Universität Stuttgart

Institut für Wasser- und Umweltsystemmodellierung

Mitteilungen

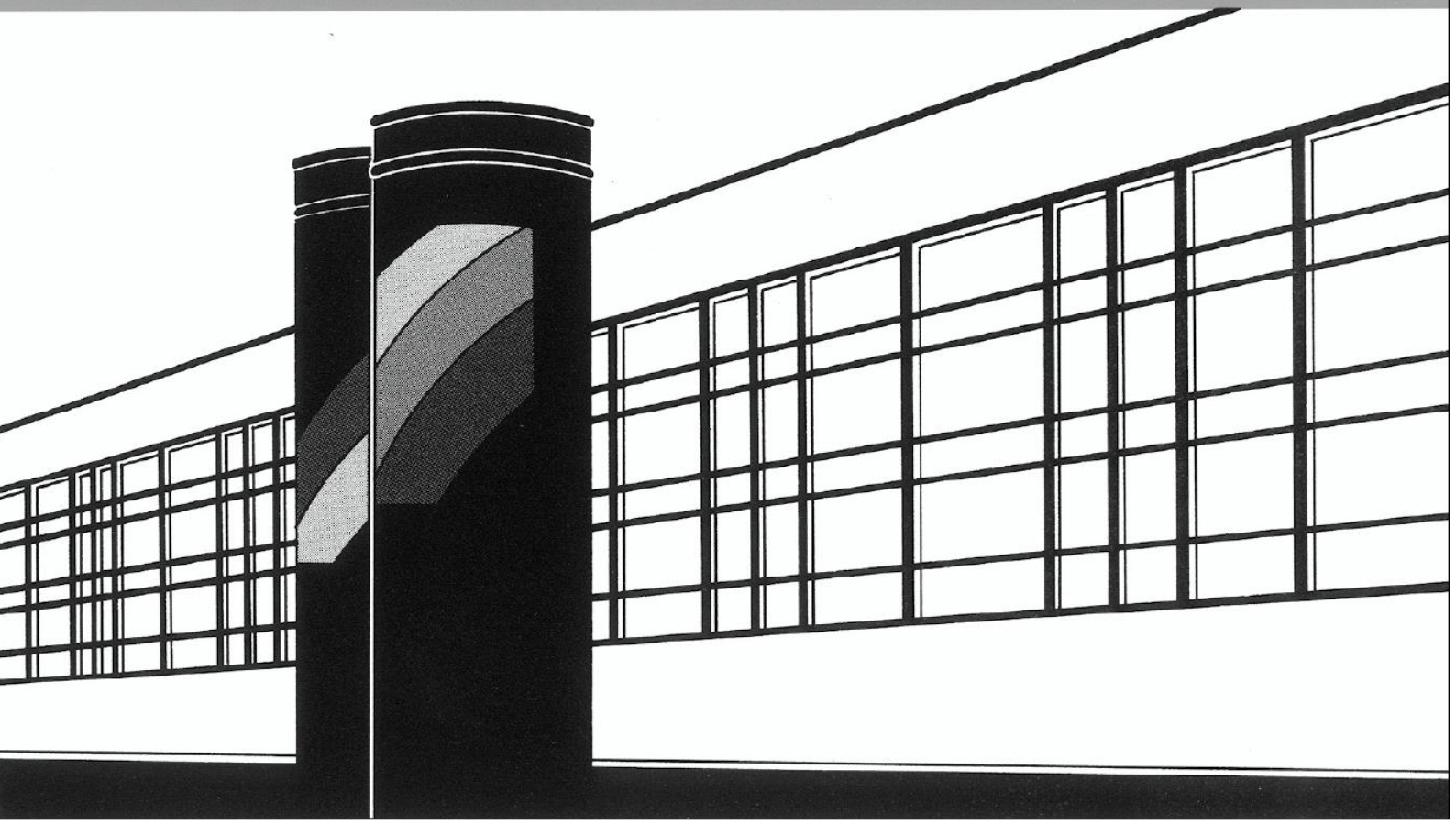

Heft 282 Felix Beckers

Investigations on Functional Relationships between Cohesive Sediment Erosion and Sediment Characteristics

Investigations on Functional Relationships between Cohesive Sediment Erosion and Sediment Characteristics

von der Fakultät Bau- und Umweltingenieurwissenschaften der
Universität Stuttgart zur Erlangung der Würde eines
Doktor-Ingenieurs (Dr.-Ing.) genehmigte Abhandlung

vorgelegt von
Felix Beckers
aus Leutkirch im Allgäu, Deutschland

Hauptberichterin:	Prof. Dr.-Ing. Silke Wieprecht
Mitberichter:	Prof. Dr.-Ing. Jochen Aberle

Tag der mündlichen Prüfung: 21.05.2021

Institut für Wasser- und Umweltsystemmodellierung
der Universität Stuttgart
2021

Heft 282

Investigations on Functional Relationships between Cohesive Sediment Erosion and Sediment Characteristics

von
Dr.-Ing.
Felix Beckers

Eigenverlag des Instituts für Wasser- und Umweltsystemmodellierung
der Universität Stuttgart

D93 Investigations on Functional Relationships between Cohesive Sediment Erosion and Sediment Characteristics

Bibliografische Information der Deutschen Nationalbibliothek
Die Deutsche Nationalbibliothek verzeichnet diese Publikation in der Deutschen Nationalbibliografie; detaillierte bibliografische Daten sind im Internet über http://www.d-nb.de abrufbar

Beckers, Felix:
Investigations on Functional Relationships between Cohesive Sediment Erosion and Sediment Characteristics, Universität Stuttgart. - Stuttgart: Institut für Wasser- und Umweltsystemmodellierung, 2021

(Mitteilungen Institut für Wasser- und Umweltsystemmodellierung, Universität Stuttgart: H. 282)
Zugl.: Stuttgart, Univ., Diss., 2021
ISBN 978-3-942036-86-3

NE: Institut für Wasser- und Umweltsystemmodellierung <Stuttgart>: Mitteilungen

Herausgegeben 2021 vom Eigenverlag des Instituts für Wasser- und Umweltsystem-modellierung

Druck: DCC Kästl e.K., Ostfildern

Acknowledgements

I would like to thank Prof. Dr.-Ing. Silke Wieprecht, chair of the Department of Hydraulic Engineering and Water Resources Management of the Institute for Modelling Hydraulic and Environmental Systems at the University of Stuttgart. From the very first moment, she was involved in my academic journey. As supervisor during my internship in 2007, as lecturer in the years 2009-2013, as examiner of my diploma thesis in 2014, as Professor during my time as research associate from 2014 to date, and as supervisor of my doctoral thesis. I am extremely grateful for her guidance and support I received throughout the years.

Furthermore, I would like to extend my sincere thanks to Prof. Dr.-Ing. Jochen Aberle, chair of the Department of Hydraulic Engineering and River Morphology of the Leichtweiß Institute for Hydraulic Engineering and Water Resources at the University of Braunschweig. I met him the first time while I have been working on my diploma thesis at the NTNU in Trondheim and am very pleased that he is the second examiner of my doctoral thesis.

I owe particular thanks to Prof. Dr.-Ing. Markus Noack and Stefan Haun, PhD. They gave me the opportunity to develop own ideas but were always at hand with help and advice, which enabled me to adapt and improve my competences in the broad field of hydraulic engineering and water resources management.

Many more persons accompanied and supported me throughout the last years and a big thank you goes to all my colleagues with whom I had the great pleasure to work with. In particular, I would like to thank my (former) office-colleagues Najibullah Sadid, Aline Schäfer Rodrigues Silva, and Kaan Koca for the numerous fruitful discussions and for an always relaxed and productive atmosphere. Many thanks go to the workshop-team around Gerhard Schmid, Henning Eickhoff, Marko Schmitt, Steffen Hägele, and Bojan Skodic. They were always at hand and provided innovative solutions whenever I needed something for any kind of project.

I highly appreciated the work of various student assistants and graduates who contributed to this thesis. At this point, special thanks go to Ruslan Biserov and Caleb Inskeep. They supported me on a large number of time-consuming erosion experiments, which would not have been possible without their passion and effort.

I also wish to thank Dr.-Ing. Matthias Schneider and apl. Prof. Dr.-Ing. Sergey Oladyshkin. Both of them introduced me with great dedication to their research areas, which challenged me

but taught me valuable skills to broaden my view and think outside the box. Furthermore, the CHARM-colleagues from Konstanz and Freiburg taught me how exciting and interesting it is to work in a transdisciplinary research project. Thank you very much for this great experience.

My deepest gratitude goes to my parents, my sister, and my family for their persistent encouragement and moral support throughout the entire duration of my studies and my doctoral thesis. They made a lot of things possible for me, for which I am always grateful to them. I cannot begin to express my thanks to Bärbel and my daughter Romy, who fill my life with endless joy, happiness, and deepest satisfaction. It is beyond words to express my gratitude to their patience, love, and unconditional support - Thank you for being there for me.

Felix Beckers

February 28, 2021

Stuttgart, Germany

Contents

List of Figures

List of Tables

Notations

The following symbols are used in this thesis:

A_e	[mm^2]	total area of erosion
d	[μm]	particle size diameter
d_m	[μm]	mean particle size diameter
d_{50}	[μm]	median particle size diameter
j	[-]	pixel
M	[mg s^{-1} mm^{-2}]	mass erosion rate (related to an area)
Q	[l s^{-1}]	flow rate
u'	[m s^{-1}]	longitudinal velocity fluctuation
v'	[m s^{-1}]	vertical velocity fluctuation
$\langle\overline{u'v'}\rangle$	[m^2 s^{-2}]	double-averaged covariance of the velocity fluctuations
y	[mm]	longitudinal dimensions of the SETEG erosion flume in the local coordinate system of the LDV

ΔV	[mm^3]	average erosion volume
$\Delta V^{(j)}$	[mm^3]	erosion volume per pixel
$\Delta x^{(j)}$	[mm]	metric length dimension per pixel in x-direction
$\Delta y^{(j)}$	[mm]	metric length dimension per pixel in y-direction
Δz	[mm]	average deepening
$\Delta z^{(j)}$	[mm]	elevation change per pixel
Δz_s	[mm]	specific deepening
ε	[mm s^{-1}]	volumetric erosion rate (related to an area)
ρ	[g cm^{-3}]	fluid density
ρ_b	[g cm^{-3}]	bulk density
τ	[Pa]	shear stress
τ_c	[Pa]	critical shear stress

Abbreviations

The following abbreviations are used in this thesis:

ASSET flume	Adjustable Shear Stress Erosion and Transport Flume
CEC	cation exchange capacity
CHL-a	chlorophyll-a
CMOS	complementary metal-oxide-semiconductor
DIN	German standard
DIN EN	European standard
EFA flume	Erosion Function Apparatus
EPS	extracellular polymeric substances
EPS-p	proteins of the EPS fractions
EPS-c	carbohydrates of the EPS fractions
GBS	Großer Brombachsee
ICOLD	International Commission on Large Dams
ISO	International Organization for Standardization
KBS	Kleiner Brombachsee
LDV	Laser Doppler velocimetry
MFM	magnetic flow meter
PHOTOSED	PHOTOgrammetric Sediment Erosion Detection
PVC	polyvinyl chloride
ROI	region of interest
SBT	Schwarzenbachtalsperre
SEDCIA	Sediment Erosion Rate Detection by Computerised Image Analyses
SEDFlume	Sediment Erosion at Depth Flume
SETEG	Strömungskanal zur Ermittlung der Tiefenabhängigen Erosionsstabilität von Gewässersedimenten
TOC	total organic carbon

Abstract

Every fluvial system transports sediments and in pristine conditions a long-term equilibrium between sediment erosion and deposition exists. An anthropogenic disturbance of this morphodynamic equilibrium has a negative impact on the morphology, ecology, and consequently on the vitality of the whole system. For example, dam construction interrupts the longitudinal sediment continuity. This causes sediment accumulation upstream and sediment deficit downstream of the structure. Consequently, sedimentation and erosion problems arise, which require maintenance measures to counteract negative morphological, ecological, and also economic effects. This means that strategies for sustainable sediment management in reservoirs are necessary to mitigate sedimentation and to remobilize already accumulated sediments when required.

In many reservoirs, sediment deposits consist largely of fine sediments of the clay and silt fraction ($d<63\mu m$). Generally, an exact description of the erodibility of fine sediment deposits is challenging because fine sediments tend to develop a shear strength dominated by cohesive effects. Thus, their erosion and remobilization potential differs considerably from coarse and non-cohesive material ($d>63\mu m$). This is due to complex interactions between physical, chemical, and biological effects, which contribute to the erosion resistance of cohesive sediments against flow-induced shear stress making it difficult to analytically describe their erosion processes.

For this reason, experimental research is essential to study the characteristics and the erodibility of cohesive reservoir sediments. At the same time high-resolution measurement techniques are required, which are capable to resolve the spatio-temporal variability of cohesive sediment erosion to investigate fundamental erosion processes.

This thesis explores the erodibility of fine reservoir deposits to unravel functional relations between fine sediment erosion and underlying sediment characteristics. The present research is concerned with four main objectives, which are addressed in four scientific publications. These publications are the main part of this thesis and are included at the end. Furthermore, a detailed summary of these articles is given in the text.

The first step was the removal of undisturbed sediment cores from the deposits of three reservoirs (Kleiner Brombachsee, Großer Brombachsee, and Schwarzenbachtalsperre) for further experimental investigations (characterizing analyses and erosion experiments). In a second step,

experiments were conducted in a laboratory erosion flume (SETEG) and the erosion behavior was recorded with a novel measurement technique (PHOTOSED) that is capable to measure the erosion with high spatio-temporal resolution. Next, the erosion behavior, the erosion variability, and specific emerging erosion forms were assessed based on the data obtained. This was followed by the evaluation of critical erosion thresholds (initiation of motion and a change in the erosion behavior) for the experimentally investigated sediments. Finally, the critical erosion thresholds were correlated with a set of analyzed sediment characteristics to explore functional relationships between cohesive sediment erosion and their physical, chemical, and biological sediment characteristics.

The results obtained indicate that it is possible to remove undisturbed sediment cores from reservoir deposits using an adapted Frahm Sediment Sampler. These cores can be experimentally eroded in the SETEG/PHOTOSED-system to investigate their depth-dependent erosion potential. Likewise, removed sediment cores can be used to analyze the depth-dependent sediment characteristics in distinct layers including physical (bulk density, particle size distribution, sediment composition, and percentiles), chemical (total organic carbon and cation exchange capacity), and biological parameters (extracellular polymeric substances and chlorophyll-a).

The developed method PHOTOSED is capable to explore the erodibility of cohesive sediments and allows the detection of erosion volumes for several orders of magnitude (lowest investigated volume during calibration was 13 mm^3, mean absolute deviation for this volume was $\approx 9.2\%$). This is an essential benefit when investigating the erodibility of cohesive sediments and non-cohesive/cohesive sediment mixtures, which are known to be highly variable in space, time, and erosion magnitude.

Detailed investigations using the SETEG/PHOTOSED-system revealed that due to the high spatio-temporal resolution of PHOTOSED, it is possible to measure the erosion process of cohesive sediments dynamically and pixel-based with a vertical resolution in the sub-millimeter range. This allows detecting and distinguishing between two fundamental erosion processes. These fundamental processes being the emergence of individual erosion spots caused by surface erosion and the formation of large holes that were torn open through the detachment of aggregate chunks. Moreover, interrelated processes as a temporal consequence of ongoing erosion can be measured. These are the propagation of the erosion in the longitudinal and lateral direction (which eventually leads to the merging of disconnected erosion areas) and the progression of the erosion in the vertical direction (ongoing deepening). The analysis of the spatio-temporal erosion variability revealed that the largest erosion events are confined to only a few time steps during temporal progression. In this event they exceed the time-averaged median of the deepening significantly (between 7 and 16 times the median was measured).

The functional relationships between critical erosion thresholds of fine reservoir sediments

and a collection of physical, chemical, and biological sediment characteristics were explored by multivariate correlation analyses (case studies: Großer Brombachsee and Schwarzenbachtalsperre). For the deposits of the Großer Brombachsee the results indicate strong positive correlations between the critical erosion thresholds and the clay content, and to a less extent with the bulk density. Strong negative correlations are observed between the erosion thresholds and the total organic carbon content. For the deposits of the Schwarzenbachtalsperre the results show strong negative correlations between the erosion thresholds and the clay content, which can be attributed to a comparatively high sand content. The increased sand content is strongly associated with increasing erosion thresholds in the first 10 cm of the sediment cores, but this relation diminishes in deeper located sediment layers.

The findings gained by this research provide valuable knowledge to the field of fine sediment erosion and contribute significantly to the process understanding of cohesive sediment erosion. Particularly, it was shown that it is possible to remove undisturbed sediment cores for further experimental investigations from deep reservoir deposits. The SETEG/PHOTOSED system used to erode these cores is capable to measure the complex erosion of cohesive sediments dynamically and with high spatio-temporal resolution in order to explore fundamental erosion processes including specific erosion forms. This allows to obtain confident erosion thresholds from the cumulative erosion volume to be correlated with analyzed sediment characteristics. In doing so, functional relationships between the erosion stability and physical, chemical, and biological sediment properties could be explored. It was shown that mainly the clay content and the bulk density correlated positively with the erosion stability, while the organic matter content correlated predominantly negatively. However, the results obtained also show that the relations are complex and the identification of individual key parameters is challenging for natural cohesive sediments. It is therefore advisable to pursue analytical evaluations with combinatorial approaches in future.

Future research should aim at taking into account the effect of turbulent shear stress fluctuations and dynamic roughness changes on the erodibility of cohesive sediments. The high spatio-temporal resolution of PHOTOSED allows evaluating geometric roughness changes of the sediment surface from the dynamically measured erosion data. In combination with advanced hydraulic measurements at the SETEG-flume, this enables to study flow–sediment interactions. This would serve basic research on the cause and origin of the - *now measurable* - fundamental erosion processes at the water-sediment-interface.

Kurzfassung

Einleitung und Motivation Jedes natürliche Fließgewässer transportiert Sedimente. Eine Störung des natürlichen Sedimenthaushalts durch anthropogene Eingriffe wirkt sich negativ auf Morphodynamik, Ökologie und somit auf die Vitalität eines Gewässers aus. Deutlich wird diese Problematik am Beispiel von Stauräumen. Die zum Aufstau des Wassers benötigten Querbauwerke führen zu einer Unterbindung der longitudinalen Sedimentdurchgängigkeit. Dies hat zur Folge, dass sich oberstrom der Bauwerke Sedimente ablagern und unterstrom ein Sedimentdefizit herrscht, was zu Anlandungs- und Erosionsproblemen führt. Während im 20. Jahrhundert der Bau neuer Stauräume im Fokus stand, so gilt es heutzutage durch nachhaltige Managementstrategien bereits akkumulierte (und sich kontinuierlich akkumulierende) Sedimente zu (re)mobilisieren, um den Betrieb und die Wirtschaftlichkeit von Stauräumen langfristig sicherzustellen.

In vielen Stauräumen bestehen die Sedimentablagerungen überwiegend aus Feinsedimenten. Insbesondere die Beschreibung und Vorhersage deren Erosionspotentials unter hydraulischer Beanspruchung stellt eine Herausforderung an die Sedimentforschung dar. Grund dafür sind kohäsive Bindungskräfte, die von Feinsedimenten der Ton- und Schlufffraktion ($d<63\mu m$) ausgebildet werden. Daraus resultieren interpartikuläre Wechselwirkungen, die Einzelpartikel zu Aggregaten zusammenschließen lässt, was die Erosionsstabilität der Sedimente bestimmt. Aufgrund dieser Wechselwirkungen, die sowohl durch komplexe interagierende physikalische und chemische als auch biologische Parameter hervorgerufen werden, ist eine exakte analytische Vorhersage der Erosionsstabilität kohäsiver Sedimente bisher nicht möglich. Folglich sind experimentelle Untersuchungen die einzige Möglichkeit, um die Eigenschaften und das damit verbundene Erosionspotential kohäsiver Sedimente zu untersuchen und zu bewerten. Hierfür werden hochauflösende Messverfahren benötigt, die in der Lage sind, die räumlich-zeitliche Variabilität der kohäsiven Sedimenterosion zu erfassen. Dieser Forschungsbedarf zur Erosion kohäsiver Sedimente wird in dieser Arbeit aufgegriffen.

Das wesentliche Ziel dieser Arbeit ist es, das Erosionsverhalten, die Erosionsstabilität und deren funktionale Zusammenhänge mit physikalischen, chemischen und biologischen Sedimentparametern von natürlichen Stauraumsedimenten zu untersuchen, um zum Prozessverständnis der kohäsiven Sedimenterosion beizutragen. Zu diesem Zweck wurden bestehende Techniken (Frahm-Lot) an die besonderen Randbedingungen von Stauräumen

angepasst und zur Entnahme von ungestörten Sedimentkernen aus Tiefensedimenten weiterentwickelt. Es wurden neue Messmethoden zur Erfassung der kohäsiven Sedimenterosion (PHOTOSED) und Analysemethoden zur Bewertung des Erosionsverhaltens kohäsiver Feinsedimente entwickelt. Damit war es möglich Sedimente aus drei Stauräumen (Kleiner Brombachsee, Großer Brombachsee und Schwarzenbachtalsperre) zu entnehmen, deren physikalische, chemische und biologische Sedimenteigenschaften zu untersuchen und das Erosionspotential in einer Erosionsrinne (SETEG) experimentell zu erforschen. Schließlich wurden die erhobenen Daten multivariat analysiert, um wesentliche Zusammenhänge zwischen der Erosionsstabilität und den charakteristischen Eigenschaften der Stauraumsedimente zu identifizieren.

Die wesentlichen Forschungsfragen sind in vier wissenschaftlichen Publikationen erschienen, welche am Ende der Arbeit zu finden sind. Die darin enthaltenen Ergebnisse und wesentlichen Erkenntnisse sind nachfolgende zusammengefasst:

Publikation I: Experimental investigation of reservoir sediments In dieser Publikation werden die Möglichkeiten zur Entnahme von ungestörten Sedimentkernen aus Stauraumablagerungen eruiert und die theoretischen Konzepte zur Verschneidung der gemessenen Erosionsstabilität über die Sedimenttiefe (unter Verwendung des SETEG/PHOTSED-Systems) mit einer Reihe von analysierten Sedimenteigenschaften (physikalische, chemische und biologische Parameter) überprüft.

Mit Hilfe eines Frahm-Lots, welches an die Bedingungen von Stauräumen adaptiert wurde, werden von einer schwimmenden Plattform aus Sedimentkerne aus Stauraumablagerungen entnommen (Untersuchungsgebiet: Kleiner Brombachsee). Die gewonnenen Sedimentkerne sind ungestört, sodass sie im SETEG/PHOTOSED-System experimentell erodiert werden können, um ihr tiefenabhängiges Erosionspotential zu erforschen. Des Weiteren werden die entnommenen Sedimentkerne verwendet, um die Sedimenteigenschaften in verschiedenen tiefenabhängigen Schichten zu analysieren. Neben physikalisch-chemischen Parametern (Lagerungsdichte, Perzentilwerte der Partikelgrößenverteilung, gesamter organischer Kohlenstoffgehalt und Kationenaustauschkapazität) werden auch biologische Parameter (extrazelluläre polymere Substanzen und Chlorophyll-a) analysiert.

Die Ergebnisse dieser Studie bestätigen das theoretische Konzept und zeigen, dass es möglich ist, die experimentell gemessene Erosionsstabilität mit den analysierten Sedimentparametern zu korrelieren. Insbesondere unterstreichen die Ergebnisse, dass neben den physikalisch-chemischen Sedimenteigenschaften auch biologische Parameter berücksichtigt werden sollten, um Zusammenhänge zur kohäsiven Erosionsstabilität zu erforschen.

Publikation II: PHOTOSED - PHOTOgrammetric Sediment Erosion Detection In dieser Publikation wird die entwickelte photogrammetrische Messmethode PHOTOSED (PHOTOgrammetric Sediment Erosion Detection) zur Erfassung des Erosionsverhaltens kohäsiver Feinsedimente vorgestellt. Der Artikel erläutert den theoretischen Hintergrund und gibt Informationen zur Kalibrierung und Verifizierung von PHOTOSED.

PHOTOSED projiziert mit einem Halbleiterlaser ein pseudozufälliges Muster von Lichtpunkten auf eine Sedimentoberfläche. Während eines Erosionsversuchs, wird die Sedimentoberfläche und die, aus einer Erosion resultierende, Verschiebung von Lichtpunkten mit einer Kamera überwacht und aufgenommen. In einer post-processing-Routine berechnet PHOTOSED aus den vorliegenden Videos die Erosionsvolumina innerhalb einer Region of Interest (ROI) unter Verwendung von Farnebäck's dense optical flow Algorithmus.

Die Ergebnisse der umfangreichen Kalibrierungs- und Verifizierungsexperimente zeigen, dass PHOTOSED die Messung von Erosionsvolumina für mehrere Größenordnungen ermöglicht (kleinstes untersuchtes Volumen war 13 mm^3, mittlere absolute Abweichung zur Messung betrug $\approx$ 9,2%). Dies ist ein wesentlicher Vorteil bei der Erforschung der kohäsiven Sedimenterosion, da deren Erosionsverhalten räumlich und zeitlich stark variieren kann. PHOTOSED bietet somit die Möglichkeit, das Erosionsverhalten von kohäsiven Sedimenten detailliert zu untersuchen.

Publikation III: High spatio-temporal resolution measurements of cohesive sediment erosion In dieser Publikation werden mehrere Aspekte der bisherigen Forschung kombiniert. Zunächst wird die SETEG-Erosionsrinne vorgestellt und hydraulisch charakterisiert. Als nächstes werden die Messgrößen von PHOTOSED hergeleitet und erläutert sowie die Vorteile und Vielseitigkeit der Methode zur Messung der kohäsiven Sedimenterosion beschrieben. Schließlich werden detaillierte Ergebnisse von drei Erosionsversuchen vorgestellt (Untersuchungsgebiet: Schwarzenbachtalsperre). Dies beinhaltet die Analyse und Bewertung des Erosionsverhaltens und die Auswertung der räumlich-zeitlichen Variabilität der kohäsiven Sedimenterosion.

Die Ergebnisse zeigen, dass es aufgrund der hohen räumlich-zeitlichen Auflösung von PHOTOSED möglich ist, den Erosionsprozess von kohäsiven Sedimenten dynamisch und pixelbasiert mit einer vertikalen Auflösung im Submillimeterbereich zu messen. Dies ermöglicht das Erkennen und Unterscheiden zweier grundlegender Erosionsprozesse. Hierbei handelt es sich um sporadisch auftretende, einzelne Erosionsbereiche und um die Entstehung von großen Löchern durch das Herausreißen von ganzen Aggregatbrocken. Darüber hinaus können zusammenhängende Prozesse als zeitliche Folge der fortschreitenden Erosion gemessen werden. Dies sind die Ausbreitung der Erosion in Längs- und Querrichtung (was

schließlich zur Verbindung einzelner Erosionsbereiche führt) und die anhaltende vertikale Erosion (zunehmende Eintiefung).

Die Auswertungen der räumlich-zeitlichen Erosionsvariabilität zeigen, dass sich die größten Erosionsereignisse auf wenige Zeitschritte im zeitlichen Verlauf beschränken. In diesem Fall übersteigen sie den zeitlich gemittelten Median der Erosion deutlich (eine Erhöhung um das 7- bis 16-fache des Medians wurde gemessen). Außerdem fällt die größte Eintiefung nicht zwangsläufig mit der größten Erosionsfläche zusammen, was durch die grundlegenden Erosionsprozesse und deren spezifische Erosionsformen (Flocken-/Aggregaterosion, Ablösung von Aggregatbrocken) zu erklären ist.

Wichtigste Erkenntnis dieser Arbeit ist, dass die mit dem SETEG/PHOTOSED-System durchgeführten Erosionsversuche zuverlässige und hochauflösende Messdaten, einschließlich detaillierter Informationen über die spezifischen Erosionsformen, liefern. Dadurch ist eine robuste Bewertung des kohäsiven Erosionsverhaltens möglich.

Publication IV: Functional relationships between critical erosion thresholds of fine reservoir sediments and their sedimentological characteristics In dieser Publikation werden die entwickelten Methoden und gewonnenen Erkenntnisse zusammengeführt, um die funktionalen Zusammenhänge zwischen den kritischen Erosionsschwellen der untersuchten Stauraumsedimente und deren sedimentologischen Eigenschaften zu erforschen. Zu diesem Zweck wird ein umfangreicher Datensatz durch experimentelle Erosionsversuche mit dem SETEG/PHOTOSED-System für zwei Stauräume (Untersuchungsgebiete: Großer Brombachsee und Schwarzenbachtalsperre) erhoben. Die Erosionsdaten werden hinsichtlich kritischer Erosionsschwellen mit einem pseudo-automatischen Steigungskriterium ausgewertet, um eine sichere Bewertung der Erosionsstabilität zu gewährleisten. Diese Schwellenwerte werden mit einer Auswahl an physikalischen, chemischen und biologischen Sedimenteigenschaften mittels multivariater Statistik korreliert, um funktionale Zusammenhänge zwischen diesen Parametern und der Erosionsstabilität der untersuchten Stauraumsedimente zu analysieren.

Es wird gezeigt, dass kritische Erosionsschwellen mit Hilfe des angewandten Algorithmus (Steigungskriterium) verlässlich aus den kumulativen Erosionsvolumina abgeleitet werden können. Es werden zwei kritische Erosionsschwellen betrachtet: (i) Die Schubspannung bei Erosionsbeginn, die durch den erstmaligen Anstieg des kumulativen Erosionsvolumens identifizierbar ist und (ii) die Schubspannung bei einem Wechsel des Erosionsregimes (Erosionsverhaltens), die durch die maximale Steigungsänderung des kumulierten Erosionsvolumens gekennzeichnet ist. Die ermittelten kritischen Schubspannungswerte werden mit den gemessenen physikalischen (Lagerungsdichte, Sedimentzusammensetzung, Perzentilwerte der Partikelgrößenverteilung), chemischen (gesamter organischer Kohlenstoff, Kationenaustauschkapazität) und biologischen (Chlorophyll-a, extrazelluläre polymere Substanzen getrennt in Pro-

teine und Kohlenhydrate) Parametern korreliert.

Die Ergebnisse für die Sedimente des Großen Brombachsees zeigen starke positive Korrelationen zwischen den kritischen Erosionsschwellen mit dem Tongehalt und in geringerem Maße mit der Lagerungsdichte. Starke negative Korrelationen sind zwischen den Erosionsschwellen und dem Gesamtgehalt an organischem Kohlenstoff zu beobachten. Darüber hinaus nehmen die Korrelationen der Erosionsschwellen mit den Sedimenteigenschaften über die Sedimenttiefe kontinuierlich ab. Die Ergebnisse für die Sedimente der Schwarzenbachtalsperre weisen eine negative Korrelation zwischen den Erosionsschwellen und dem Tongehalt auf, was auf einen vergleichsweise hohen Sandgehalt zurückzuführen ist. Der erhöhte Sandgehalt ist in den ersten 10 cm der Sedimentkerne stark mit den Erosionsschwellen korreliert, dieser Zusammenhang nimmt jedoch in tiefer gelegenen Sedimentschichten ab.

Fazit und Ausblick Die durch diese Arbeit gewonnenen Erkenntnisse tragen wesentlich zum Prozessverständnis der kohäsiven Sedimenterosion bei. Im Wesentlichen wird gezeigt, dass es möglich ist, ungestörte Sedimentkerne für weitergehende experimentelle Untersuchungen aus dem Tiefenbereich von Stauräumen zu entnehmen. Das eingesetzte SETEG/PHOTOSED-System ermöglicht es, die komplexen Erosionsvorgänge dynamisch und hochaufgelöst zu messen, um Rückschlüsse auf die grundlegenden Erosionsprozesse zu ziehen. Eine anschließende Korrelation der ermittelten Erosionsstabilitäten mit analysierten Sedimentparametern ermöglicht es, funktionale Zusammenhänge zwischen der Erosion und physikalischen, chemischen und biologischen Sedimenteigenschaften zu entschlüsseln. Für die untersuchten Stauraumsedimente hat sich gezeigt, dass insbesondere der Tongehalt und die Lagerungsdichte überwiegend positiv und der Gehalt an organischem Material überwiegend negativ mit der Erosionsstabilität korreliert. Jedoch zeigt sich auch, dass die Zusammenhänge bei natürlichen Sedimenten sehr komplex sind und sich nur stark vereinfachend auf einzelne Schlüsselparameter reduzieren lassen. Es ist daher ratsam die analytische Auswertung zukünftig mit kombinatorischen Ansätzen zu ergänzen.

Weitergehender Forschungsbedarf besteht insbesondere in der messtechnischen Detektion turbulenter Schubspannungsspitzen und dynamischer Rauheitsänderungen während experimenteller Versuche mit dem SETEG/PHOTOSED-System sowie einer Bewertung deren Einflüsse auf die Hydraulik und Sedimenterosion. Dies würde der Grundlagenforschung zu den Ursachen und Entstehung der - *nun messbaren* - grundlegenden Erosionsprozesse an der Wasser-Sediment-Grenzschicht dienen.

The thesis may contain similar and/or identical material from my publications:

”Experimental investigation of reservoir sediments”,
”PHOTOSED - PHOTOgrammetric Sediment Erosion Detection”,
”High spatio-temporal resolution measurements of cohesive sediment erosion”, and
”Functional relationships between critical erosion thresholds of fine reservoir sediments and their sedimentological characteristics”.

I omit a clear identification for readability and use these parts from the articles with kind permission from the publisher.

1. Introduction

Every fluvial system moves and transports sediment particles through its current (fluvial sediment transport). Depending on the sediment type and the hydraulic condition, sediment transport can occur as bedload or suspended load. Bedload describes the transport of coarse sediment along the bed (sliding, rolling, and saltation). Suspended load describes the transport of fine sediments in the water column, which are kept in suspension due to the turbulence levels of the flow and thus move above the bedload layer (Wu, 2008). Together, bedload and suspended load form the total load. Usually bedload accounts for 5–25% (Wu, 2008) and suspended load represents the remaining majority of the total load (Pye, 1994).

In a pristine river, a morphodynamic equilibrium exists, which means there is a long-term balance between sediment erosion and deposition. An anthropogenic disturbance of this dynamic equilibrium has a negative impact on the morphology and ecology of the whole system (e.g., Hinderer et al., 2013). For example, dam construction interrupts the longitudinal sediment continuity and alters the hydraulic conditions of the impacted area. This causes sediment accumulation upstream and sediment deficit downstream of the structure. Consequently, sedimentation and erosion problems arise, which require maintenance measures to counteract negative morphological, ecological, and also economic effects (e.g., Kondolf et al., 2014; Peteuil et al., 2018). This means that strategies for sustainable sediment management in reservoirs are necessary to mitigate sedimentation and to remobilize already accumulated sediments when required (e.g., Brandt, 2000; Kondolf et al., 2014; Schleiss et al., 2016).

In many reservoirs, sediment deposits consist largely of fine sediments of the clay and silt fraction ($d<63\mu m$) (e.g., Morris and Fan, 1998; Beckers et al., 2018b). Generally, an exact description of the erodibility of fine sediment deposits is challenging because fine sediments tend to develop a shear strength dominated by cohesive effects. Thus, their erosion and remobilization potential differs considerably from coarse and non-cohesive material ($d>63\mu m$). This is due to complex interactions between physical, chemical, and biological effects, which control the erosion resistance of cohesive sediments and make it difficult to describe their erosion processes (e.g., Pye, 1994; Debnath and Chaudhuri, 2010; Wu, 2016). Despite a large number of scientific studies on this topic, no generally accepted approaches are available to reliably model cohesive sediment erosion (e.g., Grabowski et al., 2011; Walder, 2016; Karamigolbaghi et al., 2017; Van Rijn, 2020). For this reason, experimental investigations are essential to study

the characteristics and the erodibility of cohesive sediments (Mehta and Lee, 1994; Witt, 2004; Briaud, 2008; Noack et al., 2015). While this is possible for intertidal, estuarine, and riverine sediments, it is difficult for reservoir sediments since the deposits are hard to access, mainly due to their depth.

1.1. Reservoir sedimentation

Reservoirs serve a multitude of purposes such as hydropower production, drinking and irrigation water supply, flood retention, and recreation (e.g., Beckers et al., 2018a; Annandale et al., 2018). The single process that all reservoirs worldwide share to a different degree in common is sedimentation (Morris and Fan, 1998). From a hydro-morphodynamic perspective, reservoir sedimentation occurs due to a continuous decrease of both, flow forces and turbulence levels from the head of a reservoir towards the dam. While bed load and coarse fractions of the suspended load settle primarily and form delta deposits, fine sediment particles are transported far into the reservoir (Morris and Fan, 1998). Consequently, downstream sediment fining occurs and the deposits are often composed of fine sediments with cohesive properties (Fan and Morris, 1992; Mouris et al., 2018; Beckers et al., 2018a).

According to ICOLD (2020), approximately 58,500 large dams exist worldwide to impound water to form reservoirs (large dam: dam height $\geq$ 15 m or dam height 5-15 m with $>$0.003 km^3 storage capacity). The significance of reservoirs is highly increasing due to anthropogenic influences exacerbated by climate and demographic changes and the need for renewable energy (Zarfl et al., 2015). Zarfl et al. (2015) reported at least 3,700 major dams for hydropower production are either planned or under construction, each with a capacity of more than 1 MW. This trend will likely continue and more and larger dams will be built in coming decades (Mulligan et al., 2020). Accordingly, an increasing fragmentation of rivers by dams is expected as well as increasing sediment trapping by reservoirs.

The loss of reservoir storage capacity is a costly phenomenon (e.g., Vörösmarty et al., 1997a,b) and estimates exist that quantify the trapped sediment on a global scale. Vörösmarty et al. (2003) yields a range of 4-5 billion tons of sediment per year being intercepted by all registered reservoirs. Syvitski (2005) estimated that worldwide, reservoirs are responsible for trapping 1.4$\pm$0.3 billion tons of sediment per year, which consequently does not reach the coasts. Some studies yield a percentage loss of global reservoir storage, such as two works from the late 1980s and early 1990s, which estimated a loss of 1% per year (Mahmood, 1987; Yoon, 1992) whereas Sumi (2004) estimated a loss of 0.52% per year. This range between 0.5-1% global loss of water storage per year due to sedimentation was confirmed by Basson (2009) and Schleiss et al. (2016). Accordingly, Kondolf et al. (2014) concluded that independent of the estimate, sediment trapping by reservoirs is of primary global importance. This is also the reason for

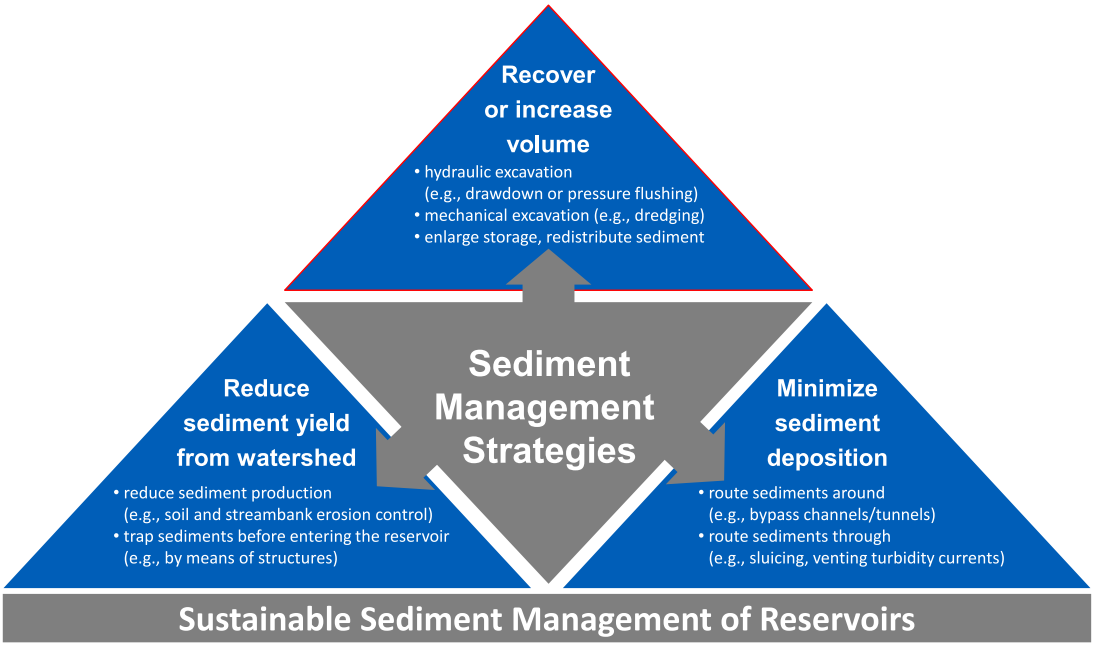

Figure 1.1. Sediment management strategies in reservoirs to sustain storage capacity (modified after Kondolf et al. (2014)).

one of the main messages raised at the Third World Water Forum, Japan (2003): *While in the 20th century the focus was on reservoir development, the focus in the 21st century will be on sediment management aiming at converting non-sustainable reservoirs to sustainable infrastructures for future generations.*

1.2. Sediment management in reservoirs

In instances where the accumulated sediments have negative impacts on the operation or the lifetime of the reservoir, sediment management strategies are necessary to counteract sedimentation (e.g., Kondolf et al., 2014; Schleiss et al., 2016; Peteuil et al., 2018). Figure 1.1 provides an overview on sediment management strategies from the perspective of sustaining reservoir storage capacity (modified after Kondolf et al., 2014).

Generally, sediment management strategies are classified into three categories: measures in the watershed to reduce the sediment yield into a reservoir, measures to minimize sediment deposition, and measures to recover or increase the storage volume of a reservoir (Kondolf et al., 2014; Kantoush and Sumi, 2010).

The measures to reduce the sediment yield are aimed at erosion control in the watershed (e.g., afforestation, terracing, bank protection) or on trapping of sediment prior to entering the reservoir (e.g., by checkdams). Measures to minimize sediment deposition contain sedi-

ment routing around (e.g., bypass tunnels/channels) and through (e.g., sediment sluicing) the reservoir. Principally, many of these techniques require constructive measures (e.g., bypass tunnels/channels, checkdams, or sediment traps). Ideally, these technical requirements were considered already during design and construction of the dam or, in case possible, must be build at a later stage.

The measures of the third category (see top of Figure 1.1) maintain reservoir capacity by recovering (e.g., mechanical excavation) or increasing the storage volume (e.g., enlargement of existing reservoir). One important possibility to recover volume by remobilizing already deposited material is reservoir flushing . Generally, during flushing operation bottom outlets (or flushing gates) are opened in order to release water to erode deposited material by hydraulic excavation. Through this procedure it is intended to flush sediment from the reservoir into the downstream section (Brandt, 1999). Detailed information on reservoir flushing is provided by Morris and Fan (1998), Brandt (1999), or Wen Shen (1999).

For planning and conducting an efficient flushing operation, several integral aspects should be considered. For example, the topographic and geometric boundary conditions of a reservoir considerably influence the flushing efficiency (e.g., Olsen, 1999; Kantoush and Sumi, 2010; Haun, 2012). Furthermore, detailed knowledge on the sediment deposits regarding their distribution (e.g., location, magnitude), their composition (e.g., clay, silt, sand), and particularly on their depth-dependent erodibility is key to the success of reservoir flushing and generally to sediment management in reservoirs (e.g., Peteuil et al., 2018; Wen Shen, 1999; Morris and Fan, 1998). Especially in case the reservoir deposits are composed of fine sediments with cohesive properties, this remains challenging due to the difficulty in describing the erodibility of cohesive materials.

1.3. Motivation and objectives

A variety of experimental studies are available, which explore the erodibility of cohesive sediments and non-cohesive/cohesive sediment mixtures from diverse environments (e.g., Mitchener and Torfs, 1995; Panagiotopoulos et al., 1997; Righetti and Lucarelli, 2007; Kothyari and Jain, 2008; Noack et al., 2015; Zhang and Yu, 2017; Wu et al., 2018; Beckers et al., 2019). Great effort has been made in revealing functional relationships between erodibility and sediment characteristics (e.g., Grabowski et al., 2011; Wu et al., 2018). Yet no generally accepted model exists to predict cohesive sediment erosion (e.g., Van Rijn, 2020).

This is due, in part, to the complex interconnections between various influencing factors (physical, chemical, and biological) that dominate the resistance of cohesive sediment beds against flow induced shear stress (e.g., Pye, 1994; Van Rijn, 2020). Considering all potential parameters

is a labor intensive undertaking and not feasible or economically practical in an applied engineering or research context. This is why most studies focus on physico-chemical sediment characteristics (such as bulk density, particle size distribution, and organic content) but often neglect biological characteristics. However, evidence for biostabilization of naturally composed cohesive sediments exists in marine (e.g., Black et al., 2002) but also in riverine environments (e.g., Thom et al., 2015; Gerbersdorf and Wieprecht, 2015).

At the same time, many of the existing studies that contributed significantly to process understanding use artificial sediment mixtures or remolded sediments (e.g., Panagiotopoulos et al., 1997; Kothyari and Jain, 2008; Briaud et al., 2017; Zhang and Yu, 2017). Transferring these findings to natural sediments is challenging since these are much more complex mixtures. Natural sediments are examined less frequently, although studies are available that investigate sediments obtained from the field in laboratory studies (ex-situ) (e.g., Roberts et al., 2003; Beckers et al., 2018b), in-situ at their place of origin (e.g., Black et al., 2002), or combine ex-situ and in-situ experiments (e.g., Widdows et al., 2007; Noack et al., 2015).

The last challenge arises from the fact that very little information is available on technology that is capable of measuring the spatial and temporal variability of the cohesive sediment erosion process (see Tolhurst et al., 2006; Van Prooijen and Winterwerp, 2010). High-resolution measurement data are a pending requirement when it is intended to objectively assess the highly variable erosion progress of cohesive sediments. In this context, dynamically measured erosion caused by specific erosion forms (e.g., flocs, aggregates, aggregate chunks, etc.) could help to increase knowledge on the fundamental processes as well as their interactions. This encompasses the evaluation of specific erosion forms and the identification of characteristic erosion conditions for the assessment of the sediment stability (such as critical erosion thresholds).

As detailed, there is still a lack in the understanding of cohesive sediment erosion, particularly, in terms of functional relationships between the cohesive erosion stability of reservoir deposits and their sediment characteristics. This thesis aims at contributing to this understanding by increasing the scientific knowledge on the erosion process of cohesive reservoir deposits to fill existing knowledge gaps.

In order to meet these requirements, main objectives have been formulated, which will be addressed in this thesis by a number of specific objectives. The first main objective is the removal of undisturbed sediment cores from reservoir deposits for erosion experiments. In a second step, experiments are conducted in a laboratory erosion flume and the erosion behavior is recorded with a novel measurement technique capable to measure the erosion with high spatio-temporal resolution. Next, the erosion behavior, the erosion variability, and specific emerging erosion forms are assessed based on the data obtained. This is followed by the evaluation of critical erosion thresholds for the investigated reservoir deposits. The findings are finally correlated with their corresponding sediment characteristics to reveal functional rela-

tionships between cohesive sediment erosion and physical, chemical, and biological sediment characteristics.

The specific objectives addressed by this thesis are listed below:

- Removal of undisturbed sediment cores from the deposits of three reservoirs for erosion experiments and sediment characterization.
- Verification of theoretical concepts to relate the erosion stability to the sediment characteristics.
- Development, calibration, and verification of a photogrammetric method to detect (cohesive) sediment erosion.
- Measurement of cohesive sediment erosion with high spatio-temporal resolution to investigate fundamental erosion processes.
- Measurement of cohesive sediment erosion with high spatio-temporal resolution to quantify the variability of the erosion during temporal progression.
- Identification of confident critical erosion thresholds to assess the (depth-dependent) erosion stability of the investigated reservoir sediments.
- Exploration of functional relationships between the erosion stability and the sedimentological characteristics of the investigated reservoir deposits.

1.4. Outline of this thesis

The *Introduction* (chapter 1) is followed by *Fundamentals of Cohesive Sediment Erosion* (chapter 2). This chapter provides insights into the fundamentals of cohesive sediment erosion including relevant information on the classification of cohesive sediments as well as their erodibility and erosion behavior. Additionally, chapter 2 gives insight into facilities to measure cohesive sediment erosion. The *Materials and Methods* used and applied in this thesis are detailed in chapter 3. The main part consists of four scientific papers, which contain the results obtained while working on this thesis. Chapter 4 contains the *Summary of Scientific Papers* and the full papers are included in the chapters: Publication I , publication II, publication III, and publication IV. Finally, the *Conclusions and Recommendations* are given in chapter 5.

2. Fundamentals of Cohesive Sediment Erosion

Fluvial sediments are classified as non-cohesive (cohesionless) and cohesive sediments. The erosion of non-cohesive sediments mainly depends on the submerged weight of individual particles and their initiation of motion is well described by the curve from Shields (1936) and its versions (see Buffington and Montgomery, 1997). In contrast, the erosion of cohesive sediments is insufficiently understood and no generally accepted empirical approach, similar to that of Shields (1936), is available (e.g., Kothyari and Jain, 2008; Van Rijn, 2020). The reason for this non-existance is that surface rather than gravitational forces control the erosion behavior of cohesive sediments due to their high surface area to mass ratio (Morris and Fan, 1998; Craig, 2004). Interparticular forces between individual sediment particles cause them to join together and to form aggregates, which additionally provide friction interlocking and therefore control the resistance against fluid induced shear stress (Kothyari and Jain, 2008). Consequently, the entire erosion process of cohesive sediments is influenced by interactions between a multitude of sediment and fluid properties (Craig, 2004), thus causing a complex and highly variable erosion behavior (see Beckers et al., 2020).

2.1. Classification of cohesive sediments

Cohesive sediments are sediments, whose properties are mainly characterized by fine clay and silt size particles, while non-cohesive sediments are characterized by sand and gravel size particles (Craig, 2004). This means that cohesive sediments contain a sufficient concentration of fines and colloids to impart plastic properties at a specific water content and consequently have the ability to resist shear stress (Morris and Fan, 1998).

Generally, sediments are classified according to a variety of parameters, such as origin, mineralogy, particle size, particle shape, or settling velocity. In practice, one of the most important parameters for the classification of sediments is the particle size diameter and the concept of particle size classes. Therefore, sediment particles are assigned to a particle size class based on their equivalent spherical diameter. Most sedimentologists use the logarithmic Udden–Wentworth grade scale or similar scales, which are characterized by more subgroups and

Table 2.1. Particle size scale according to ISO 14688-1:2017 (2017).

Descriptive terminology		Particle size [mm]
boulder	large boulder	> 630
	boulder	> 200 and ≤ 630
	cobble	> 63 and ≤ 200
gravel	coarse gravel	> 20 and ≤ 63
	medium gravel	> 6.3 and ≤ 20
	fine gravel	> 2.0 and ≤ 6.3
sand	coarse sand	> 0.63 and ≤ 2.0
	medium sand	> 0.2 and ≤ 0.63
	fine sand	> 0.063 and ≤ 0.20
silt	coarse silt	> 0.02 and ≤ 0.063
	medium silt	> 0.0063 and ≤ 0.02
	fine silt	> 0.002 and ≤ 0.0063
clay		≤ 0.002

finer gradation (Blott and Pye, 2001). Table 2.1 shows the scale according to ISO 14688-1:2017 (2017), which is used in this thesis.

A division into cohesive and non-cohesive material is often made based on the threshold for the silt fraction at d=63 μm (e.g., Mitchener and Torfs, 1995; Van Ledden, 2003; Kurtenbach et al., 2010; Van Rijn, 2020). While sediments with d>63 μm can be regarded as non-cohesive, sediments with d<63 μm are cohesive when containing a certain clay content because it is the concentration of the clay minerals which is responsible for cohesion (Raudkivi, 1982). For example, coarse silt shows little to no cohesive behavior (Wu, 2008; Wu et al., 2018) and although the finest rock flour particles may be of clay size, they are not clay minerals and therefore do not possess cohesion (see Craig, 2004).

Some studies suggest a threshold between cohesive and non-cohesive behavior in the range between d=16-40 μm (see Ackers and White, 1973; Stevens, 1991). This range was confirmed by Mehta and Lee (1994), who refer to the Stokes' law and settling velocity data. The authors point to d=20 μm as a reliable size indicator for cohesion since the settling velocity increases significantly for smaller sized particles. In any case, cohesive behavior is correlated with a decrease in particle size (e.g., Grabowski et al., 2011). Nonetheless, an exact classification of sediments by only their particle size into cohesive and non-cohesive material is not sufficient and should be supplemented by further mineralogical classification (see Raudkivi and Tan, 1984).

2.2. Erodibility of cohesive sediments and influencing parameters

Most natural cohesive sediments consist of a graded mixture and are composed of particles from more than one particle size range (Table 2.1). The composition of the sediments and the relative proportions of different sized particles yields a variable bed shear strength, which substantially affects sediment erodibility. Moreover, natural sediments contain not only mineralogical (inorganic) components but also organic matter and are exposed to biological activity as well as ecological changes. This makes them a complex mixture, whose properties are difficult to characterize since various physical, chemical, and biological factors affect their structure and consequently their erodibility. As a result, natural cohesive sediments are often referred to as mud indicating a mixture dominated by mainly clay and silt-sized particles.

Berlamont et al. (1993) studied the erosion and transport behavior of cohesive coastal and estuarine sediments and identified 28 parameters to characterize the sediment properties. The authors grouped the parameters into physico-chemical properties of the overflowing fluid, physico-chemical properties of the sediment, characteristics of bed structure, and water-bed exchange processes. The authors emphasize that some parameters are interdependent and that it is a tentative list. Nevertheless the number of parameters shows how complex the erosion and transport mechanisms of cohesive sediments are and how difficult it is to characterize all involved factors. It is worth noting that the authors did not include biological parameters to describe the sediment properties although biological effects on cohesive sediment stability are widely accepted (e.g., Thom et al., 2015; Gerbersdorf et al., 2007).

Witt (2004) studied cohesive sediment erosion and divided the influencing parameters into those related to flow induced shear stresses and those related to resistive forces of the sediment (expressed as erosion stability). The latter was grouped into physical, geochemical, and biological parameters and a table was compiled, which is based on an evaluation of the information available in literature. The author concluded that the erosion stability of cohesive sediments is not a function of a single parameter, but is always a combinatory function of multiple physical, chemical, and biological processes.

Grabowski et al. (2011) reviewed the importance of sediment properties on the erodibility of cohesive sediments. The authors explicitly limited their review to sediment properties that dictate the resistive forces against the flow and identified several key physical, geochemical, and biological parameters and properties. Grabowski et al. (2011) emphasize that the described sediment properties are dynamically linked. Thus, the net erodibility of cohesive sediments depends on the interactions between these properties and changes in their features may generate significant spatial and temporal variations.

Table 2.2 compiles the parameters with an influence on the erodibility of cohesive sediments based on the studies from Berlamont et al. (1993), Witt (2004), and Grabowski et al. (2011). It

Table 2.2. Compilation of literature data on physical, chemical, and biological parameters influencing the erodibility of cohesive sediments. *Please note that the terminology was not changed and corresponds to the wording of the references.*

	Grabowski et al. (2011)	**Witt (2004)**	**Berlamont et al. (1993)**
physical	particle size distribution	particle size distribution	particle size distribution and sand content
	bulk density	bulk density	bulk density
	water content		
	temperature	temperature	temperature
		gas content	gas content
			specific surface area
chemical	clay mineralogy	mineralogy	mineralogical composition
		clay type and clay content	
	total salinity	total salinity	
	organic content	organic content	organic content
	relative cation concentrations		
		cation exchange capacity	cation exchange capacity
			Na-, K-, Mg-, Ca-, Fe-, Al-Ions
	pH	pH	pH
	metal concentrations		
		pore water composition	
			chlorinity
			oxygen content
			redox potential
biological	bioturbation	bioturbation	
	feeding and egestion by organisms		
	biogenic and extracellular polymeric substances	extracellular polymeric substances	
		colonization of sediment	

has to be noted that the shown parameters from Berlamont et al. (1993) are restricted to the physico-chemical properties of the sediment. Table 2.2 does not claim to include all potential parameters but provides an overview of important parameters influencing the erodibility of cohesive sediments.

2.3. Important parameters influencing cohesive sediment erosion

In this thesis, important sediment parameters are analyzed to characterize the investigated reservoir deposits and to correlate them with the experimentally investigated erodibility (see Beckers et al., 2018b, 2020, 2021). These parameters and their influence on the erodibility are briefly presented below.

Physico-chemical parameters

Particle size distribution and sediment composition The particle size distribution provides the means to distinguish between different sediment size fractions (Table 2.1) in order to derive the sediment composition of a graded mixture. This allows natural cohesive sediment mixtures to be characterized by their clay, silt, and sand content. Furthermore, standard statistical parameters from the sediment distribution can be evaluated, such as the mean (d_m) and median (d_{50}) particle size diameter.

In general, the mean and median particle size is one of the most important and widely used indicator for cohesive sediment erosion (Grabowski et al., 2011). For example, a negative correlation between the critical shear stress and the median diameter was found during field experiments on natural marine mud by Thomsen and Gust (2000). Briaud et al. (2017) also found a negative correlation between critical shear stresses and median diameters for a variety of cohesive sediment mixtures. The authors explain existing scatter in their data (see Fig. 1 in publication IV) with the fact that other forces besides gravity influence the erosion threshold of cohesive sediments. They suggest to define an upper and lower limit based on the median diameter in order to envelop the critical shear stress data for a first-order estimate of cohesive sediment erodibility.

The influence of the clay content on the erodibility has been intensively studied and various authors found a positive correlation between an increase in clay content and sediment stability expressed as critical shear stress (e.g., Kamphuis and Hall, 1983; Panagiotopoulos et al., 1997; Debnath et al., 2007; Schäfer Rodrigues Silva et al., 2018; Perkey et al., 2020). Similar studies were conducted using mud (natural mixtures of clay and silt) and positive correlations between the mud content and the sediment stability were found as well (e.g., Mitchener and Torfs, 1995; Van Rijn, 2020). However, studies also exist that report no correlation between clay, silt, and the critical shear stress (e.g., Kimiaghalam et al., 2016).

Gerbersdorf et al. (2007) studied the erosion behavior of riverine sediments over depth. The authors found a positive correlation between the silt content and a negative correlation between the sand content and the critical shear stress. This seems reasonable as layers of sand may form

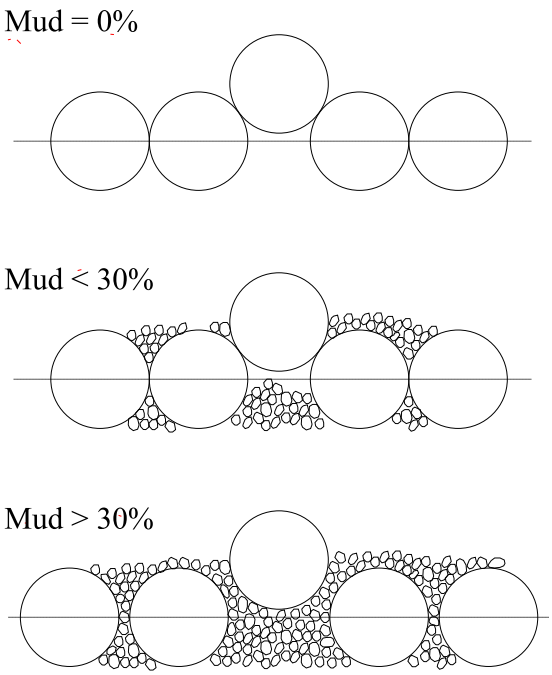

Figure 2.1. Conceptual model on the influence of mud on fine sandy sediments by Panagiotopoulos et al. (1997) (modified after Debnath and Chaudhuri (2010)).

with lower erosion thresholds than consolidated muds due to changing flow and depositional events in natural environments (Grabowski et al., 2011).

It is significant that even relatively small proportions of clay or mud (clay and silt) have a strong influence on the erosion behavior of a non-cohesive/cohesive sediment mixture. The effect of an increasing mud content (and thus clay content) on the erodibility can be visualized using the conceptual model of Panagiotopoulos et al. (1997) for mud/sand mixtures, which is based on the considerations by Wiberg and Smith (1987). The model is shown in Figure 2.1.

When mud is added to a sediment mixture initially consisting of only sand, the mud begins to surround the sand particles. At low mud contents (<30%), the sand particles are still in contact with each other but the voids are already filled with the mud particles. At increasing mud contents (>30%), the mud starts to fully surround the sand particles and also pushes them apart. Consequently, the sand particles are no longer in contact with each other and the resistance against erosion is fully controlled by the mud and the clay fraction. Eventually resulting in the mixture eroding in the same manner as cohesive sediments (Panagiotopoulos et al., 1997).

However, there is disagreement on the transition range between non-cohesive and cohesive behavior. Mitchener and Torfs (1995) found this range to be between 3-15% mud added to sand by weight. Panagiotopoulos et al. (1997) found that the erodibility of mud and sand mixtures are controlled by the mud upon exceedance of 30%, where the mud had a clay content of

11-14%. Debnath et al. (2007) confirmed cohesive erosion behavior for mixtures with a mud content >15%. The research by Spork (1997) provided a similar range for the clay content and reports a strongly influenced erosion behavior of sediment mixtures when exceeding a clay content between 5-10%.

It has also been reported that a maximum critical shear stress is obtained after certain proportions of mud are added to sand. Mitchener and Torfs (1995) found the maximum shear strength when the mud-sand mixture contains 30-50% mud. Perkey et al. (2020) found a similar range and obtained a maximum critical shear stress when the mud content reaches 30-40%.

The main differences of these studies arise from different types of mud and clay and the imprecise information on the clay minerals in the mud, which explains the discrepancies between the results.

Bulk density The bulk density is a sum parameter and depends on the particle size distribution, sediment composition, particle density, water content, organic content, and gas content. Additionally, the bulk density is also directly related to the consolidation of a sediment mixture. Consolidation describes a compaction process of sediment deposits due to gravity and water pressure by the effect of dewatering over time (Wu, 2008). Consequently, the bulk density often varies over depth in natural cohesive sediments (Gerbersdorf and Wieprecht, 2015; Beckers et al., 2018b).

The effect of the bulk density on cohesive sediment erosion has been intensively studied, is well supported in literature (Grabowski et al., 2011), and is one of the most frequently used parameters to model critical shear stresses (Zhu et al., 2008).

For artificial sediment mixtures a negative correlation between the bulk density and the erodibility is generally reported (e.g., Mitchener and Torfs, 1995; Jepsen et al., 1997; Lick and McNeil, 2001). However, for natural cohesive sediments no clear relationship was found (e.g., Mitchener and Torfs, 1995; McNeil et al., 1996; Panagiotopoulos et al., 1997; Gerbersdorf et al., 2007). This is also supported by the findings of Schäfer Rodrigues Silva et al. (2018), who investigated the erodibility of natural cohesive sediments from two rivers (Rhine and Saale). While the erosion data (moment of critical erosion) from the Rhine river correlated with the bulk density, the erosion data from the Saale river did not. This can be explained by the presence of sand in naturally composed sediments as it has been the case in upper layers of the Saale sediments. Sand typically has a greater density than mud but often a lower critical shear stress (e.g., Gerbersdorf et al., 2007). In turn, this means that the bulk density does not reflect the cohesive strength of a mixture and does not necessarily correlate with the erodibility.

Total organic carbon The total organic carbon content describes the quantity of organic matter per sediment mass. It contains all forms of organic matter and does not differentiate

between specific types of material (such as dead or alive organic compounds). The organic content has long been recognized to affect the erodibility of cohesive sediments , which is supported by field and laboratory investigations (Grabowski et al., 2011). However, no clear effect on the erosion stability is reported by the literature.

In general, it is assumed that organic material affects the interparticular forces between clay particles (Grabowski et al., 2011). Colloidal organic mass is negatively charged and thus small amounts of organic matter can considerably increase sediment stability by introducing additional bonds between mineral particles (Parchure, 1984; Van Leussen, 1988). On the contrary, Mehta (1991) reported of a decrease in stability with increasing organic content by a change in the sediment matrix and structure due to a lower number of interparticular bonds (see Schweim, 2005). For remolded sediments, Lick and McNeil (2001) found that the removal of natural organic material changes the initial bulk density, the consolidation process, and subsequently affects the erosion rates.

Primarily, experimental investigations support the stabilizing effect of natural cohesive sediments by the presence of organic material. Parchure and Davis (2005) analyzed mud samples with an organic content in the range of 1-75%. The authors showed that an increase in organic matter decreases the erodibility significantly, particularly for organic contents exceeding 10%. Righetti and Lucarelli (2007) found that the erosion stability of limnic cohesive sediments depends strongly on the organic content (5-fold increase of stability between 8-25% organic content). Furthermore, the authors point to a maximum stabilizing effect, which was reached at an organic matter content between 12–14%. A positive correlation between the organic content and critical shear stresses of cohesive sediments are also reported for riverine sediments (e.g., Aberle et al., 2004; Gerbersdorf et al., 2007). Aberle et al. (2004) observed the stabilizing effect results from fibrous organic material, such as decomposing leaves and root systems, which has immense resistance to erosion and shelters underlying sediment.

Cation exchange capacity The cation exchange capacity is a measure for the capacity of clay minerals to retain cations and thus a proxy for the electrochemical properties of a soil or sediment. Cation exchange capacity is expressed as units of exchangeable cations per volume or mass and tend to be highest in soils with high clay and organic contents (Ellis and Mellor, 1995). In soil sciences, the cation exchange capacity is used as an indicator for quality and productivity of soils (for details see Ellis and Mellor (1995) or Pye (1994)). A high cation exchange capacity is indicative of an electrochemically active clay with a high charge density (Grabowski et al., 2011) and thus influences its cohesiveness.

Although relatively few studies measure the cation exchange capacity, it has been found to correlate well with the erodibility of cohesive sediments (e.g., Gerbersdorf et al., 2007). For example, Gerbersdorf et al. (2007) concluded from their erosion data of riverine sediments that

interparticular forces had the largest influence on stability and specifically included the cation exchange capacity in their considerations (next to the particle size classes, total organic carbon content, and polymeric substances such as proteins and carbohydrates). Furthermore, Kimiaghalam et al. (2016) found a general trend of increasing shear strength along with an increasing cation exchange capacity for natural soil samples from different river banks in Manitoba, Canada.

Biological parameters

All natural sediments are inhabited by organisms and therefore show evidence of biological activity (Paterson and Black, 1999; Grabowski et al., 2011). This alters the erosion behavior of the sediments and both stabilizing and destabilizing effects can be a consequence. Although biostabilization (and destabilization) is an important factor influencing the erodibility (e.g., Paterson and Black, 1999; Gerbersdorf and Wieprecht, 2015; Thom et al., 2015), it is a complex phenomenon itself and it remains a challenge to distinguish the biologically induced binding forces from the interparticular cohesive forces (Gerbersdorf and Wieprecht, 2015).

At this point, it is neither intended to review this topic nor to detail the processes responsible for the biostabilization of cohesive sediments. Instead, the biological parameters analyzed to address biostabilization in the investigated reservoir sediments are briefly introduced and their influence on the erodibility is described. For further details on biostabilization of cohesive sediments, the reviews from Grabowski et al. (2011) and Gerbersdorf and Wieprecht (2015) are recommended.

Extracellular polymeric substances Extracellular polymeric substances are secreted by microphytobenthos, such as diatoms or cyanobacteria, and heterotrophic bacteria, which allow them to aggregate and form biofilms (e.g., Thom et al., 2015). These biofilms continue to secret extracellular polymeric substances and produce a mucilaginous matrix (de Brouwer et al., 2000; Gerbersdorf et al., 2007; de Deckere et al., 2001; Gerbersdorf et al., 2020), which literally glues mineral particles together (Gerbersdorf and Wieprecht, 2015). As a result, biofilms act as protective layer (Paterson, 1997) and stabilize sediments, resulting in a higher erosion threshold (e.g., Gerbersdorf and Wieprecht, 2015; Gerbersdorf et al., 2020).

Recent studies suggest the secreted extracellular polymeric substances of the biofilm are primarily responsible for sediment stabilization. Since extracellular polymeric substances are secreted by almost all microorganisms, including chemotrophic microorganisms (Costerton et al., 1987; Decho and Moriarty, 1990), it is likely that not only biofilms at the sediment surface but also deeper, microbially active, layers experience biostabilization (Westrich et al., 2000).

This is supported by the study of Gerbersdorf et al. (2007), who provide evidence for biological stabilization by extracellular polymeric substances for natural riverine sediments not only at the surface but also over depth (0-35cm). The authors concluded it is not the biomass of the potential producers of extracellular polymeric substances (e.g., algae or bacteria), which are responsible for sediment stability, but their excretion products, in particular carbohydrates and proteins. These findings are supported by results obtained on biofilms from intertidal flats (e.g., Perkins et al., 2001; Smith and Underwood, 2001).

Le Hir et al. (2007) studied the effect of extracellular polymeric substances on the erosion threshold of muddy beds and demonstrated a 5-fold increase in sediment strength due to a protective biofilm of less than 1 mm thickness. However, the authors note that an effect of biostabilization on the erosion rate is debatable since once the protective biofilm is broken and eroded, the underlying sediment is exposed and erodes in the same way as bare sediment.

Chlorophyll-a The chlorophyll-a concentration is a proxy for phototrophic biomass. Therefore, it is a characteristic parameter indicating the microphytobenthos growth on sediments (Westrich et al., 2000). The latter are potential producers of extracellular polymeric substances. Thus, the distribution of chlorophyll-a concentration can be linked directly to the distribution of extracellular polymeric substances under specific conditions (Underwood and Smith, 1998; Paterson and Black, 1999). Consequently, microphytobenthos have a high stabilizing effect on the sediment, which might be even more significant in comparison to other microbial communities (Yallop et al., 2000). Generally, high chlorophyll-a values are related to small particle sizes since these offer large surface areas for settlement (de Brouwer et al., 2002; Meyer-Reil, 2005).

Regarding the erodibility, a significant relationship between the critical shear stress and chlorophyll-a for intertidal muddy sands were found by Defew et al. (2003), provided that the chlorophyll-a exceeds 100 mg m^{-2}. Le Hir et al. (2007) found differences in the range of the critical shear stresses for low chlorophyll-a (little range of erosion thresholds) and when chlorophyll-a exceeds 30 mg m^{-2} (high range of erosion thresholds). It is also shown that these findings are supported by data in literature, e.g., by Defew et al. (2003). However, the authors note that the published correlations between shear strength and chlorophyll-a scatter considerably, allowing for no universal relationship except the general tendency for shear strength to increase with chlorophyll-a concentration.

Gerbersdorf et al. (2007) found for riverine sediments that chlorophyll-a is mostly concentrated at the surface or within the top 2 cm of the sediment. Furthermore, they reported their measured concentrations were similar to those measured by de Brouwer et al. (2003) for high photosynthetic active biofilms on intertidal flats. However, no correlations between chlorophyll-a and the critical shear stresses were found for the studied riverine sediments.

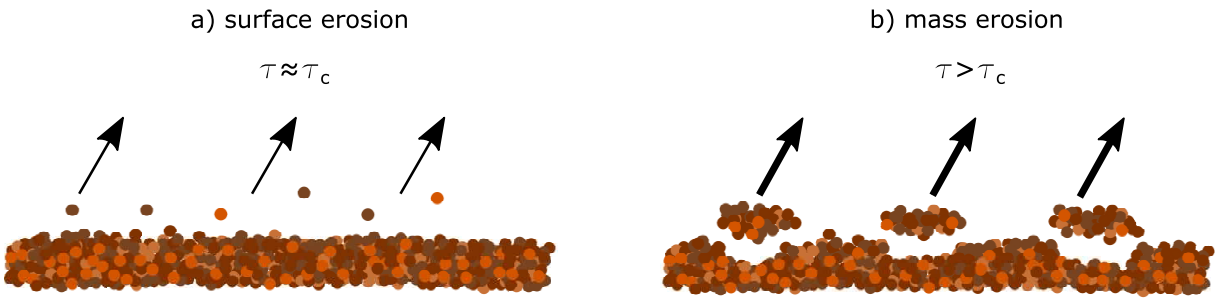

Figure 2.2. Principle modes of cohesive sediment erosion: (a) surface erosion (particle or floc erosion) and (b) mass erosion (erosion of clusters or aggregate chunks) (modified after Mehta (1991); Schweim (2005)).

2.4. Erosion behavior of cohesive sediments

Fluvial erosion is the detachment of sediments by hydrodynamic forces from the bed or deposits but also from banks of a waterbody. It is widely accepted that for sediment motion, the flow induced shear stress impacting on the bed, denoted as τ, must exceed the shear strength (resistive forces or stabilizing forces) of the sediment, denoted as τ_c, to initiate erosion (excess shear stress approach). This threshold indicating the initiation of motion, that is the critical shear stress, is one of the most important parameters in experimental erosion studies (Briaud, 2008). The reason is that for a number of hydraulic engineering and environmental issues it is fundamental to know the conditions when sediments begin to move (Noack, 2012), such as for an efficient reservoir flushing operation (see section 1.2). The erosion rate, which quantifies the amount of sediment being eroded per unit area and unit time, completes the description of cohesive sediment erosion. The erosion rate is denoted as M in case the eroded sediment mass is considered or as ε in case the volumetric change is the quantity of interest. M is related to ε by $M = \varepsilon\rho_b$; where ρ_b is the bulk density.

Two principle modes of cohesive sediment erosion are typically described in literature: surface erosion and mass erosion. Surface erosion is characterized by particle or floc erosion of sediments triggered by the fact that the flow forces locally exceed the shear strength ($\tau \approx \tau_c$). Mass erosion is the response of the sediment bed to a dynamic shear load ($\tau > \tau_c$) (Mehta and Partheniades, 1982) resulting in the erosion of clusters or lumps of aggregates (Zhu et al., 2008) or even in the erosion of layers due to bed failure along planes (Wu et al., 2018). Figure 2.2 illustrates these two erosion modes. A third but special erosion mode is the entrainment of sediments from a layer of stationary suspension (fluid-mud). In case of high sediment concentrations, fluid-mud layers may evolve from dense mobile layers before they consolidate to settled beds (Kirby, 1988). Vice versa, a similar phase of low shear strength can form due to bed fluidization and a destabilization of the water-sediment interface (Mehta, 1986; Wu, 2016). From this phase, sediments are easily re-entrained.

Besides the erosion modes, two main erosion types referred to as *Type I* and *Type II* were identified by Mehta and Partheniades (1982) through an interpretation of time-concentration profiles of resuspension rates. They differ in that under constant shear stress over time, *Type I* erosion asymptotically decreases and approaches a constant value, whereas *Type II* erosion does not and proceeds continuously. The cause of this behavior is due to the vertical stratification of a sediment bed and either uniform or non-uniform bed shear strength over depth.

For comprehension, a *Type I* sediment bed has an increasing shear strength over depth due to, e.g., stratification or consolidation. In case a constant shear stress impacts on the sediment, erosion stops when a layer is reached which has a shear strength equal or larger to the shear stress applied. A *Type II* sediment bed has a uniform shear strength over depth and erosion occurs and continues as long as the shear stress is larger than the shear strength of the bed (see also Sanford and Maa, 2001). This is why these erosion types are also classified as depth-limited or supply-limited erosion (*Type I*) and steady-state or unlimited erosion (*Type II*) (e.g., Parchure and Mehta, 1985; Aberle, 2008; Van Prooijen and Winterwerp, 2010). Since the transition between these erosion types might be smooth and does not allow for a clear distinction (Grabowski et al., 2011), complementary descriptions can be found that combine features of both types (e.g., Amos et al., 1992; Debnath et al., 2007; Aberle, 2008).

In addition, various specific erosion forms are described in literature, which were mainly visually observed in studies on the erosion behavior of cohesive sediments. For example, McNeil et al. (1996) reported that, during erosion, individual particles are entrained before chunks of sediment are plucked from the surface leaving holes or pits behind (compare with Figure 2.2). Righetti and Lucarelli (2007) observed a multistep entrainment phenomenon beginning with a sporadic, discontinuous motion of relatively small aggregates. This is followed by an increasing number of primary particle aggregates coupled with the sporadic entrainment of larger aggregates. Finally, a gradual enhancement of floc entrainment was observed until an abrupt change in the erosive process takes place (described as a sudden increase in quantity and size of the eroded flocs). Kothyari and Jain (2008) describe the erosion of clumps and layers and identify three stages of initiation of motion: pothole, line, and mass erosion.

2.5. Facilities to investigate the erosion behavior of cohesive sediments

Globally, a variety of facilities and devices are in use to investigate the erosion process of cohesive sediments. They are employed to study individual or multiple erosion parameters. These are mainly erosion thresholds and erosion rates while some erosion facilities study transport rates, emerging bed forms, or flocculation and settling properties (see Wu, 2016). In general, the erosion facilities and devices can be separated into laboratory flumes, benthic in-situ flumes,

and miscellaneous devices (such as jet erosion tests (see Charonko and Wynn, 2010) and hole erosion tests (see Wan and Fell, 2004)).

Laboratory and benthic in-situ flumes

Erosion flumes (both laboratory and benthic in-situ flumes) can be grouped into straight flumes and annular flumes (Black and Paterson, 1997; Aberle, 2008). They can be further subdivided into open or closed annular and straight flumes. The advantage of rotating annular flumes is that they are theoretically of infinite length and no pumps influence the hydraulics. However, the rotating of such flumes develops a complex flow profile with transverse effects on a bed. Straight flumes develop a more homogeneous and uniform flow field when sufficiently long to minimize disturbances at the inflow and outflow. For this reason, annular flumes are increasingly used to explore the transport behavior of fine sediments in suspension (e.g., Spork, 1997; Hillebrand, 2008), whereas straight flumes are mainly used for erosion studies. An overview on available laboratory erosion flumes can be found in Mehta and Parchure (2000) and on in-situ flumes in Aberle (2008). Moreover, Wu (2016) provides a list of existing erosion flumes based on a review on transport and erosion experiments conducted with non-cohesive/cohesive sediment mixtures. Another, and the probably most comprehensive summary including a description of the listed devices, can be found in Lee and Mehta (1994) (please note: this summary also contains miscellaneous erosion devices).

An advantage of in-situ devices is that they can be operated over undisturbed beds (Black and Paterson, 1997) where non-disturbing placement is possible. Their disadvantage is that they can only be used to erode surface sediment layers (Noack et al., 2015). However, many engineering and ecological issues require depth-dependent information on the erodibility of sediments, such as the management of reservoir deposits (see sections 1.2 and 1.3). This demand can be met using laboratory flumes capable to measure the depth-dependent erosion behavior of undisturbed sediment samples ex-situ (e.g., McNeil et al., 1996; Kern et al., 1999; Briaud et al., 2001; Roberts et al., 2003). Their design follows a general principle: sediment core samples are locked into an erosion channel from below. The sediment is then slowly raised into the current and the time to erode the protruding sediment is measured to provide a bulk erosion rate (i.e., the bed elevation changes over time).

Some important and frequently employed laboratory flumes that serve this purpose are the SEDFlume (sediment erosion at depth flume (McNeil et al., 1996)), the ASSET flume (Adjustable Shear Stress Erosion and Transport Flume that is a next generation SEDflume (Roberts et al., 2003)), and the EFA flume (Erosion Function Apparatus (Briaud et al., 2001)). In this study, the SETEG erosion flume (Kern et al., 1999) is employed to investigate the depth-dependent erosion potential of cohesive sediments. It is a straight, rectangular, and closed

flow-through flume that is operated under pressurized flow. It resembles the SEDflume but uses different methods to measure the erosion (details provided in section 3.5).

Shear stress determination Most studies investigate the sediment response to changing flow conditions following a flume-specific protocol, which eventually results in a set of erosion rates as a function of flow. Then, the corresponding shear stress to the flow is either calculated using standard methods (Walder, 2016) or taken from a hydraulic calibration curve (e.g., Beckers et al., 2020).

For example, the shear stress of the EFA flume is calculated from the flow rate based on empirical relations and by means of the chart by Moody (1944). This was found to be the most suitable approach after studying the influence of core protrusion on the bed shear stress by measuring the pressure gradients immediately before and after the sediment sample (Briaud et al., 2001; Briaud, 2008).

In case of the SEDflume, the bed shear stress is determined from the flow rate by using a calibrated relation between the mean flow and the bed shear stress. This relation is based on an implicit formula relating the wall shear stress to the mean flow obtained from Prandtl's universal law of friction (see McNeil et al., 1996; Schlichting and Gersten, 2017). Since the hydrodynamics of the ASSET flume are equivalent to those of the SEDflume, the ASSET flume is calibrated in the same way (Roberts et al., 2003). Moreover, a recent study conducted with the SEDflume by Perera et al. (2020) also refers to the calibrated relation between the mean flow and the bed shear stress obtained by McNeil et al. (1996).

For earlier investigations, the bed shear stress in the SETEG-flume was also derived from a relationship, which was based on theoretical considerations and empirical equations (Kern et al., 1999). This previous relationship was replaced by a calibrated relationship between the flow rates and the double-averaged near-bed Reynolds shear stresses obtained from high-resolution LDV measurements (Beckers et al., 2020). Generally, the Reynolds shear stress can be calculated as follows:

$$\tau = -\rho \left\langle \overline{u'v'} \right\rangle \tag{2.1}$$

where τ is the near-bed Reynolds shear stress, ρ is the fluid density, and $\left\langle \overline{u'v'} \right\rangle$ is the double-averaged (time and space) covariance of the longitudinal and vertical velocity fluctuations at a considered flow rate.

The mean velocity and velocity fluctuations can be calculated from the measured instantaneous velocity in longitudinal and vertical direction using Reynolds decomposition. This enables the near-bed turbulent stress to be calculated directly from the velocity measurements and not

from idealized equations. Thus, uncertainties arising from flume construction or from potential errors in flow control are avoided. Furthermore, spatial and temporal variations in the shear stress can be considered (details provided in Beckers et al., 2020).

The approach to relate the flow rate with the near-bed Reynolds shear stress for the hydraulic calibration of erosion flumes is also reported from other studies (e.g., Aberle et al., 2006; Debnath et al., 2007).

Erosion rate measurements As previously mentioned, some flumes operating with sediment core samples raise the sediment into the current and measure the time to erode the protruding sediment. This provides a change in bed elevation over time, that is, the erosion rate (e.g., McNeil et al., 1996; Briaud et al., 2001; Roberts et al., 2003; Jacobs et al., 2011; Kimiaghalam et al., 2016).

Many of the existing erosion flumes, both in-situ or laboratory devices, use optical backscatter sensors to measure suspended sediment concentrations during erosion experiments, which are then used to calculate the resuspension rate (e.g., Mehta and Partheniades, 1982; Amos et al., 1992; Black et al., 2002; Aberle, 2008; Droppo et al., 2015). Although this is widely applied, the resuspension rate can not necessarily be equated with the erosion rate due to the fact that bed load may contribute to cohesive sediment erosion, especially when dealing with non-cohesive/cohesive sediment mixtures (Mitchener and Torfs, 1995; Roberts et al., 2003; Aberle et al., 2004; Debnath et al., 2007; Wu, 2016). Some studies exist, which have aimed at addressing this point by complementary measurement equipment, such as bed load traps (e.g., Roberts et al., 2003; Debnath et al., 2007; Jacobs et al., 2011).

Moreover, measurement techniques exist which monitor changes of the sediment surface. This yields the eroded volume change of sediment over time and results directly in the erosion rate, since the measurements are insensitive to the transport mode after erosion (account for bed load and suspended load). For example, the SETEG flume was equipped with the SED-CIA method (Sediment Erosion Rate Detection by Computerised Image Analyses (Witt, 2004)), which was then replaced by PHOTOSED (PHOTOgrammetric Sediment Erosion Detection (Noack et al., 2018)).

Evaluation of critical erosion thresholds One of the most important parameters in experimental erosion studies is the threshold indicating the initiation of motion (Briaud, 2008). However, due to the complexity of cohesive sediment erosion and the variable erosion behavior (see section 2.4), various definitions exist, often referring to different erosion thresholds. This results in uncertainty in the existing cohesive erosion threshold data and additional complexity for data interpretation (Sanford and Maa, 2001; Debnath and Chaudhuri, 2010).

In general, two concepts for identifying critical erosion conditions can be distinguished: (i) the visual determination or (ii) the analytic evaluation of the recorded erosion data by means of data analysis techniques.

While the visual determination is always subjective, it allows to add information on the erosion behavior (such as particle entrainment or floc erosion). For example, Schäfer Rodrigues Silva et al. (2018) visually determined the initiation of motion for riverine sediments and defined the threshold as the shear stress where the entrainment of particles from the sediment surface occurred. The study by Van Rijn (2020) presents thresholds for critical bed-shear stresses for particle, surface, and mass erosion, which were visually determined from flume experiments.

Analytic concepts based on an evaluation of the recorded erosion data are less subjective but depend on reliable measurement technology for data recording as well as on robust data analysis techniques. Mainly slope criteria are applied to find significant changes during temporal progression of the erosion (e.g., Gularte et al., 1980; Righetti and Lucarelli, 2007; Beckers et al., 2021). Additionally, back-extrapolating of the erosion rate data to the shear stress at zero erosion is conducted (e.g., Partheniades, 1965; Sanford and Halka, 1993). It should be further noted that the analytic concepts are often supplemented by additional visual observations on the erosion behavior.

Generally, the evaluation of critical erosion thresholds is always influenced by external conditions, such as experimental configurations, the test procedure, and experimental protocols. Reviews on the evaluation of critical erosion thresholds can be found in Debnath and Chaudhuri (2010) and Sanford and Maa (2001). Moreover, additional threshold definitions exist and are discussed in Beckers et al. (2021).

3. Materials and Methods

As previous mentioned, the main goal of this thesis is to explore functional relationships between the erosion potential of reservoir deposits and their sediment characteristics. To achieve this goal, individual tasks were conducted to address the specific objectives (presented in section 1.3). This includes the selection of representative study sites (reservoirs), sediment core removal from their deposits, as well as the realization of various measurements and experiments to characterize the sediment deposits and determine their erosion potential. This chapter presents the materials and methods used to meet the requirements of the raised objectives.

First, the reservoirs are briefly introduced, whose deposits were investigated during this thesis. These reservoirs serve different purposes (see Beckers et al., 2018a) and their sediment deposits differ in their characteristics but also in their accessibility (due to their depth). Sediment cores were removed using a Frahm Sediment Sampler, which was adapted to meet the demands of core sampling in reservoirs (Beckers et al., 2018b). The collected sediment cores were investigated in two ways: either the sediments were analyzed in terms of their characteristics over depth (by means of physical, chemical, and biological parameters) or they were used to experimentally investigate their depth-dependent erosion potential by employing an erosion flume coupled with a novel high-resolution measurement technique (see Noack et al., 2018) to reveal the erosion behavior (see Beckers et al., 2021). Relating these results develops functional relationships between the erosion potential and the sediment characteristics of the investigated reservoir deposits (see Beckers et al., 2021). The bulk of experiments conducted enable a generalized assessment of the methods since they were tested for different boundary conditions (sediment from different reservoirs, sediment of different composition, sediment with different erosion behavior, etc.). Moreover, this ensures the transferability of the applied methods.

3.1. Investigated reservoir deposits

Sediment from the deposits of three reservoirs are investigated and the findings are presented in publications I, III, and IV. These are the reservoirs Kleiner Brombachsee, Großer Brombachsee, and Schwarzenbachtalsperre (in the following sorted thematically and not according to their chronological appearance in the publications).

Kleiner Brombachsee This reservoir is located in the Franconian Lake district of Bavaria, Germany (49°08'08.0"N 10°53'15.0"E). It serves as a pre-reservoir for the Großer Brombachsee (see next paragraph) but can be considered as an independent reservoir due to its size (Deutsches Talsperren Komitee e.V., 2013). The reservoir was built from 1975 until 1986, has a water surface of 2.58 km^2 and a total storage volume of 14.72x10^3 m^3 at maximum operation level (411 m.a.s.l.) (Deutsches Talsperren Komitee e.V., 2013).

Großer Brombachsee Also located in Bavaria, Germany, the Großer Brombachsee is the largest reservoir of the Franconian Lake district (49°07'47.6"N 10°55'60.0"E). It was built during 1983 and 1992 for the purpose of low water regulation of the Regnitz-Main catchment but is additionally used for recreation (Daus et al., 2019). At maximum operation level (410.5 m.a.s.l.), the reservoir has a water surface of 8.63 km^2 and a total storage volume of 143.73x10^3 m^3 (Deutsches Talsperren Komitee e.V., 2013).

Schwarzenbachtalsperre Located in the Northern Black Forest of Germany (48°39'25.6"N 8°19'28.9"E), the Schwarzenbachtalsperre was built between 1922 and 1926 and is the upper reservoir in a pump-storage system. At maximum operation level (668.5 m.a.s.l.; minimum operation level 628 m.a.s.l), the Schwarzenbach reservoir has a water surface of 0.66 km^2 and provides a total storage volume of 14.42x10^6 m^3. The reservoir has a maximum length of 2.2 km, maximum width of 600 m, and maximum depth of 47 m (Mouris et al., 2018; Deutsches Talsperren Komitee e.V., 2013). In addition to the pumped water volume, the reservoir is fed by two natural inflows and a transition tunnel.

3.2. Sediment core removal from reservoir deposits

The basic requirement for a detailed investigation of reservoir deposits is the removal of sediment cores. In general, core removal from sediment deposits is a common practice and has been conducted with different coring techniques. Morris and Fan (1998) mainly reported on gravity and piston corers used to determine parameters such as bulk density, grain size distribution, and chemical characteristics of the removed sediment. From different environments, especially marine science, a variety of coring studies are available (see Dück et al., 2019a). For the purpose of geochemical investigations of the sediment often vibra cores, gravity cores, drilling cores, and pressure cores have been used (e.g., Burgay et al., 2020). Although these cores are taken for similar investigations, the requirements for sediment removal from reservoirs for subsequent erosion tests differ significantly. Primarily, reservoir sediment removal requires navigation on a lake and is often associated with great water depths, eliminating the possibility to work with scuba divers. Furthermore, the reliability of core sampling impinges on the sample remaining

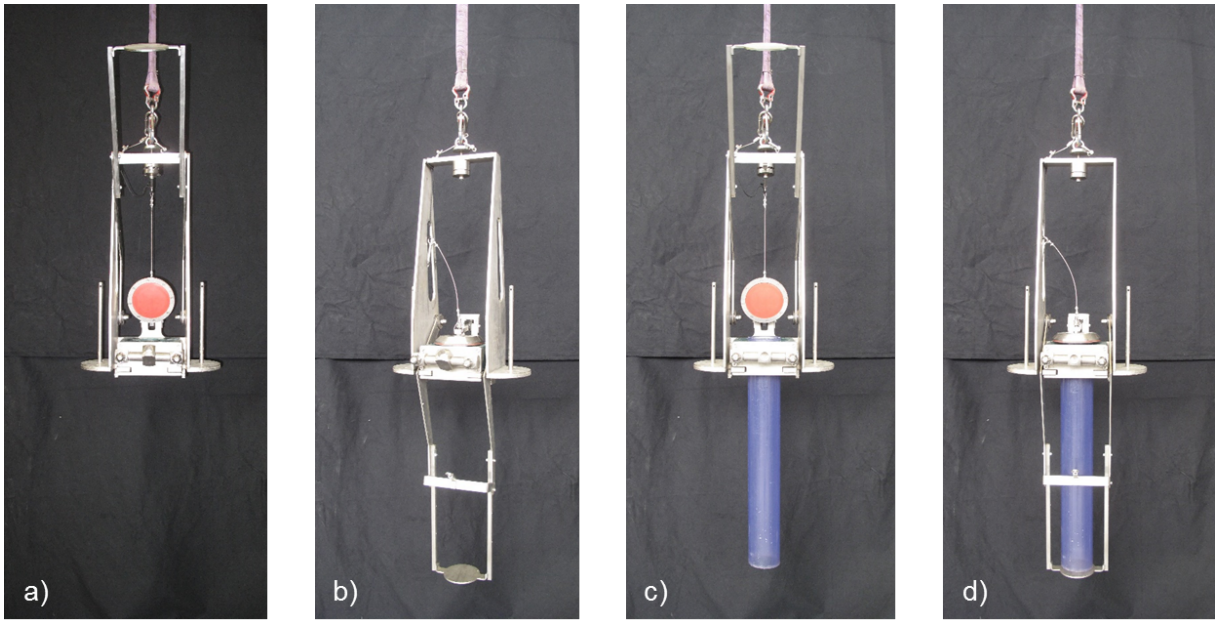

Figure 3.1. Frahm Sediment Sampler (a) with open lid and clasp, (b) closed lid and clasp, (c) with open lid and clasp including PVC-tube, (d) closed lid and clasp including PVC-tube (Beckers et al., 2019).

undisturbed, which creates its own challenges (e.g., Blomqvist, 1985). For instance, McIntyre (1971) reported the necessity to use cores of $\geq$0.1 m diameter in order to overcome sampling problems stemming from the sediment-water interface. Consequently, a sufficiently large core diameter is required to attenuate coring disturbances (see Dück et al., 2019b).

To address these challenges, a Frahm Sediment Sampler was used. This coring device was developed at the Leibniz Institute for Baltic Sea Research and is distributed by the Meerestechnisches Büro Turla GmbH. It was previously used in marine technology to close the gap between piston and gravity cores (Reikowski, 2015) and was adapted to meet the demands of sediment core sampling from reservoir deposits (Beckers et al., 2018b). In comparison to conventional corers, the advantage is that a lid generates a vacuum at the time of sediment withdrawal and a sideways movable clasp seals the sediment core immediately after removal from the bed. Thus, with the Frahm Sediment Sampler relatively undisturbed sediment cores with a diameter of 0.1 m can be extracted from submerged sediment deposits.

Prior to core sampling, PVC-tubes are fixed to the main device with a quick-action connector. Then the lid and the movable clasp are locked in position by a taut rope. Afterwards, the device can be lowered to the reservoir bed. Upon contact with the bed, the mass of the device presses the PVC-tube into the sediment (the total mass can be increased by additional weight). As soon as the rope tension reduces, the lid and the movable clasp release and close the PVC-tube containing the sediment core sample. After core removal, the PVC-tubes are sealed with a plug at the bottom and with a lid on the top. The sediment cores are stored vertically in a dark

Figure 3.2. Platform used to operate the Frahm Sediment Sampler (a) after assembly on land, (b) completely equipped with tripod, electric winch, and Frahm Sediment Sampler (on rack) on the water (Beckers et al., 2019).

cooling chamber to avoid disturbances of the sediment layers and to minimize biochemical processes. The PVC-tubes have an inner diameter of 0.1 m (wall thickness of 0.005 m) and a length of 1 m. This diameter was chosen to minimize effects of wall friction on the sediment cores. Furthermore, the walls of all the PVC-tubes are cut off diagonally at an angle of 5° and the wall is beveled to minimize penetration disturbances.

Figure 3.1 shows the Frahm Sediment Sampler at different operational phases. Figure 3.1 a) and b) show the Frahm Sediment Sampler open and closed without PVC-tube. Correspondingly, Figure 3.1 c) and d) show the Frahm Sediment Sampler open and closed with a transparent PVC-tube used for sediment core removal.

The Frahm Sediment Sampler is operated from a floating platform, which can be navigated by a combustion engine or electric motor depending on the reservoirs local water law requirements. The platform is equipped with a tripod and an electric winch (12 V). The speed of the winch ranges between 20 m min^{-1} and 10 m min^{-1} (without load/with load). The maximum operational depth is currently 100 m. It is worth noting that the device can be operated from alternative constructions as well as with different drive technologies (e.g., boat and hydraulic cranes). Figure 3.2 shows (a) the platform used for sampling on land and (b) the full setup used for sampling floating on a reservoir. For more information see Beckers et al. (2019).

3.3. Experimental preparations and procedure

The bulk density is the only sediment parameter which is measured non-destructively by means of a gamma-ray-densitometer. Thus, it has a decisive role for the further experimental procedure since it is assumed that sediment cores from similar sampling area with similar bulk density profiles also have similar sediment characteristics and erosion behaviors.

For this reason, the depth-dependent bulk density profiles are measured first for all collected sediment cores, usually with a vertical resolution of 1-5 cm. Based on related bulk density profiles, sediment cores are assigned to each other and appointed to further destructive analyses (sediment characterization or erosion experiment).

The sediment cores assigned to each other are then divided into vertical sediment layers. The sediment layers of one core are analyzed in terms of their erosion potential using the SETEG/PHOTOSED-system, which eventually results in a depth-dependent information on the erosion. The sediment from the other core is extracted from the vertical layers (equivalent depths to the eroded core) and is subsequently analyzed in terms of its physico-chemical and biological characteristics. Details can be read in Beckers et al. (2018b, 2019, 2021).

3.4. Analysis of physico-chemical and biological sediment characteristics

The extracted sediment from the vertical layers is analyzed in terms of physico-chemical and biological sediment parameters (see section 2.3) to, first, characterize the sediment deposits and, second, to be correlated with the measured erosion stability (see Beckers et al., 2018b, 2021).

A group of parameters was selected to narrow down the multitude of influencing parameters (see Table 2.2) to those which are most relevant for cohesive sediment erosion. As detailed in section 2.2 and 2.3, this selection is based on current knowledge on parameters influencing the erodibility of cohesive sediments (see Grabowski et al., 2011). Moreover, parameters with high relevance for further applications were selected, such as for numerical modeling of sediment management strategies in reservoirs (e.g., Haun, 2012; Olsen, 1999).

The analyzed sediment parameters are summarized in Table 3.1. A detailed description of these parameters can be found in section 2.3. In this section, the methods for the analysis of the sediment parameters are briefly introduced. In case no standard document is published by the international organization for standardization (ISO), the method for the analysis is described in detail.

Table 3.1. Overview of analyzed physical, chemical, and biological sediment parameters.

physical	bulk density
	particle size distribution and sediment composition
chemical	total organic carbon
	cation exchange capacity
biological	chlorophyll-a
	extracellular polymeric substances (proteins/carbohydrates)

Physico-chemical parameters

Bulk density The vertical bulk density profile of each removed sediment core is measured with a gamma-ray densitometer (see Beckers et al., 2018b). The measurement principle of the gamma-ray attenuation method is based on the Beer-Lambert law, which describes the absorption of gamma radiation by a penetrated medium (for details see Mayar et al. (2019)). This allows to measure the bulk density of the sediment non-destructively within the PVC-tube. The measurement unit consists of a radioactive source of ^{137}CS with a decay energy of 662 keV. The detector unit consists of a scintillator of Sodium Iodide doped with Thalium (NaI(TI)) and a photomultiplier.

Beckers et al. (2019) described the measurement procedure as follows: The sediment core (PVC-tube containing the sediment) is placed between a traverse system that automatically moves down the core to measure the gamma absorption at predefined layers. At the beginning of each measurement, the system is carefully calibrated against the attenuation of the PVC-tube containing, first, the media air and, second, the media water to consider the influence of the tube walls. Measurements are conducted for sediment layers with a defined spacing (usually steps of 1-5 cm). Once a sediment layer is reached, the measurement starts and is conducted for a time of 300 s. Gamma quants are emitted by the source, attenuated by the sediment core, received by the scintillator on the opposite side of the core, converted to photo impulses by the photomultiplier, and finally counted and stored by a computer. The count rate is proportional to the attenuated gamma quants which is used to derive the bulk density of the sediment (see also Mayar et al. (2019)). Figure 3.3 shows a schematic drawing of the gamma-ray densitometer.

Particle size distribution and sediment composition The particle size distribution of the extracted sediment samples (layers) is determined by laser diffraction using a Malvern Mastersizer 2000 (Malvern Instruments, 2007). The instrument enables the measurement of particle sizes in the millimeter, micrometer, and nanometer range (0.02-2,000 μm), allowing the user to

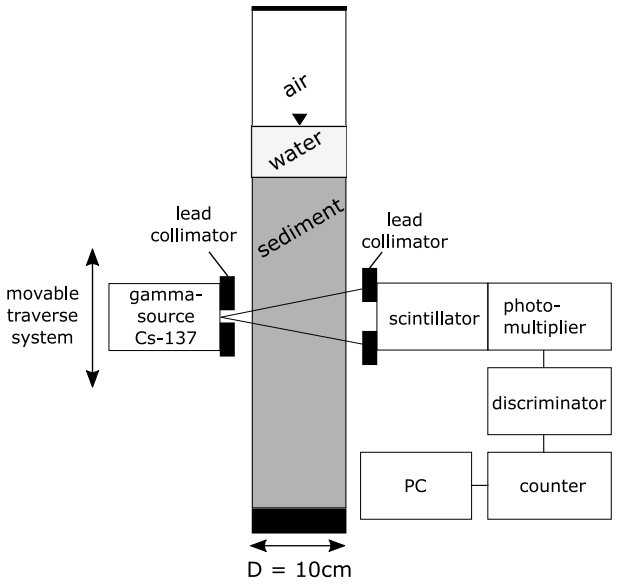

Figure 3.3. Setup for bulk density measurements with gamma-ray densitometer (Beckers et al., 2018b).

analyze a large range of particle sizes of natural cohesive sediments.

From the measured particle sizes, the sediment composition is derived according to ISO 14688-1:2017 (2017) (Table 2.1). In addition, the particle sizes at the 10th-, 50th-, and 90th-percentiles are determined from the measured particle size distribution.

Total organic carbon In the extracted sediment layers, the total organic carbon content is determined by loss on ignition according to the international standard DIN EN 13137 (2001). It is worth mentioning that the total organic carbon contains all forms of organic matter and does not differentiate between dead or alive organic compounds.

Cation exchange capacity For a set of extracted sediment layers, the effective cation exchange capacity is determined by exchange with a hexamminecobalttrichloride solution according to the international standard ISO 23470:2018 (2018). An evaluation of the individual exchanged ions was not conducted.

Biological parameters

Extracellular polymeric substances Extracellular polymeric substances are analyzed by determining the proteins and carbohydrates/sugars fractions in the sediment. The proteins

are determined with the modified Lowry method (Raunkjær et al., 1994) and the carbohydrates/sugars are determined with the method of DuBois et al. (1956). Details on the exact procedure for the analysis of proteins and carbohydrates can be found in Gerbersdorf et al. (2005, 2007).

Chlorophyll-a The Chlorophyll-a concentration in the sediment is determined using a photometric analysis according to DIN 38412-16:1985-12 (1985). Details on the analysis of Chlorophyll-a can be found in Gerbersdorf et al. (2005, 2007).

3.5. Erosion experiments using the SETEG/PHOTOSED-system

The SETEG/PHOTOSED-system is located at the Institute for Modelling Hydraulic and Environmental Systems (IWS, University of Stuttgart). It consists of the SETEG erosion flume (Kern et al., 1999) and the PHOTOSED method (Noack et al., 2018) to measure the depth-dependent erosion potential of cohesive sediments and non-cohesive/cohesive sediment mixtures. The setup of the SETEG/PHOTOSED-system is shown in Figure 3.4.

The technical description of PHOTOSED as well as information on calibration and verification are published in Noack et al. (2018). A detailed description of the SETEG erosion flume, a summary of PHOTOSED, and an introduction to the measurement outputs and variables are presented in Beckers et al. (2020). Furthermore, the following section gives a compilation of this information.

SETEG erosion flume

The SETEG erosion flume is constructed as a straight, rectangular, and closed flume that is operated under pressurized flow. It has a length of 8.00 m, a width of 0.142 m, and a height of 0.10 m (inner dimensions) and allows to investigate flow rates from 1 to 65 $\mathrm{l\,s^{-1}}$. The measuring section consists of a circular opening in the bottom of the flume where sediment cores with diameters between 0.1 and 0.135 m can be locked in position. The center of the measuring section is located 7.64 m downstream of the inflow to ensure a fully developed turbulent flow field (Figure 3.4).

By means of a piston and a lifting spindle (side view of Figure 3.4), the sediment sample can be moved vertically to position various sediment layers at individually selected core depths. When a desired layer is reached, the vertical movement stops and the protruding sediment is cut off with a wire, leaving the sediment layer flush with the bottom (see Beckers et al., 2019).

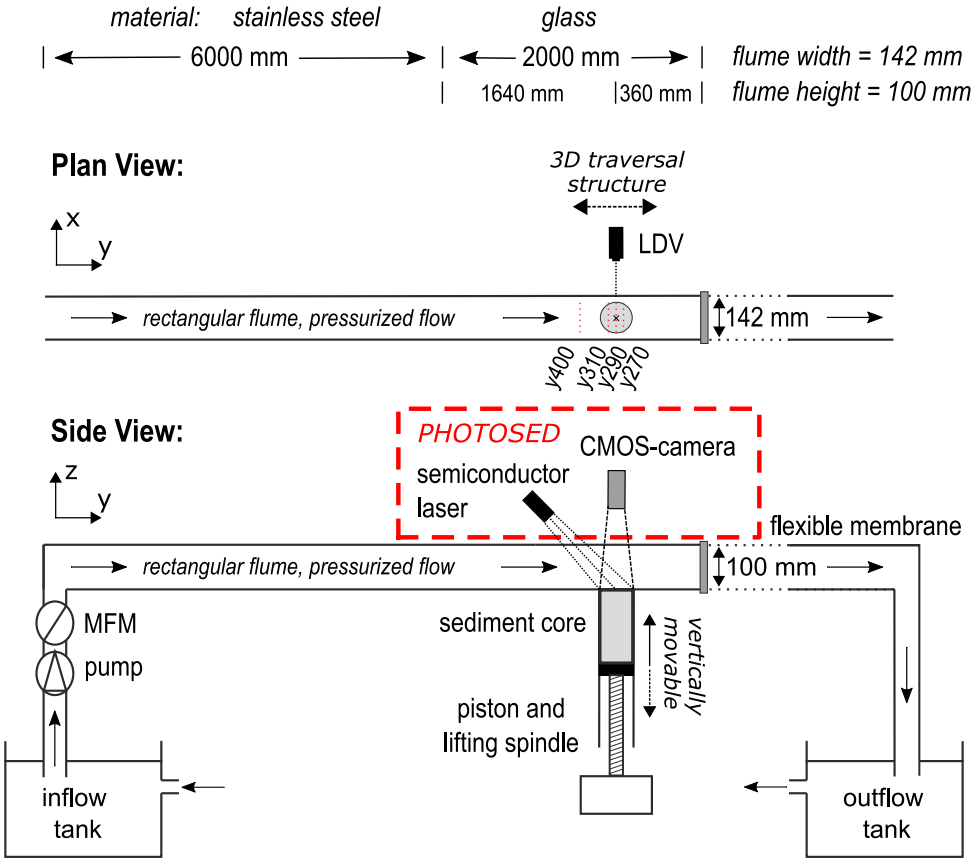

Figure 3.4. Schematic plan and side view of the SETEG/PHOTOSED-system including dimensions. The measurement setup of the 2D LDV used for hydraulic calibration (plan view) and of PHOTOSED for the photogrammetric detection of sediment erosion (side view) are included (modified from Beckers et al. (2019) and Beckers et al. (2020)).

Through this minimally invasive procedure, each experiment begins with a user-set and defined hydraulic condition. Next, the sediment surface is exposed to incrementally increasing flow rates starting below the critical erosion threshold. Each flow is applied for constant time periods, usually for 600 s, to study the temporal erosion behavior until surface failure is observed. This procedure is carried out for various sediment layers to obtain depth-dependent information on the erodibility of the investigated sediment core.

Hydraulic characterization and calibration The SETEG erosion flume is hydraulically calibrated in order to ensure a fully developed turbulent flow field and to obtain a relationship between the flow rate and the near-bed Reynolds shear stress (Q-τ-relation). For this purpose, laser Doppler velocimetry measurements using a 2D LDV were conducted (TSI Inc., Shoreview, MN, USA). The setup of the LDV on the SETEG erosion flume is shown on the plan view of Figure 3.4. The detailed procedure of the measurements is described in Beckers et al. (2020),

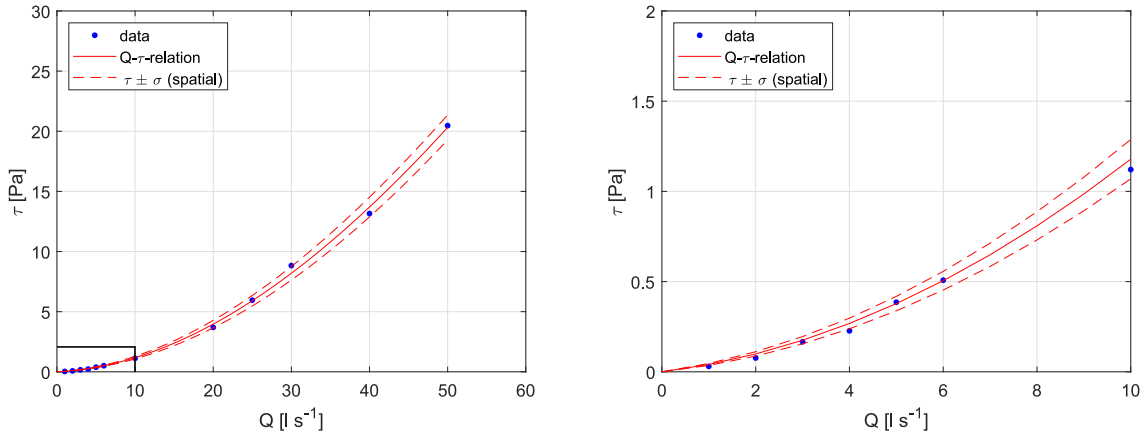

Figure 3.5. Calibration curve (Q-τ-relation) of the SETEG erosion flume for the full range (left) and a zoomed section (right) of flow rates. The solid line represents the near-bed double-averaged Reynolds shear stress while the dashed lines indicate the variation among the spatial standard deviation.

including results on the flow and turbulence development in the form of double-averaged vertical distributions for four longitudinal cross-sections. These cross-sections are visible in the plan view of Figure 3.4 (y400, y310, y290, and y270).

The lowest measured points (2 mm above the flume bottom) at each of the three cross-sections located on the measuring sections (y310, y290, and y270) are used to create the calibration curve (Q-τ-relation). Therefore, the double-averaged near-bed Reynolds shear stress is evaluated from the turbulent fluctuations of the velocity components u' and v' according to equation 2.1. Given the three cross-sections evaluated, the spatial variation of the near-bed Reynolds shear stress can be derived.

The calibration curve is shown in Figure 3.5 including the spatial standard deviation over the measuring section. By means of this Q-τ-relation, the flow rates can be converted to shear stresses.

PHOTOSED

The PHOTOgrammetric Sediment Erosion Detection method (PHOTOSED) is coupled with the SETEG erosion flume. It was developed for erosion measurements for a variety of cohesive and non-cohesive/cohesive sediment mixtures. The setup consists of a semiconductor laser with a diffraction optic and a CMOS camera (2 MP, 10Hz, Imaging Development Systems GmbH, Obersulm, Germany). Figure 3.4 (side view) shows the complete setup of PHOTOSED (red box). During an erosion experiment, the laser projects a structured light pattern (approximately 24,000 light points) on the investigated sediment surface. While erosion proceeds, the sediment

surface and displacement of light points is continuously monitored with the camera. In a post-processing routine, consecutive frames are extracted from the captured time series at given time intervals. Next, PHOTOSED computes the volumetric change between these frames within a user-specified region of interest (ROI) by applying Farnebäck's dense optical flow algorithm (Farnebäck, 2003).

In general, PHOTOSED enables the detection of volumetric changes from approximately 1 mm^3 between two consecutive frames, provided the erosion takes place over an area of 35 pixels (corresponding to approximately 10 mm^2) (Beckers et al., 2020). The system provides the elevation change per pixel j defined as $\Delta z^{(j)}$ where $j = 1, \ldots, n$. Through multiplication with the known metric length dimensions $\Delta x^{(j)}$ and $\Delta y^{(j)}$ of each pixel j in the domain defined by the ROI, the erosion volume per pixel, $\Delta V^{(j)}$, can be calculated. Aggregation of the discrete volumes over all pixels j in the area defined by the ROI results in the spatially averaged erosion volume change ΔV.

By means of additional transformations, further erosion parameters can be derived. Among those are the spatially averaged deepening Δz, the erosion rate ε, the total area of erosion A_e, and the specific deepening Δz_s. Additional details are published in Beckers et al. (2020). Further procedures to evaluate the collected erosion data, such as the detection of critical erosion thresholds by applying a slope criterion, are explained and discussed in Beckers et al. (2021).

As a whole, the SETEG/PHOTOSED-system allows the erosion of cohesive and non-cohesive/cohesive sediment mixtures to be studied with high spatio-temporal resolution in order to address pending challenges in cohesive sediment research.

4. Summary of Scientific Papers

The results obtained during the work on this thesis are published in peer-reviewed articles of scientific conferences (publication I) and journals (publication II, III, and IV). This chapter briefly summarizes these scientific publications. Each summary contains the objectives and the main findings for each study. The published articles are attached at the end of this thesis (publication I, II, III, and IV). Any details can be taken directly from its corresponding article.

All publications deal with the experimental investigation of cohesive sediment erosion. Their content reflects the chronological steps that were undertaken to scientifically explore the points raised in the objectives of this thesis (section 1.3).

4.1. Publication I: Experimental investigation of reservoir sediments

The purpose of this study was to investigate the ability of the coring equipment to remove sediment cores from reservoir deposits. Moreover, the theoretical concept is presented by combining the experimentally measured erosion stability over the sediment depth (using the SETEG/PHOTSED-system) with a set of analyzed sediment characteristics (containing physical, chemical, and biological parameters).

This publication shows that a Frahm Sediment Sampler operated from a floating platform is suitable to successfully remove sediment cores from reservoir deposits (case study: Kleiner Brombachsee). The obtained sediment cores were undisturbed, allowing them to be experimentally eroded in the SETEG/PHOTOSED-system to investigate their depth-dependent erosion potential. Likewise, removed sediment cores were used to analyze the depth-dependent sediment characteristics in distinct layers. Beside physico-chemical parameters (bulk density, particle size distribution, total organic carbon, and cation exchange capacity), biological parameters (extracellular polymeric substances and chlorophyll-a) were also considered to address recent discoveries in cohesive sediment research.

The results obtained by this study confirm the theoretical concept and indicate that it is possible to correlate the explored erosion stability with the analyzed sediment parameters. Specifically, the results emphasize that apart from physico-chemical sediment characteristics, biologi-

cal characteristics should also be considered when it is intended to reveal interactions between sediment parameters and cohesive erosion stability.

4.2. Publication II: PHOTOSED - PHOTOgrammetric Sediment Erosion Detection

In this method paper the developed measurement technique PHOTOSED (PHOTOgrammetric Sediment Erosion Detection) is introduced. The paper elucidates the theoretical background of PHOTOSED and provides information on the calibration and verification of the method.

PHOTOSED was specifically designed to measure the erosion of cohesive sediments and non-cohesive/cohesive sediment mixtures. The method uses a semiconductor laser to project a pseudo-random pattern of light points on a sediment surface and monitors the displacement during erosion with a camera. In a post processing routine, PHOTOSED applies Farnebäck's dense optical flow algorithm (Farnebäck, 2003) and calculates the erosion volumes within a user-specified, rectangular region of interest (ROI).

The outcomes of the intensive calibration and verification experiments show that the PHOTOSED method allows the detection of erosion volumes for several orders of magnitude (lowest investigated volume was 13 mm^3, mean absolute deviation for this volume was $\approx 9.2\%$). This is an essential benefit when investigating the erosion potential of natural non-cohesive/cohesive sediment mixtures, which are known to be highly variable in space, time, and magnitude. Therefore, PHOTOSED provides the means to study the erosion behavior of (natural) cohesive sediments and non-cohesive/cohesive sediment mixtures in detail.

4.3. Publication III: High spatio-temporal resolution measurements of cohesive sediment erosion

This paper combines several aspects of the previously conducted research. First, the SETEG erosion flume is introduced and hydraulically characterized. Second, the measurement variables of PHOTOSED are derived and the advantages and versatility of the method is described. Third, detailed results of three erosion experiments are presented. This includes the evaluation and analysis of the changing erosion behavior and the evaluation of the spatial and temporal variability of cohesive sediment erosion.

The results show that due to the high spatio-temporal resolution of PHOTOSED, it is possible to measure the erosion process of cohesive sediments and non-cohesive/cohesive sediment mixtures dynamically and pixel-based with a vertical resolution in the sub-millimeter range.

This enables to detect and distinguish between two fundamental erosion processes. These fundamental processes being the emergence of individual erosion spots caused by surface erosion and the formation of large holes that were torn open through the detachment of aggregate chunks. Moreover, interrelated processes as a temporal consequence of ongoing erosion can be measured. These are the propagation of the erosion in the longitudinal and lateral direction (which eventually leads to the merging of disconnected erosion areas) and the progression of the erosion in the vertical direction (ongoing deepening).

The results of the spatio-temporal erosion variability reveal that the largest erosion events are confined to only a few time steps during temporal progression. In this event they exceed the time-averaged median of the deepening significantly (between 7 and 16 times the median were measured). Moreover, the largest deepening does not necessarily coincide with the largest erosion area. This can be explained since these relationships are controlled by the fundamental erosion processes and their specific occurring erosion forms (floc/aggregate erosion, detachment of aggregate chunks). As a whole, erosion experiments conducted with the SETEG/PHOTOSED-system provide reliable high-resolution data and the means for a robust assessment of the cohesive erosion behavior including detailed information on specific erosion forms.

4.4. Publication IV: Functional relationships between critical erosion thresholds of fine reservoir sediments and their sedimentological characteristics

This paper ultimately combines the methods and the knowledge gained during the work on this thesis and explores the functional relationships between critical erosion thresholds of fine (cohesive) reservoir sediments and their sedimentological characteristics. For this purpose, an extensive erosion data set was obtained with the SETEG/PHOTOSED-system for two investigated reservoir deposits (Großer Brombachsee and Schwarzenbachtalsperre). The erosion data was evaluated regarding critical erosion thresholds using a pseudo-automatic approach to identify confident erosion threshold values. These threshold values were eventually correlated with a collection of physical, chemical, and biological sediment characteristics using multivariate statistics to unravel functional relationships between these parameters and the erosion stability of the deposits.

It is shown that critical erosion thresholds can be confidently derived from the cumulative erosion volume by means of a slope criterion. Two critical erosion thresholds were considered: First, the shear stress for incipient motion that is indicated by the initial rise of the cumulative volume. Second, the shear stress at a change in the erosion regime (erosion behavior) that is indicated by the maximum change in the slope of the cumulative volume. The identified

shear stress values were correlated with a collection of physical (bulk density, sediment composition, percentiles), chemical (total organic carbon, cation exchange capacity), and biological (chlorophyll-a and extracellular polymeric substances separated into proteins and carbohydrates) sediment characteristics.

The results for the deposits of the Großer Brombachsee reveal strong positive correlations between the critical erosion thresholds and the clay content, and to a less extent with the bulk density. Strong negative correlations are observed between the erosion thresholds and the total organic carbon content. Furthermore, the correlations of the erosion thresholds and the sediment characteristics consistently decrease over sediment depth. The results for the deposits of the Schwarzenbachtalsperre reveal strong negative correlations between the erosion thresholds and the clay content, which can be attributed to a comparatively high sand content. The increased sand content is strongly associated with increasing erosion thresholds in the first 10 cm of the sediment cores, but this relation diminishes in deeper located sediment layers.

5. Conclusions and Recommendations

Reservoir deposits are often characterized by fine sediment accumulations, which tend to be cohesive in their erosion behavior. For a sustainable sediment management in reservoirs, it is essential to have sound knowledge on the characteristics of the deposits and particularly on their depth-dependent erosion stability. However, cohesive sediment erosion is a complex phenomenon which requires detailed experimental research using advanced quantitative methods to unravel functional relationships between cohesive erosion thresholds and sediment characteristics.

Regarding the objectives raised at the beginning of this thesis, which were addressed in detail in publication I, II, III, and IV, the following **conclusions** can be summarized:

- In total 56 undisturbed sediment cores were successfully removed from three reservoirs (depth of sediment removal: 5-40 m) by the use of the Frahm Sediment Sampler in order to be used for further experimental investigations (*publication I, III, and IV*).
- The theoretical concept of relating the experimentally investigated erosion stability to a collection of quantified sediment characteristics was successfully verified (*publication I*).
- The developed PHOTOSED method was successfully calibrated and verified. It is capable to detect erosion volumes for several orders of magnitude with a minimum detection limit of $\sim$15 mm^3. This enables high-resolution erosion measurements in order to investigate in detail the erosion behavior of cohesive sediments and non-cohesive/cohesive sediment mixtures (*publication II*).
- Given the spatio-temporal resolution of PHOTOSED, it is possible to detect and distinguish between two fundamental processes of cohesive sediment erosion: (i) the emergence of individual erosion spots caused by surface erosion and (ii) the formation of large holes that were torn open by detached aggregate chunks. Additionally, interrelated processes as a consequence of ongoing erosion were detected: (iii) the propagation of the erosion in the longitudinal and lateral direction, which eventually led to the merging of disconnected erosion areas, and (iv) the progression of the erosion in the vertical direction (ongoing deepening) (*publication III*).
- The spatio-temporal erosion variability reveals that the largest erosion events are confined to only a few time steps during temporal progression. In this event, they exceeded

the time-averaged median of the deepening significantly (factors between 7 and 16 were measured) (*publication III*).

- Critical erosion thresholds were evaluated from the time-series of the cumulative erosion volume by means of a slope criterion. This procedure enables to reliably identify the initial rise of the recorded volume (indicates incipient motion) and the maximum change in slope (indicative of a change in erosion behavior). As a whole, the applied criterion allows a robust assessment of the data and yields confident critical erosion thresholds to assess the erosion stability for distinct layers over the sediment core depth (*publication IV*).
- The extensively explored functional relationships between the critical erosion thresholds and the sedimentological characteristics reveal (i) strong positive correlations with the clay content and the bulk density and a strong negative correlation with the organic matter content for the deposits of the Großer Brombachsee. At the same time, (ii) a strong positive relation between the erosion stability and the sand content and a negative correlation with the clay content is found for the deposits of the Schwarzenbachtalsperre (*publication IV*).

In addition to the conclusions, the following **recommendations** can be summarized:

Although an extensive collection of sediment parameters was analyzed in this work, it does not provide a fully comprehensive parameter description of the sediment characteristics. For example, the sediment deposits of the Schwarzenbachtalsperre suggest that the gas content can be an important parameter, which should be quantified and used to evaluate the erosion stability in future studies. Other parameters can be found in the literature that may also indicate functional relationships with the erosion stability (e.g., mineralogy).

In addition to unraveling parameter-specific functional relations, it seems advisable to pursue combinatorial approaches. Because of the mutual interdependencies of individual sediment parameters, such approaches may provide additional opportunities to better understand the complex relationships involved in the process of fine sediment erosion.

In particular, the results from the Schwarzenbachtalsperre indicate the complexity in identifying unambiguous, functional relationships between the erosion stability and sedimentological characteristics of fine reservoir sediments. This complexity should be addressed by extending the data pool to perform more advanced statistical analyses (complemented for example by further depth-sequencing of the data). The methods and routines developed by this work are verified, robust, and ready to use, ensuring that the data pool can be readily expanded with additional experimental data in future.

A key point for future fundamental erosion research is taking into account the effect of dynamic roughness changes induced by ongoing erosion and of turbulence-induced shear stress

fluctuations. The versatility of the SETEG/PHOTOSED-system, especially the high spatio-temporal resolution of PHOTOSED, allows to evaluate geometric roughness changes of the sediment surface from the dynamically measured erosion data. In combination with advanced hydraulic measurements, this enables to study flow–sediment-interactions at the water-sediment-interface, for example, by correlating turbulence intensities with erosion and roughness distribution functions.

To increase the knowledge on sustainable sediment management in reservoirs, it is advisable to investigate sediments of additional deposits with diverse characteristics using the introduced approaches and the generated knowledge. This includes, but is not limited to, sediment core collection with greater spatial variability to evaluate local differences in the sediment deposits. Eventually, the amount of experimentally investigated erosion data can be used as input data for numerical models. These models, in turn, can be used to evaluate the effectiveness of different scenarios allowing for an assessment of sediment management strategies in reservoirs.

References

Aberle, J. (2008). *Measurement techniques for the estimation of cohesive sediment erosion*, Hydraulic Methods for Catastrophes: Floods, Droughts, Environmental Disasters, Publications of the Institute of Geophysics, Polish Academy of Sciences.

Aberle, J., Nikora, V. and Walters, R. (2004). Effects of bed material properties on cohesive sediment erosion, *Marine Geology* **207**(1-4): 83–93.

Aberle, J., Nikora, V. and Walters, R. (2006). Data Interpretation for In Situ Measurements of Cohesive Sediment Erosion, *Journal of Hydraulic Engineering* **132**(6): 581–588.

Ackers, P. and White, W. R. (1973). Sediment Transport: New Approach and Analysis, *Journal of the Hydraulics Division* **99(HY11)**(11): 2041–2060.

Amos, C. L., Daborn, G., Christian, H., Atkinson, A. and Robertson, A. (1992). In situ erosion measurements on fine-grained sediments from the Bay of Fundy, *Marine Geology* **108**(2): 175–196.

Annandale, G. W., Randle, T. J., Langendoen, E. J., Hotchkiss, R. H. and The United States national reservoir sedimentation and sustainability team (NRSST) (2018). Reservoir sedimentation management: a sustainable development challenge, *Hydrolink* **3**: 72 – 75.

Basson, G. R. (2009). Management of siltation in existing and new reservoirs. General Report Q. 89, *Proc. of the 23rd Congress of the Int. Commission on Large Dams CIGB-ICOLD (vol. 2)*.

Beckers, F., Biserov, R. and Wieprecht, S. (2019). Experimental Investigation of Sediment Stability at Reservoirs on the Rhône River, *Technical Report 09/2019*, Institute for Modelling Hydraulic and Environmental Systems (IWS), Stuttgart, Germany.

Beckers, F., Haun, S., Gerbersdorf, S. U., Noack, M., Dietrich, D. R., Martin-Creuzburg, D., Peeters, F., Hofmann, H., Glaser, R. and Wieprecht, S. (2018a). CHARM - CHAllenges of Reservoir Management - Meeting Environmental and Social Requirements, *Hydrolink* **3**: 80 – 82.

Beckers, F., Haun, S. and Noack, M. (2018b). Experimental investigation of reservoir sediments, *E3S Web of Conferences* **40**: 03030.

Beckers, F., Inskeep, C., Haun, S., Schmid, G., Wieprecht, S. and Noack, M. (2020). High spatio-temporal resolution measurements of cohesive sediment erosion, *Earth Surface Processes and Landforms* **45**(11): 2432–2449.

Beckers, F., Koca, K., Haun, S., Noack, M., Gerbersdorf, S. U. and Wieprecht, S. (2021). Functional relationships between critical erosion thresholds of fine reservoir sediments and their sedimentological characteristics, *submitted to the Journal of Hydraulic Engineering. Preprint available in chapter: publication IV* .

Berlamont, J., Ockenden, M., Toorman, E. and Winterwerp, J. (1993). The characterisation of cohesive sediment properties, *Coastal Engineering* **21**: 105 – 128.

Black, K. S. and Paterson, D. M. (1997). Measurement of the erosion potential of cohesive marine sediments: A review of current in situ technology, *Journal of Marine Environmental Engineering* **4**: 43–83.

Black, K. S., Tolhurst, T. J., Paterson, D. M. and Hagerthey, S. E. (2002). Working with natural cohesive sediments, *Journal of Hydraulic Engineering* **128**(1): 2–8.

Blomqvist, S. (1985). Reliability of core sampling of soft bottom sediment - an in situ study, *Sedimentology* **32**(4): 605–612.

Blott, S. J. and Pye, K. (2001). GRADISTAT: a grain size distribution and statistics package for the analysis of unconsolidated sediments, *Earth Surface Processes and Landforms* **26**(11): 1237–1248.

Brandt, S. A. (1999). *Reservoir desiltation by means of hydraulic flushing: sedimentlogical and geomorphological effects in reservoirs and downstream reaches as illustrated by the Cachi Reservoir and the Reventazon River, Costa Rica*, Copenhagen. OCLC: 637131590.

Brandt, S. A. (2000). A review of reservoir desiltation, *International Journal of Sediment Research* **15**(3).

Briaud, J.-L. (2008). Case Histories in Soil and Rock Erosion: Woodrow Wilson Bridge, Brazos River Meander, Normandy Cliffs, and New Orleans Levees, *Journal of Geotechnical and Geoenvironmental Engineering* **134**(10): 1425–1447.

Briaud, J.-L., Govindasamy, A. V. and Shafii, I. (2017). Erosion Charts for Selected Geomaterials, *Journal of Geotechnical and Geoenvironmental Engineering* **143**(10): 04017072.

Briaud, J.-L., Ting, F. C. K., Chen, H. C., Cao, Y., Han, S. W. and Kwak, K. W. (2001). Erosion Function Apparatus for Scour Rate Predictions, *Journal of Geotechnical and Geoenvironmental Engineering* **127**(2): 105–113.

Buffington, J. M. and Montgomery, D. R. (1997). A systematic analysis of eight decades of incipient motion studies, with special reference to gravel-bedded rivers, *Water Resources Research* **33**(8): 1993–2029.

Burgay, F., Abollino, O., Buoso, S., Costa, E., Giacomino, A., La Gioia, C., Garofalo, S. F., Pecoraro, G. and Malandrino, M. (2020). Geochemical characterization of a marine sediment core from the Joides Basin, Ross Sea, Antarctica, *Marine Geology* **428**: 106286.

Charonko, C. and Wynn, T. (2010). Evaluation of an in situ measurement technique for streambank critical shear stress and soil erodibility, Las Vegas, NV, p. 10.

Costerton, J. W., Cheng, K. J., Geesey, G. G., Ladd, T. I., Nickel, J. C., Dasgupta, M. and Marrie, T. J. (1987). Bacterial Biofilms in Nature and Disease, *Annual Review of Microbiology* **41**(1): 435–464.

Craig, R. F. (2004). *Craig's soil mechanics*, 7th edn, Spon Press, London and New York.

Daus, M., Koberger, K., Gnutzmann, N., Hertrich, T. and Glaser, R. (2019). Transferring Water While Transforming Landscape: New Societal Implications, Perceptions and Challenges of Management in the Reservoir System Franconian Lake District, *Water* **11**(12): 2469.

de Brouwer, J. F. C., Bjelic, S., de Deckere, E. M. G. T. and Stal, L. J. (2000). Interplay between biology and sedimentology in a mudflat (Biezelingse Ham, Westerschelde, The Netherlands), *Continental Shelf Research* **20**(10-11): 1159–1177.

de Brouwer, J. F. C., de Deckere, E. M. G. T. and Stal, L. J. (2003). Distribution of extracellular carbohydrates in three intertidal mudflats in Western Europe, *Estuarine, Coastal and Shelf Science* **56**(2): 313–324.

de Brouwer, J., Ruddy, G., Jones, T. and Stal, L. J. (2002). Sorption of EPS to sediment particles and the effect on the rheology of sediment slurries, *Biogeochemistry* **61**: 57–71.

de Deckere, E. M. G. T., Tolhurst, T. J. and de Brouwer, J. F. C. (2001). Destabilization of Cohesive Intertidal Sediments by Infauna, *Estuarine, Coastal and Shelf Science* **53**(5): 665–669.

Debnath, K. and Chaudhuri, S. (2010). Cohesive sediment erosion threshold: a review, *ISH Journal of Hydraulic Engineering* **16**(1): 36–56.

Debnath, K., Nikora, V., Aberle, J., Westrich, B. and Muste, M. (2007). Erosion of Cohesive Sediments: Resuspension, Bed Load, and Erosion Patterns from Field Experiments, *Journal of Hydraulic Engineering* **133**(5): 508–520.

Decho, A. W. and Moriarty, D. J. W. (1990). Bacterial exopolymer utilization by a harpacticoid copepod: A methodology and results, *Limnology and Oceanography* **35**(5): 1039–1049.

Defew, E. C., Tolhurst, T. J., Paterson, D. M. and Hagerthey, S. E. (2003). Can the stability of intertidal sediments be predicted from proxy parameters? An in situ investigation, *in* D. Raffaelli, M. Solan, D. Paterson, A. Buck and J. Pomfret (eds), *Estuarine and Coastal Sciences Association*, Vol. 5, pp. 61–77.

Deutsches Talsperren Komitee e.V. (ed.) (2013). *Talsperren in Deutschland [Dams and reservoirs in Germany]*, Springer Fachmedien Wiesbaden, Wiesbaden.

DIN 38412-16:1985-12 (1985). *German standard methods for the examination of water, waste water and sludge; test methods using water organisms (group L); determination of chlorophyll-a in surface water (L 16)*.

DIN EN 13137 (2001). *Characterization of waste - Determination of total organic carbon (TOC) in waste, sludges and sediments*.

Droppo, I. G., D'Andrea, L., Krishnappan, B. G., Jaskot, C., Trapp, B., Basuvaraj, M. and Liss, S. N. (2015). Fine-sediment dynamics: towards an improved understanding of sediment erosion and transport, *Journal of Soils and Sediments* **15**(2): 467–479.

DuBois, M., Gilles, K. A., Hamilton, J. K., Rebers, P. A. and Smith, F. (1956). Colorimetric method for determination of sugars and related substances, *Analytical chemistry* **28**(3): 350–356.

Dück, Y., Liu, L., Lorke, A., Ostrovsky, I., Katsman, R. and Jokiel, C. (2019a). A novel freeze corer for characterization of methane bubbles and assessment of coring disturbances, *Limnology and Oceanography: Methods* **17**: 305–319.

Dück, Y., Lorke, A., Jokiel, C. and Gierse, J. (2019b). Laboratory and field investigations on freeze and gravity core sampling and assessment of coring disturbances with implications on gas bubble characterization, *Limnology and Oceanography: Methods* **17**: 585–606.

Ellis, S. and Mellor, A. (1995). *Soils and environment*, Routledge, London and New York. OCLC: 52751707.

Fan, J. and Morris, G. L. (1992). Reservoir Sedimentation. I: Delta and Density Current Deposits, *Journal of Hydraulic Engineering* **118**(3): 354–369.

Farnebäck, G. (2003). Two-Frame Motion Estimation Based on Polynomial Expansion, *in* G. Goos, J. Hartmanis, J. van Leeuwen, J. Bigun and T. Gustavsson (eds), *Image Analysis*, Vol. 2749, Springer Berlin Heidelberg, Berlin, Heidelberg, pp. 363–370.

Gerbersdorf, S. U., Jancke, T. and Westrich, B. (2005). Physico-chemical and biological sediment properties determining erosion resistance of contaminated riverine sediments – Temporal and vertical pattern at the Lauffen reservoir/River Neckar, Germany, *Limnologica* **35**(3): 132–144.

Gerbersdorf, S. U., Jancke, T. and Westrich, B. (2007). Sediment Properties for Assessing the Erosion Risk of Contaminated Riverine Sites. An approach to evaluate sediment properties and their covariance patterns over depth in relation to erosion resistance. First investigations in natural sediments (11 pp), *Journal of Soils and Sediments* **7**(1): 25–35.

Gerbersdorf, S. U., Koca, K., de Beer, D., Chennu, A., Noss, C., Risse-Buhl, U., Weitere, M., Eiff, O., Wagner, M., Aberle, J., Schweikert, M. and Terheiden, K. (2020). Exploring flow-biofilm-sediment interactions: Assessment of current status and future challenges, *Water Research* **185**: 116182.

Gerbersdorf, S. U. and Wieprecht, S. (2015). Biostabilization of cohesive sediments: revisiting the role of abiotic conditions, physiology and diversity of microbes, polymeric secretion, and biofilm architecture, *Geobiology* **13**(1): 68–97.

Grabowski, R. C., Droppo, I. G. and Wharton, G. (2011). Erodibility of cohesive sediment: The importance of sediment properties, *Earth-Science Reviews* **105**(3-4): 101–120.

Gularte, R. C., Kelly, W. E. and Nacci, V. A. (1980). Erosion of cohesive sediments as a rate process, *Ocean Engineering* **7**(4): 539–551.

Haun, S. (2012). *Three-dimensional numerical modelling of sediment transport during the flushing of hydropower reservoirs*, PhD thesis, Norwegian University of Science and Technology, Trondheim, Norway.

Hillebrand, G. (2008). *Transportverhalten kohäsiver Sedimente in turbulenten Strömungen - Untersuchungen im offenen Kreisgerinne [Transport behavior of cohesive sediments in turbulent currents - investigations in an open annular flume]*, PhD thesis, Universität Karlsruhe, Karlsruhe.

Hinderer, M., Kastowski, M., Kamelger, A., Bartolini, C. and Schlunegger, F. (2013). River loads and modern denudation of the Alps - A review, *Earth-Science Reviews* **118**: 11–44.

ICOLD (2020). ICOLD: World register of dams: General synthesis.

ISO 14688-1:2017 (2017). *Geotechnical investigation and testing – Identification and classification of soil – Part 1: Identification and description (ISO 14688-1:2017)*.

ISO 23470:2018 (2018). *DIN EN ISO 23470, Soil quality – Determination of effective cation exchange capacity (CEC) and exchangeable cations using a hexamminecobalttrichloride solution (ISO 23470:2018)*.

Jacobs, W., Le Hir, P., Van Kesteren, W. and Cann, P. (2011). Erosion threshold of sand–mud mixtures, *Continental Shelf Research* **31**(10): S14–S25.

Jepsen, R., Roberts, J. and Lick, W. (1997). Effects of bulk density on sediment erosion rates, *Air, Soil, and Pollution* **99**: 21–31.

Kamphuis, J. W. and Hall, K. R. (1983). Cohesive Material Erosion by Unidirectional Current, *Journal of Hydraulic Engineering* **109**(1): 49–61.

Kantoush, S. A. and Sumi, T. (2010). River Morphology and Sediment Management Strategies for Sustainable Reservoir in Japan and European Alps, *Annuals of Disaster Prevention Research Institute, Kyoto University* **No. 53B**: 19.

Karamigolbaghi, M., Ghaneeizad, S. M., Atkinson, J. F., Bennett, S. J. and Wells, R. R. (2017). Critical assessment of jet erosion test methodologies for cohesive soil and sediment, *Geomorphology* **295**: 529–536.

Kern, U., Haag, I., Schürlein, V., Holzwarth, M. and Westrich, B. (1999). Ein Strömungskanal zur Ermittlung der tiefenabhängigen Erosionsstabilität von Gewässersedimenten: das SETEG-System, *Wasserwirtschaft* **89**: 72–77.

Kimiaghalam, N., Clark, S. P. and Ahmari, H. (2016). An experimental study on the effects of physical, mechanical, and electrochemical properties of natural cohesive soils on critical shear stress and erosion rate, *International Journal of Sediment Research* **31**(1): 1–15.

Kirby, R. (1988). High Concentration Suspension (Fluid Mud) Layers in Estuaries, *in* J. Dronkers and W. van Leussen (eds), *Physical Processes in Estuaries*, Springer, Berlin, Heidelberg, p. 25.

Kondolf, G. M., Gao, Y., Annandale, G. W., Morris, G. L., Jiang, E., Zhang, J., Cao, Y., Carling, P., Fu, K., Guo, Q., Hotchkiss, R., Peteuil, C., Sumi, T., Wang, H.-W., Wang, Z., Wei, Z., Wu, B., Wu, C. and Yang, C. T. (2014). Sustainable sediment management in reservoirs and regulated rivers: Experiences from five continents, *Earth's Future* **2**(5): 256–280.

Kothyari, U. C. and Jain, R. K. (2008). Influence of cohesion on the incipient motion condition of sediment mixtures, *Water Resources Research* **44**(4).

Kurtenbach, A., Bierl, R., Schorer, M., Eisold, B., Symader, W. and Gallé, T. (2010). Kohäsive Feinpartikel in fluvialen Systemen: einige Gedanken zu Erkenntnissen und Forschungsdefiziten [Cohesive fine particles in fluvial systems: some thoughts on findings and research deficits], *Umweltwissenschaften und Schadstoff-Forschung* **22**(6): 631–644.

Le Hir, P., Monbet, Y. and Orvain, F. (2007). Sediment erodability in sediment transport modelling: Can we account for biota effects?, *Continental Shelf Research* **27**(8): 1116–1142.

Lee, S.-C. and Mehta, A. J. (1994). Cohesive sediment erosion, *Technical Report DRP-9406*, Coastal and Oceanographic Engineering Department, University of Florida, Gainesville, Florida.

Lick, W. and McNeil, J. (2001). Effects of sediment bulk properties on erosion rates, *The Science of The Total Environment* **266**(1-3): 41–48.

Mahmood, K. (1987). Reservoir sedimentation: Impact, extent, and mitigation, *World Bank technical paper WTP71*, International Bank for Reconstruction and Development, Washington, DC, USA.

Malvern Instruments (2007). *Mastersizer 2000 - User Manual*, man0384-1.0 edn, Malvern Instruments Ltd., Worcestershire, United Kingdom.

Mayar, M. A., Schmid, G., Wieprecht, S. and Noack, M. (2019). Optimizing vertical profile measurements setup of gamma ray attenuation, *Radiation Physics and Chemistry* **164**: 108376.

McIntyre, A. D. (1971). Deficiency of Gravity Corers for sampling Meiobenthos and Sediments, *Nature* **231**(5300): 260–260.

McNeil, J., Taylor, C. and Lick, W. (1996). Measurements of Erosion of Undisturbed Bottom Sediments with Depth, *Journal of Hydraulic Engineering* **122**(6): 316–324.

Mehta, A. J. (1986). Characterization of Cohesive Sediment Properties and Transport Processes in Estuaries, *Estuarine Cohesive Sediment Dynamics*, Vol. 14, Springer-Verlag, pp. 290–325.

Mehta, A. J. (1991). *Characterization of cohesive soil bed surface erosion, with special reference to the relationship between erosion shear strength and bed density*, Coastal and Oceanographic Engineering Department, University of Florida, Gainesville, Florida.

Mehta, A. J. and Lee, S.-C. (1994). Problems in Linking the Threshold Condition for the Transport of Cohesionless and Cohesive Sediment Grain, *Journal of Coastal Research* **10**(1): 9.

Mehta, A. J. and Parchure, T. M. (2000). Surface erosion of fine-grained sediment revisited, *Proceedings in Marine Science*, Vol. 2, Elsevier, pp. 55–74.

Mehta, A. J. and Partheniades, E. (1982). Resuspension of Deposited Cohesive Sediment Beds, Coastal Engineering Research Council, Cape Town, South Africa, pp. 1569–1588.

Meyer-Reil, L.-A. (2005). *Mikrobiologie des Meeres: eine Einführung [Microbiology of the sea: an introduction]*, number 2679 in *UTB*, Facultas Universitätsverlag, Wien.

Mitchener, H. and Torfs, H. (1995). Erosion of mud-sand mixtures, *Coastal Engineering 29 (1996) 1-25* .

Moody, L. (1944). Friction Factors for Pipe Flow, *Transactions of American Society Mechanical Engineers* **66**: 671–678.

Morris, G. L. and Fan, J. (1998). *Reservoir sedimentation handbook: design and management of dams, reservoirs, and watersheds for sustainable use*, McGraw-Hill, New York.

Mouris, K., Beckers, F. and Haun, S. (2018). Three-dimensional numerical modeling of hydraulics and morphodynamics of the Schwarzenbach reservoir, *E3S Web of Conferences* **40**: 03005.

Mulligan, M., van Soesbergen, A. and Sáenz, L. (2020). GOODD, a global dataset of more than 38,000 georeferenced dams, *Scientific Data* **7**(1): 31.

Noack, M. (2012). *Modelling approach for interstitial sediment dynamics and reproduction of gravel-spawning fish*, number 214 in *Mitteilungen des Instituts für Wasser- und Umweltsystemmodellierung, Universität Stuttgart*, Inst. für Wasser- und Umweltsystemmodellierung, Stuttgart.

Noack, M., Gerbersdorf, S., Hillebrand, G. and Wieprecht, S. (2015). Combining Field and Laboratory Measurements to Determine the Erosion Risk of Cohesive Sediments Best, *Water* **7**(9): 5061–5077.

Noack, M., Schmid, G., Beckers, F., Haun, S. and Wieprecht, S. (2018). PHOTOSED - PHOTOgrammetric Sediment Erosion Detection, *Geosciences* **8**(7): 243.

Olsen, N. R. B. (1999). Two-dimensional numerical modelling of flushing processes in water reservoirs, *Journal of Hydraulic Research* **37**(1): 3–16.

Panagiotopoulos, I., Voulgaris, G. and Collins, M. B. (1997). The influence of clay on the threshold of movement of fine sandy beds, *Coastal Engineering 32 (1997) 19-43* .

Parchure, T. M. (1984). *Erosional Behavior of Deposited Cohesive Sediments*, Doctor of Philosophy (PhD), Coastal and Oceanographic Engineering Department, University of Florida, Gainesville, Florida.

Parchure, T. M. and Davis, J. E. (2005). Effect of Organic Materials on Bulk Density and Erodibility of Fine Sediment Beds, *Technical Report ERDC/CHL TR-05-7*, Vicksburg, Mississippi.

Parchure, T. M. and Mehta, A. J. (1985). Erosion of Soft Cohesive Sediment Deposits, *Journal of Hydraulic Engineering* **111**(10): 1308–1326.

Partheniades, E. (1965). Erosion and Deposition of Cohesive Soils, *Journal of the Hydraulics Division* **Vol. 91**(1): 105–139.

Paterson, D. M. (1997). Biological mediation of sediment erodibility: ecology and physical dynamics, *in* N. Burt, R. Parker and J. Watts (eds), *Cohesive Sediments*, Wiley Interscience, New York, pp. 215–230.

Paterson, D. M. and Black, K. S. (1999). Water Flow, Sediment Dynamics and Benthic Biology, *Advances in Ecological Research*, Vol. 29, Elsevier, pp. 155–193.

Perera, C., Smith, J., Wu, W., Perkey, D. and Priestas, A. (2020). Erosion rate of sand and mud mixtures, *International Journal of Sediment Research* **35**(6): 563–575.

Perkey, D. W., Smith, S. J. and Priestas, A. M. (2020). Erosion Thresholds and Rates for Sand-Mud Mixtures, *TR-20-13*, The U.S. Army Engineer Research and Development Center (ERDC), Vicksburg, Mississippi.

Perkins, R. G., Underwood, G. J. C., Brotas, V., Snow, G. C., Jesus, B. and Ribeiro, L. (2001). Responses of microphytobenthos to light: primary production and carbohydrate allocation over an emersion period, *Marine Ecology Progress Series* **223**: 101–112.

Peteuil, C., Jodeau, M., De Linares, M., Valette, E., Alliau, D., Wirz, C., Fretaud, T., Antoine, G. and Sécher, M. (2018). Toward an operational approach for the characterization and modelling of fine sediments dynamics in reservoirs, *E3S Web of Conferences* **40**: 03028.

Pye, K. (1994). *Sediment transport and depositional processes*, Blackwell Scientific Publications, Oxford and Boston.

Raudkivi, A. J. (1982). Kohäsive Sedimente [cohesive sediments], *Grundlagen des Sedimenttransports*, Springer, Berlin, Heidelberg, pp. 127–165.

Raudkivi, A. J. and Tan, S. K. (1984). Erosion of cohesive soils, *Journal of Hydraulic Research* **22**(4): 217–233.

Raunkjær, K., Hvitved-Jacobsen, T. and Nielsen, P. H. (1994). Measurement of pools of protein, carbohydrate and lipid in domestic wastewater, *Water Research* **28**(2): 251–262.

Reikowski, A. (2015). *Betriebsanleitung FRAHM-LOT [Manual FRAHM-LOT]*, 1.1 edn, MBT Underwater Technology.

Righetti, M. and Lucarelli, C. (2007). May the Shields theory be extended to cohesive and adhesive benthic sediments?, *Journal of Geophysical Research* **112**(C05039).

Roberts, J. D., Jepsen, R. A. and James, S. C. (2003). Measurements of Sediment Erosion and Transport with the Adjustable Shear Stress Erosion and Transport Flume, *Journal of Hydraulic Engineering* **129**(11): 862–871.

Sanford, L. P. and Halka, J. P. (1993). Assessing the paradigm of mutually exclusive erosion and deposition of mud, with examples from upper Chesapeake Bay, *Marine Geology* **114**(1-2): 37–57.

Sanford, L. P. and Maa, J. P.-Y. (2001). A unified erosion formulation for fine sediments, *Marie Geology 179 (2001) 9-23* .

Schäfer Rodrigues Silva, A., Noack, M., Schlabing, D. and Wieprecht, S. (2018). A data-driven fuzzy approach to simulate the critical shear stress of mixed cohesive/non-cohesive sediments, *Journal of Soils and Sediments* **18**(10): 3070–3081.

Schleiss, A. J., Franca, M. J., Juez, C. and De Cesare, G. (2016). Reservoir sedimentation, *Journal of Hydraulic Research* **54**(6): 595–614.

Schlichting, H. and Gersten, K. (2017). *Boundary-Layer Theory*, 9th edn, Springer, Berlin, Heidelberg.

Schweim, C. (2005). *Modellierung und Prognose der Erosion feiner Sedimente [Modeling and prediction of fine sediment erosion]*, PhD thesis, RWTH Aachen, Aachen.

Shields, A. (1936). *Anwendung der Ähnlichkeitsmechanik und der Turbulenzforschung auf die Geschiebebewegung [Application of mechanical similarity and turbulence research to bedload motion]*, PhD thesis, Preussischen Versuchsanstalt für Wasserbau, Berlin.

Smith, D. J. and Underwood, G. J. C. (2001). The production of extracellular carbohydrates by estuarine benthic diatoms: the effects of growth phase and light and dark treatment, *Journal of Phycology* **36**(2): 321–333.

Spork, V. (1997). *Erosionsverhalten feiner Sedimente und ihre biogene Stabilisierung [Erosion behavior of fine sediments and their biogenic stabilization]*, Band 114 der Reihe Mitteilungen des Lehrstuhls und Instituts für Wasserwirtschaft, RWTH Aachen, Aachen.

Stevens, R. L. (1991). Grain-size distribution of quartz and feldspar extracts and implications for flocculation processes, *Geo-Marine Letters* **11**(3-4): 162–165.

Sumi, T. (2004). Reservoir sedimentation management with bypass tunnels in Japan, *Proceedings of 9th International Symposium on River Sedimentation*, Yichang, China, pp. 1036–1043.

Syvitski, J. P. M. (2005). Impact of Humans on the Flux of Terrestrial Sediment to the Global Coastal Ocean, *Science* **308**(5720): 376–380.

Third World Water Forum, Japan (2003). Sedimentation Management Challenges for Reservoir Sustainability, Kyoto, Shiga and Osaka, Japan.

Thom, M., Schmidt, H., Gerbersdorf, S. U. and Wieprecht, S. (2015). Seasonal biostabilization and erosion behavior of fluvial biofilms under different hydrodynamic and light conditions, *International Journal of Sediment Research* **30**(4): 273–284.

Thomsen, L. and Gust, G. (2000). Sediment erosion thresholds and characteristics of resuspended aggregates on the western European continental margin, *Deep Sea Research Part I: Oceanographic Research Papers* **47**(10): 1881–1897.

Tolhurst, T. J., Defew, E. C., de Brouwer, J. F. C., Wolfstein, K., Stal, L. J. and Paterson, D. M. (2006). Small-scale temporal and spatial variability in the erosion threshold and properties of cohesive intertidal sediments, *Continental Shelf Research* **26**(3): 351–362.

Underwood, G. J. C. and Smith, D. J. (1998). Predicting Epipelic Diatom Exopolymer Concentrations in Intertidal Sediments from Sediment Chlorophyll a, *Microbial Ecology* **35**(2): 116–125.

Van Ledden, M. (2003). *Sand-mud segregation in estuaries and tidal basins*, PhD thesis, Delft.

Van Leussen, W. (1988). Aggregation of Particles, Settling Velocity of Mud Flocs A Review, *in* J. Dronkers and W. van Leussen (eds), *Physical Processes in Estuaries*, Springer, Berlin, Heidelberg, pp. 347–403.

Van Prooijen, B. C. and Winterwerp, J. C. (2010). A stochastic formulation for erosion of cohesive sediments, *Journal of Geophysical Research* **115**(C01005).

Van Rijn, L. C. (2020). Erodibility of Mud–Sand Bed Mixtures, *Journal of Hydraulic Engineering* **146**(1): 04019050.

Vörösmarty, C. J., Meybeck, M., Fekete, B. and Sharma, K. (1997a). The potential impact of neo-Castorization on sediment transport by the global network of rivers, *in* D. Walling and J.-L. Probst (eds), *Human Impact on Erosion and Sedimentation*, IAHS Press, Wallingford, UK, pp. 261–272.

Vörösmarty, C. J., Meybeck, M., Fekete, B., Sharma, K., Green, P. and Syvitski, J. P. M. (2003). Anthropogenic sediment retention: major global impact from registered river impoundments, *Global and Planetary Change* **39**(1-2): 169–190.

Vörösmarty, C. J., Sharma, K., Fekete, B., Copeland, A. H., Holden, J., Marble, J. and Lough, J. A. (1997b). The storage and aging of continental runoff in large reservoir systems of the world, *Ambio* **26**(4): 210–219.

Walder, J. S. (2016). Dimensionless Erosion Laws for Cohesive Sediment, *Journal of Hydraulic Engineering* **142**(2): 04015047.

Wan, C. F. and Fell, R. (2004). Investigation of Rate of Erosion of Soils in Embankment Dams, *Journal of Geotechnical and Geoenvironmental Engineering* **130**(4): 373–380.

Wen Shen, H. (1999). Flushing sediment through reservoirs, *Journal of Hydraulic Research* **37**(6): 743–757.

Westrich, B., Haag, I. and Kern, U. (2000). Mobilität von Schadstoffen in den Sedimenten staugeregelter Flüsse - Dynamik und Bilanzierung von Schwebstoffen und Schwermetallen in einer Stauhaltungskette [Mobility of pollutants in sediments of regulated rivers],

Forschungsbericht FZKA-BWPLUS, Institut für Siedlungswasserbau, Wassergüte und Abfallwirtschaft, Universität Stuttgart, Stuttgart.

Wiberg, P. L. and Smith, J. D. (1987). Calculations of the critical shear stress for motion of uniform and heterogeneous sediments, *Water Resources Research* **23**(8): 1471–1480.

Widdows, J., Friend, P. L., Bale, A. J., Brinsley, M. D., Pope, N. D. and Thompson, C. E. L. (2007). Inter-comparison between five devices for determining erodability of intertidal sediments, *Continental Shelf Research* **27**(8): 1174–1189.

Witt, O. (2004). *Erosionsstabilität von Gewässersedimenten und deren Bedeutung für den Stofftransport bei Hochwasser am Beispiel ausgewählter Stauhaltungen des Oberrheins [Erosion stability of riverine sediments and their importance for sediment transport during floods on the example of selected reservoirs at the Upper Rhine]*, Vol. 127 of *Mitteilungen des Instituts für Wasserbau, Universität Stuttgart*, Institut für Wasserbau, Stuttgart.

Wu, W. (2008). *Computational river dynamics*, Taylor & Francis, London and New York.

Wu, W. (2016). Mixed cohesive and noncohesive sediment transport: a state of the art review, *River Sedimentation: Proceedings of the 13th International Symposium on River Sedimentation*, Stuttgart, pp. 9–18.

Wu, W., Perera, C., Smith, J. and Sanchez, A. (2018). Critical shear stress for erosion of sand and mud mixtures, *Journal of Hydraulic Research* **56**(1): 96–110.

Yallop, M. L., Paterson, D. M. and Wellsbury, P. (2000). Interrelationships between Rates of Microbial Production, Exopolymer Production, Microbial Biomass, and Sediment Stability in Biofilms of Intertidal Sediments, *Microbial Ecology* **39**(2): 116–127.

Yoon, Y. N. (1992). The state and the perspective of the direct sediment removal methods from reservoirs, *International Journal of Sediment Research* **7(2)**: 99–116.

Zarfl, C., Lumsdon, A. E., Berlekamp, J., Tydecks, L. and Tockner, K. (2015). A global boom in hydropower dam construction, *Aquatic Sciences* **77**(1): 161–170.

Zhang, M. and Yu, G. (2017). Critical conditions of incipient motion of cohesive sediments, *Water Resources Research* **53**(9): 7798–7815.

Zhu, Y., Lu, J., Liao, H., Wang, J., Fan, B. and Yao, S. (2008). Research on cohesive sediment erosion by flow: An overview, *Science in China Series E: Technological Sciences* **51**(11): 2001.

Publication I.

Experimental investigation of reservoir sediments

Table 5.1. Metadata of publication I

Title	Experimental investigation of reservoir sediments
Authors	**Felix Beckers**, Stefan Haun, Markus Noack
Journal	E3S Web of Conferences (River Flow 2018)
submitted	February 5, 2018
accepted	April 25, 2018
published	September 5, 2018
DOI	https://doi.org/10.1051/e3sconf/20184003030

Experimental investigation of reservoir sediments

Felix Beckers[1,*], *Stefan* Haun[1], and *Markus* Noack[1]

[1]Institute for Modelling Hydraulic and Environmental Systems, University of Stuttgart, Pfaffenwaldring 61, 70569 Stuttgart, Germany

Abstract. This study presents an experimental approach to investigate cohesive reservoir sediments. It is shown, how adjacent sediment cores can be extracted from reservoir beds with a Frahm Sediment Sampler. The cores are subsequently used for detailed investigations in a hydraulic laboratory. In a first step, related cores are identified based on their bulk density profiles. One part of the related cores is used to analyze the sediment properties over depth by means of potential stability parameters. The other part is used to determine the depth-dependent erosion stability in an erosion flume (SETEG-system). In the SETEG-system, a photogrammetric method is applied to measure the erosion rates of pre-defined sediment layers at different exposed shear stresses. Subsequently, the critical shear stress can be derived, which leads to an objective evaluation and allows a systematic approach. Finally, both results are combined to investigate possible correlations between the evaluated depth-dependent stability parameters and the measured erosion stability. The approach is presented on sediment cores from the case study "Kleiner Brombachsee", a reservoir that is located in Middle Franconia, Germany.

1. Introduction

Reservoir sedimentation can reduce the lifetime of reservoirs and may have negative impacts on the operation as well as on the downstream river region [1]. Thus, sustainable sediment management strategies are required to minimize reservoir sedimentation, to remobilize already deposited sediments and to restore the natural sediment continuity at its best. However, successful measures can only be derived when detailed knowledge regarding the sediment properties and the erosion stability of the deposited sediment as well as their mutual interaction exists. Moreover, depth-dependent stability information is important to address the changing sediment properties between surface layers and buried layers. In this context, especially the description of fine sediment mixtures consisting of clay, silt and sand is a challenging task due to their cohesive erosion behavior. Fine sediments, however, often dominate reservoir sediments. Therefore, this study presents an experimental approach to investigate the depth-dependent erosion stability of cohesive reservoir sediments and their sedimentological properties by taking into account physical, chemical and biological stability parameters.

* Corresponding author: felix.beckers@iws.uni-stuttgart.de

2. Material and methods

2.1. Study area

The approach is presented on the case study "Kleiner Brombachsee". This reservoir was built between 1975 and 1986 as a pre-reservoir of the "Großer Brombachsee" and for the purpose of low water regulation of the Regnitz-Main catchment. It is located in Middle Franconia, Germany (49° 8′ 8″ N, 10° 53′ 15″ E) and provides a water surface of 2.58 km² and a total storage volume of 14.72 Mio. m³ at maximum operation level (411 m a.s.l.) [2].

2.2. Collection of undisturbed sediment samples

In a first step, adjacent sediment cores are taken from the reservoir with a so called Frahm Sediment Sampler ("Frahm-Lot"). This device was developed at the "Leibniz Institute for Baltic Sea Research" and is distributed by the "Meerestechnisches Büro Turla GmbH (MBT)" [3]. It was previously used in marine technology to close the gap between piston and gravity cores and is applied in inland waters for the first time.

With the Frahm Sediment Sampler undisturbed sediment cores with a diameter of 0.1 m and a length of up to 1 m can be extracted from the reservoir. The advantage is that a lid and a sideways movable clasp seal the sediment core immediately after removal from the bed. It can be operated from a floating platform that is equipped with a tripod and a winch. The maximum depth of operation is currently 100 m. The sampling can be either conducted manually or electrically (12 V) to adapt to the present water law requirements. In the case of electric drive, the speed of the winch ranges between 20 m min^{-1} and 10 m min^{-1} (without load/with load). Fig. 1. a-c shows the jacked up Frahm Sediment Sampler with closed lid and clasp, the floating platform with the tripod equipped for operation and an extracted sediment core.

a)  b)  c) 

Fig. 1. a) Frahm Sediment Sampler in inactive state in the laboratory; b) equipped floating platform for the sampling of undisturbed sediment cores; c) sediment core taken with the Frahm Sediment Sampler.

2.3. Laboratory analysis

After their removal, the sediment cores are prepared for transportation to be analyzed in the hydraulic laboratory of the Institute for Modelling Hydraulic and Environmental Systems (IWS). The investigations in the laboratory are conducted for one core at a time. Thus, the remaining cores are vertically stored in a darkened cooling chamber to avoid any influences on the sediment layers and to reduce biological activity.

Bulk density and core allocation for destructive analysis

First of all, the vertical bulk density profile is determined for all cores by using a non-destructive gamma-ray attenuation method. For this purpose, the sediment core is placed between a traverse system that automatically moves along the core to determine the bulk density at predefined spacing. It consists of a radioactive source of ^{137}CS with a decay energy of 662 keV as well as a detector unit with a scintillator of Sodium Iodide doped with Thalium (NaI(TI)) and a photomultiplier (see Fig. 2. a). The principle is to measure the absorption of gamma radiation by a penetrated media. Since the system is carefully calibrated against the attenuation of air and water, the bulk density of the sediment core can be derived.

The measurement of the bulk density profiles is the only non-destructive analysis used during the investigations. Because of that, the bulk density profiles serve as basis to identify related cores with same/similar sediment properties, to assign them to each other and to select them for the further destructive analysis. This is either the investigation of potential stability parameters or the measurement of the erosion stability. Since the cores are analyzed over depth, the bulk density profiles are also used to pre-define horizontal layers in which the further measurements take place.

Sediment properties and stability parameters

The sediment gets extracted from the cores in the pre-defined horizontal layers to be subsequently analyzed with respect to a selection of potential stability parameters. For this purpose, a construction with a lifting spindle and custom-made plugs are used to push the sediment out of the core from bottom to top. As soon as the respective layer reaches the top, three sub-samples (triplets) with a diameter of 4.5 cm are taken for further processing. This subdivision into triplets takes place to address the spatial heterogeneity of the sediments within a layer. After their removal, each single triplet sample is homogenized and prepared for the subsequent analyses. This leads to three representative vertical profiles of the investigated parameters along the cores.

The analyzed stability parameters included in this study are the particle size distribution (PSD), the total organic carbon (TOC), the cation exchange capacity (CEC) and to address biostabilization of cohesive sediments the extracellular polymeric substances (EPS) and Chlorophyll-a (CHL-a) [4]. The PSD is determined by laser diffraction with a Malvern Mastersizer 2000 (Malvern Instruments Ltd, Malvern, UK). The TOC is determined by loss on ignition [5], CEC by exchange with barium chloride [6], EPS proteins with the modified Lowry method [7], EPS sugars with the Dubois method [8] and CHL-a by a photometric analysis [9].

Erosion stability using the SETEG-system

Cores selected for the measurement of the depth-dependent erosion stability are analyzed with the SETEG-system of the IWS (SETEG = Strömungskanal zur Ermittlung der tiefenabhängigen Erosionsstabilität von Gewässersedimenten).

The SETEG-system was established in 2004 and has been continuously developed further to investigate the sediment stability over depth [10-11]. It consists of a straight, rectangular and closed flume, which is operated under pressurized flow. It has a total length of 8.32 m, a width of 0.145 m and a height of 0.10 m as it can be seen in Fig. 2. b. Sediment cores are locked in position on the bottom side of the flume. The sediment sample can then be moved vertically by means of a lifting spindle. As soon as the desired sediment layer has been reached, the protruding sediment is cut off, leaving the desired layer flush with the

bottom so the erosion test can start. During an erosion test, the sediment layer is exposed to stepwise increasing discharges of regular intervals and of constant time periods (t = 600 s). The corresponding shear stresses are determined by a hydraulic calibration curve (Q-τ-relation) that was created from high-resolution LDA-measurements in the area of interest prior to the experiment [11]. At the same time, a photogrammetric measurement of the erosion rates is conducted. For this purpose, a random grid pattern (24,000 points) is projected on the sediment surface and surveyed by a camera (frame rate: 3 fps). During post-processing, images can be extracted from the recorded video of different time intervals (Δt) and regions of interest (ROI). Surface erosion leads to a shift of the single points on the sediment surface. If erosion occurred between two images, the volume change can be calculated with a dense optical flow algorithm from the OpenCV library (https://opencv.org/). The erosion rate is subsequently calculated by dividing the detected volume by the region of interest (ROI) and by the considered time interval (Δt). The optical distortion due to the angled mounting and the different penetrated media (air, glass, water) is spatially and vertically corrected by a polynomial function of second degree that was obtained during calibration experiments. The advantage of this volumetric approach is that it captures both, sediment which gets transported in suspension and sediment transported as bed load after remobilization. Moreover, the volumetric detection limit is very low and in the range of 5 to 10 mm^3 per single event.

After the erosion of a sediment core, the measured erosion rates can be plotted over the corresponding shear stresses for each investigated layer separately. Based on that, the critical shear stress that serves as indicator for sediment stability can be calculated by extrapolating the shear stress for an erosion rate to 0 mm s^{-1} [12-15]. This allows an objective assessment of the sediment stability.

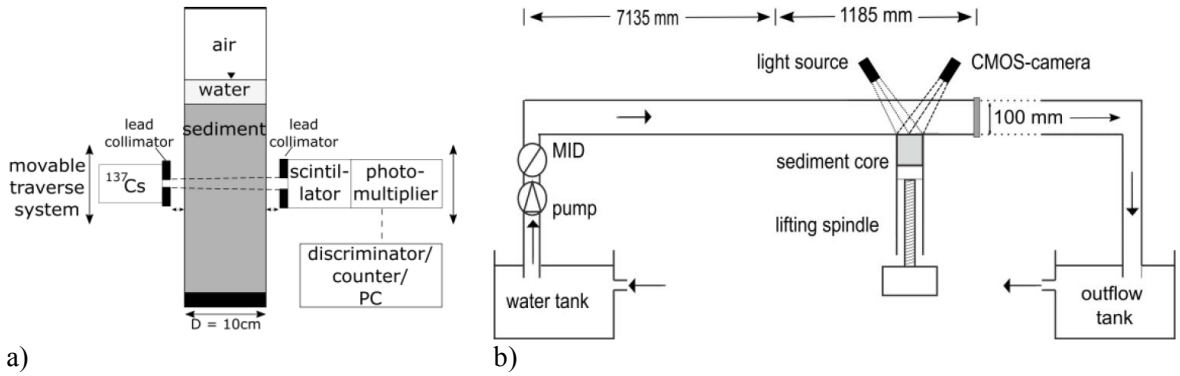

Fig. 2. a) Schematic side-view of the gamma-ray densitometer and b) the SETEG-system.

Combination of results

Finally, all results of the related cores can be compared with each other to investigate the depth-dependent influence of the investigated stability parameters on the measured sediment stability. For clarification, the results are subsequently presented in a single figure as standardized values to focus on the benefits of the approach.

3. Results and Discussion

In total, 10 adjacent sediment cores with a sediment thickness between 0.15 m to 0.5 m were collected from the bed of the reservoir "Kleiner Brombachsee" on May 16 and May 29, 2017. The cores were collected from water depths between 4 to 5 m in a field of (40 x 25) m^2 close to a preservation area slightly behind the dam (49° 8′ 0.5″ N, 10° 53′ 19″

E). At first glance it could be seen that most of the samples contain clayey material at the bottom part. The subsequent laboratory analysis revealed that this is grown soil. This led to the positive side effect that the current sediment thickness became visible (0.05 m to 0.35 m) and the local sedimentation rate could be calculated with the known date of impoundment (1986). Thus, the local sedimentation rate varies between 0.16 cm a^{-1} to 1.13 cm a^{-1}.

3.1. Bulk density and core allocation

The results of the bulk density measurements are shown over sediment depth in Fig. 3. a. Four main characteristics can be pointed out: the profiles have different lengths according to the sediment thickness, the bulk density increases over depth, the total range of bulk densities varies between 1 g cm^{-3} and 2 g cm^{-3} and two groups can be identified due to a different characteristic increase over depth. In this context, the strong increase of the bulk density (> 1.7 g cm^{-3}) indicates the transition from the natural sediment into the grown soil. This means, that the natural sediment layer is very thin in the cores where this behavior occurs within the top 0.1 m. Thus, they are excluded from further investigations leading to the remaining sediment cores shown in Fig. 3. b, which are used for the destructive analyses. For illustration purposes, the stability parameters of core "KB16-1" and the erosion stability of core "KB29-4" are presented in this study.

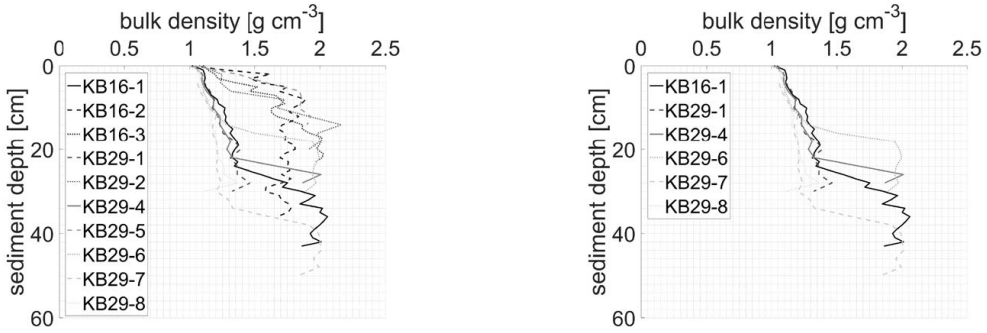

a) b)

Fig. 3. a) Complete and b) adjusted set of bulk density profiles of adjacent sediment cores. The cores were taken from the reservoir "Kleiner Brombachsee" on May 16 and May 29, 2017 as indicated by their names.

3.2. Sediment properties and stability parameters

The sediment properties are investigated by means of stability parameters in different horizontal layers. The parameters PSD, TOC, CEC, EPS (separated in proteins and sugars) and CHL-a are shown for core "KB16-1" as vertical profiles in Figure 7 a-f. T1, T2 and T3 (dashed lines) represent the evaluated triplet samples within each layer, whereas the solid line shows their mean.

Fig. 4 a shows the percentile values d_{10}, d_{50} and d_{90} of the PSD over depth. It can be seen, that the mean of d_{10} and d_{50} decreases from top to a depth of 0.2 m, which corresponds to a decreasing grain diameter. Below this depth, a sharp increase indicates the transition of the deposited sediment into the natural soil (see also Fig. 3). The mean of the d_{90} shows a pronounced peak in a depth of 0.1 m, which is due to a high sand content in this sediment layer. Apart from that, it increases nearly constant towards the end. The mean of the TOC, CEC, EPS (proteins and sugars) and CHL-a, shown in Fig. 4 b-f, decreases over depth, apart from a few oscillations, which are mainly caused by the spatial heterogeneity of the sediments within a layer (analyzed by the triplets T1, T2 and T3). It can be clearly

seen, that the heterogeneity reduces below 0.2 m (natural soil). An exception is EPS (proteins), here the reduction starts at 0.25 m. As a result of these findings the CEC was only analyzed in the upper 0.2 m.

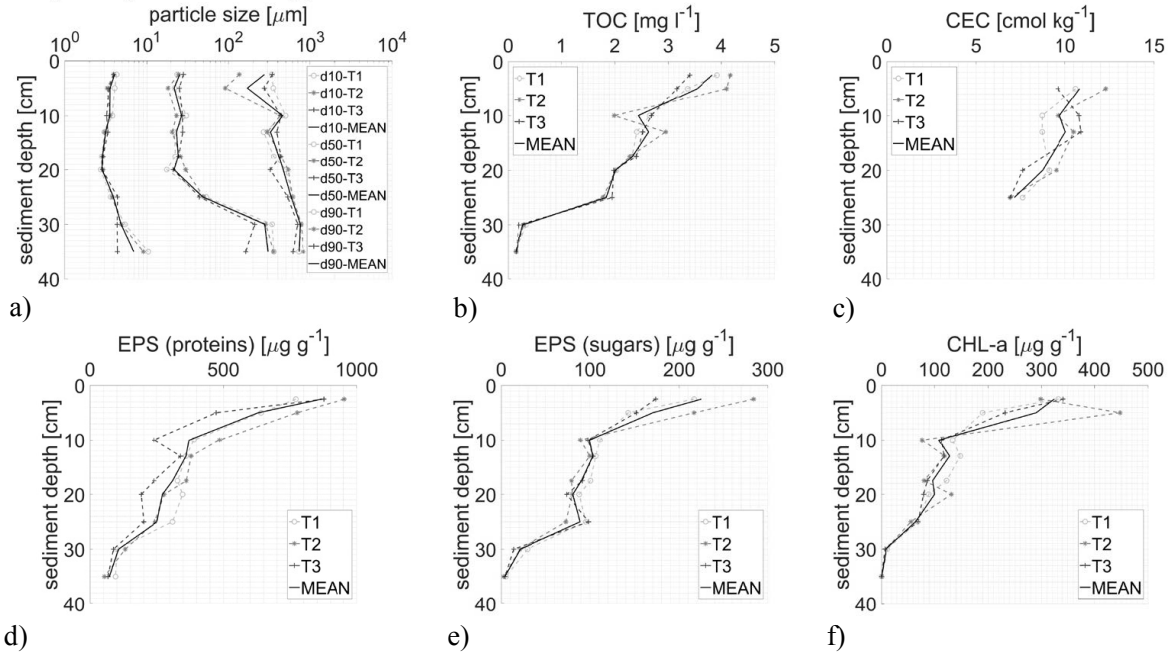

Fig. 4. Vertical profiles of investigated stability parameters: a) particle size distribution (PSD) shown as percentile values d_{10}, d_{50} and d_{90}; b) total organic carbon (TOC); c) cation exchange capacity (CEC); d) extracellular polymeric substances - proteins (EPS); e) extracellular polymeric substances - sugars (EPS) and f) chlorophyll-a (CHL-a). The analyzed triplets (T1, T2 and T3) and their mean are shown.

3.3. Erosion stability using the SETEG-system

The results of the erosion stability tested in the SETEG-system are shown in Fig. 5 for core "KB29-4". The core is eroded at seven layers (4 cm, 7 cm, 10 cm, 13 cm, 16 cm, 19 cm and 22 cm). During the erosion test, the measured erosion rates are used to determine the critical shear stress for each layer by calculating the shear stress for an extrapolated erosion rate of E = 0 mm s^{-1}.

It can be seen, that in the first two layers, the critical shear stress and the sediment stability is comparatively low (around 0.3 N m^{-2}). In the next two layers a strong increase occurs to the maximum stability of τ_{crit} = 1.27 N m^{-2}, reached at a depth of 0.13 m. A following decrease to the end is interrupted by another raise at a depth of 0.19 m. It is likely, that the "younger" sediment on top is easier to remobilize, whereas the deeper located sediment layers are consolidated and thus more stable. The low value in the last layer might already indicate the sandy natural soil (see also Fig. 3.).

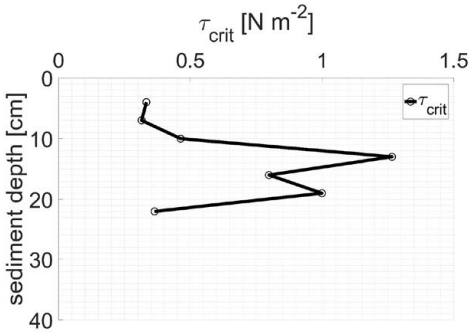

Fig. 5. Depth-dependent sediment stability of core "KB29-4" expressed as critical shear stress.

3.4. Combination of results

In a next step, the vertical profiles of the stability parameters and of the erosion stability can be compared with each other to investigate possible relationships. The results are presented as normalized values in Fig. 6.

Fig. 6. a shows the physical stability parameters ("KB16-1") and the measured erosion stability of core "KB29-4". It can be seen for instance, that the local increase in d_{90} at a depth of 0.1 m corresponds to a relative low erosion stability. Vice versa, the following decrease of d_{90} in the layer below (0.13 m) leads to a significant higher erosion stability. This can be explained with a decreasing particle size and an increasing cohesiveness in the sediment layer at 0.13 m leading to a higher sediment stability.

Fig. 6. b shows the chemical and biological stability parameters ("KB16-1") and the measured erosion rate of core "KB29-4". Here, the decreasing trend of the stability parameters can be seen. However, at the highest measured shear stress in the layer at 0.13 m a local peak is discernible. Here the chemical and biological parameters may additionally reinforce the stabilizing effect induced by the physical parameters and finally contribute to the increased stability. However, further investigations are necessary to reveal these interactions.

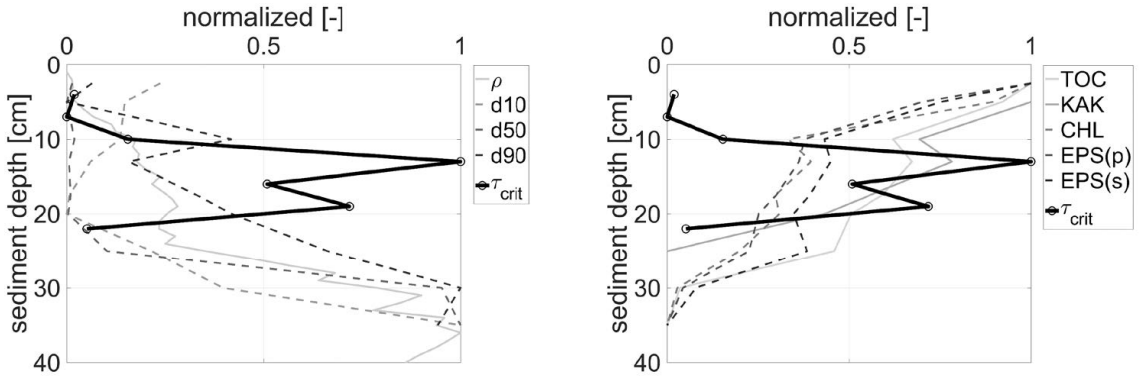

a) b)

Fig. 6. a) Combination of physical stability parameters ("KB16-1") and b) chemical and biological stability parameters ("KB16-1") with the measured erosion stability of core "KB29-4". All results are shown as normalized values.

4. Conclusions

In this study, an experimental approach to investigate cohesive reservoir sediments is presented. For this purpose, undisturbed sediment cores are successfully extracted from the reservoir bed with a Frahm Sediment Sampler. They are used to investigate the depth-dependent sediment properties and the erosion stability in laboratory analyses. The investigated stability parameters (particle size distribution (PSD), total organic carbon (TOC), cation exchange capacity (CEC), extracellular polymeric substances (EPS proteins and EPS sugars) and Chlorophyll-a (CHL-a)) are compared with the erosion stability, determined with the SETEG-system to examine possible correlations.

It can be seen for the cores obtained from the case study "Kleiner Brombachsee", that there is a negative visual correlation between the d_{90} and the sediment stability in some of the investigated top layers. In addition, reinforcement due to chemical and biological stability parameters is likely but must be further investigated. In the lower layers no visual correlation can be found.

In general, the presented approach is applicable to investigate reservoir sediments, to describe their properties, their erosion stability and to identify key-parameters that govern cohesive sediment stability. Finally, this information can be used to derive site-specific sediment management strategies for sustainable reservoir operation.

This study was conducted within the project CHARM - Challenges of Reservoir Management - Meeting Environmental and Social Requirements. The project is part of the Water Research Network Baden-Württemberg. It is funded by the Ministry of Science, Research and Arts of the federal state of Baden-Württemberg, Germany.

References

1. G.L. Morris, J. Fan, *Reservoir sedimentation handbook: design and management of dams, reservoirs, and watersheds for sustainable use* (McGraw-Hill, New York, 1998)
2. Deutsches TalsperrenKomitee e. V. (Ed.), *Talsperren in Deutschland* (Springer Fachmedien Wiesbaden, Wiesbaden, 2013)
3. Reikowski, A., *Manual FRAHM-LOT*, (MBT Underwater Technology, V 1.1)
4. S.U. Gerbersdorf, S. Wieprecht, *Biostabilization of cohesive sediments: revisiting the role of abiotic conditions, physiology and diversity of microbes, polymeric secretion, and biofilm architecture*, Geobiology **13**, 68–97 (2015)
5. DIN EN 13137:2001-12, *Characterization of waste - Determination of total organic carbon (TOC) in waste, sludges and sediments* (2001)
6. DIN ISO 13536:1997-04, *Soil quality - Determination of the potential cation exchange capacity and exchangeable cations using barium chloride solution buffered at pH = 8,1 (ISO 13536:1995)* (1997)
7. K. Raunkjaer, T. Hvitvedjacobsen, P.H. Nielsen, *Measurement of pools of protein, carbohydrate and lipid in domestic waste-water,* Water research **28**, 251–262 (1994)
8. M. Dubois, K.A. Gilles, J.K. Hamilton, P.A. Rebers, F. Smith, *Colorimetric method for determination of sugars and related substances,* Analytical chemistry **28**, 350–356 (1956)
9. DIN 38412-16:1985-12, *German standard methods for the examination of water, waste water and sludge; test methods using water organisms (group L); determination of chlorophyll-a in surface water (L 16)* (1985)
10. O. Witt, B. Westrich, *Quantification of erosion rates for undisturbed contaminated cohesive sediment cores by image analysis*, The Interactions between Sediments and Water. Springer, pp. 271–276 (2003)
11. M. Noack, S.U. Gerbersdorf, G. Hillebrand, S. Wieprecht, *Combining Field and Laboratory Measurements to Determine the Erosion Risk of Cohesive Sediments Best*, Water **7**, 5061–5077 (2015)
12. A. Schaefer Rodrigues Silva, G. Schmid, M. Noack, S. Wieprecht, *Erosionsmessungen an Sedimentkernen aus dem Oberwasser der Wehranlage Marckolsheim und Rhinau (No. 03/2017)*, Institut für Wasser- und Umweltsystemmodellierung (2017)
13. T.M. Ravens, P.M. Gschwend, *Flume measurements of sediment erodibility in Boston Harbor*, Journal of Hydraulic Engineering **125**, 998–1005 (1999)
14. L.P. Sanford, J.P. Halka, *Assessing the paradigm of mutually exclusive erosion and deposition of mud, with examples from upper Chesapeake Bay,* Marine Geology 37–57 (1993)
15. T.J. Tolhurst, R. Riethmüller, D.M. Paterson, *In situ versus laboratory analysis of sediment stability from intertidal mudflats,* Continental Shelf Research (2000)

Publication II.

PHOTOSED - PHOTOgrammetric Sediment Erosion Detection

Table 5.2. Metadata of publication II

Title	PHOTOSED - PHOTOgrammetric Sediment Erosion Detection
Authors	Markus Noack, Gerhard Schmid, **Felix Beckers**, Stefan Haun, Silke Wieprecht
Journal	Geosciences 8, 243
submitted	June 2, 2018
accepted	June 29, 2018
published	June 30, 2018
DOI	https://doi.org/10.3390/geosciences8070243

geosciences

MDPI

Article

PHOTOSED—PHOTOgrammetric Sediment Erosion Detection

Markus Noack *, Gerhard Schmid, Felix Beckers, Stefan Haun and Silke Wieprecht

Institute for Modelling Hydraulic and Environmental Systems, University of Stuttgart, Pfaffenwaldring 61, 70569 Stuttgart, Germany; gerhard.schmid@iws.uni-stuttgart.de (G.S.); felix.beckers@iws.uni-stuttgart.de (F.B.); stefan.haun@iws.uni-stuttgart.de (S.H.); silke.wieprecht@iws.uni-stuttgart.de (S.W.)

* Correspondence: markus.noack@iws.uni-stuttgart.de; Tel.: +49-711-685-64774

Received: 2 June 2018; Accepted: 29 June 2018; Published: 30 June 2018

Abstract: This work presents a novel high-resolution photogrammetric measuring technique (PHOTOSED) to study in detail the erosion behavior of cohesive sediments, or cohesive/non-cohesive sediment mixtures. PHOTOSED uses a semiconductor laser to project a pseudo-random pattern of light points on a sediment surface and applies the Dense Optical Flow (DOF) algorithm to measure the erosion volume based on displacements of the projected light points during the sediment erosion process. Based on intensive calibration and verification experiments, the accuracy and applicability of the method has been validated for a wide range of erosion volumes, encompassing several orders of magnitude, which is required for investigations of natural sediment mixtures. The high spatial resolution of PHOTOSED is especially designed to detect the substantial variability of erosion rates during exemplary erosion experiments, which allows for further in-depth investigations of the erosion process of cohesive sediments and cohesive/non-cohesive sediment mixtures.

Keywords: cohesive sediments; cohesive/non-cohesive sediment mixtures; erosion behavior; high-spatial resolution measurements; photogrammetric measurements

1. Introduction

The erosion of cohesive sediments and non-cohesive/cohesive sediment mixtures represents a crucial issue for many engineering and ecological applications. Consequently, the erosion behavior has been intensively studied over recent decades in laboratories, as well as in the field. The typical erosion modes for cohesive sediments have been described by several authors in form of particle erosion and the erosion of aggregates (e.g., [1]), which has been extended by Kothyari and Jain [2], and Wu et al. [3] for non-cohesive/cohesive mixtures considering different ratios of cohesive and non-cohesive sediments. Moreover, current scientific literature distinguishes between depth-limited erosion and steady-state erosion [4], dependent on vertical sediment properties. In addition, many efforts have been made to find correlations between critical shear stress, critical velocity, or erosion rates to parameters involved in erosion processes of cohesive sediments, resulting in an immense variety of different formulae (e.g., [3,5–9]). Yet the results of the developed formulae show large differences to each other, are all empirical, and with poor universality [10]. Reasons for these differences are the complex interactions between physical, chemical, and biological parameters (e.g., [11–15]), along with the excessive variety of different devices and methods that were applied to study the erosion process of cohesive sediments [10].

In this context, accurate measurements of erosion rates for cohesive sediment surfaces play an essential role in developing approaches to describe the erosion behavior of non-cohesive/cohesive sediment mixtures. In general, the surface erosion rate is defined as the mass or volume of eroded sediments per surface area and time [16] and is commonly related to the exposed flow conditions

(e.g., as excess shear stress [9]). Aberle et al. [17] have provided an extended overview of different measuring techniques to obtain erosional characteristics of cohesive sediments in the laboratory and field. This review includes recirculating flumes (e.g., [18,19]), straight flow-through flumes (e.g., [20–22]), and miscellaneous devices, such as jet tests (e.g., CSM, cohesive strength meter, Paterson, 1989), hole erosion tests [23], microcosm experiments [24], and erosion bells [25].

Despite the considerable variety of devices, information about the spatial and temporal variability of erosion rates and the capability of the devices to resolve the spatial and temporal variability is rare in literature. Most often, the erosion rates are determined for larger areas, such as the entire surfaces of sediment cores, or the dimensions of open-bottom measuring sections (e.g., [20,21,26]). However, the surface erosion process of cohesive sediments, or non-cohesive/cohesive mixtures, is not homogeneously distributed over the measuring areas. Instead, it shows a high spatial and temporal heterogeneity during the erosion experiments, resulting in a strong structured surface [2]. In addition, the surface evolution to structured surfaces due to erosion leads to different local roughness changes, which affects the local hydraulics and shear stresses, and thus the further progression of erosion. Therefore, this article introduces a novel laboratory method called PHOTOSED (PHOTOgrammetric Sediment Erosion Detection), for the high-resolution measurements of erosion rates from cohesive sediments and non-cohesive/cohesive sediment mixtures using a photogrammetric approach.

2. Materials and Methods

2.1. Experiments in the Erosion Flume—SETEG

The PHOTOSED method was developed for the SETEG-flume (Stroemungskanal zur Ermittlung der tiefenabhängigen Erosionsstabilitaet von Gewaessersedimenten; [22,26,27], Figure 1), which is in use at the Institute for Modelling Hydraulic and Environmental Systems, of the University of Stuttgart, for measuring depth-oriented erosion rates and critical shear stresses for nearly 20 years. The flume (with a height: 0.090 m, width: 0.142 m, and length: 8.320 m) consists of a closed rectangular channel with pressurized flow to obtain optical access for photogrammetric measurements. The measuring section consists of a circular opening in the bottom of the flume where cylindrical sediment cores, with a maximum diameter of 135 mm, can be inserted and are exposed to the fully developed flow. A jack-stepping motor controls vertical movement of the sediments in the core to ensure that the sediment surface is flush with the flume bottom. This arrangement allows for different depths of the sediment core to be investigated independently to obtain depth-oriented information about the erosion behavior. During an erosion experiment, the discharge is increased stepwise until the entrainment of sediment particles, or aggregates, can be observed. The resulting critical shear stress is determined by a hydraulic calibration function (Q-τ-relation), which was obtained by previously conducted high-resolution LDA measurements (TSI Inc., Shoreview, MN, USA). To obtain vertical profiles along the cores, the measurements are typically conducted at depth intervals of 10 mm to 50 mm.

2.2. PHOTOSED—PHOTOgrammetric SEDiment Erosion Detection

For the photogrammetric detection of sediment erosion (PHOTOSED), the SETEG-flume is equipped with a semiconductor laser, with a diffraction optic (Laser2000 GmbH, Wessling, Germany) at the light source, to project a pseudo-random pattern of approximately 24,000 light points on the 143 cm^2 sediment surface (based on the maximum diameter of a sediment core). In addition, a CMOS-camera (2 MP, IDS GmbH, Ettlingen, Germany) is installed for image acquisition, with a temporal resolution of 10 Hz. The laser is mounted outside the flume, and projects down onto the sediment surface in the direction of flow at an angle of 45°, while the CMOS-camera is mounted vertically above the sediment surface. An adjustable pump and magnetic inductive flow-meter (MID) control the flow within the SETEG-flume. Figure 1 shows a schematic overview of the SETEG-flume with the photogrammetric measuring setup.

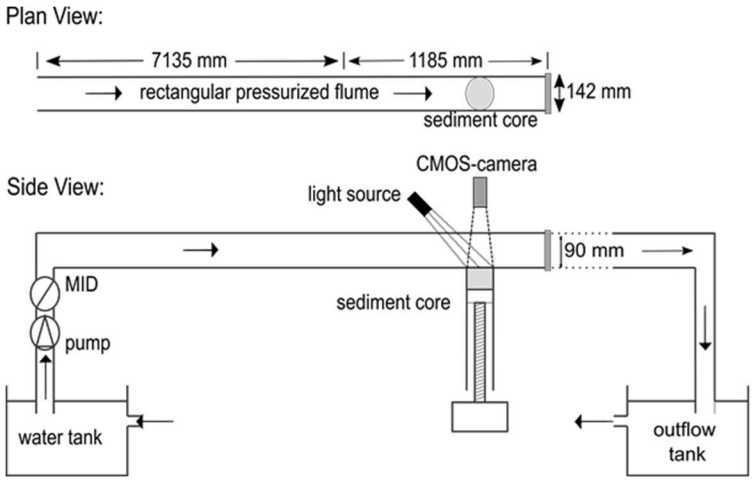

Figure 1. Schematic overview of the SETEG-flume including the experimental setup of PHOTOSED to measure high-resolution erosion rates of cohesive sediments (modified from [22,26,27]).

The measurement of erosion volumes for determining erosion rates considers both bed and suspended load. This represents an advantage compared to devices that determine the erosion rate based solely on suspended load measurements. Several studies showed that bed load could contribute significantly to total erosion [6,13,28]. Within the SETEG-flume, the detection of erosion rates is based on measured erosion volumes in specific time intervals, which depend on the temporal resolution of the CMOS-camera but also on the minimal detectable erosion volume.

PHOTOSED analyzes the displacement of the projected light points for consecutive time-steps that are extracted from continuous image acquisitions of the CMOS-camera. Therefore, an ROI (Region Of Interest) is specified, encompassing a rectangle with a maximum area of 10,426 mm^2 (1600 $\times$ 1300 px), to focus on the center of the circular sediment surface and to minimize boundary effects, such as potential erosions at the transition zones between the sediment surface and the flume bottom. To assess the erosion volume between two consecutive images, a Dense Optical Flow (DOF) algorithm of the OpenCV library (Open Source Computer Vision, OpenCV 2.4.10) is used to evaluate the displacements of the projected light points during the erosion process. In contrast to the method of Lucas and Kanade [29], who used the Lagrange tracking method for optical flow assessment to obtain the movement of certain specific pixels (also known as sparse optical flow), the DOF method, developed by Farnebäck [30], is applied. The DOF method is based on a Eulerian approach considering the potential displacement of all pixels between two consecutive images. Therefore, the algorithm searches for identical features between two consecutive images and within a neighborhood of each pixel to approximate the displacements by a polynomial expansion function. The coefficients of the polynomial function are estimated from a weighted least squares fit to the features of the neighboring block. The scale of the block determines the features to which the algorithm is sensitive. A small displacement of the image portions (blocks) can analytically be determined by changing the coefficients of the polynomial expansion at each pixel. For large displacements, the Farnebäck-algorithm is applied on several image pyramid levels to convert the initial large movement into a detectable movement. To use the Farnebäck-algorithm for erosion experiments, the projected random light points are required to provide image features, which are only related to the local surface position, because erosion may result in the image features continuously changing between two consecutive images. The DOF algorithm is implemented into a Python script (version 2.7.8) for the calculation of the erosion volume by using neighboring blocks that are represented by approximately 35 pixels (based on previous investigations with sizes between 15 px and 70 px). The erosion rates are subsequently calculated by considering the time interval between two consecutive images.

2.3. Calibration and Verification Method

To apply photogrammetric approaches for the assessment of erosion volumes using the proposed setup, an in-depth calibration process is required. This must be done to mitigate the optical distortion due to the different refraction indices of the penetrated media (air, water, and glass) and different optical paths between the observed sediment surface and the camera sensor for all pixels. To this end, a calibration setup was developed consisting of a round panel with three circular test areas of different sizes and known geometry. Screws allow for the precise adjustment of the height in the test area, with a full rotation corresponding to a height adjustment of 0.5 mm. To determine the optical distortion, the test areas were vertically shifted for known lengths resulting in known volumes compared to the planar situation. To cover the whole ROI during the calibration process, the test panel was mounted in four different orientations. With this setup, 2D-polynomial correction functions can be determined to account for the optical distortion in x, y, and z-direction and to convert the results from pixel to metric scale.

Figure 2A shows an image of the CMOS-camera including the round panel with the three different test areas, the projected light points, and the ROI. Figure 2B–D exemplary represents a visualization of the DOF algorithm for each test area. For all experiments the camera properties were identical (focal distance: 6.0 mm, aperture: 8, shutter speed: 100–300 ms according to the reflectivity of the sediment surface).

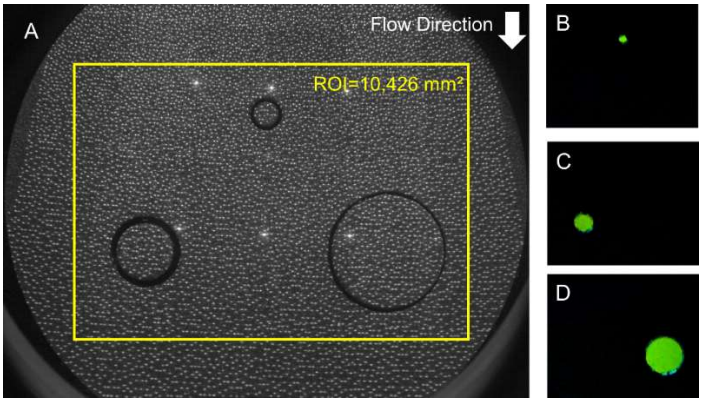

Figure 2. Image of the CMOS-camera showing the round panel of the calibration setup with three different test areas (**A**). Exemplary visualization of the DOF algorithm for each test area, the color represents the drop of the test areas (**B**–**D**).

The projected light pattern in Figure 2A is not uniformly distributed over the ROI due to the angled mounting of the semiconductor laser. This results in a higher point density in the upper part of the ROI and a lower point density in the lower part of the ROI. However, given the high total number of projected points (24,000), the influence on the spatial resolution is only marginal. One projected light point corresponds to 3–6 pixel in diameter depending on the position of the light point. However, the size in pixels for each projected light point is not affecting the accuracy of PHOTOSED because the DOF algorithm detects the displacement of characteristic patterns that consist of several light points. The exemplary visualization of the results of the DOF algorithm (Figure 2B–D) represents the spatial detection of elevation changes for the three different test areas with respect to their initial elevation level. Especially at the edges of the test areas, some imprecise detections can be observed because high gradients of elevation changes may cause erroneous displacement calculations. This impreciseness is also influenced by the chosen block size for the DOF algorithm of 35 px. However, previous investigations showed that a larger block size would degrade the spatial detection for small areas, and a smaller block size would result in a higher noise due to erroneous detections and in a limitation for detecting high surface gradients. For the calibration and

verification of PHOTOSED, the test areas were shifted vertically, which represents in this context a worst-case scenario.

3. Results and Discussion

3.1. Calibration and Verification

To determine the calibration factors in *x*-, *y*- and *z*-direction due to the optical distortion, the three test areas of the calibration panel were stepwise decreased, and the positions were photogrammetrically recorded. To account for different vertical positions, seven positions were measured at a step interval of dz = 0.5 mm. In a second calibration, four vertical positions were measured at a step interval of dz = 1.0 mm. In addition, the orientation of the calibration panel was changed four times to test the influence of the non-uniformly projected light pattern. In total, this calibration concept resulted in 84 different measurements for dz = 0.5 mm (seven vertical positions) and 48 measurements for dz = 1.0 mm (four vertical positions).

For the longitudinal and lateral directions (*x*- and *y*-component), the distortion is nearly symmetrical because of the centered vertical mounting of the camera above the ROI. The mean calibration factor in *x*-direction is dx = 69.2 µm/px, with a standard deviation of σ_x = 0.9 µm/px, while in the *y*-direction the mean calibration factor yields dy = 69.6 µm/px and a standard deviation of σ_y = 1.49 µm/px. Given the symmetry, an equal calibration factor of 69.4 µm/px, with the standard deviation of σ_{xy} = 1.25 µm/px, was chosen for the following procedure.

For the correction in *z*-direction, a 2D-polynomial function is required because of the angled mounting of the semiconductor laser. Figure 3 shows the spatial variation of the calibration factor in *z*-direction for the entire ROI.

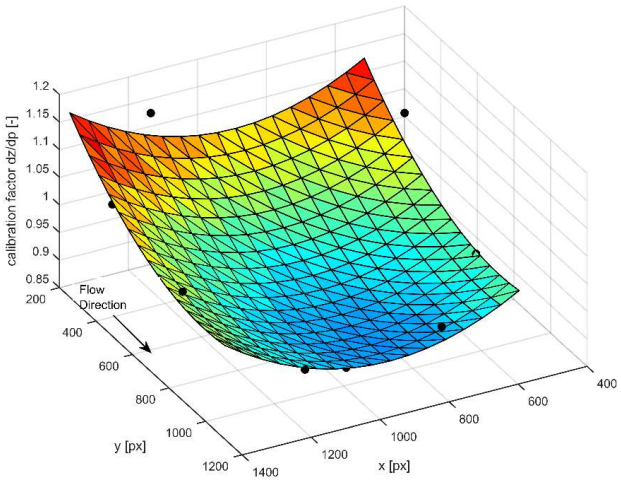

Figure 3. Calibration factor for the vertical scaling from pixel into metric scale of the distorted camera images. The plotted points (n = 12) represent the measurements while the mesh represents their spatial interpolation.

The mean calibration factor in *z*-direction is dz = 111.5 µm/px with a standard deviation of σ_z = 10.3 µm. This calibration factor needs to be multiplied with the position-dependent correction factors in Figure 3 to obtain the correct displacement in the *z*-direction.

3.2. Accuracy of PHOTOSED

Figure 4 represents the measuring accuracy after an incremental shift of the three different test areas of dz = 0.5 mm (Figure 4A) and dz = 1.0 mm (Figure 4B).

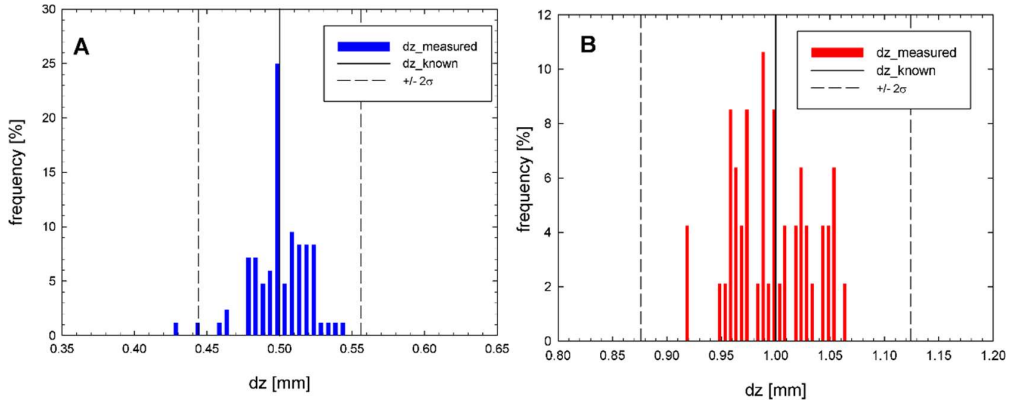

Figure 4. Vertical measuring accuracy of PHOTOSED for given incremental vertical shifts of dz = 0.5 mm (**A**) and dz = 1.0 mm (**B**). The dashed lines represent the median ± the doubled standard deviation (± 2σ).

For Figure 4A, a total of 84 measuring values were evaluated against the known vertical incremental shift of dz = 0.5 mm (in seven vertical positions). 95.45% of all values (2σ) show a deviation of less than 0.028 mm. In Figure 4B, a total of 48 measuring points were evaluated for an incremental shift of dz = 1.0 mm (in four vertical positions) leading to a doubled standard deviation of 2σ = 0.062 mm. Although the doubled standard deviation for a vertical incremental shift of dz = 1.0 mm is higher compared to the vertical shift of dz = 0.5 mm indicating a higher scattering of the obtained data, the relative accuracy (dz/2σ) remains constant. Hence, only the absolute accuracy is affected. The higher scattering results from the angled mounting of the semiconductor laser leading to obscuring and hiding effects regarding projected light points at the boundaries of the displaced area. This effect becomes larger for more pronounced erosion depths. However, the occurred erosion depth between two consecutive images for investigations on sediment surfaces can be subdivided into intermediate stages by shortening the time interval between the two consecutive images given the high temporal resolution of the CMOS-camera (10 Hz).

These measuring results prove the applicability of PHOTOSED for highly accurate measurements of vertical changes based on the DOF algorithm and the applied calibration method.

Figure 5 illustrates the comparison between all predefined and measured volumes with PHOTOSED over several orders of magnitude.

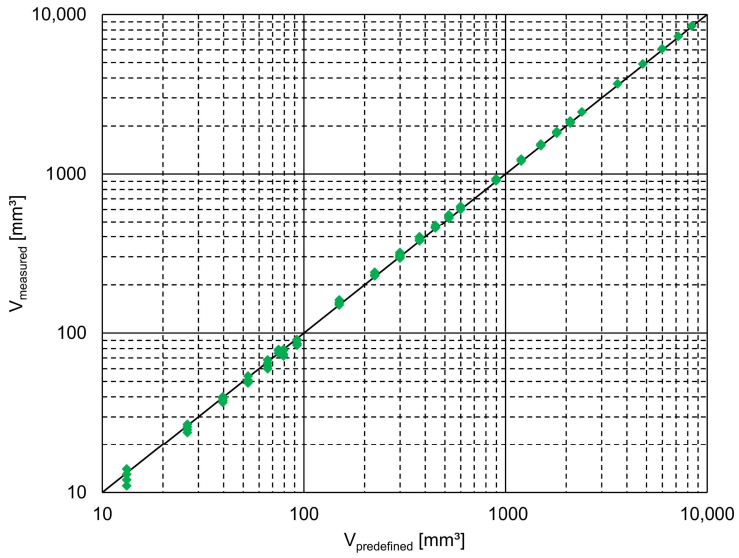

Figure 5. Comparison between photogrammetrically determined volumes against predefined volumes using the three different test areas.

Figure 5 demonstrates the applicability of PHOTOSED for volumes comprising several orders of magnitude ranging from 13 to 8476 mm^3. The mean absolute deviation between photogrammetrically determined volumes to the predefined volumes is 3.24%.

Figure 5 also indicates the lower limits and minimal detectable erosion volumes. For the lowest investigated volume of V = 13 mm^3, the mean absolute deviation reaches a maximum value of 9.2%. This lower detection limit is a result of the point density of the projected light pattern and the required specification of the block size for the DOF algorithm (35 px). The DOF algorithm requires several projected light points for a correct pattern detection; hence, the spatial resolution depends directly on the density of the projected light points. This is predominantly affecting the accuracy on the edges of surface changes. Accordingly, the larger the edges are in comparison to the surface size, the higher the inaccuracy, resulting in a lower detection limit.

Since the erosion of cohesive sediments is highly dynamic and complex, it is often described as a stochastic process given the turbulent nature of flow (e.g., [8]), and the immense number of involved parameters and processes (e.g., [10,11]). The resulting erosion rates can easily vary by several orders of magnitude for the same flow rates [9,26,31]. In this context, the developed photogrammetric method PHOTOSED represents a novel and high-resolution measuring concept to resolve this huge variability of erosion rates for cohesive sediments and offers a wide range of opportunities to perform in-depth investigations of the erosion phenomena of cohesive sediments, or non-cohesive/cohesive sediment mixtures.

3.3. Exemplary Erosion Experiments

After the successful calibration and verification of PHOTOSED, two erosion experiments for one sediment surface, consisting of a cohesive/non-cohesive mixture and two different flow conditions (Q_1 = 7.5 L/s, Q_2 = 11.3 L/s), were conducted to demonstrate the spatial resolution of the photogrammetric approach and to show the spatial and temporal heterogeneity of the measured erosion rates. The particle size distribution of the sediment surface consisted of 8% clay, 83% silt and 9% sand, while the wet bulk density was 1.42 g/cm^3. The flow rates correspond to Reynolds shear stresses of 0.7 Pa (Re = 64,500) and 1.3 Pa (Re = 97,400), respectively. The sediment surface was exposed to the two flow rates for a total time of 600 s each and consecutive images were captured in a temporal resolution of 1.0 s. Figure 6 shows three dimensional plots of the sediment surface at the end of both erosion experiments (t = 600 s) for a flow of Q_1 = 7.5 L/s and Q_2 = 11.3 L/s, respectively.

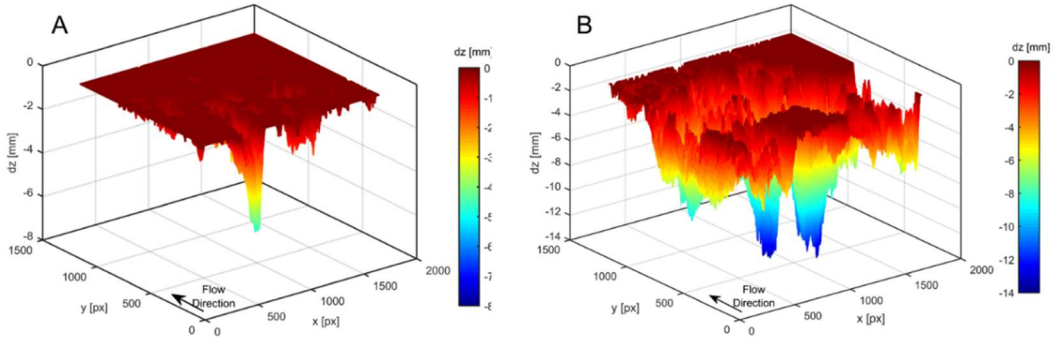

Figure 6. Three-dimensional plots of the sediment surfaces at the end of the erosion experiments after t = 600 s for Q_1 = 7.5 L/s (**A**) and Q_2 = 11.3 L/s (**B**).

The heterogeneity of the occurred erosion is clearly visible for both erosion experiments. For a discharge of Q_1 = 7.5 L/s (Figure 6A) one erosion peak located at the edge of the ROI is observed, indicating a large local erosion. The surrounding smaller erosion peaks are presumably a result of the adjacent erosion peak at the edge of the ROI, which leads to local changes in the topography and roughness. Other areas of the ROI are not eroded at all. For Q_2 = 11.3 L/s (Figure 6B) the erosion is further

developed, showing a second peak with large erosion and a spatial distribution of medium erosion. However, some areas of the surface remain stable without any erosion. Moreover, it becomes obvious that the roughness of such a structured surface will change compared to the initial surface and, consequently, the local shear stresses to which the sediments are exposed to during the erosion experiment.

To quantify the variability of erosion rates of the sediment surface over time, during both erosion experiments, box plots are derived for each pixel ($n = 1.9 \times 10^6$) showing the erosion rates for time intervals of 30 s (Figure 7).

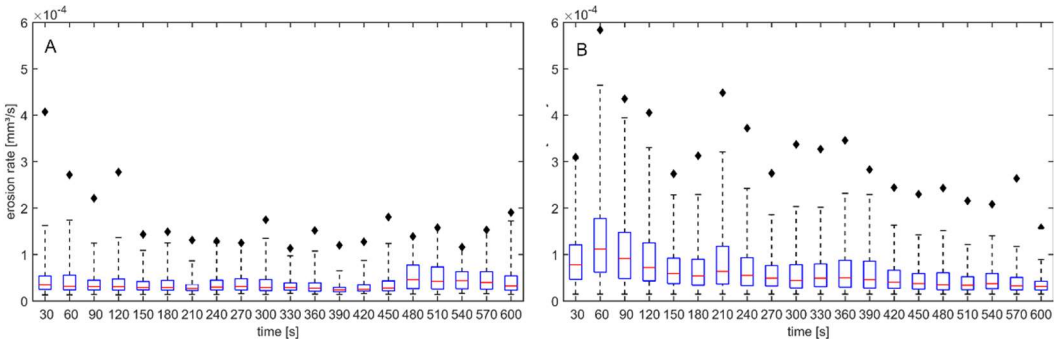

Figure 7. Variability of erosion rates for time intervals of t = 30 s throughout the entire erosion experiments for Q_1 = 7.5 L/s (**A**) and Q_2 = 11.3 L/s (**B**).

In the box plots of Figure 7, the red line for each time-step represents the median value of erosion rates while the bottom and top edges indicate the interquartile range (25th and 75th percentiles) and the whiskers extend to 99.9th percentiles. The filled diamonds represent the maximum measured erosion rate per each time interval of 30 s. For the erosion experiment with Q_1 = 7.5 L/s (Figure 7A), the median of the erosion rates varies between 0.24×10^{-4} mm^3/s and 0.46×10^{-4} mm^3/s, which represents almost a factor of two. The maximum value yields 4.1×10^{-4} mm^3/s during the beginning of the experiment at t = 30 s, when the sediments are first exposed to the flow. However, parts of the sediment surface show no erosion at all. The variability of the erosion rates within each time interval is even higher. Therefore, the median is compared to the maximum values as a criterion for the degree of variability, leading to factors from 2.7 (minimum at t = 540 s) to 11 (maximum at t = 30 s), with a mean value of 5.6, which indicates an extremely high heterogeneity of the obtained erosion rates.

The erosion experiment with Q_2 = 11.3 L/s (Figure 7B) shows, as expected, higher erosion rates with median values ranging from 0.31×10^{-4} to 1.12×10^{-4} mm^3/s. The maximum value for the entire experimental duration is 5.84×10^{-4} mm^3/s (t = 60 s). The minimum variability within one time interval results in a factor of 4.0 at t = 30 s, while the maximum variability yields a factor of 8.1 at t = 570 s. The mean variability yields a value of 6.1 and is slightly higher compared to the erosion experiment with Q_1 = 7.5 L/s.

Both erosion experiments show a high spatial heterogeneity regarding the measured erosion rates. Moreover, it proves that the peak erosion rates occur only very locally (outside the 99.9th percentile) emphasizing the need for high-resolution measurements of erosion rates.

Another strength of PHOTOSED with its high-resolution measurements is the feasibility for detailed investigations of the temporal erosion progress and the eventual formation of erosion patterns over time.

Figure 8A–F show the erosion progress (x-y-plane) for six selected time-steps (Δt = 100 s) of the erosion experiment with a flow rate of Q_2 = 11.3 L/s.

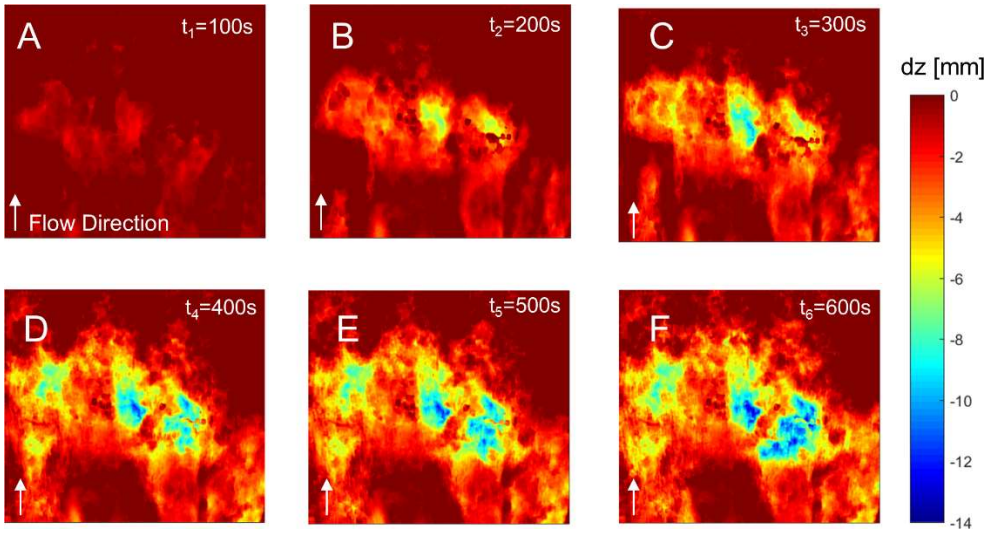

Figure 8. Temporal erosion progress of the erosion experiment with Q_2 = 11.3 L/s (*x*-*y*-plane) at six selected time-steps (Δt = 100 s).

Next to the variability of erosion rates, the visualized erosion progress in Figure 8A–F shows a continuously growing erosion pattern. The locations of initial erosion (Figure 8A) become larger and deeper over time (Figure 8B–F) indicating a relationship between erosion, surface roughness, and hydraulic forces. The local changes of the surface may lead to local peaks of turbulent fluctuations that result in different formations of erosion patterns. Although the selected time-step in Figure 8 is 100 s, the currently used CMOS-camera is capable for temporal resolutions up to 10 Hz, allowing for deeper analysis of the progressive erosion patterns of cohesive sediments, or non-cohesive/cohesive sediment mixtures.

4. Conclusions

A novel and high-resolution photogrammetric approach for the detection of erosion rates for cohesive sediments, or non-cohesive/cohesive sediment mixtures, has been introduced (PHOTOSED). The method allows for detailed insights in the erosion phenomena of both cohesive sediments and non-cohesive/cohesive sediment mixtures. The experimental setup uses a semiconductor laser with a diffraction optic to project a pseudo-random pattern of light points on a sediment surface, a CMOS-camera for image acquisition, and a dense optical flow (DOF) algorithm with the OpenCV library that evaluates the displacements of the light points of two consecutive images during the erosion process to assess the erosion volume. The calibration and verification procedure showed that the PHOTOSED method allows the detection of erosion volumes for several orders of magnitude with a minimum detection limit of approx. 15 mm^3 and enabling high-resolution measurements of erosion rates, as well as in-depth investigations of the erosion behavior of cohesive sediments and cohesive/non-cohesive sediment mixtures. One limitation is the shading of projected light points in cases of instantaneous and severe erosion depths with nearly vertical gradients given to the angled mounting of the semiconductor laser. However, the DOF algorithm returns an erosion volume based on two consecutive images for a selected time interval. This erosion volume and thus the occurred erosion depth can be subdivided into intermediate erosion stages by shortening the time interval between these two consecutive images given the high temporal resolution of the CMOS-camera (10 Hz).

The PHOTOSED method was subsequently applied to a sediment surface consisting of a cohesive/non-cohesive sediment mixture at two different flow rates. The results identify a high variability of the erosion rates within time intervals of 30 s and variability factors up to 10 between the median erosion rate and the maximum erosion rate. The high variability of erosion rates distributed over the entire sediment surface emphasizes the need to study the erosion phenomena of cohesive

sediments, or cohesive/non-cohesive sediment mixtures, in detail using high-resolution measurements. Although the sediment characteristics can significantly influence the dimensions of erosion rates, they are not limiting the accuracy of PHOTOSED because the method is based on the detection of erosion volumes, which also represents an advantage compared to devices working with suspended load measurements for the detection of erosion rates. However, if the erosion rates are related to hydraulic forces in form of shear stresses, the overall erosion pattern should not be too pronounced because of the influence of changing roughness on local hydraulics.

The high spatial and temporal resolution of PHOTOSED allows for the detection of different erosion patterns providing a high potential for further research including e.g., detailed studies of the interactions at the water-sediment interface or the unraveling of the complex interactions of physical, chemical and biological variables that are involved in determining the erosion stability. In addition, many practical issues in terms of sediment management in rivers, navigation channels, harbors or reservoirs can be addressed.

Author Contributions: The manuscript was written by M.N. with support of all co-authors. G.S. wrote the Python-Script to apply the DOF algorithm and did the calibration and verification experiments. F.B. and S.H. contributed by analyzing the spatial and temporal variability of the erosion processes. S.W. reviewed and edited the manuscript.

Acknowledgments: The authors gratefully acknowledge the assistance of undergraduate research assistants for their support during field measurements and data analyses. In addition, the authors express their sincere thanks to Caleb Inskeep for reviewing the script and language editing. The authors also gratefully acknowledge the financial support from the Water and Shipping Authority in Freiburg (WSA Freiburg), the German Federal Institute for Hydrology, and the Ministry of Science, Research and Arts in Baden-Württemberg, Germany. We also would like to acknowledge the anonymous reviewers for the valuable feedbacks.

Conflicts of Interest: The authors declare no conflict of interest.

References

1. Mirtskhoulava, T.E. Scouring by flowing water of cohesive and noncohesive beds. *J. Hydraul. Res.* **1991**, *29*, 341–354. [CrossRef]
2. Kothyari, U.C.; Jain, R.K. Erosion characteristics of cohesive sediment mixtures. In *River Flow 2010: Proceedings of the 5th International Conference on Fluvial Hydraulics (Vol. 1); Braunschweig, Germany, 8–10 September 2010*; Bundesanstalt für Wasserbau: Karlsruhe, Germany, 2010.
3. Wu, W.; Perera, C.; Smith, J.; Sanchez, A. Critical shear stress for erosion of sand and mud mixtures. *J. Hydraul. Res.* **2017**, *56*, 1–15. [CrossRef]
4. Paterson, D.M.; Black, K.S. Water flow, sediment dynamics and benthic biology. *Adv. Ecol. Res.* **1999**, *29*, 155–196. [CrossRef]
5. Parchure, T.M.; Mehta, A.J. Erosion of Soft Cohesive Sediment Deposits. *J. Hydraul. Eng.* **1985**, *111*, 1308–1326. [CrossRef]
6. Mitchener, H.; Torfs, H. Erosion of mud/sand mixtures. *Coast. Eng.* **1996**, *29*, 1–25. [CrossRef]
7. Sanford, L.P.; Maa, J.P.-Y. A unified erosion formulation for fine sediments. *Mar. Geol.* **2001**, *179*, 9–23. [CrossRef]
8. Van Prooijen, B.C.; Winterwerp, J.C. A stochastic formulation for erosion of cohesive sediments. *J. Geophys. Res.* **2010**, *115*, C01005. [CrossRef]
9. Walder, J.S. Dimensionless erosion laws for cohesive sediment. *J. Hydraul. Eng.* **2015**, *142*. [CrossRef]
10. Zhu, Y.; Lu, J.; Liao, H.; Wang, J.; Fan, B.; Yao, S. Research on cohesive sediment erosion by flow: An overview. *Sci. China Ser. E Technol. Sci.* **2008**, *51*, 2001–2012. [CrossRef]
11. Berlamont, J.; Ockenden, M.; Toorman, E.; Winterwerp, J.C. The characterisation of cohesive sediment properties. *Coast. Eng.* **1993**, *21*, 105–128. [CrossRef]
12. Black, K.S.; Tolhurst, T.J.; Paterson, D.M.; Hagerthey, S.E. Working with natural cohesive sediments. *J. Hydraul. Eng.* **2002**, *128*, 2–8. [CrossRef]
13. Aberle, J.; Nikora, V.; Walters, R. Effects of bed material properties on cohesive sediment erosion. *Mar. Geol.* **2004**, *207*, 83–93. [CrossRef]

14. Gerbersdorf, S.U.; Jancke, T.; Westrich, B. Physico-chemical and biological sediment properties determining erosion resistance of contaminated riverine sediments—Temporal and vertical pattern at the lauffen reservoir/river neckar, Germany. *Limnol.-Ecol. Manag. Inland Waters* **2005**, *35*, 132–144. [CrossRef]
15. Grabowski, R.C.; Droppo, I.G.; Wharton, G. Erodibility of cohesive sediment: The importance of sediment properties. *Earth-Sci. Rev.* **2011**, *105*, 101–120. [CrossRef]
16. Mehta, A.J.; Partheniades, E. Resuspension of deposited cohesive sediment beds. *Coast. Eng. Proc.* **1982**, *1*, 1569–1588.
17. Aberle, J. Measurement techniques for the estimation of cohesive sediment erosion. In *Hydraul. Methods for Catastrophes: Floods, Droughts, Environmental Disasters*; Rowiński, P.M., Ed.; Publications of the Institute of Geophysics, Polish Academy of Sciences: Warsaw, Poland, 2008; Volume 406, pp. 5–20.
18. Maa, J.P.-Y.; Wright, L.D.; Lee, C.-H.; Shannon, T.W. VIMS sea carousel: A field instrument for studying sediment transport. *Mar. Geol.* **1993**, *115*, 271–287. [CrossRef]
19. Bale, A.J.; Widdows, J.; Harris, C.B.; Stephens, J.A. Measurements of the critical erosion threshold of surface sediments along the Tamar Estuary using a mini-annular flume. *Cont. Shelf Res.* **2006**, *26*, 1206–1216. [CrossRef]
20. McNeil, J.; Taylor, C.; Lick, W. Measurements of erosion of undisturbed bottom sediments with depth. *J. Hydraul. Eng.* **1996**, *122*, 316–324. [CrossRef]
21. Roberts, J.D.; Jepsen, R.A.; James, S.C. Measurements of sediment erosion and transport with the adjustable shear stress erosion and transport flume. *J. Hydraul. Eng.* **2003**, *129*, 862–871. [CrossRef]
22. Noack, M.; Gerbersdorf, S.U.; Hillebrand, G.; Wieprecht, S. Combining field and laboratory measurements to determine the erosion risk of cohesive sediments best. *Water* **2015**, *7*, 5061–5077. [CrossRef]
23. Wan, C.F.; Fell, R. Investigation of rate of erosion of soils in embankment dams. *J. Geotech. Geoenviron. Eng.* **2004**, *130*, 373–380. [CrossRef]
24. Gust, G.; Muller, V. Interfacial hydrodynamics and entrainment functions of currently used erosion devices. In *Cohesive Sediments*; Burt, N., Parker, R., Watts, J., Eds.; John Wiley & Sons, Ltd.: Chichester, UK, 1997; pp. 149–174.
25. Tolhurst, T.J.; Black, K.S.; Paterson, D.M.; Mitchener, H.J.; Termaat, G.R.; Shayler, S.A. A comparison and measurement standardisation of four in situ devices for determining the erosion shear stress of intertidal sediments. *Cont. Shelf Res.* **2000**, *20*, 1397–1418. [CrossRef]
26. Witt, O.; Westrich, B. Qunatification of erosion rates for undistrubed contaminated cohesive sediment cores by image analysis. *Hydrobiologia* **2003**, *494*, 271–276. [CrossRef]
27. Kern, U.; Haag, I.; Schürlein, V.; Holzwarth, M.; Westrich, B. Ein strömungskanal zur ermittlung der tiefenabhängigen erosionsstabilität von gewässersedimente. *Wasserwirtschaft* **1999**, *89*, 72–77.
28. Debnath, K.; Nikora, V.; Aberle, J.; Westrich, B.; Muste, M. Erosion of cohesive sediments resuspension, bed load, and erosion patterns from field experiments. *J. Hydraul. Eng.* **2007**, *133*, 508–520. [CrossRef]
29. Lucas, B.D.; Kanade, T. An iterative image registration technique with an application to stereo vision. In Proceedings of the 7th International Joint Conference on Artificial Intelligence, Vancouver, BC, Canada, 24–28 August 1981.
30. Farnebäck, G. Two-frame motion estimation based on polynomial expansion. In *Image Analysis*; Lecture Notes in Computer Science; Springer: Berlin, Heidelberg, 2003; pp. 363–370.
31. Noack, M.; Hillebrand, G.; Seidenkranz, U.; Wieprecht, S. Investigation on the erosion stability of cohesive sediment deposits in the weir channel of the barrage Iffezheim, river rhine. *Hydrol. Wasserbewirtsch.* **2016**, *60*, 164–175. [CrossRef]

Publication III.

High spatio-temporal resolution measurements of cohesive sediment erosion

Table 5.3. Metadata of publication III

Title	High spatio-temporal resolution measurements of cohesive sediment erosion
Authors	**Felix Beckers**, Caleb Inskeep, Stefan Haun, Gerhard Schmid, Silke Wieprecht and Markus Noack
Journal	Earth Surface Processes and Landforms
submitted	December 23, 2018
accepted	May 1, 2020
published	May 9, 2020 (online)
DOI	https://doi.org/10.1002/esp.4889

EARTH SURFACE PROCESSES AND LANDFORMS
Earth Surf. Process. Landforms , (2020)

Published online in Wiley Online Library
(wileyonlinelibrary.com) DOI: 10.1002/esp.4889

High spatio-temporal resolution measurements of cohesive sediment erosion

Felix Beckers,[1]* Caleb Inskeep,[1] Stefan Haun,[1] Gerhard Schmid,[1] Silke Wieprecht[1] and Markus Noack[1,2]
[1] Institute for Modelling Hydraulic and Environmental Systems, Department of Hydraulic Engineering and Water Resources Management, University of Stuttgart, Pfaffenwaldring 61, Stuttgart 70569, Germany
[2] Faculty of Architecture and Civil Engineering, Karlsruhe University of Applied Science, Moltkestrasse 30, Karlsruhe 76133, Germany

Received 23 December 2018; Revised 29 April 2020; Accepted 1 May 2020

*Correspondence to: Felix Beckers, Institute for Modelling Hydraulic and Environmental Systems, Department of Hydraulic Engineering and Water Resources Management, University of Stuttgart, Pfaffenwaldring 61, 70569 Stuttgart, Germany. E-mail: felix.beckers@iws.uni-stuttgart.de

ESPL
Earth Surface Processes and Landforms

ABSTRACT: In this study, we present a novel approach to measure fundamental processes of cohesive sediment erosion. The experimental setup consists of a laboratory erosion flume (SETEG) and a photogrammetric method to detect sediment erosion (PHOTOSED). Detailed data are presented for three erosion experiments, which were conducted with a natural non-cohesive/cohesive sediment mixture at increasing sediment depths (4, 8, 16 cm). In each experiment, the sediment was exposed to a set of incrementally increasing shear stresses and the erosion was measured dynamically, pixel-based, and approximate to the process scale given the resolution of PHOTOSED. This enables us to distinguish between (i) individual emerging erosion spots caused by surface erosion and (ii) large holes torn open by detached aggregate chunks. Moreover, interrelated processes were observed, such as (iii) propagation of the erosion in the longitudinal and lateral direction leading to merging of disconnected erosion areas and (iv) progressive vertical erosion of already affected areas. By complementing the (bulk) erosion volume profiles with additional quantitative variables, which contain spatial information (erosion area, specific deepening, number of disconnected erosion areas), conclusions on the erosion behaviour (and the dominant processes) can be drawn without requiring qualitative information (such as visual observations). In addition, we provide figures indicating the spatio-temporal erosion variability and the (bulk) erosion rates for selected time periods. We evaluate the variability by statistical quantities and show that significant erosion is mainly confined to only a few events during temporal progression, but then considerably exceeds the time-averaged median of the erosion (factors between 7.0 and 16.0). Further, we point to uncertainties in using (bulk) erosion rates to assess cohesive sediment erosion and particularly the underlying processes. As a whole, the results emphasise the need to measure cohesive sediment erosion with high spatio-temporal resolution to obtain reliable and robust information. © 2020 The Authors. Earth Surface Processes and Landforms published by John Wiley & Sons Ltd

KEYWORDS: PHOTOSED; SETEG; cohesive sediments; non-cohesive/cohesive sediment mixtures; photogrammetric measurements; spatio-temporal erosion variability

Introduction

Detailed knowledge regarding the erodibility and erosion behaviour of cohesive sediments and non-cohesive/cohesive sediment mixtures is of particular importance for many engineering and ecological applications. Consequently, many studies investigate the influence of sediment characteristics and the eroding fluid on the erodibility of cohesive sediments and non-cohesive/cohesive sediment mixtures, or intend to approximate these relationships mathematically (e.g. Gularte *et al.*, 1980; Mehta and Partheniades, 1982; Raudkivi and Tan, 1984; Berlamont *et al.*, 1993; Mitchener and Torfs, 1995; Panagiotopoulos *et al.*, 1997; Black *et al.*, 2002; Tolhurst *et al.*, 2006; Gerbersdorf *et al.*, 2007; Righetti and Lucarelli, 2007; Mostafa *et al.*, 2008; Noack *et al.*, 2015; Perera and Wu, 2016; Wu *et al.*, 2018). Although sizeable progress has been made in uncovering relations between sediment properties and erodibility (Grabowski *et al.*, 2011), cohesive sediment erosion has not yet been fully understood.

In order to improve this understanding, more reliable laboratory and field data are needed (e.g. Zhu *et al.*, 2008; Grabowski *et al.*, 2011; Wu, 2016). This demand can be met with ongoing experimental research using various existing erosion devices. An overview on available *in-situ* devices and measurement techniques can be found in Black and Paterson (1997) and Aberle (2008), who make a classification from recirculating flumes, flow-through flumes, and other miscellaneous devices. Examples of miscellaneous devices include jet-testing apparatuses (Hanson and Cook, 2004) and cohesive strength meters (Paterson, 1989). The erosion flumes can be further subdivided into straight open flumes, closed tunnels, and annular flumes,

[Correction added on 30 June 2020 after first online publication: the formatting of Table 3 has been amended, and the overbar and tilde symbols have been corrected in Table 4 and the caption of Figure 2 in this version.]

which have been used for field experiments but are also used for laboratory investigations as well (e.g. Wu *et al.*, 2018). While an advantage of *in-situ* devices is that they can be operated over undisturbed beds (Black and Paterson, 1997) where non-disturbing placement is possible, their disadvantage is that they can only be used to erode surface sediment layers (Noack *et al.*, 2015). However, many engineering and ecological issues require depth-dependent information on the erodibility of sediments, such as the assessment of the vertical erosion risk of buried contaminated sediments (e.g. McNeil *et al.*, 1996; Gerbersdorf *et al.*, 2007) or the assessment of the vertical erosion potential of reservoir deposits (e.g. Beckers *et al.*, 2018). To serve this purpose, laboratory flumes have been developed and applied to measure the depth-dependent erosion behaviour (e.g. McNeil *et al.*, 1996; Kern *et al.*, 1999; Briaud *et al.*, 2001; Lick and McNeil, 2001; Roberts *et al.*, 2003; Righetti and Lucarelli, 2007; Jacobs *et al.*, 2011; Kimiaghalam *et al.*, 2016). Their design follows a general principle: sediment core samples are locked into an erosion channel from below. The sediment is then slowly raised into the current and the time to erode the protruding sediment is measured to provide a bulk erosion rate (i.e. the bed elevation changes over time). The sediment response to changing flow conditions is tested, eventually results in a set of erosion rates as a function of flow, and standard methods are used to calculate the corresponding shear stress (Walder, 2016).

Many of the existing erosion devices, both *in-situ* and laboratory devices, use optical backscatter sensors to measure suspended-sediment concentration during erosion experiments, which is then used to calculate the resuspension rate (e.g. Mehta and Partheniades, 1982; Amos *et al.*, 1992; Black *et al.*, 2002; Aberle, 2008; Droppo *et al.*, 2015). The disadvantage of the latter is that the resuspension rate cannot necessarily be equated with the erosion rate, due to the fact that the bed load may contribute to cohesive sediment erosion, especially when dealing with non-cohesive/cohesive sediment mixtures (Mitchener and Torfs, 1995; Roberts *et al.*, 2003; Aberle *et al.*, 2004; Debnath *et al.*, 2007; Wu, 2016). Thus, recent studies have aimed to address this point by complementary measurements, including bed load traps or bed elevation monitoring (e.g. Roberts *et al.*, 2003; Debnath *et al.*, 2007; Jacobs *et al.*, 2011; Ye *et al.*, 2011). However, even if resuspension rates are complemented with additional bed load measurements, they result in a bulk erosion rate with respect to the available measuring area, although cohesive sediment erosion is described as a highly dynamic process due to the temporal and spatial variability of naturally composed sediments (Black *et al.*, 2002; Gerbersdorf *et al.*, 2007; Aberle, 2008). Further, the non-uniformity of natural sediments results in variable bed shear strength and, in combination with the turbulent characteristic of flow, a random behaviour is induced during erosion (e.g. Van Prooijen and Winterwerp, 2010; Schäfer Rodrigues Silva *et al.*, 2018).

Following non-cohesive erosion modes, two principle modes of cohesive sediment failure are typically described in the literature: surface erosion and mass erosion. While the first is characterised by particle or floc erosion of surficial sediments triggered by the fact that the shear strength is locally exceeded by the flow forces, the latter is the response of the bed to a dynamic shear load (Mehta and Partheniades, 1982), resulting in the erosion of clusters or lumps of aggregates (Zhu *et al.*, 2008) or even in the erosion of layers due to bed failure along planes (Wu *et al.*, 2018). Mehta and Partheniades (1982) identified two main erosion types, referred to as *Type I* and *Type II*, through an interpretation of time–concentration profiles of bulk resuspension rates. They differ in that under constant shear stress over time, *Type I* erosion asymptotically decreases and approaches a constant value, whereas *Type II* erosion does not. The cause of this behaviour is the vertical stratification of a sediment bed, and either uniform or non-uniform bed shear strength over depth. This is why these erosion types are also classified as depth-limited or supply-limited erosion (*Type I*) and steady-state or unlimited erosion (*Type II*) (e.g. Parchure and Mehta, 1985; Aberle, 2008; Van Prooijen and Winterwerp, 2010). However, the transition between these erosion types might be smooth and does not allow for a clear distinction (Grabowski *et al.*, 2011). Consequently, complementary descriptions can be found that combine features of both types (e.g. Amos *et al.*, 1992; Debnath *et al.*, 2007; Aberle, 2008). Yet, all these erosion types describe a bulk erosion effect and do not make a distinction between the underlying erosion processes, although specific erosion forms have been visually observed in studies on cohesive sediments.

McNeil *et al.* (1996) report that, during erosion, individual particles are entrained before chunks of sediment are plucked from the surface, leaving holes or pits behind. Righetti and Lucarelli (2007) observe a multistep entrainment phenomenon and distinguish between a sporadic, discontinuous motion of relatively small aggregates, followed by an increasing number of primary particle aggregates, coupled with the sporadic entrainment of larger aggregates. Finally, a gradual enhancement of floc entrainment is observed, until an abrupt change in the erosive process takes place, which is described as a sudden increase in quantity and size of the eroded flocs. Kothyari and Jain (2008) describe the entrainment of clumps and layers, and identify three stages of initiation of motion: pothole, line, and mass erosion.

Although a considerable variety of experimental studies can be found in the literature, very little information is available on measurement technology that is capable of resolving the spatial and temporal variability of the cohesive erosion process (see Tolhurst *et al.*, 2006; Van Prooijen and Winterwerp, 2010). However, high-resolution measurement data are a pending requirement when it is intended to objectively assess the highly variable erosion progress of cohesive sediments. In this context, dynamically measured erosion caused by specific erosion forms could help to increase knowledge on the fundamental as well as interacting processes.

In this study, we propose a novel approach based on high-resolution photogrammetric measurements for detailed investigations of cohesive sediment erosion, including quantitative evaluations of the spatio-temporal erosion variability. First, we introduce our apparatus, consisting of an erosion flume (SETEG) and a photogrammetric method to detect sediment erosion (PHOTOSED). This includes the hydraulic characterisation of the flume and the derivation of the measurement variables provided by PHOTOSED. Next, we show for three experiments a selection of the spatio-temporal erosion progress, illustrate the ability of our approach to identify fundamental erosion processes caused by specific erosion forms, and present the full temporal development of erosion profiles containing spatial information. We narrow these results down to characteristic changes in the erosion behaviour, assess the spatio-temporal erosion variability by statistical quantities, and present the erosion rates derived from the volumetric measurements. Finally, we critically discuss our results and the key findings of this study. We expect that obtaining high spatio-temporal resolution data will help in identifying the fundamental erosion processes and eventually increase our knowledge on the erosion of cohesive sediments and non-cohesive/cohesive sediment mixtures.

Materials and Methods

SETEG erosion flume

The SETEG erosion flume (*erosion flume to determine the depth-dependent erosion stability of aquatic sediments*) is

located at the Institute for Modelling Hydraulic and Environmental Systems (IWS, University of Stuttgart). It is a straight, rectangular, and closed flume to measure critical shear stresses and erosion rates of sediments over depth. The flume is operated under pressurized flow (Kern *et al.*, 1999) and has been continuously developed further to address challenges in sediment research (Witt and Westrich, 2003; Noack *et al.*, 2015, 2018). The setup of the SETEG-erosion flume is presented in Figure 1. The dimensions are as follows: length 8.00 m, width 0.142 m, and height 0.10 m (inner dimensions). The flow is measured with a magnetic flow meter (MFM, Endress+Hauser, Promag 50W1F DN150, error $\leq$ 0.5%) and can be controlled by the operator to investigate flow rates from 1 up to 65 l s^{-1}. The measuring section consists of a circular opening in the flume bottom where sediment cores with diameters between 100 and 135 mm can be locked in position. The centre of the measuring section is located 7.64 m downstream of the inflow. By means of a piston and a lifting spindle, the sediment sample can be moved vertically to position various sediment layers at individually selected core depths. When a desired layer is reached, the vertical movement stops and the protruding sediment is cut off with a wire (using a specially designed apparatus). It is removed from the flume, leaving the sediment layer flush with the bottom. Through this minimally invasive procedure, each experiment begins with a user-set/defined hydraulic condition. Furthermore, the removed sediment can be used to study the sediment characteristics. Next, the erosion experiment starts and the sediment surface is exposed to incrementally increasing flow rates and, consequently, incrementally increasing shear stresses. They are applied for constant time periods to study the temporal erosion behaviour until surface failure is observed. This procedure is carried out for various sediment layers to obtain depth-dependent information on the erodibility of the investigated sediment (Beckers *et al.*, 2018). Given the pressurized flow conditions and the surrounding glass walls, all-round visibility is given as well as access for hydraulic (LDV) and photogrammetric (PHOTOSED) measurements.

Hydraulic characterisation and calibration

For the range of possible flow rates (Q = 1–65 l s^{-1}), the Reynolds number based on the hydraulic radius of the SETEG-erosion flume is constantly high (Re $\geq$ 8.3 $\times$ 10^3) and the entrance length for fully turbulent flow development can be approximated as 4.7 m (Nikuradse, 1932). In order to ensure a fully developed turbulent flow field and to obtain a hydraulic calibration function (Q–τ relation), we conducted high-resolution 2D laser Doppler velocimetry (LDV) measurements (TSI Inc., Shoreview, MN, USA). The setup of the LDV is shown in the upper panel of Figure 1. It was located on a traversal structure and mounted with the probe head axis at an angle of 8° in air (6° in water) to the bottom and perpendicular to the flume. During the measurements we used the software's coincidence mode (TSI Inc., 2011) to collect the velocity data in the longitudinal and vertical direction simultaneously. One single measurement at one position was completed once 20000 valid samples were collected. In total, 168 points per flow rate were measured to characterise the flow field. Each point is referred to a local coordinate system, where y (mm) denotes the direction of flow, z (mm) the vertical direction, and x (mm) the lateral direction. Points were distributed on four longitudinal cross-sections located 11 cm upstream (y400), 2 cm upstream (y310), in the centre (y290), and 2 cm downstream (y270) of the measuring section (with respect to the centre). On the vertical axis,

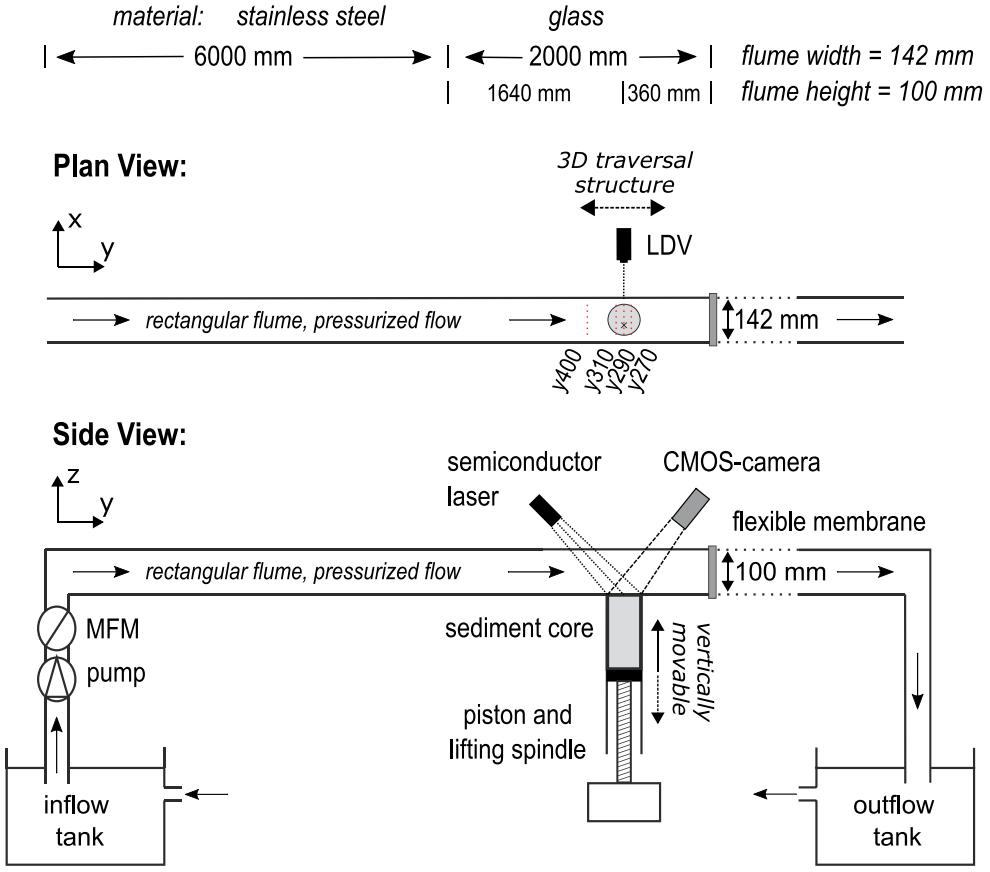

Figure 1. Schematic plan and side view of the SETEG erosion flume with dimensions. The measurement setup of a 2D LDV (plan view) and PHOTOSED (side view) are included (modified from Kern et al., 1999; Witt and Westrich, 2003; Noack et al., 2018). [Colour figure can be viewed at wileyonlinelibrary.com]

seven points were measured at increasing height positions. The lowest accessible position was 2 mm (z154) above the bed and, due to symmetry considerations, the highest measured point was the centre of the flume located 50 mm (z106) above the bed. The remaining positions were irregularly distributed at the following positions above the bed: 4 mm (z152), 6 mm (z150), 10 mm (z146), 18 mm (z138), and 34 mm (z122). Along a cross-section the velocity components were measured at six points (x220, x230, x240, x250, x260, x270).

From the measured velocity components, we calculate the mean velocity and the velocity fluctuations using Reynolds' decomposition, which is generally written as $u_i = \overline{u_i} + u'_i$. Here, u_i are the instantaneous (measured) velocity components, $\overline{u_i}$ are the time-averaged velocities, u'_i are the turbulent fluctuations, and i denotes the ith component of the velocity vector. Based on the spatially resolved measurements, we calculate the double-averaged velocity components commonly used in environmental hydraulics (e.g. Nikora *et al*., 2007): $\langle u_i \rangle = \langle \overline{u_i} \rangle + \langle u'_i \rangle$. Here, the angle brackets denote the additional spatial averaging.

In our case, i=1,2; the double-averaged near-bed Reynolds shear stress can be derived for a specific flow rate $Q^* \rightarrow \tau^*$ from u'^* and v'^* according to

$$\tau^* = -\rho \left\langle \overline{u'^* v'^*} \right\rangle \tag{1}$$

where τ^* is the near-bed Reynolds shear stress, ρ is the fluid density, and $\left\langle \overline{u'^* v'^*} \right\rangle$ is the double-averaged (time and space) covariance of the longitudinal and vertical velocity fluctuations at a considered flow rate Q^*.

The hydraulic calibration curve is created by correlating the evaluated shear stresses with their corresponding flow rates. For this curve, the measured points at 2 mm (z154) above the flume bed are selected from the three cross-sections located along the measuring section (y310, y290, and y270). By means of this Q–τ relation, the near-bed Reynolds shear stress is derived at discrete values along the curve. The range of shear stresses applied in this study, and their evaluated spatial standard deviations, are provided in Table 1. The values of the standard deviations indicate that the spatial shear stress variation is approximately 11% on average.

Both the mean flow and the turbulence development is shown in Figure 2 by means of vertical distributions for two flow rates, namely 2 and 10 l s^{-1}. The measurements were conducted over a smooth surface as this represents the initial condition at the start of an erosion experiment. Figure 2a contains the double-averaged flow profiles and Figure 2b contains the covariance of the longitudinal u' and vertical v' velocity fluctuations. The Reynolds numbers are 1.7×10^4 (2 l s^{-1}) and 8.3×10^4 (10 l s^{-1}). Both flow and turbulence development is ensured, since the profiles show a good degree of fit along the vertical for all four longitudinal cross-sections.

PHOTOSED

The PHOTOSED method (photogrammetric sediment erosion detection) was developed for erosion measurements for a variety of cohesive and non-cohesive/cohesive sediment mixtures (Noack *et al*., 2018). The PHOTOSED setup consists of a semiconductor laser with a diffraction optic (Laser2000 GmbH, Wessling, Germany) that is mounted diagonally over the measuring section of the SETEG erosion flume at an angle of 41° in air (59° in water) against the flow direction (see Figure 1). This allows us to project a structured light pattern consisting of approximately 24000 light points (for a maximum core diameter of 135 mm) on the investigated sediment layer. During an erosion experiment, the sediment surface and displacement of light points is continuously monitored with a CMOS camera (2 MP, 10 Hz, Imaging Development Systems GmbH, Obersulm, Germany). The camera is mounted diagonally across the laser and captures images at an angle of 35° in air (41° in water) against the flow direction (see Figure 1). In a post-processing routine, consecutive frames are extracted from the captured time series at given time intervals. These files are then further processed using a Python script, which applies Farnebäck's Dense Optical Flow algorithm (Farnebäck, 2003) from the OpenCV library (Open Source Computer Vision, OpenCV 2.4.10) to calculate the erosion volumes within a user-specified, rectangular region of interest (ROI). PHOTOSED enables the detection of volumetric changes from approximately 1 mm^3 between two consecutive frames, provided the erosion takes place over an area of 35 pixels (corresponding to approximately 10 mm^2). A detailed technical description of PHOTOSED and the intense calibration and verification process can be found in Noack *et al*. (2018).

An image captured with the CMOS camera prior to the start of an erosion experiment, showing the projected light points, can be seen in Figure 3a. The ROI used in this study is also shown, denoted in yellow. The ROI was defined with a minimum distance of 1.5 cm from the core boundary to minimise possible boundary effects. It is worth noting that the scaling of the captured images is pixel-based. During post-processing, a conversion to metric scale is performed based on the known metric positions, resulting in a parallelogram as shown in Figure 3b.

Measurement outputs and variables

PHOTOSED detects the topographic change of a sediment surface during erosion for consecutive time frames within a neighbourhood block for each pixel. The system provides the elevation change $\Delta z^{(j)}$ per pixel, defined as

$$\Delta z^{(j)} = z^{(j)}_{t+\mathrm{d}t} - z^{(j)}_t \tag{2}$$

where $\Delta z^{(j)}$ (mm) is the elevation change per pixel j (j=1,...,n) defined by the ROI, t and t+dt define the time steps of two consecutive frames separated by the time interval dt, and $z^{(j)}$ is the instantaneous elevation per pixel.

Table 1. Relationship between flow rates (Q) and near-bed Reynolds shear stresses (τ) in the SETEG erosion flume including spatial standard deviation (SD). The shear stresses are derived from a Q–τ relation that was obtained from LDV measurements (2 mm above the bed, three cross-sections over measuring section). The values in bold denote the measured flow rates

Q (l s^{-1})	**1.0**	1.5	**2.0**	2.5	**3.0**	3.5	**4.0**	4.5	**5.0**	**6.0**	7.0	8.0	**10.0**
τ (Pa)	**0.04**	0.07	**0.10**	0.13	**0.17**	0.22	**0.27**	0.32	**0.38**	**0.50**	0.65	0.81	**1.18**
SD (Pa)	**0.005**	0.009	**0.012**	0.016	**0.020**	0.025	**0.029**	0.035	**0.040**	**0.052**	0.064	0.078	**0.109**

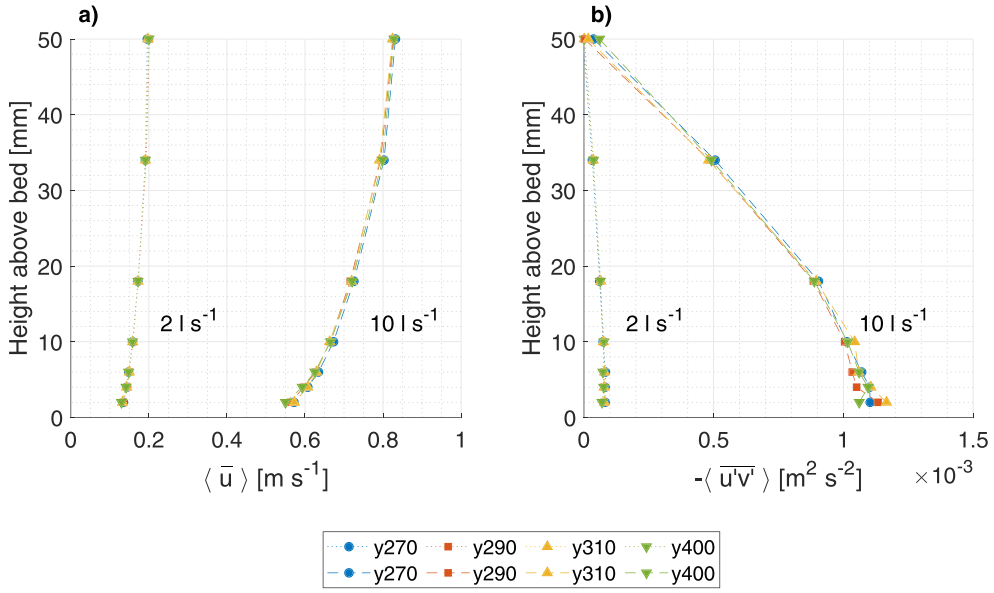

Figure 2. Flow and turbulence development in the form of double-averaged vertical distributions for four longitudinal cross-sections (located 11 cm upstream (y400), 2 cm upstream (y310), in the centre (y290), and 2 cm downstream (y270) of the measuring section). (a) Longitudinal velocity $\langle \overline{u} \rangle$ for 2 and 10 l s^{-1} and (b) covariance of the longitudinal and vertical velocity fluctuations $-\langle \overline{u'v'} \rangle$ for 2 and 10 l s^{-1}. [Colour figure can be viewed at wileyonlinelibrary.com]

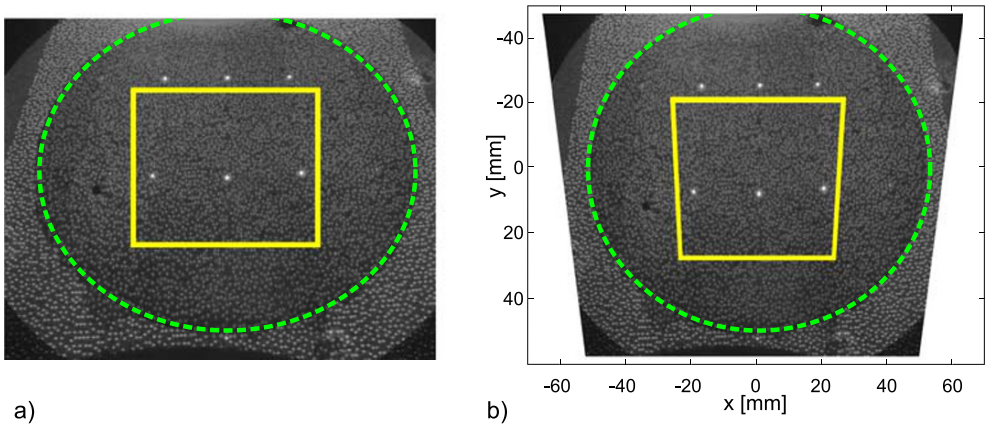

Figure 3. Image showing the initial state of the sediment surface before the start of the erosion experiment in (a) pixel scale and (b) metric scale. The green circle denotes the sediment core boundary, and the yellow square indicates the region of interest used in this study (A_{ROI} = 2642 mm^2). [Colour figure can be viewed at wileyonlinelibrary.com]

The erosion volumes for two consecutive time steps can be calculated as follows:

$$V_t^{(j)} = z_t^{(j)} \Delta x^{(j)} \Delta y^{(j)} \tag{3}$$

$$V_{t+\mathrm{d}t}^{(j)} = z_{t+\mathrm{d}t}^{(j)} \Delta x^{(j)} \Delta y^{(j)} \tag{4}$$

where $V_t^{(j)}$ and $V_{t+\mathrm{d}t}^{(j)}$ (mm^3) are the erosion volumes, and $\Delta x^{(j)}$ and $\Delta y^{(j)}$ are the known metric length dimensions of pixel j in the domain defined by the ROI.

With Equations 3 and 4, we can calculate the erosion volume difference per pixel:

$$\Delta V^{(j)} = V_{t+\mathrm{d}t}^{(j)} - V_t^{(j)} = \left(z_{t+\mathrm{d}t}^{(j)} - z_t^{(j)} \right) \Delta x^{(j)} \Delta y^{(j)} = \Delta z^{(j)} \Delta x^{(j)} \Delta y^{(j)} \tag{5}$$

Aggregation of the discrete values obtained from Equation 5 over all pixels j, in the area defined by the chosen ROI, provides the spatially averaged erosion volume difference

$$\Delta V = \sum_{j=1}^{n} \Delta V^{(j)} \tag{6}$$

Next, a spatially averaged deepening is calculated by dividing the spatially averaged erosion volume by the area of the ROI (A_{ROI}):

$$\Delta z = \frac{\Delta V}{A_{ROI}} \tag{7}$$

where Δz (mm) is the average deepening, ΔV is the spatially averaged erosion volume difference between two consecutive time frames, and A_{ROI} is the area of the entire ROI. The erosion rate results from a division of Equation 7 by the considered time interval between the two consecutive frames:

$$\varepsilon = \frac{\Delta V}{A_{ROI}\, \mathrm{d}t} \tag{8}$$

where ε (mm s^{-1}) is the erosion rate, and dt (s) is the considered time interval.

As a result of the high spatial resolution of PHOTOSED, individual and disconnected areas of erosion can be detected. These individual erosion areas can be aggregated to a total area of erosion

$$A_e = \sum_{i=1}^{m} a_i \tag{9}$$

where A_e (mm^2) is the aggregated erosion area of all individual erosion areas, a_i (i=1,...,m) (mm^2) is the area of an individual erosion area, and m is the total number of individual erosion areas.

Subsequently, the specific deepening can be derived from Equation 7 by replacing the area of the ROI (A_{ROI}) with the aggregated area of erosion (A_e) obtained from Equation 9. Consequently, the specific deepening can be written as follows:

$$\Delta z_s = \frac{\Delta V}{A_e} \tag{10}$$

where Δz_s (mm) is the specific deepening.

Advantages and versatility

The ROI and time intervals are variable and can be specified during data evaluation due to the photogrammetric approach. This allows the user to select an ROI with sufficient distance from the core boundary to exclude possible boundary effects and to adapt the evaluation according to the observed erosion behaviour, for instance by modifying the considered time step while the ROI is kept constant. For example: the ROI is constant (A_{ROI} = 2642 mm^2) and the time interval is dt = 15 s. According to Equation 8 and the detection limits of PHOTOSED (Δz_{min}~ 0.1 mm on approximately 10 mm^2), the minimum detectable erosion rate is ε = 2.5 × 10^{-5} mm s^{-1}. Whereas if we integrate over a time interval of dt = 30 s, the minimum detectable erosion rate is ε = 1.3 × 10^{-5} mm s^{-1}. An added benefit of PHOTOSED is that the captured time series of frames may be reviewed at any time to verify the data and to ensure the reliability of the results. Furthermore, the measurements are insensitive to the transport mode after erosion due to the photogrammetric approach.

A specific example summarising the relevant advantages of the method is given in Figure 4. It shows enlarged segments of four consecutive frames (dt = 1 s) taken during an erosion experiment. The segments display the top right corner of a sediment surface, the ROI (yellow), and the sediment core boundary (green). An aggregate chunk gets detached within a second (between t = 111 and 112 s) at the top right corner of the ROI. It is apparent that this erosion is not triggered by any boundary effect, since the ROI was defined with sufficient distance from the core edge (1.5 cm, see also Figure 3).

Experimental procedure and sediment characterisation

This study presents the data of three erosion experiments (EI, EII, EIII). They have been conducted within a sediment core (diameter 10 cm) obtained from a reservoir located in the northern Black Forest, Germany (48°39′25″ N, 8°19′29″ E) on 26 September 2017. The experiments have been conducted at increasing vertical core depths. These depths were 4, 8, and 16 cm (measured from the top level of sediment). Each sediment surface was exposed to a set of shear stresses, applied consecutively and kept constant for t = 600 s. The increments of increase were chosen in such a way that the critical shear stress was exceeded during each erosion experiment. Table 2 summarises the investigated shear stresses for the three conducted erosion experiments.

Table 3 summarises depth-dependent sediment characteristics. The bulk density was measured using a gamma-ray densitometer (Beckers *et al.*, 2018), the total organic carbon (TOC) was determined by loss on ignition (DIN EN 13137, 2001), and particle size measurements were conducted with a Malvern Mastersizer 2000 (Malvern Instruments Ltd, Malvern, UK) that works with the principle of laser diffraction. The composition of the sediment mixture is given according to the classification scale of Wentworth (1922).

Results

Spatio-temporal evaluation of erosion progress

Figure 5 visualises the spatio-temporal erosion progress for erosion experiments EI, EII, and EIII at selected time steps. The selection was made since no relevant erosion was detected during the previously applied shear stresses (later confirmed by Figure 11) and due to the large collection of data. The figures are obtained by rolling out the pixel-based measurements ($\Delta z^{(j)}$) as cumulated values to the entire area of the ROI (A_{ROI} = 2642 mm^2). For this purpose, a time interval of dt = 100 s was chosen and the erosion progress is shown in the xy-plane for three time steps (t = 200, 400, and 600 s). For better presentation, the results are shown in pixel scale since the conversion to metric scale would result in a parallelogram according to Figure 4b. It should be emphasised that the edge of the subfigures corresponds to the edge of the ROI and not to the edge of the sediment core, as a minimum distance of 1.5 cm from the core

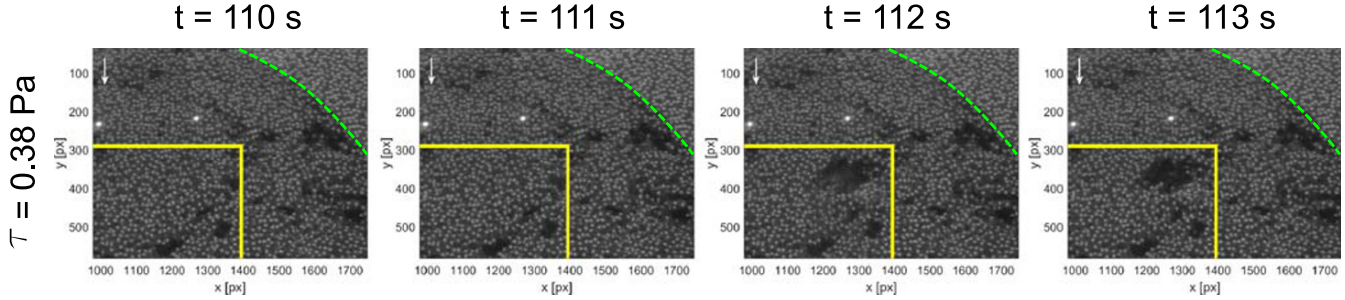

Figure 4. Four consecutive frames separated by a time interval of dt = 1 s, indicating the detachment of an aggregate chunk in the top right corner of the ROI (yellow) during an erosion experiment. The green line denotes the sediment core boundary. [Colour figure can be viewed at wileyonlinelibrary.com]

Table 2. Consecutively applied shear stresses for erosion experiment EI, EII, and EIII. Each shear stress was kept constant for $t = 600$ s. Detailed results are presented for selected shear stresses, which are denoted in bold

Name	Sediment layer (cm)	Shear stress (Pa)										
EI	4	0.07	0.10	0.13	**0.17**	**0.22**	0.27	0.32	0.38	0.50	0.65	
EII	8		0.10	0.13	0.17	0.22	0.27		**0.38**	**0.50**		
EIII	16				0.17		0.27		0.38	0.50	**0.65**	**0.81**

Table 3. Depth-dependent sediment characteristics over core depth

Sediment layer (cm)	Sediment composition (%)			Percentiles (μm)			Bulk density (g m^{-3})	TOC (%)
	Clay	Silt	Sand	d_{10}	d_{50}	d_{90}		
4	2.5	76.2	21.3	4.7	21.3	96.7	1.04	13.8
8	2.4	71.4	26.2	5.0	24.2	127.1	1.05	12.3
16	3.3	80.6	16.1	3.8	18.1	72.3	1.09	9.1

boundary is maintained (see Figures 3 and 4). The white arrow in the first subfigures denotes the flow direction (top to bottom).

The sediment surface in EI was least resistant towards erosion and experienced surface erosion (caused by flocs and small aggregates) during the first, second, and third applied shear stresses. This led to individual erosion spots with depths up to 1.7 mm by the end of $\tau = 0.13$ Pa (Figure 5b). Individual erosion spots of similar magnitude were further detected throughout the total duration of the erosion experiment, as a result of the same (surface) erosion processes.

During the higher shear stresses presented in Figures 5c and d, a variety of aggregates were detached from the surface. Consequently, these erosion forms created large spatial erosion areas through propagation in the flow and lateral direction, which resulted in the merging of individual erosion areas. Moreover, progressive vertical erosion was detected, as confirmed by Figures 5a–d. Yet parts of the surface remained unaffected by erosion at the end of $\tau = 0.22$ Pa (Figure 5d).

The sediment surface in EII initially showed a similar response compared to EI (4 cm). It experienced randomly distributed surface erosion, indicated by emerging individual erosion spots that did not exceed depths of more than 1.6 mm during shear stresses of $\tau = 0.22$, 0.27, and 0.38 Pa (Figures 5e–g). However, the applied shear stresses that initiated sporadic surface erosion differed by, on average, a factor of 2.8. The last applied shear stress ($\tau = 0.50$ Pa) tore large holes (maximum depth 8.1 mm) into the surface, which decreased in magnitude over time and formed a lateral connected erosion pattern by the end of the experiment (Figure 5h).

EIII was most resistant towards erosion, although a distinct erosion hole with a depth of 5.9 mm emerged upon increase to a shear stress of $\tau = 0.38$ Pa (Figure 5i). This event was caused by the detachment of a single aggregate chunk (the event is captured in Figure 4). In contrast, EII showed surface erosion for the same applied shear stress (Figure 5g). During the next two shear stresses ($\tau = 0.50$, 0.65 Pa), new individual erosion spots could be detected resulting from entrained flocs and aggregates (maximum depth 2.7 mm). Compared to similar erosion forms measured in EI, this results in a shear stress increase by an average factor of 5.0. During the last shear stress ($\tau = 0.81$ Pa), additional material was torn from the surface and a second distinct erosion hole opened up at the end with a depth of 4.6 mm (Figure 5l). It is worth noting that the initially emerged erosion hole did not deepen further during the proceeding erosion experiment.

Identification of erosion processes and relation to specific erosion forms

In each of the experiments, recurring erosion patterns have been detected. They were caused by different erosion processes and indicate that specific erosion forms are dominant during progressing erosion. In particular, two processes can be identified: (i) individual erosion spots emerging sporadically on the sediment surface and (ii) large holes that were torn open during erosion.

Figure 6 illustrates process (i) and Figure 7 illustrates process (ii). Both figures represent an extract from the previous Figure 5. They are thus equivalently evaluated for $dt = 100$ s. For clarification purposes, the upper panels show the relative erosion between the presented time steps, while the lower panels show the cumulative (absolute) erosion at each time step (see also Figure 5). While the first process is an effect of surface erosion and is indicative of floc and aggregate entrainment (Figure 6), the second process reveals local bed failure as a result of detached aggregate chunks (Figure 7).

During temporal progression of the erosion, interrelated processes could be measured and identified. These were (iii) a propagation of the erosion in the longitudinal as well as the lateral direction, leading eventually to merging of separated erosion areas and (iv) progressing vertical erosion (ongoing deepening). Examples of these interrelated processes are illustrated in Figures 8, 9, and 10. Again, the top panels indicate the relative erosion and the lower panels the cumulative (absolute) erosion at each time step. The processes shown are also taken from the time series provided in Figure 5. It is worth noting that these interrelated processes can be caused by new emerging individual erosion spots as a result of surface erosion (Figure 8) and by the formation of large holes through the detachment of aggregate chunks (Figure 9).

Given the relative erosion in the top panels and the cumulative erosion in the lower panels, the processes (i)–(iv) can be clearly identified in the presented examples in Figures 6–10. Moreover, from the measured processes one can infer the cause of specific erosion forms.

Temporal development of erosion profiles containing spatial information

For a combined comparison of the entire erosion results of the experiments (EI, EII, and EIII), Figure 11 contrasts the temporal development of (a) the erosion volumes (ΔV), (b) the erosion

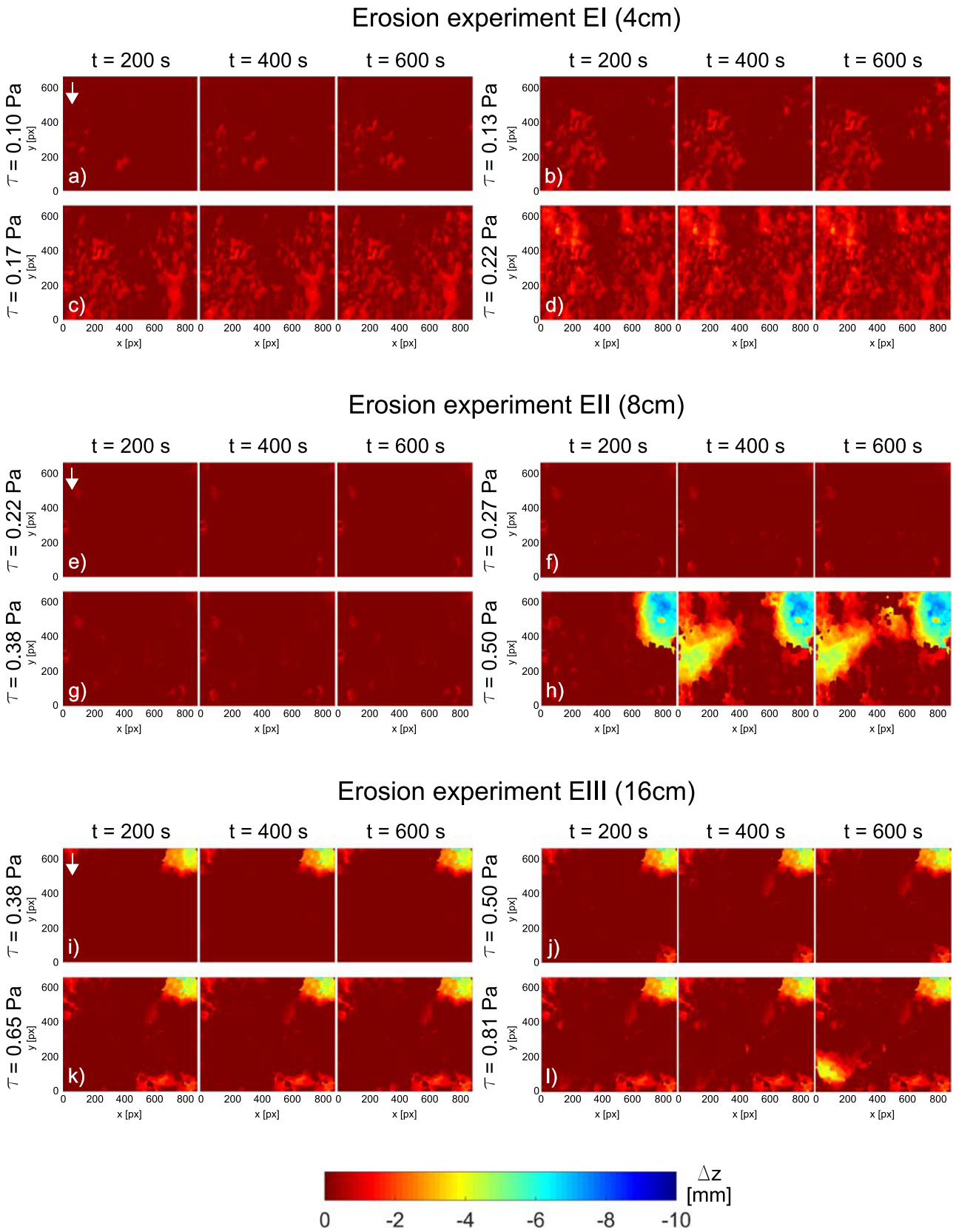

Figure 5. Spatial distribution of the cumulative erosion progress within the entire ROI (A_{ROI} = 2642 mm^2) for four consecutively applied shear stresses: experiment EI (4 cm), experiment EII (8 cm), and experiment EIII (16 cm). The erosion progress during each applied shear stress is shown at time steps t = 200, 400, and 600 s. The white arrow in the top left subfigure denotes the flow direction. [Colour figure can be viewed at wileyonlinelibrary.com]

areas (A_e), (c) the specific deepening (Δz_s), and (d) the number of disconnected erosion areas (m). All variables contain the aggregated results throughout the entire ROI. The erosion volume and area are displayed as cumulative values. Since the increments of the consecutively applied shear stresses differ among the experiments, some gaps exist for EII and EIII, as indicated in Table 3.

As expected, the profiles of the erosion volume initially show no response, because we deliberately started each erosion experiment below a critical erosion threshold. At the end of the

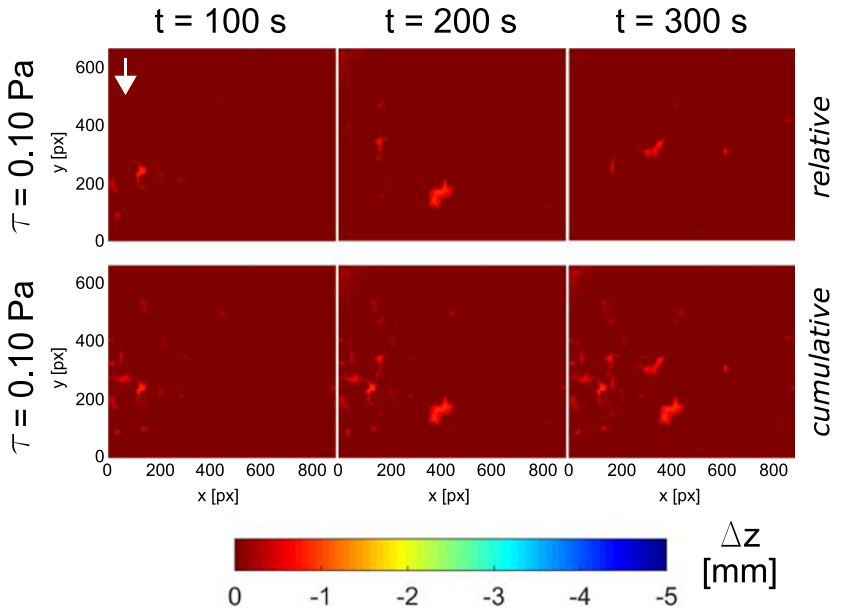

Figure 6. Example from experiment EI (4 cm) for sporadically emerging individual erosion spots. [Colour figure can be viewed at wileyonlinelibrary.com]

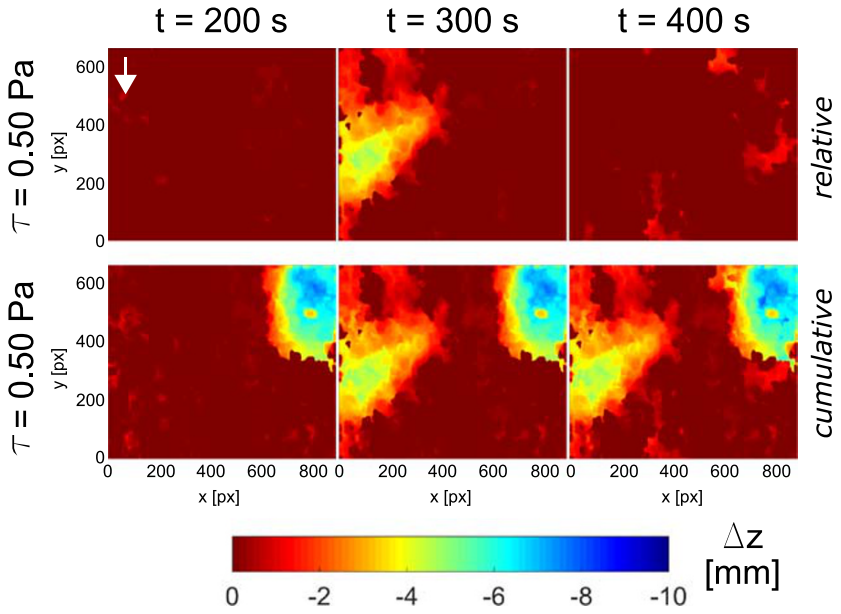

Figure 7. Example from experiment EII (8 cm) for the formation of large holes. [Colour figure can be viewed at wileyonlinelibrary.com]

experiments, the largest erosion volume is measured for EI (5504 mm^3), followed by EII (4113 mm^3) and finally EIII (1174 mm^3). In experiment EI, the final erosion affected an area of 2582 mm^2 (98%), while in EII it affected 1754 mm^2 (66%), and in EIII it affected 1068 mm^2 (40%). However, in EI most of the area was already affected in an early stage of the experiment (τ = 0.22 Pa), whereas in EII and EIII the surface experienced erosion at a later stage (τ = 0.50 and 0.38 Pa, respectively), as confirmed by Figure 5.

The significance of the actual occurring erosion is reflected in the specific deepening, since it relates the eroded volume to the affected area (Figure 11c). Consequently, distinct erosion events of high significance were measured in EII with a specific deepening of 2.9 mm (τ = 0.50 Pa) and in EIII with a specific deepening of 1.9 mm (τ = 0.38 Pa). These events could be attributed to deep holes torn into the surface by the sudden detachment of aggregate chunks, as confirmed by Figures 5e–l (see also Figure 7). In contrast, the profile of the specific deepening of EI does not contain events of comparable significance. This can be explained by the erosion mainly being characterised by a variety of individually emerging erosion spots to indicate continuous surface erosion (confirmed by Figures 5a–d; see also Figure 6). As a result, the sediment surface in EI was not prone to sudden failure like the deeper located surfaces (EII and EIII).

The disconnected erosion areas follow a general trend, which is shown to be consistent for each experiment (Figure 11d). First, the number of disconnected erosion areas increases continuously, indicating new emerging erosion areas. This can be traced back to sporadic surface erosion and suggests the entrainment of flocs and small aggregates, since the erosion volume and area affected stay relatively low. The initial rise of

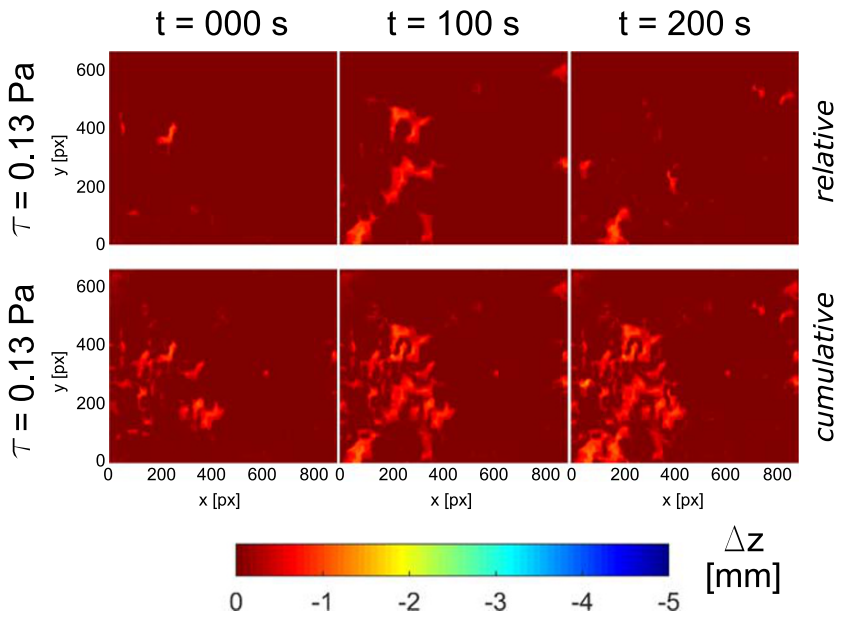

Figure 8. Example from experiment EI (4 cm) for the propagation of the erosion in longitudinal as well as lateral direction induced by individual emerging erosion spots. [Colour figure can be viewed at wileyonlinelibrary.com]

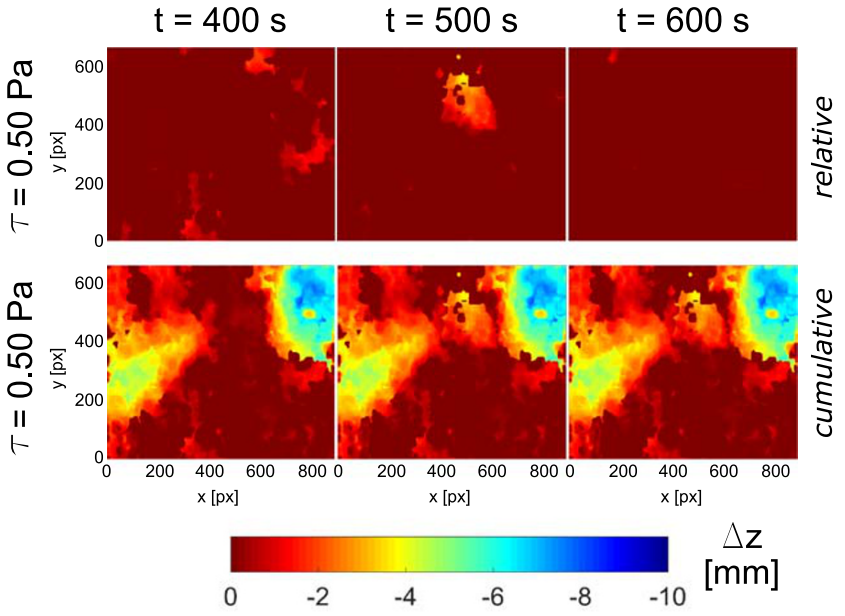

Figure 9. Example from experiment EII (8 cm) for the propagation of the erosion in longitudinal as well as lateral direction induced by the formation of erosion holes. [Colour figure can be viewed at wileyonlinelibrary.com]

the disconnected erosion areas was detected for EI at a shear stress of τ = 0.07 Pa, for EII at a shear stress of τ = 0.17 Pa, and for EIII at a shear stress of τ = 0.27 Pa. Second, a drop in the number of disconnected areas coincides with an increase in the erosion volume and erosion area, indicating that the erosion behaviour has changed – since disconnected erosion areas must have grown together while erosion proceeds (see also Figure 5). This characteristic case was measured for EI at a shear stress of τ = 0.17 and 0.22 Pa, and for EII at a shear stress of τ = 0.50 Pa. It is not as clear for EIII, but a similar trend was measured at the end of a shear stress of τ = 0.81 Pa (Figure 11). Based on these results, the following time periods were selected for detailed evaluation in the following section: EI (4 cm): τ = 0.17 and 0.22 Pa; EII (8 cm): τ = 0.38 and 0.50 Pa; EIII (16 cm): τ = 0.65 and 0.81 Pa (see also Table 3).

In general, it can be observed that the erosion decreased from EI to EIII, thus over the sediment core depth. This is indicated by the staggered arrangement of the erosion volume and the erosion area, as well as by the temporal offset in the disconnected erosion areas (Figure 11). As a result, the sediment characteristics in Table 2 indicate that erosion decreased with a higher bulk density, a refinement of the sediment composition, and a decreasing organic content.

Spatio-temporal erosion variability for selected time periods

Figures 12a–f show the range of detected erosion for the two consecutively applied shear stresses that were selected based

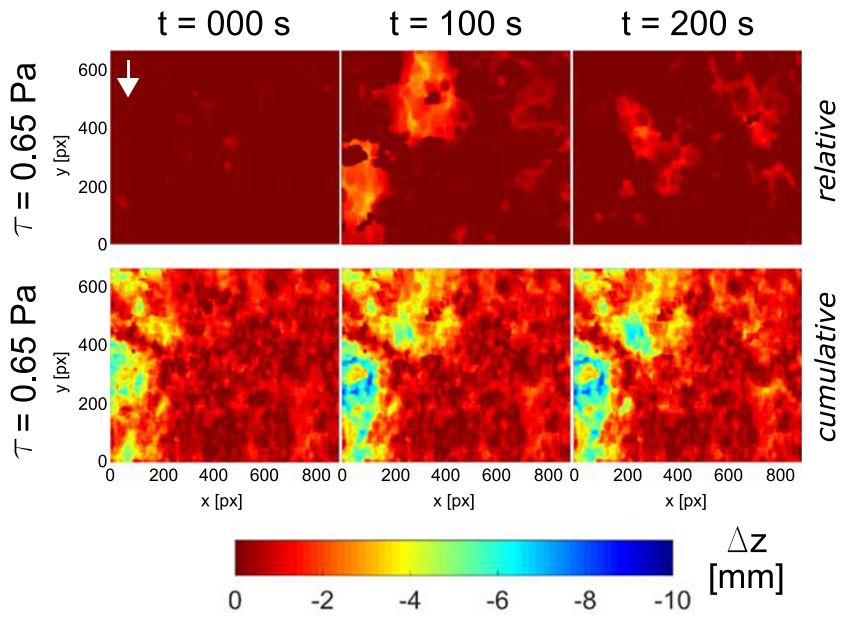

Figure 10. Example from experiment EI (4cm) for progressing vertical erosion (ongoing deepening). [Colour figure can be viewed at wileyonlinelibrary.com]

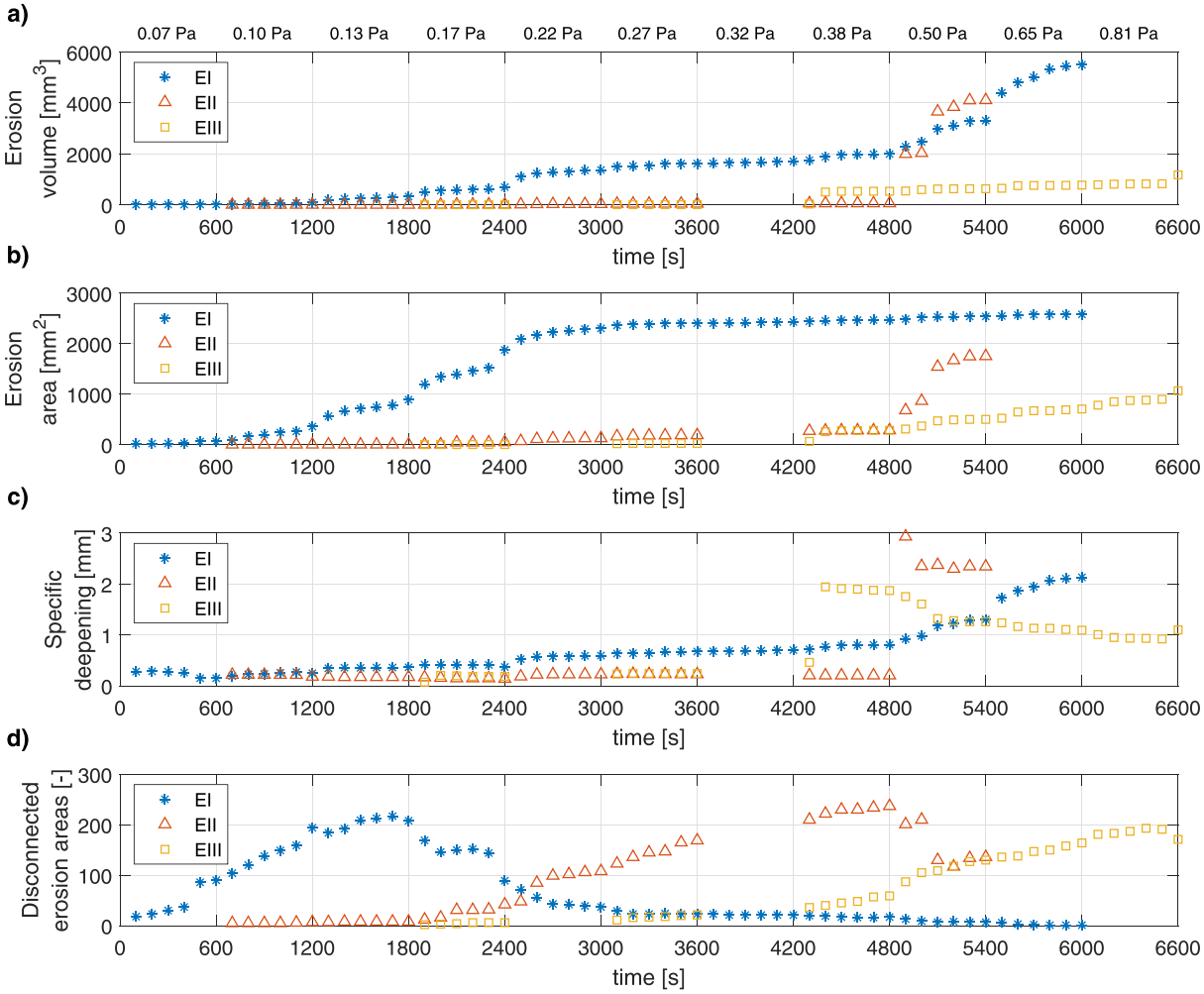

Figure 11. Comparison of (a) erosion volume, (b) erosion area, (c) specific deepening, and (d) number of disconnected erosion areas for the three conducted erosion experiments EI (4cm), EII (8cm), and EIII (16cm). The evaluation was conducted with a time step of d*t* = 100s. The consecutively applied shear stresses are listed above the upper panel. [Colour figure can be viewed at wileyonlinelibrary.com]

on the characteristic temporal change in the erosion behaviour (see also Table 3). The distribution of the erosion ($\Delta z^{(j)}$) is presented by means of boxplots and their concurrent bar graphs, which provide information about the aggregated erosion area (A_e). The time interval has been refined to dt = 30s to obtain a higher temporal resolution. In doing so, the spatial erosion variability can be shown while still being able to group the data temporally. The central mark (denoted by the hollow circle) represents the median, the top and bottom of the blue box represent the 25th and 75th percentiles, respectively, and the whiskers cover the data that are not considered to be outliers and correspond to $\pm 2.7\sigma$. The maximum point of deepening is denoted by the filled circle and confines the outliers. The horizontal dashed lines represent the time-averaged values of the maximum deepening (red), the median deepening (dark blue), and the erosion area (light blue). Please note that the scaling of the vertical axis is not consistent between the plots and changes with the magnitude of the erosion. The time-averaged statistical quantities of the measured deepening are presented in Table 4.

On average, the diversity of the deepening was in the order of one magnitude for all experiments. Moreover, the measurements indicate that the deepening followed a consistent pattern in four out of six measurements, with the largest impact happening in the first third, followed by a general decrease over time (Figure 12). Only the second presented shear stress of EII (Figure 12d) and EIII (Figure 12f) oppose this trend and show large impacts in the second and last third, respectively. Generally, large impacts are often confined to just a few time steps during temporal progression, but then clearly exceed the time-averaged values (Figure 12). In EI the time-averaged median was exceeded by the maximum measured deepening by a factor of 13.3 during τ = 0.17Pa (at 30s), whereas during τ = 0.22Pa it was exceeded by a factor of 16.0 (at 90s). In EII the equally evaluated factors result in 7.0 (at 60s) and 10.5 (at 60s) during τ = 0.38and 0.50Pa, respectively. Finally, the time-averaged median of EIII was exceeded by the maximum measured deepening by a factor of 9.8 during a shear stress of τ = 0.65Pa (at 150s), whereas it was exceeded by a factor of 12.3 during τ = 0.81Pa (at 540s).

Overall, the results show that the distribution of the deepening had a consistently positive skew, since the upper whiskers in each of the boxplots are longer and the time-averaged mean is constantly higher than the median (Figure 12). This is further represented by the time-averaged maximum erosion compared to the median and underlines that the erosion was not normally distributed (Table 4).

The boxplots are plotted alongside the percentage of aggregated erosion area, which is the area within the ROI that experiences erosion. Table 5 presents the time-averaged and the maximum detected erosion areas. The results indicate that the time-averaged mean area affected by erosion is small with regard to the total area of the ROI (Table 5). Out of all six results, it was never exceeded by more than eight events (Figure 12b). Finally, a large erosion area does not necessarily coincide with a large deepening. While large area and deepening coincide in EII and EIII, this is not the case for EI and thus suggests an influence of the erosion behaviour.

Temporal development of erosion rates for selected time periods

Figures 13a–f show the temporal development of the erosion rates (ε) for the time periods, with a characteristic temporal change in the erosion behaviour for EI, EII, and EIII (see also Table 3 and Figure 12). They are all related to the entire area of the chosen ROI (A_{ROI} = 2642mm^2). Furthermore, the erosion rates are presented for the following five time intervals: dt = 15, 30, 60, 100, and 120s (denoted by different colours), to encompass those time intervals used in the previous evaluations. The erosion rates are shown on a semi-logarithmic plot to account for the large range of variations. Further, the erosion rates contain blank time steps in the event that no erosion rate was detected. The horizontal dashed line in each graph denotes the time-averaged erosion rates obtained with dt = 100s. Table 6 summarises these time-averaged mean erosion rates and the maximum detected erosion rate next to their time period of occurrence.

It is shown in Figure 13 that small time intervals reveal a fluctuating trend and indicate that the erosion rates can vary significantly during temporal progression (e.g. Figures 13a, b, and d). On the contrary, large time intervals provide an averaged erosion rate due to integration over a longer period and are thus capable of measuring low rates (e.g. Figures 13e and f). Figure 13c presents only an initial response followed by two individual measured erosion rates as a result of hardly existing erosion, and confirms previous knowledge (e.g. Figure 5g).

On average, the diversity of the detected erosion rates is one order of magnitude in Figures 13a and c, whereas it is two orders of magnitude in Figures 13b, d, e, and f. High erosion rates were predominantly detected in the first third (Figures 13a, b, c, and e), but also notably in the second third (Figure 13d) and in the final third (Figure 13f) of the measurement (see also Table 6). By using existing erosion types, the rates presented in Figure 13c can be classified as erosion *Type I* (depth-dependent). The rates in Figures 13a, b, and e share features of *Type I* and *Type II* erosion, with the highest rates being detected at the beginning, but ultimately the erosion did not cease. The erosion rates presented in Figures 13d and f do not follow *Type I* (depth-limited) or *Type II* (steady-state) erosion within the considered period of time, and thus cannot be classified with the common erosion types.

Discussion of Results

The high spatio-temporal resolution measurements provide the means to distinguish between two fundamental erosion processes caused by specific erosion forms, which could be measured and identified in our experiments: (i) the emergence of individual erosion spots as a result of surface erosion (i.e. floc and aggregate entrainment) and (ii) the formation of large holes torn open by detached aggregate chunks (Figures 6 and 7). Whereas individual erosion spots were a recurring phenomenon that could be continuously measured during low and high shear stresses, large erosion holes were measured primarily at shear stresses that exceeded τ = 0.38Pa (Figure 5). The chronology of these processes and their causing specific erosion forms are in qualitative agreement with the observations of many authors (e.g. Parchure and Mehta, 1985; Amos *et al.*, 1992; Mitchener and Torfs, 1995; McNeil *et al.*, 1996; Roberts *et al.*, 2003; Debnath *et al.*, 2007; Righetti and Lucarelli, 2007; Jacobs *et al.*, 2011). Given the photogrammetric approach and the available time series of frames, the specific erosion forms can always be verified by overviewing the raw data (e.g. Figure 4).

The temporal development of the erosion experiments reveals interrelated processes, namely (iii) the propagation of the erosion in the longitudinal and lateral direction, leading eventually to a merging of disconnected erosion areas, and (iv) progressive vertical erosion of already affected areas (Figures 8–10). Understandably, processes (iii) and (iv) are a

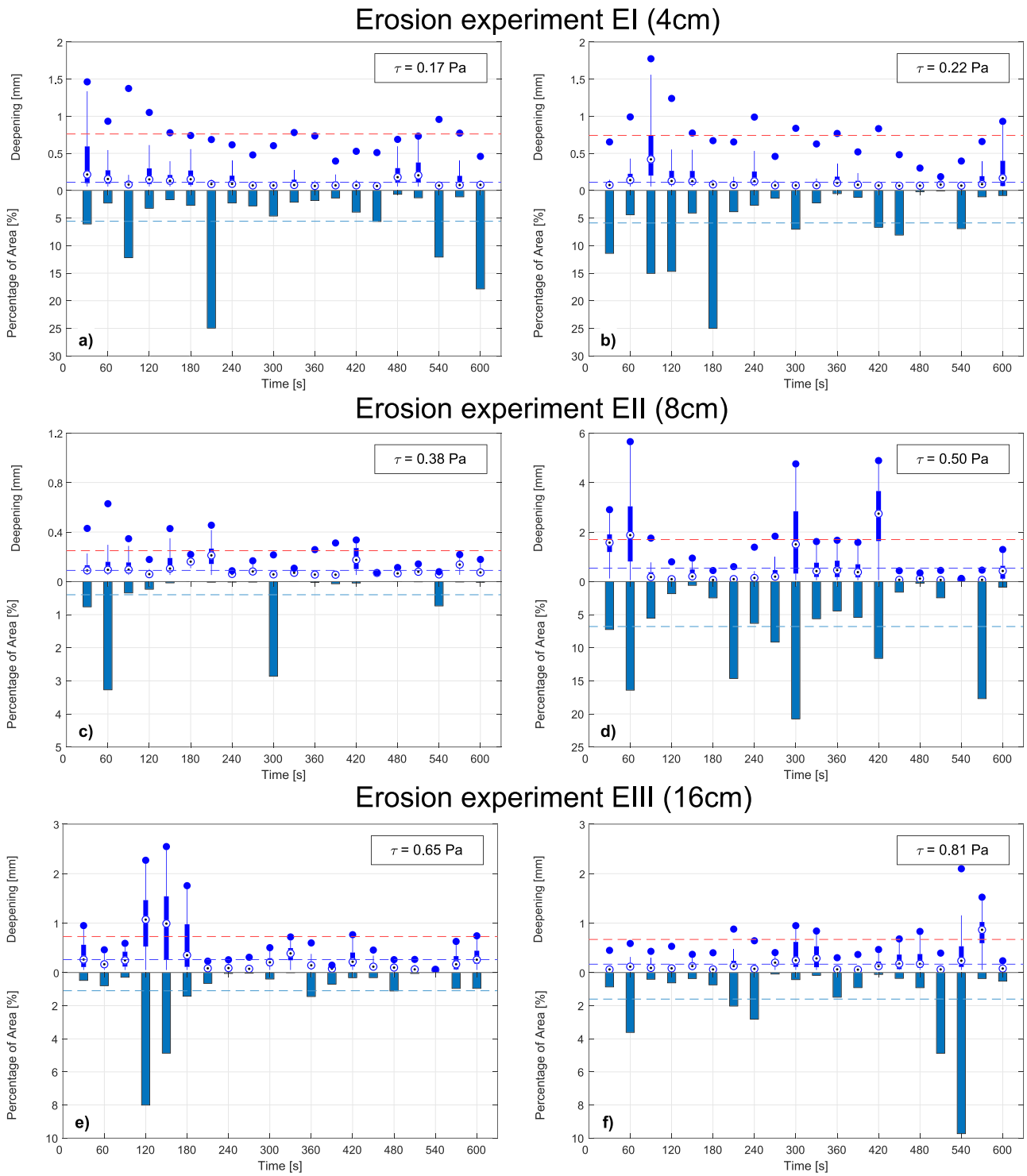

Figure 12. Spatio-temporal variability of the measured deepening per pixel plotted over the percentage of affected erosion area with respect to the entire ROI (A_{ROI} = 2642 mm^2; 580800 pixels). Results are shown for two consecutive shear stresses per experiment EI (4 cm), EII (8 cm), and EIII (16 cm). The horizontal dashed lines denote the time-averaged maximum deepening (red), the median deepening (dark blue), and the erosion area (light blue). [Colour figure can be viewed at wileyonlinelibrary.com]

logical temporal consequence during ongoing erosion, but in contrast to non-cohesive sediments, these processes have been insufficiently studied on relevant scales due to the fact that high spatio-temporal resolution data of cohesive sediment erosion were very limited or completely unavailable (e.g. Tolhurst *et al.*, 2006). However, these processes should be addressed, since erosion is a self-reinforcing process and likely progresses from already affected erosion areas as confirmed throughout Figures 5–10.

As a result of the high-resolution data obtained, the profile of the erosion volume can be complemented with the profiles of the affected erosion area, the specific deepening, and the number of disconnected erosion areas to take into consideration spatial information (Figure 11). While the specific deepening is a quantitative parameter that provides information on the significance of an occurring erosion, the number of disconnected erosion areas is a solely qualitative parameter as it contains no information on the actual erosion magnitude. Still, it is a robust variable that intuitively provides information on the spatial distribution of the erosion within a considered area (in this study, the ROI). Further, the incipient rise of the disconnected erosion areas marks the initiation of surface erosion (Figure 11d), as the

Table 4. Time-averaged statistical quantities of deepening for the selected shear stresses per erosion experiment. The median is denoted by $\widetilde{\Delta z^{(j)}}$, the mean by $\overline{\Delta z^{(j)}}$, the standard deviation by SD, and the maximum values by $\overline{\Delta z_{max}^{(j)}}$

Name	Sediment layer (cm)	Shear stress (Pa)	$\widetilde{\Delta z^{(j)}}$ (mm)	$\overline{\Delta z^{(j)}}$ (mm)	SD (mm)	$\overline{\Delta z_{max}^{(j)}}$ (mm)
		0.17	0.11	0.15	0.12	0.76
EI	4	0.22	0.11	0.15	0.11	0.74
		0.38	0.09	0.10	0.04	0.25
EII	8	0.50	0.54	0.58	0.39	1.70
		0.65	0.26	0.28	0.17	0.73
EIII	16	0.81	0.17	0.20	0.12	0.67

Table 5. Time-averaged erosion area $\left(\overline{A_e}\right)$ and maximum detected erosion area ($A_{e,max}$) with respect to the entire area of the ROI (A_{ROI} = 2642 mm^2) for the selected shear stresses per erosion experiment

Name	Sediment layer (cm)	Shear stress (Pa)	$\overline{A_e}$ (%)	$A_{e,max}$ (%)
		0.17	5.6	25.0
EI	4	0.22	5.9	25.0
		0.38	0.4	3.3
EII	8	0.50	6.8	20.8
		0.65	1.1	8.0
EIII	10	0.81	1.6	9.7

variable counts already the emerging individual erosion spots (process (i)). It is worth noting that surface erosion (flocs, small aggregates) marginally contributes to the total erosion volume (Figure 11a). Conversely, initiation of surface erosion could not readily be deduced from the time series of the erosion volume. A drop in the disconnected erosion areas, combined with an increasing erosion volume and erosion area, is evidence of a change in the erosion behaviour and implies that processes (iii) and (iv) are present.

A characteristic increase in the specific deepening indicates erosion events of high significance. Such an increase is most distinct in EII and EIII, since deep holes were torn open by the sudden detachment of aggregate chunks (process (ii); see also Figures 5e–l). Similar effects have been visually observed (but not dynamically measured) by various authors. For example, Mitchener and Torfs (1995) reported aggregated clumps of material being removed from a cohesive surface, McNeil *et al*. (1996) reported chunks of eroded sediment that leave holes or pits behind, and Zhu *et al*. (2008) referred to clusters and lumps of aggregates during erosion (see also Debnath *et al*., 2007; Aberle, 2008). Although no uniform terms are used, the specific erosion forms described are likely to be the same. Certainly, such events will result in the same erosion process, namely the formation of large holes, which is reflected in the specific deepening of EII and EIII (Figure 11; see also Figures 5-e–l).

The necessity to address the spatial distribution alongside the eroded volume is reflected by cross-comparing the results of EI, EII, and EIII (Figure 11). When taking into account the erosion volume only (Figure 11a), misinterpretations of erosion data can be a consequence as the development suggests a resemblance among erosion experiments EI and EII. In general, erosion volume profiles can only be evaluated with regard to an initial rise, a change in the slope, and the final eroded (bulk) volume. Thus, it is not possible to assess the spatial distribution of the occurring erosion nor to obtain information on the dominant erosion process, making user-specific descriptions necessary (e.g. Mehta and Partheniades, 1982; Amos *et al*., 1992; Mitchener and Torfs, 1995; Debnath *et al*., 2007; Righetti and Lucarelli, 2007). Only with the addition of the affected erosion area (Figure 11b) and the specific deepening (Figure 11c) does it become obvious that the experiments EI and EII must have experienced erosion of different spatial extent and different behaviour.

As a whole, it is possible to draw conclusions on the erosion behaviour by means of erosion profiles, in case they contain spatial information. This is an integral finding of this study, since we obtained quantitative results which can be interpreted in terms of the dominant erosion forms and their spatial distribution without requiring supporting qualitative information (such as visual observations).

Based on the full temporal development of the erosion profiles per experiment (Figure 11), two consecutive shear stresses indicating a change in the erosion behaviour were (exemplarily) selected for detailed evaluations (see Figure 12, Tables 4 and 5). In general, the spatio-temporal erosion variability indicates that the distribution of the erosion is right-skewed and not normally distributed for all considered time steps and over all experiments (Figure 12 and Table 4). This corresponds to the general understanding of cohesive sediment erosion, since locally increased erosion is likely due to the mutual interference of surface changes and flow changes initiating progressing erosion (as confirmed by the detected processes (iii) and (iv) shown in Figures 8–10) (see also Van Prooijen and Winterwerp, 2010; Schäfer Rodrigues Silva *et al*., 2018). More specifically, the (now quantifiable) variability indicates that the deepening can vary significantly during temporal progression. When relating the maximum measured deepening to the time-averaged median, this results in variability factors ranging from 7.0 to 16.0 (Figure 12). Such factors are reasonable, as it has been shown that strong impacts are mostly confined to a few erosion events. This is most evident for experiment EII during exposure to a shear stress of τ = 0.50 Pa, where three characteristic impacts at 60, 300, and 420 s dominate the erosion (Figure 12d). Each impact corresponds to one of the three large holes that were torn into the surface (cf. Figure 5h). As expected, the median and maximum detected deepening of each impact exceeded the time-averaged values considerably (Figure 12d, Table 4). These results make clear the significant variability of cohesive sediment erosion during temporal progression.

Another insight is that the largest deepening does not necessarily correlate with the largest measured erosion area. This can also be explained with the erosion behaviour and the dominant erosion processes. Individual emerging erosion spots induced by surface erosion may affect a large erosion area but usually do not result in a large deepening (e.g. Figure 12b). On the contrary, it is likely that large holes torn open by the sudden detachment of aggregate chunks (i.e. a large deepening) coincide with a large erosion area at this time step (e.g. Figure 12d). This emphasises the need to measure cohesive

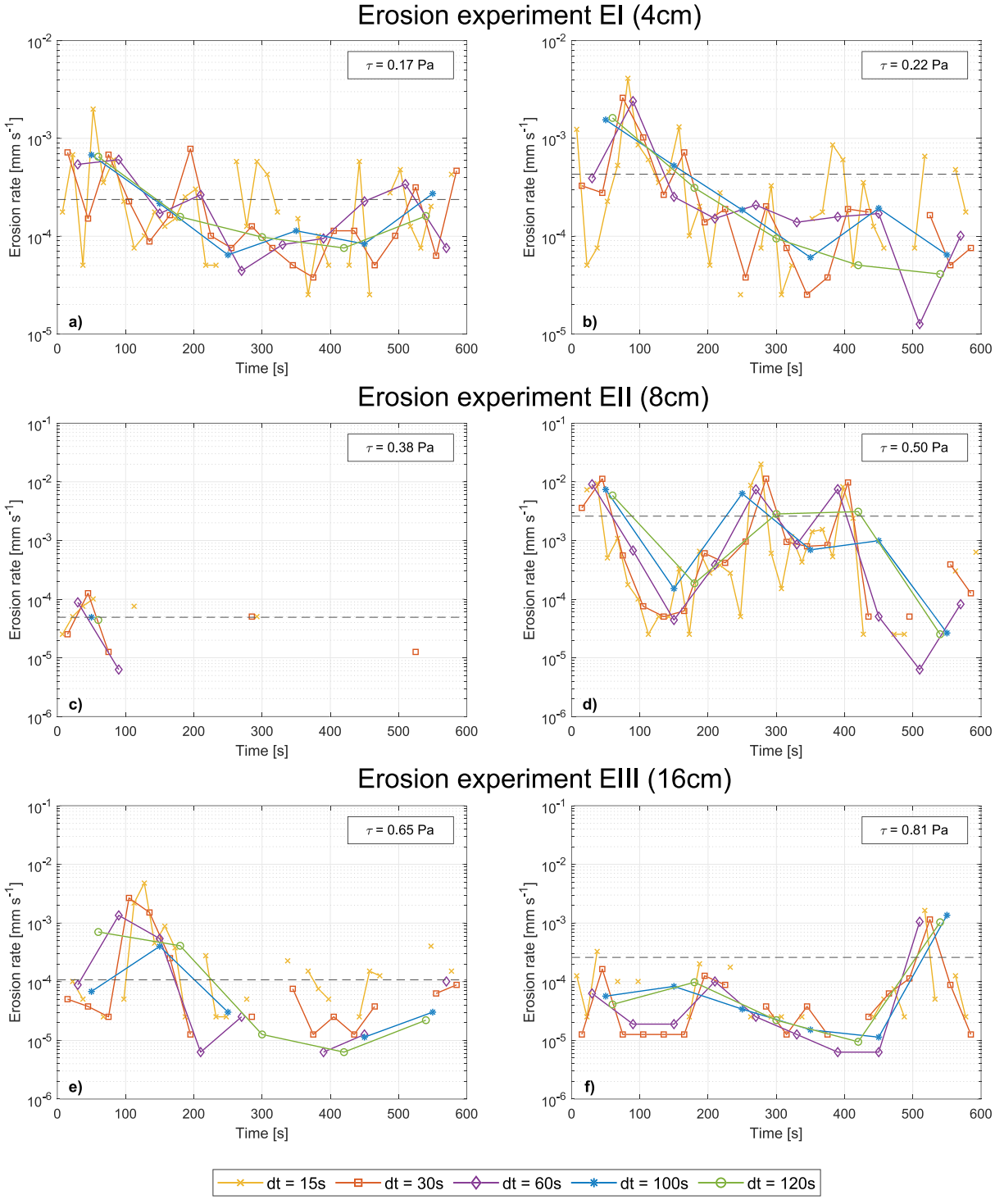

Figure 13. Erosion rates evaluated with respect to the entire ROI (A_{ROI} = 2642 mm^2) for five different time intervals (dt = 15, 30, 60, 100, 120 s). Results are shown for two consecutive shear stresses per experiment: EI (4 cm), EII (8 cm), and EIII (16 cm). The horizontal dashed line denotes the time-averaged erosion rate for dt = 100 s. [Colour figure can be viewed at wileyonlinelibrary.com]

sediment erosion, spatially resolved and with high resolution, to verify such relationships and the erosion processes responsible.

The need for high-resolution measurements is further reflected in the presented erosion rates (Figure 13). Four out of six presented erosion rates can be classified using common erosion types (*Type I* and *Type II*). The remaining two erosion rates presented in Figures 13d and f do not follow one of these existing types. This can be explained when comparing Figure 13 with the previous Figures 5–10. All peaks in the erosion rates, including the maximum rate detected, can be attributed to erosion events induced by specific processes. Among these are the emergence of individual erosion spots (e.g. Figures 13a and b; see also Figures 5c and d), as well as the formation of large holes, which were torn open by detached aggregate chunks (e.g. Figures 13d–f; see also Figures 5h–l). Since the common erosion types refer to resuspension rates (Mehta and Partheniades, 1982), an inability exists to classify aggregate chunks due to their highly probable bed load transport mode after detachment (e.g. Mitchener and Torfs, 1995; Roberts *et al.*, 2003; Debnath *et*

Table 6. Time-averaged mean erosion rates ($\bar{\varepsilon}$) obtained with dt = 100 s and maximum measured erosion rates (ε_{max}) as well as their time period of occurrence for the selected shear stresses per erosion experiment

Name	Sediment layer (cm)	Shear stress (Pa)	$\bar{\varepsilon}$ (mm s^{-1})	ε_{max} (mm s^{-1})	Time period (s)
		0.18	0.0002	0.002	45–60
EI	4	0.22	0.0004	0.041	75–90
		0.38	0.00005	0.0001	30–60
EII	8	0.51	0.0026	0.02	270–285
		0.65	0.0001	0.0048	120–135
EIII	10	0.80	0.0003	0.0016	510–525

al., 2007). As shown, such events occur within our data (particularly reflected in Figures 13d and f) as our measurements are insensitive to the transport mode after erosion (photogrammetric approach; erosion rates calculated using Equation 8). However, any information on the erosion processes cannot be deduced from erosion rate profiles. This underlines once again that there is a need for spatially resolved measurements. Only by considering additional spatial information is it possible to draw conclusions on the erosion behaviour and on the fundamental processes of cohesive sediment erosion.

A general assessment of the erosion experiments EI, EII, and EIII reveals that the erosion in EI is characterised by mainly (i) individual emerging erosion spots as a result of surface erosion and the further interrelated processes (iii) and (iv) (Figures 5a–d and 11–13). These observations suggest that the sediment sample has a vertical gradient in bed shear strength, leading to depth-limited or supply-limited erosion (e.g. Aberle, 2008) (i.e. *Type I* erosion), as proven in Figures 13a and b. This erosion type, in turn, is typical for stratified surficial sediment beds (Mehta and Partheniades, 1982), which are weakly consolidated. Due to the shallow sediment depth (4 cm) and sediment characteristics (Table 2), this holds true for EI. Consequently, our results confirm previous knowledge that surface erosion and further interrelated processes (such as (iii) and (iv)) are dominant in surficial and weakly consolidated sediment beds. The erosion of EII and EIII was mainly characterised by the formation of deep holes, which were torn into the surface through the detachment of aggregate chunks (Figures 5e–l and 11–13). Given the sediment depths (8 and 16 cm) and sediment characteristics (Table 2), we attribute this behaviour to a more consolidated bed. Although little information is available on the erosion behaviour of consolidated or compacted cohesive sediments (Zhu *et al.*, 2008), this conclusion corresponds well to the visual observations of Debnath *et al.* (2007) and Aberle (2008), who report on large aggregates and lumps of material eroded from consolidated, cohesive beds. Furthermore, the remaining holes in the surface of EII and EIII (Figures 5h and l) resemble observations made with compacted sediment mixtures (e.g. pothole erosion described by Kothyari and Jain, 2008).

Overall, it can be concluded that the erosion decreased over depth (Figures 5 and 11) and thus with a higher bulk density, a refinement of the sediment composition, and a decreasing organic content (Table 2). This is in general agreement with previous knowledge on the erosion stability of natural non-cohesive/cohesive sediment mixtures (McNeil *et al.*, 1996; Lick and McNeil, 2001; Righetti and Lucarelli, 2007; Schäfer Rodrigues Silva *et al.*, 2018).

The potential limitations of this study were more commonly due to the erosion flume (SETEG) than to the applied photogrammetric method (PHOTOSED). One complication is the roughness transition from the smooth flume bed to the sediment surface. To counteract this issue, we selected our ROI with a minimum distance of 1.5 cm from the sediment core boundary (Figures 3 and 4), despite Roberts *et al.* (2003) concluding for a similar flume that the effect would be negligible and contribute minimally to overall experimental results. Further, the hydraulic calibration shown in Table 1 presents double-averaged shear stress values and their spatial standard deviations, which are 11% on average. Although a spatial distribution over the sample exists, this cannot explain the large measured erosion variability. The shear stress might also underestimate the effective near-bed Reynolds shear stress since the roughness of the sediment bed deviates during an erosion experiment (e.g. Berlamont *et al.*, 1993; Black and Paterson, 1997; Aberle *et al.*, 2006; Debnath *et al.*, 2007; Aberle, 2008). Taking into account the effect of dynamic roughness changes induced by ongoing erosion, as well as turbulence-induced shear stress fluctuations, remains a topic for future research. To address these issues, high spatio-temporal resolution measurements are a crucial requirement, as geometric roughness changes of a surface can be derived from the dynamically measured erosion data (e.g. with the approach of Aberle *et al.*, 2010). This enables us to study flow–sediment interactions and also to correlate turbulence intensities with erosion distribution functions.

Summary and Conclusions

The presented study demonstrates that due to the high spatio-temporal resolution of our method (PHOTOSED), it is possible to measure the erosion process of cohesive sediments and non-cohesive/cohesive sediment mixtures, dynamically and pixel-based with a vertical resolution in the sub-millimetre range. Consequently, we are able to detect and distinguish between two fundamental erosion processes: (i) the emergence of individual erosion spots caused by surface erosion and (ii) the formation of large holes that were torn open by detached aggregate chunks. Furthermore, interrelated processes as a temporal consequence of ongoing erosion were detected: (iii) the propagation of the erosion in the longitudinal and lateral direction, which eventually led to the merging of disconnected erosion areas and (iv) the progression of the erosion in the vertical direction (ongoing deepening).

It has further been shown that the ability to consider spatial information (such as erosion area, specific deepening, and number of disconnected erosion areas) – besides volumetric erosion profiles – allows us to draw conclusions on the erosion behaviour by quantitative means without requiring additional qualitative information. This is an essential requirement for a robust assessment of erosion data, which volumetrically resemble each other but ultimately experience a different erosion behaviour.

The evaluation of the spatio-temporal erosion variability for selected time periods revealed that the largest erosion events are confined to only a few time steps during temporal progression. In this event they exceeded the time-averaged median of the deepening significantly (factors between 7.0 and 16.0). It has been proven that the largest deepening does not necessarily coincide with the largest erosion area, since these relationships are controlled by the fundamental erosion processes and the specific erosion forms. On the contrary, such substantial information cannot be deduced from common (bulk) erosion rates. In summary, the findings emphasise the need for temporally and spatially resolved measurements – especially when addressing research topics in cohesive erosion research, such as the investigation of flow–sediment interactions.

In addition, for the three presented erosion experiments it can be concluded that (i) individual erosion spots caused by surface erosion and the interrelated processes (iii) and (iv) were

characteristic for the weakly consolidated sediment layer (4 cm), while (ii) the formation of large holes caused by detached aggregate chunks was characteristic for the more consolidated sediment layers (8 and 16 cm). Overall, the erosion decreased over sediment core depth and, thus, with a higher bulk density, a refinement of the sediment composition, and a decrease in organic content.

The key conclusion is that we measured fundamental erosion processes caused by specific emerging erosion forms, derived descriptive variables to consider spatial information in (bulk) erosion profiles, and quantified the spatio-temporal erosion variability (while minimising possible boundary effects by means of the photogrammetric approach). As a whole, this provides reliable high-resolution data of cohesive sediment erosion and the means for robust assessments of the erosion behaviour.

According to Grabowski *et al*. (2011) and Wu (2016), it is an essential prerequisite to generate comparable and more reliable (cohesive) erosion data from the field and laboratory. We add that this data should be of high spatio-temporal resolution. Therefore, we recommend developing and implementing the use of more high spatio-temporal resolution measurements in cohesive sediment research. This will serve towards a common goal: to give rise to further dependable erosion data that will develop deeper insights into the complex erosion of cohesive sediments and non-cohesive/cohesive sediment mixtures.

Acknowledgements—This study was carried out within the project CHARM – Challenges of Reservoir Management – Meeting Environmental and Social Requirements. The project is part of the Water Research Network Baden-Württemberg. It is funded by the Ministry of Science, Research, and Arts of the federal state of Baden-Württemberg, Germany.

We gratefully acknowledge the help of Ruslan Biserov, who conducted various time-consuming erosion experiments. We would also like to thank Kaan Koca, Sergey Oladyshkin, and James Nodwell-Taylor for their valuable assistance.

Conflict of Interest

The authors have no conflict of interest to declare.

Data Availability STATEMENT

The data sets used and/or analysed during the current study are available from the corresponding author on reasonable request.

References

Aberle J. 2008. Measurement techniques for the estimation of cohesive sediment erosion, Hydraulic Methods for Catastrophes: Floods, Droughts, Environmental Disasters. Publications of the Institute of Geophysics, Polish Academy of Sciences.

AberleJ., Nikora V., Henning M., Ettmer B., Hentschel B.. 2010. Statistical characterization of bed roughness due to bed forms: A field study in the Elbe River at Aken, Germany. *Water Resources Research*, **46**(3), W03521. https://doi.org/10.1029/2008wr007406.

Aberle J, Nikora V, Walters R. 2006. Data interpretation for in situ measurements of cohesive sediment erosion. *Journal of Hydraulic Engineering* **132**: 581–588. https://doi.org/10.1061/(ASCE)0733-9429(2006)132:6(581).

Aberle J, Nikora V, Walters R. 2004. Effects of bed material properties on cohesive sediment erosion. *Marine Geology* **207**: 83–93. https://doi.org/10.1016/j.margeo.2004.03.012.

Amos CL, Daborn GR, Christian HA, Atkinson A, Robertson A. 1992. In situ erosion measurements on fine-grained sediments from the Bay of Fundy. *Marine Geology* **108**: 175–196. https://doi.org/10.1016/0025-3227(92)90171-D.

Beckers F, Haun S, Noack M. 2018. Experimental investigation of reservoir sediments. *E3S Web Conferences* **40**: art. 03030. https://doi.org/10.1051/e3sconf/20184003030.

Berlamont J, Ockenden M, Toorman E, Winterwerp J. 1993. The characterisation of cohesive sediment properties. *Coastal Engineering* **21**: 105–128.

Black KS, Paterson DM. 1997. Measurement of the erosion potential of cohesive marine sediments: a review of current in situ technology. *Journal of Marine Environmental Engineering* **4**: 43–83.

Black KS, Tolhurst TJ, Paterson DM, Hagerthey SE. 2002. Working with natural cohesive sediments. *Journal of Hydraulic Engineering* **128**: 2–8.

Briaud JL, Ting FCK, Chen HC, Cao Y, Han SW, Kwak KW. 2001. Erosion function apparatus for scour rate predictions. *Journal of Geotechnical and Geoenviromental Engineering* **127**: 105–113. https://doi.org/10.1061/(ASCE)1090-0241(2001)127:2(105).

Debnath K, Nikora V, Aberle J, Westrich B, Muste M. 2007. Erosion of cohesive sediments: resuspension, bed load, and erosion patterns from field experiments. *Journal of Hydraulic Engineering* **133**(5) 508–520. https://doi.org/10.1061/(ASCE)0733-9429(2007)133:5(508).

DIN EN 13137. 2001. Characterization of waste – determination of total organic carbon (TOC) in waste, sludges and sediments. European Standard.

Droppo IG, D'Andrea L, Krishnappan BG, Jaskot C, Trapp B, Basuvaraj M, Liss SN. 2015. Fine-sediment dynamics: towards an improved understanding of sediment erosion and transport. *Journal of Soils and Sediments* **15**: 467–479. https://doi.org/10.1007/s11368-014-1004-3.

Farnebäck G. 2003. Two-frame motion estimation based on polynomial expansion. In *Image Analysis*, Bigun J, Gustavsson T (eds). Springer: Berlin; 363–370.

Gerbersdorf SU, Jancke T, Westrich B. 2007. Sediment properties for assessing the erosion risk of contaminated riverine sites. An approach to evaluate sediment properties and their covariance patterns over depth in relation to erosion resistance. First investigations in natural sediments (11 pp). *Journal of Soils and Sediments* **7**: 25–35. https://doi.org/10.1065/jss2006.11.190.

Grabowski RC, Droppo IG, Wharton G. 2011. Erodibility of cohesive sediment: the importance of sediment properties. *Earth Science Reviews* **105**: 101–120. https://doi.org/10.1016/j.earscirev.2011.01.008.

Gularte RC, Kelly WE, Nacci VA. 1980. Erosion of cohesive sediments as a rate process. *Ocean Engineering* **7**: 539–551. https://doi.org/10.1016/0029-8018(80)90051-7.

Hanson GJ, Cook KR. 2004. Apparatus, test procedures, and analytical methods to measure soil erodibility in situ. *Applied Engineering in Agriculture* **20** 455–462. https://doi.org/10.13031/2013.16492.

Jacobs W, Le Hir P, Van Kesteren W, Cann P. 2011. Erosion threshold of sand–mud mixtures. *Continental Shelf Research* **31**: S14–S25. https://doi.org/10.1016/j.csr.2010.05.012.

Kern U, Haag I, Schürlein V, Holzwarth M, Westrich B. 1999. Ein Strömungskanal zur Ermittlung der tiefenabhängigen Erosionsstabilität von Gewässersedimenten: das SETEG-System. *WasserWirtschaft* **89**: 72–77.

Kimiaghalam N, Clark SP, Ahmari H. 2016. An experimental study on the effects of physical, mechanical, and electrochemical properties of natural cohesive soils on critical shear stress and erosion rate. *International Journal of Sediment Research* **31**: 1–15. https://doi.org/10.1016/j.ijsrc.2015.01.001.

Kothyari UC, Jain RK. 2008. Influence of cohesion on the incipient motion condition of sediment mixtures. *Water Resources Research* **44**: W04410. https://doi.org/10.1029/2007WR006326.

Lick W, McNeil J. 2001. Effects of sediment bulk properties on erosion rates. *Science of the Total Environment* **266**: 41–48. https://doi.org/10.1016/S0048-9697(00)00747-6.

McNeil J, Taylor C, Lick W. 1996. Measurements of erosion of undisturbed bottom sediments with depth. *Journal of Hydraulic Engineering* **122**: 316–324. https://doi.org/10.1061/(ASCE)0733-9429(1996)122:6(316).

Mehta AJ, Partheniades E. 1982. Resuspension of deposited cohesive sediment beds. In *Proceedings of the 18th Conference on Coastal Engineering*, Cape Town; 1569–1588.

Mitchener H, Torfs H. 1995. Erosion of mud–sand mixtures. *Coastal Engineering* **29**: 1–25. https://doi.org/10.1016/S0378-3839(96)00002-6.

Mostafa TS, Imran J, Chaudhry MH, Kahn IB. 2008. Erosion resistance of cohesive soils. *Journal of Hydraulic Research* **46**: 777–787. https://doi.org/10.1080/00221686.2008.9521922.

Nikora V, McLean S, Coleman S, Pokrajac D, McEwan I, Campbell L, Aberle J, Clunie D, Koll K. 2007. Double-averaging concept for rough-bed open-channel and overland flows: applications. *Journal of Hydraulic Engineering* **133**: 884–895. https://doi.org/10.1061/(ASCE)0733-9429(2007)133:8(884).

Nikuradse J. 1932. Gesetzmäßigkeiten der turbulenten Strömung in glatten Rohren. Forschung auf d. Gebiete d. Ingenieurwesens 3, 1-36. In German (English version in NASA TT F–10, 359,1966).

Noack M, Gerbersdorf S, Hillebrand G, Wieprecht S. 2015. Combining field and laboratory measurements to determine the erosion risk of cohesive sediments best. *Water* **7**: 5061–5077. https://doi.org/10.3390/w7095061.

Noack M, Schmid G, Beckers F, Haun S, Wieprecht S. 2018. PHOTOSED—PHOTOgrammetric Sediment Erosion Detection. *Geosciences* **8**: 243. https://doi.org/10.3390/geosciences8070243.

Panagiotopoulos I, Voulgaris G, Collins MB. 1997. The influence of clay on the threshold of movement of fine sandy beds. *Coastal Engineering* **32**: 19–43. https://doi.org/10.1016/S0378-3839(97)00013-6.

Parchure TM, Mehta AJ. 1985. Erosion of soft cohesive sediment deposits. *Journal of Hydraulic Engineering* **111**: 1308–1326. https://doi.org/10.1061/(ASCE)0733-9429(1985)111:10(1308).

Paterson DM. 1989. Short-term changes in the erodibility of intertidal cohesive sediments related to the migratory behavior of epipelic diatoms. *Limnology and Oceanography* **34**: 223–234. https://doi.org/10.4319/lo.1989.34.1.0223.

Perera C, Wu W. 2016. Erosion coefficients of cohesive sediments. In *Proceedings of World Environmental and Water Resources Congress 2016*, West Palm Beach, FL; 293–302.

Raudkivi AJ, Tan SK. 1984. Erosion of cohesive soils. *Journal of Hydraulic Research* **22**: 217–233. https://doi.org/10.1080/00221688409499380.

Righetti M, Lucarelli C. 2007. May the Shields theory be extended to cohesive and adhesive benthic sediments? *Journal of Geophysical Research* **112**: C05039. https://doi.org/10.1029/2006JC003669.

Roberts JD, Jepsen RA, James SC. 2003. Measurements of sediment erosion and transport with the adjustable shear stress erosion and transport flume. *Journal of Hydraulic Engineering* **129**: 862–871. https://doi.org/10.1061/(ASCE)0733-9429(2003)129:11(862).

Schäfer Rodrigues Silva A, Noack M, Schlabing D, Wieprecht S. 2018. A data-driven fuzzy approach to simulate the critical shear stress of mixed cohesive/non-cohesive sediments. *Journal of Soils and Sediments* **18**: 3070–3081. https://doi.org/10.1007/s11368-017-1860-8.

Tolhurst TJ, Defew EC, de Brouwer JFC, Wolfstein K, Stal LJ, Paterson DM. 2006. Small-scale temporal and spatial variability in the erosion threshold and properties of cohesive intertidal sediments. *Continental Shelf Research* **26**: 351–362. https://doi.org/10.1016/j.csr.2005.11.007.

TSI Inc. 2011. *Phase Doppler Particle Analyzer (PDPA)/Laser Doppler Velocimeter (LDV) – Operations Manual*, P/N 1990048, Revision G. TSI, Inc.: Shoreview, MN.

Van Prooijen BC, Winterwerp JC. 2010. A stochastic formulation for erosion of cohesive sediments. *Journal of Geophysical Research* **115**: C01005. https://doi.org/10.1029/2008JC005189.

Walder JS. 2016. Dimensionless erosion laws for cohesive sediment. *Journal of Hydraulic Engineering* **142**: 04015047. https://doi.org/10.1061/(ASCE)HY.1943-7900.0001068.

Wentworth CK. 1922. A scale of grade and class terms for clastic sediments. *Journal of Geology* **30**: 377–392.

Witt O, Westrich B. 2003. Quantification of erosion rates for undisturbed contaminated cohesive sediment cores by image analysis. *Hydrobiologia* **494**: 271–276. https://doi.org/10.1023/A:1025495122246.

Wu W. 2016. Mixed cohesive and noncohesive sediment transport: a state of the art review. In *River Sedimentation: Proceedings of the 13th International Symposium on River Sedimentation*: 9–18. ISRS: Stuttgart.

Wu W, Perera C, Smith J, Sanchez A. 2018. Critical shear stress for erosion of sand and mud mixtures. *Journal of Hydraulic Research* **56**: 96–110. https://doi.org/10.1080/00221686.2017.1300195.

Ye Z, Cheng L, Zang Z. 2011. Experimental study of erosion threshold of reconstituted sediments. In *ASME 2011 30th International Conference on Ocean, Offshore and Arctic Engineering*. ASME: Rotterdam; 973–983.

Zhu Y, Lu J, Liao H, Wang J, Fan B, Yao S. 2008. Research on cohesive sediment erosion by flow: an overview. *Science in China, Series E: Technological Sciences* **51**: 2001–2012. . https://doi.org/10.1007/s11431-008-0232-4.

Publication IV.

Functional relationships between critical erosion thresholds of fine reservoir sediments and their sedimentological characteristics

Table 5.4. Metadata of publication IV

Title	Functional relationships between critical erosion thresholds of fine reservoir sediments and their sedimentological characteristics
Authors	**Felix Beckers**, Kaan Koca, Stefan Haun, Markus Noack, Sabine U. Gerbersdorf, Silke Wieprecht
Journal	Journal of Hydraulic Engineering
submitted	January 28, 2021
accepted	NA
published	NA
DOI	NA

FUNCTIONAL RELATIONSHIPS BETWEEN CRITICAL EROSION THRESHOLDS OF FINE RESERVOIR SEDIMENTS AND THEIR SEDIMENTOLOGICAL CHARACTERISTICS

Felix Beckers*[1], Kaan Koca*[1], Stefan Haun[1], Markus Noack[2], Sabine U. Gerbersdorf[2], and Silke Wieprecht[1]

[1]Institute for Modelling Hydraulic and Environmental Systems, Department of Hydraulic Engineering and Water Resources Management, University of Stuttgart, Stuttgart, Germany.
Email: felix.beckers@iws.uni-stuttgart.de; kaan.koca@iws.uni-stuttgart.de

[2]Faculty of Architecture and Civil Engineering, Karlsruhe University of Applied Science, Karlsruhe, Germany

[3]Ministry of Science, Research and Arts of the State of Baden-Württemberg, Stuttgart, Germany

*Equally contributing authors.

ABSTRACT

The present study investigated multivariate relationships between critical erosion thresholds of reservoir sediments and their physico-chemical and biological characteristics to unravel the effect of sedimentological parameters on fine sediment erosion. We collected 22 sediment cores from the deposits of two reservoirs located in southern Germany (Großer Brombachsee = GBS; Schwarzenbachtalsperre = SBT). An erosion flume and an advanced photogrammetric method were used to quantify critical erosion thresholds for a succession of vertical layers over sediment depth. The functional relationships between the critical erosion thresholds and a collection of sediment parameters, including bulk density, sediment composition, percentiles, cation exchange capacity, organic content, extracellular polymeric substances (EPS proteins and carbohydrates), and chlorophyll-a were examined. The clay-dominated sediments of the GBS with comparatively low

total organic carbon and sand content were on average 10 times more stable compared to the sandy sediments of the SBT. Consequently, for the clay-dominated sediments, strong positive correlations were found between the erosion thresholds and clay content. In contrast, the sandy sediment layers experienced strong positive correlations with the sand content and percentiles. The bulk density was mainly positively and the total organic carbon content was mainly negatively correlated with the erosion thresholds. Furthermore, EPS and chlorophyll-a were not good indicators for the erosion thresholds, suggesting an ambiguous influence of biology. Generally, the strength of the relations decreased for sediment layers deeper than 10 cm. Overall, our results underline the need to investigate the influence of sediment characteristics on fine sediment erodibility from varying natural environments.

INTRODUCTION

Understanding fine sediment erosion is of particular importance in various water-related fields in engineering and natural sciences. For instance, detailed process knowledge is inevitable to reliably predict morphodynamic changes in order to establish sustainable sediment management strategies (Aberle 2008; Annandale 1987). Numerous studies have investigated the erodibility of fine sediments with cohesive properties in riverine (Schäfer Rodrigues Silva et al. 2018; Noack et al. 2015), lacustrine (Righetti and Lucarelli 2007), and marine (Yang et al. 2019; Zhu et al. 2019) environments. Consequently, several empirical equations have been derived to estimate site-specific erosion potentials. Yet no universal relationships exist to model fine, cohesive sediment erosion (e.g., van Rijn 2020).

As motivation for our research, Figure 1 presents ranges of critical erosion thresholds (τ_{cr}) and their median particle size diameters (d_{50}) from previously conducted erosion studies in diverse environments, plotted together with those of the present study (GBS and SBT, see chapter 3). The figure also contains the Shields (1936) curve as a reference for coarse grains, empirical equations derived by Briaud (2008) and Briaud et al. (2017) to create upper and lower limits for the erosion thresholds of fine grained soils with a d_{50} <0.1 mm, and a refined upper limit based on our data ($\tau_{cr} = 0.001\ (d_{50})^{-2}$). Figure 1 reveals that a high range of variability exists for erosion threshold

data that cannot be accounted for by the d_{50} only and additional parametric effects beyond the d_{50} must influence the erosion threshold data (e.g., Briaud et al. 2017). This can be mainly attributed to variable physical (e.g., bulk density, sediment composition), chemical (e.g., total organic carbon content, cation-exchange capacity), and biological characteristics (e.g., contents of chlorophyll-a, extracellular polymeric substances) of natural sediments and their complex interactions (e.g., Burt et al. 1997; Berlamont et al. 1993; Grabowski et al. 2011; Kimiaghalam et al. 2016). Additionally, the capability of microbial aggregates (biofilm) to adhere to sediment particles or organic matter and bind them together have gained increasing attention recently (e.g., Gerbersdorf et al. 2020; Koca and Gerbersdorf 2019; Koca et al. 2019; Paterson et al. 2018; Gu et al. 2020). When growing on fine sediment, biofilm alters sediment properties and dynamics, leading to biostabilization (Gerbersdorf et al. 2020; Black et al. 2002; Righetti and Lucarelli 2007). For instance, Thom et al. (2015) described the erosion pattern of bio-inhabited sediment as crust or carpet-like, which was clearly different from pure sediment erosion. Despite the importance of chemical and biological sediment properties, most studies focus on physical sediment characteristics. Another challenge is the limited transferability of results to natural sediment conditions. The reason is that process understanding and existing erosion models have been mainly derived from laboratory experiments, conducted with non-cohesive/cohesive sediment mixtures or remolded sediments (e.g., Panagiotopoulos et al. 1997; Kothyari and Jain 2008; Zhang and Yu 2017). However, natural sediments are much more complex as they are graded and heterogeneous mixtures (Van Ledden 2003; Winterwerp et al. 2012; Schäfer Rodrigues Silva et al. 2018) with stratified bed properties (Lau et al. 2001), resulting in variable bed shear strengths in all directions of space (e.g., Tolhurst et al. 2006; Zhu et al. 2019; Beckers et al. 2020). Such effects can hardly be simulated with artificial non-cohesive/cohesive sediment mixtures, thus, experimental investigations with natural sediments are required. Furthermore, research on relationships between multivariate sediment properties and sediment erodibility is a pending requirement to improve our understanding in natural environments (Le Hir et al. 2007).

Erosion Thresholds for Cohesive Sediments

One of the most important parameter in experimental erosion studies is the threshold indicating the initiation of motion (Briaud 2008), that is, the critical shear stress. While the incipient motion of non-cohesive sediments can be described by the Shields (1936) curve and its versions (see Buffington and Montgomery 1997), no generally accepted relationships for the prediction of critical shear stresses are available for cohesive sediments (van Rijn 2020). The challenge in identifying a critical erosion threshold for cohesive sediments arises from the fact that multiple parameters (physical, chemical, biological) are involved in creating the shear strength (resistance) of cohesive sediments against the flow induced shear stress (e.g., Briaud 2008; Kothyari and Jain 2008; Zhu et al. 2019), leading to a complex and variable erosion behavior once the shear strength is locally exceeded.

Generally, cohesiveness forms for fine grained sediments in the clay ($\leq 2\mu$m) and silt size ($\leq 63\mu$m), although the clay concentration is primarily responsible for cohesion (Grabowski et al. 2011). Therefore, clay and silt are often combined and referred to as the 'mud' content of a mixture, where mud $\leq 63\mu$m (e.g., Mitchener and Torfs 1995; van Rijn 2020). Non-cohesive/cohesive sediment mixtures experience a cohesive erosion behavior once the mud content exceeds a certain threshold. This threshold is reported to be between 10% to 15% (Panagiotopoulos et al. 1997; Perera et al. 2020; Debnath et al. 2007; Mitchener and Torfs 1995). Furthermore, the shear strength of a non-cohesive/cohesive sediment mixture is influenced by different sediment compositions, consolidation/compaction, ion-exchange capacity, organic content, and biological activity (such as by a biofilm) (e.g., Berlamont et al. 1993). Therefore, exploring critical erosion thresholds of sediment mixtures exceeding a mud content of >5% becomes challenging, and consequently, different evaluation concepts and erosion threshold definitions exist.

Debnath and Chaudhuri (2010) reviewed and evaluated five erosion threshold definitions reported in the literature (see also Sanford and Maa 2001). These thresholds are defined by (i) the initial occurring sediment motion, (ii) significant occurring erosion, (iii) the intersect with the x-axis of a back extrapolated line from the plotted erosion rate, (iv) a sediment depth sequence

of increasing critical shear stress, and (v) an occurring burst in sediment motion (Debnath and Chaudhuri 2010; Sanford and Maa 2001). Additional threshold concepts can be found, which are often supplemented by describing the erosion behavior. Righetti and Lucarelli (2007) observed a multistep entrainment phenomenon by studying entrained particles and flocs (aggregates) in suspension using image analyses techniques. They defined a criterion to distinguish between the incipient motion of single particles and flocs or aggregates. Wu et al. (2018) considered the incipient surface erosion in their study and emphasized the effect of varying mud contents (low, moderate, high, and pure mud) on the erosion threshold. van Rijn (2020) reported thresholds of critical bed-shear stresses for particle, surface, and mass erosion which were visually determined from flume experiments. Beckers et al. (2020) measured emerging erosion spots caused by surface erosion and large holes torn open by detached aggregate chunks. Such specific erosion forms have also been visually observed by other researchers (e.g., McNeil et al. 1996; Roberts et al. 2003; Debnath et al. 2007), and their occurrence may also serve as threshold definition.

In summary, the multiple existing threshold definitions underline the complexity in identifying one universal critical erosion threshold for cohesive sediments and non-cohesive/cohesive sediment mixtures. Moreover, the existing definitions might describe different erosion and transport modes or different erosion types which are not always evident from the data (van Rijn 2020) and make the comparison additionally difficult (e.g., Aberle et al. 2006). Thus, it is deemed advisable to work with more than one threshold value to investigate multivariate relationships between critical erosion thresholds and sediment characteristics (e.g., Righetti and Lucarelli 2007; Briaud et al. 2017; van Rijn 2020; Le Hir et al. 2007).

In this study, we explore the functional relationships between the critical erosion thresholds and the sediment characteristics for the deposits of two reservoirs located in southern Germany. We removed sediment cores and investigated their erodibility in a multitude of erosion experiments using an advanced photogrammetric method. We considered incipient particle erosion (surface erosion) and the maximum occurring erosion using a slope criterion, which enables a robust assessment of the erosion data to obtain confident erosion thresholds. From a set of adjacent

sediment cores, we analyzed physico-chemical and biological sediment characteristics (bulk density, sediment composition, percentiles, total organic carbon, cation exchange capacity, chlorophyll-a, extracellular polymeric substances). Based on the collected data, we explored the multivariate relationships between the erosion thresholds and the sedimentological characteristics in vertical layers over sediment depth.

MATERIALS AND METHODS

Study Sites and Sediment Core Extraction

Two reservoirs with different sediment characteristics were investigated: i) The reservoir *Großer Brombachsee* (GBS) is the largest reservoir of the Franconian Lake district in Bavaria, Germany (49°07'47.6"N 10°55'60.0"E). It was built during 1983-1992 for the purpose of low water regulation of the Regnitz-Main catchment. In addition, it is used for recreation (Daus et al. 2019). At the maximum operation level (410.5 m.a.s.l.), the GBS has a water surface of 8.63 km^2 and a total storage volume of $143.73x10^3$ m^3 (Deutsches TalsperrenKomitee e. V. 2013). ii) The reservoir of the *Schwarzenbachtalsperre* (SBT) is located in the Northern Black Forest, Germany (48°39'25.6"N 8°19'28.9"E). It was built between 1922-1926 and is the upper reservoir in a pump-storage system. At the maximum operation level (668.5 m.a.s.l.), the Schwarzenbach reservoir has a water surface of 0.66 km^2 and provides a total storage volume of $14.42x10^6$ m^3 with a maximum length of 2.2 km, width of 600 m, and depth of 47 m (Mouris et al. 2018; Deutsches TalsperrenKomitee e. V. 2013). Two inflows, one transition tunnel, and the pumped water feed the reservoir.

In order to explore the sediment deposits, 9 and 13 sediment cores were removed from GBS and SBT, respectively (22 cores in total, Table 1). For this purpose we employed a Frahm-Sediment Sampler (see Beckers et al. 2018). With this device, relatively undisturbed sediment cores can be removed from deposits (maximum depth of operation is 100 m). This is ensured by using customized PVC-tubes to mitigate possible shearing effects during penetration. The tubes had a length of 1 m and a diameter of 0.1 m. Their lower opening was cut off diagonally at an angle of 5° and the wall was bevelled all around. Furthermore, the transparent PVC-tubes enabled a visual *in-situ* assessment of the sediment cores directly after the removal. In case of any signs of

157 disturbance, e.g., cracks or an oblique surface, the retrieved core was immediately rejected and not
158 used further (see also Beckers et al. 2019).

159 **Experimental Measurement Procedure**

160 The removed sediment cores were analyzed in several layers over core depth. First, the depth
161 distribution of bulk density (BD, see section 2) was measured for all 22 sediment cores with a
162 vertical resolution of 2 cm. Based on the similarity of the bulk density, sediment cores from an
163 investigated reservoir region (Table 1) were, first, assigned to each other and, second, assigned
164 to further destructive analyses. From the assignments made, a set of vertical layers was ana-
165 lyzed in terms of their physical and partly chemical and biological sediment characteristics (see
166 section 2). The remaining sediment layers were analyzed in terms of their erodibility using the
167 SETEG/PHOTOSED-system within the equivalent depths (see section 2). To ensure comparability
168 between sediment cores and to evaluate uncertainties associated with relating different sediment
169 cores (and layers) to each other, for either characterizing analyses or erosion experiments, percent-
170 age errors of BD were calculated. A maximum deviation of 7.5 % was allowed between two vertical
171 layers. This resulted in a correlation matrix containing 92 elements (see Beckers et al. 2021).

172 **Analysis of Physico-Chemical and Biological Sediment Parameters**

173 *Bulk Density*

174 The (wet) bulk density (BD) of each sediment core was measured non-destructively and prior
175 to any further analysis using a bulk densitometer (source: ^{137}CS with a decay energy 662 keV;
176 scintillator: NaI(TI)) (e.g., Mayar et al. 2020; Mayar et al. 2019). For the analysis, the sediment
177 core was placed between a traverse system that automatically moves down the core to measure the
178 BD at a predefined vertical spacing, here at 2 cm steps, to collect the BD profile over depth (Beckers
179 et al. 2018; Beckers et al. 2019).

180 *Sediment Composition and Percentiles*

181 The particle size distribution (PSD) was determined by laser diffraction with a Malvern Mas-
182 tersizer 2000 (Malvern Instruments Ltd, Malvern, UK). The instrument enables to measure particle

sizes in the milli-, micro- and nanometer range (0.02-2,000 μm) (Malvern Instruments 2007). From the measured particle sizes, the sediment composition (SC) was derived according to ISO 14688-1:2017 (2017). For the characterization of the deposits, we differentiated between clay, silt, and sand. Furthermore, the 10th-, 50th-, and 90th-percentiles (d_{10}, d_{50}, and d_{90}) were derived from the particle size distribution.

Total Organic Carbon and Cation Exchange Capacity

The Total Organic Carbon (TOC) was determined by loss on ignition (in percent) of dried sediment according to the European standard DIN EN 13137 (2001).

The effective Cation Exchange Capacity (CEC) was determined using hexamminecobalt(III)chloride as extracting solution to quantify the exchangeable cations using a spectrophotometric method according to the international standard ISO 23470:2018 (2018).

Extracellular Polymeric Substances and Chlorophyll-a

Extracellular Polymeric Substances (EPS) are secreted by microorganisms and mainly composed of proteins and carbohydrates (Gerbersdorf et al. 2020), accounting for 75-90% of the EPS-matrix (Tsuneda et al. 2003). The modified Lowry method (Raunkjær et al. 1994) and the phenol-sulfuric acid method by DuBois et al. (1956) were used to determine the water-extracable fraction of EPS-proteins (EPS-p) and EPS-carbohydrates (EPS-c), respectively.

Chlorophyll-a (CHL-a), a proxy for autotrophic biomass of biofilm, was extracted and quantified before and after acidification using a photometric analysis (DIN 38412-16:1985-12 1985).

Experiments for Investigating the Erosion Potential

Erosion experiments were conducted using the SETEG/PHOTOSED-system (Figure 2). The system consists of the SETEG erosion flume (Kern et al. 1999), whose general construction resembles different laboratory erosion flumes exploring the erosion potential of cohesive sediments and non-cohesive/cohesive sediment mixtures (e.g., McNeil et al. 1996; Briaud et al. 2001; Roberts et al. 2003). The flume is constructed as a straight, rectangular, transparent, and closed flume that is operated under pressurized flow. It has a length of 8.00 m, a width of 0.142 m, and a height of

0.10 m (inner dimensions) and allows to investigate flow rates from 1 to 65 ls^{-1} ($\tau \approx 0.04$ - 32 Pa). The SETEG erosion flume is complemented by PHOTOSED, a versatile photogrammetric method to detect sediment erosion (Noack et al. 2018) at high resolution (detection limit: Δz_{min}=0.1 mm on approximately 10 mm^2).

During an erosion experiment, sediment cores were locked in position at the flume bottom from below (circular opening, see Figure 1 in Beckers et al. (2020)). By means of a mechanical lifting apparatus, (pre-)selected sediment layers were vertically elevated and positioned for erosion tests. The protruding sediment was cut off by a wire, leaving the sediment layer flush with the flume bottom (see Figure 46 in Beckers et al. (2019)). Next, the sediment response against a set of incrementally increasing shear stresses (t_τ=600s), as an *a priori* calibrated function of flow (Beckers et al. 2020), was explored until sediment failure was observed. Caution was taken to start each experiment at a bed shear stress below the threshold for incipient motion. During the experiments, a semiconductor laser with a diffraction optic was projected onto the sediment surface, resulting in a structured light pattern of approximately 24,000 points (on a surface area of 143 cm^2). The changes of the sediment surface were continuously monitored by a CMOS camera (2 MP, 10 Hz, Imaging Development Systems GmbH, Obersulm, Germany).

In a post-processing routine, the volumetric change of the sediment layer between consecutive frames (here: Δt = 60 s) was computed within a user-specified region of interest (ROI with area of 2456 mm^2) using Farnebaeck's Dense Optical Flow algorithm (Farnebäck 2003). This provides the volumetric change of the sediment surface as a function of the applied shear stress over time. Consequently, the method accounts for both, eroded material being transported in suspension and along the bed. Furthermore, selecting a ROI with sufficient distance from the core edge, allows to mitigate potential boundary effects impacting on the erosion data. This provides reliable data and the means to distinguish between fundamental erosion processes and specific erosion forms (see Beckers et al. (2020)).

Identification of Critical Erosion Thresholds

The measurements with the SETEG/PHOTOSED-system provide the means to identify critical erosion thresholds (τ_c) from the time-series of the recorded erosion volumes. To address existing uncertainties in data analysis and interpretation (e.g., Aberle et al. 2006), we followed a pseudo-automatic approach to identify confident erosion threshold values. After plotting the cumulative erosion volume V_e (aggregated over the ROI) over the entire duration of an erosion experiment (investigated sediment layer at a certain core depth), we applied a slope-criterion (see also Gularte et al. 1980; Mehta and Partheniades 1982; Righetti and Lucarelli 2007) that identifies change points based on the derivative of the data (acceleration points) (Figure 3). The initial rise of the curve (Figure 3 A, τ=0.5 Pa) can be attributed to particle and surface erosion. The shear stress at this point is denoted as $\tau_{c,0}$ and often defined as the critical shear stress for incipient motion (e.g., Young and Southard 1978; Wu et al. 2018).

Furthermore, we consider the evidence of Righetti and Lucarelli (2007) who reported a multistep entrainment phenomenon with changing erosion regimes for cohesive sediment erosion. This change in the erosion regime (or in the erosion behavior) is the response of the sediment to an exceedance of the shear stress which induces significant erosion (see also Beckers et al. 2020). It is represented by the maximum change in slope (maximum acceleration) of the erosion data (Figure 3 A, τ=1.61 Pa). The shear stress applied at this threshold was also considered in our study and denoted as $\tau_{c,S}$.

It must be noted that for some cases $\tau_{c,0}$ coincides with $\tau_{c,S}$. This is particularly the case for fully consolidated and uniform sediments, because they erode at a constant rate once the erosion is initiated, which is often referred to as Type II (steady-state or unlimited) erosion (Mehta and Partheniades 1982; Sanford and Maa 2001; Aberle 2008). Consequently, no clear distinction between different erosion regimes can be made when the erosion progresses continuously over time (see Figure 3 B; $\tau_{c,0}$=$\tau_{c,S}$=1.61 Pa).

Statistical Analysis

The statistical analyses between the sediment characteristics and the critical erosion thresholds were conducted using *R* (v.3.5.1) (R Core Team 2017) with *RStudio* (v.1.1.423) (rstudio.com). Graphs and Figures were mainly produced using *ggplot2* package (Wickham 2016). The degree of potential relationships among the sediment characteristics and the critical erosion thresholds was conducted using a Pearson correlation analysis with the *Hmisc* package (Harrell Jr et al. 2020). Prior to an analysis, univariate and multivariate normality was tested using the test of Shapiro and Wilk (1965), followed by log- and arcsine square-root-transformations as needed. Transformation of data frames were performed using the *dplyr* package (Wickham et al. 2020). Pearson correlation coefficients at a significance level (p-value ≤ 0.05) between the selected variables indicating functional relationships were plotted by means of correlograms using the *Corrplot* package (Wei and Simko 2017).

Furthermore, the data was categorized into two groups of sediment depth to explore depth-dependency of the correlations. These groups were A (0-10 cm) and B (>10 cm). Draftsman plots were generated to visualize depth-dependent correlations using the *Performance Analytics* package (Peterson and Carl 2020). Next, the variations of the correlation coefficients were explored for the evaluated sediment parameters in the depth-dependent layers. In the correlation graphs, "+1" represents a perfect positive correlation and "-1" represents a perfect negative correlation, whereas "0" represents no relationship. The statistical significance of the relationships was evaluated at various significance levels, which are indicated in the results.

RESULTS AND DISCUSSION

Synthesis of Sediment Characteristics and Critical Erosion Thresholds

Table 2 provides the summary of the minimum, mean, and maximum values for all measured sediment parameters. The complete data set is freely available online (Beckers et al. 2021).

In general, the measured critical erosion thresholds $\tau_{c,0}$ and $\tau_{c,S}$ in the GBS are on average approx. 10 times higher than those in the SBT. While the lower limit of the measured values of $\tau_{c,0}$ and $\tau_{c,S}$ is of similar range, the maximum values differ by an order of magnitude (see Table 2).

The high erosion thresholds of the GBS deposits can be attributed to larger BD, mud, and clay contents. An increase of these parameters are generally associated with a higher erosion stability (e.g., Mitchener and Torfs 1995; Panagiotopoulos et al. 1997; Kothyari and Jain 2008; Van Ledden 2003; Wu et al. 2018). Along with an increase in clay content, the CEC increases since it is a proxy for the electro-chemical activity of clay minerals (Partheniades 2007). Accordingly, a high CEC suggests a high cohesive strength of a sediment mixture, and thus, results in a higher erosion stability (e.g., Gerbersdorf et al. 2007). Moreover, the GBS sediments are characterized by comparatively low TOC (≤3.7%), which is indicative of high erosion stability as an increased TOC accumulation could increase the erodibility of sediment deposits (e.g., Mehta 1991).

The lower erosion stability of the SBT deposits can be explained by an overall lower BD due to the presence of organic-rich sediments (TOC≥8.38%) and little consolidation (as indicated by the low BDs), which suggests a high water content (Fukuda and Lick 1980). Furthermore, the sand content is substantially larger (see Table 2). These sediment characteristics are generally associated with low erosion stability (see Grabowski et al. 2011) and confirm previous findings (e.g., Mitchener and Torfs 1995; Panagiotopoulos et al. 1997; Zhang and Yu 2017). It is worth mentioning that Krishnappan et al. (2020) observed similar critical thresholds (τ_c = 0.09 Pa) for fine-grained cohesive river sediment. They observed the sediment particles were interconnected through loose fibril material, which is an effect of microbial secretion or of the present organic material.

Noticeable in the SBT data are low BD values (<1 g cm^{-3}). This indicates gas in the sediment (Grabowski et al. 2011). The formation of carbon dioxide and methane mainly results from anaerobic carbon mineralization in anoxic sediments (Segers 1998). Given the sediment composition and organic content of the SBT deposits, gas formation in the SBT sediment occurs (see Peeters et al. 2019), and gas fluxes to the atmosphere have been reported (see Encinas Fernández et al. 2020). Generally, the presence of gas decreases the stability (Jepsen et al. 2000), which additionally supports the lower critical shear stresses measured for the SBT deposits.

Given the SC, low BDs (≤1.11 %), and the amount of TOC (≥8.38 %), we expected high

biological activity in the sediments of the SBT. Thus, we analyzed a set of biological parameters to consider their influence on the sediment stability (see section 3). The microalgae biomass indicated by the CHL-a content (40.68-412.71 μg g^{-1}) confirms this hypothesis, since the present range corresponds to and exceeds values of biologically active sediments (e.g., de Brouwer et al. (2003) found a range of 1.0-10.3 μg g^{-1} in the top 0.5 cm for three intertidal mudflats located in different geographical areas in Northwest Europe; Gerbersdorf et al. (2007) found a range of 35-197 μg g^{-1} in the river Neckar in the top 2.0 cm of the sediment). Similarly, the EPS contents found in the SBT sediments confirm the hypothesis of biologically active sediment. For instance, Morelle et al. (2020) observed highly productive sediments in the intertidal areas downstream of Seine estuary (Normandy, France), with EPS-c and EPS-p contents being larger than 70 μg g^{-1} in autumn and 35 μg g^{-1} in spring samples due to the higher percentage of fine particles in summer. While underlying the importance of fine sediments for biofilm production, the range of EPS contents observed by Morelle et al. (2020) is at least 10 times lower compared to those in the SBT.

Functional Relationships between Critical Erosion Thresholds and Sediment Characteristics of the GBS Deposits

Positive correlations were observed for the GBS sediments between the critical erosion thresholds and the sediment depth, bulk density, and clay content, whereas negative correlations were found with the TOC content, d_{10}, silt content, and d_{50} (Figure 4). These correlations follow typical findings of parametric dependencies with cohesive erosion thresholds. Particularly, bulk density was most closely and positively associated with the critical erosion thresholds, which is also reported from other studies (e.g., McNeil et al. 1996; Gerbersdorf et al. 2007; van Rijn 2020).

A decrease in d_{10} and d_{50} implies an increase in fine sediments. Although the silt content is negatively correlated with the critical erosion thresholds, this is outweighed by the positive correlation of the clay content (Figure 4). This highlights the role of clay content (not the silt or mud content) on the cohesive erosion resistance, supporting previous findings (e.g., Schäfer Rodrigues Silva et al. 2018; van Rijn 2020). Similar to the findings of Mehta (1991), we also observed negative correlations between the critical erosion thresholds and the TOC content. Despite

the impact of TOC on the erodibility of cohesive sediments is widely recognized (Grabowski et al. 2011), the effect on sediment stability is still ambiguous. Additionally, the erosion resistance increased with sediment depth, which confirms results obtained from experiments investigating depth-dependent erosion of natural cohesive sediments (e.g., McNeil et al. 1996; Lick and McNeil 2001) and supports the general understanding of depth-limited erosion (Mehta and Partheniades 1982).

To study a variation of functional relationships over sediment depth, we divided the results into two depth regions. Region A represents depths of 0-10 cm and B represents depths of >10 cm. The trend of the depth-sequenced correlations is mainly consistent for region A and B (Table 3 and Figure S1). The erosion resistance increases with BD and clay content and decreases with d_{10} and TOC content through regions A and B. Interestingly, the stabilizing effect of d_{50} and d_{90} changes from region A to region B, which is not reflected in Figure 4. Since the average particle sizes are only slightly different, this demonstrates the complexity in identifying functional relationships and highlights the necessity to consider parametric relationships in various depth-sequences. Moreover, an increase in silt content suggests a decrease in the erosion resistance. However, the significance levels of the correlations are in the range of p = 0.06-0.15, and thus, caution must be taken. Since the sand content in the GBS deposits is overall small (≤6.72 %), no significant correlations were found. Furthermore, it becomes evident that the different types of critical erosion thresholds ($\tau_{c,0}$ and $\tau_{c,S}$) yield different functional relationships with the sediment characteristics. The correlations between the sediment characteristics and $\tau_{c,S}$ are stronger compared to $\tau_{c,0}$ for the depth regions A (0-10 cm) and B (>10 cm). We attribute this to the fact that the identification of initial surface erosion, reflected by $\tau_{c,0}$, is difficult for sediments with a "strong cohesive erosion behavior" since tearing of flocs is highly variable due to stochastic nature of flow. In turn, the detection of a change in the erosion regime, indicated by $\tau_{c,S}$, is more robust for this type of sediments, thus, yielding stronger correlations with sediment characteristics.

Functional Relationships between Critical Erosion Thresholds and Sediment Characteristics of the SBT Deposits

For the SBT deposits, significant positive correlations were observed between the critical erosion thresholds and the d_{50} as well as the sand content, whereas significant negative correlations were observed with the clay and silt content as well as sediment depth (Figure 5).

The observed relationships seem contradictory at first, since one would rather expect positive relationships between the erosion thresholds and mud (clay and silt) content instead of the sand content. This effect was also reflected by the positive correlations between the critical erosion thresholds and d_{50}, since a positive correlation indicates an increasing erosion stability with an increasing median particle size diameter. It is interesting to note that a negative correlation between sediment stability and silt content was also observed for the GBS deposits (Figure 4). It has been reported that the highest erosion resistance of non-cohesive/cohesive sediment mixtures emerges at a certain mud/sand ratio. Mitchener and Torfs (1995) found this ratio to be 30-50% mud added to sand by weight while Perkey et al. (2020) reported the maximum critical shear stress at a mud content of 30-40% for homogeneously mixed non-cohesive/cohesive sediments. The SBT sediments showed a mud content of 71.71-85.58% and a sand content of 14.42-28.30% (Table 2). Therefore, it is conceivable that the SBT sediments with a higher sand content are closer to the optimal mud/sand ratio, and thus, leading to higher shear strength and to a positive correlation between the critical erosion thresholds and sand content and (d_{50}). The negative correlation between the erosion thresholds and the sediment depth suggests that there is no uniform vertical trend of the sediment characteristics. For example, Figure 5 indicates a negative correlation between BD and sediment depth. This implies that the SBT deposits do not show a classical trend with an increasing consolidation level over the depth. Such trends have been reported for natural sediments due to intermediate layers of differently composed sediment (e.g., Gerbersdorf et al. 2007). The SBT deposits were further weakly consolidated with low mean and minimum BDs (Table 2). This results from the organic matter content and biologically active sediment, which likely leads to gas production as reflected in the low BDs in some layers (see Beckers et al. 2021). In freshwater lakes,

the highest gas concentrations are usually found below a certain sediment depth (e.g., Thebrath et al. 1993; Kuivila et al. 1989). Thus, the presence of gas explains low BDs in the deeper located sediment layers and the negative correlation between BD and sediment depth.

By evaluating the variation of correlations over the two depth regions, multiple significant correlations with $\tau_{c,0}$ can be observed for the region A (0-10 cm) (Table 4 and Figure S2). The statistical analysis indicates that the erosion resistance of the SBT deposits significantly increases with sand content and the percentage values (d_{10}, d_{50}, and d_{90}) and decreases with contents of clay, silt, and TOC. These relationships resemble the erosion behavior of non-cohesive sediment despite the fact that the sediment of the SBT are composed of sufficient fine material to expect cohesion (Table 2). Thus, the erosion behavior can be explained by the mud/sand ratio, low BDs due to higher TOC and biologically active sediment, as well as by the weakly consolidated material in the SBT sediments (see Beckers et al. 2021). In the depth region B (>10 cm), a significant positive correlation was only found between the critical erosion threshold $\tau_{c,s}$ and BD ($R = 0.54$; $p < 0.01$), further suggesting that the erosion stability increases with BD. However, since the BD ranges between 0.91-1.11 g cm^{-3}, as result of organic matter, little consolidation, and the presence of gas, it is difficult to make any concluding statement. Rather, the findings for the SBT underline the importance of considering different depth-sequences for weakly consolidated reservoir deposits since sediment parameters change over depth in a complex and nontrivial way.

Comparison of Functional Relationships between the GBS and SBT Deposits

The overall variation of Pearson's correlation coefficients (Figure 6) indicates that the functional relationships between the critical erosion thresholds and the sediment characteristics were stronger for the region A (0-10 cm) for both, GBS and SBT deposits. The correlations decreased at deeper sediment layers represented by region B (>10 cm). Furthermore, the SBT sediments showed less significant and weaker correlations, particularly for the deeper sediment layers (region B >10 cm) (compare with Table 3 and 4). As a whole, this highlights the complexity in identifying functional relationships for strongly heterogeneous and biologically active natural sediments, such as from the SBT (see section 3), compared to deposits of moderate heterogeneity, such as from the GBS (see

section 3).

In general, the strongest parameter-specific functional relationship with the critical erosion thresholds was found for the BD. Averaged over all depth regions, the BD yielded the correlation coefficients of $R_{\tau_{c,0}}$=0.61 and $R_{\tau_{c,S}}$=0.79. Moreover, the clay content ($R_{\tau_{c,0}}$=0.57 and $R_{\tau_{c,S}}$=0.77) and d_{10} ($R_{\tau_{c,0}}$=-0.55 and $R_{\tau_{c,S}}$=-0.76) indicated strong correlations with the erosion thresholds. The weakest relationship was found for the silt content through all regions, however, the correlation was still high ($R_{\tau_{c,0}}$=0.47 and $R_{\tau_{c,S}}$=0.67). These results support various findings reported in previous studies (van Rijn 2020; Schäfer Rodrigues Silva et al. 2018; Mitchener and Torfs 1995; Panagiotopoulos et al. 1997).

LIMITATIONS AND RECOMMENDATIONS

The use of sediment cores for depth-dependent erosion tests is a common practice (e.g., Schäfer Rodrigues Silva et al. 2018; McNeil et al. 1996; Briaud et al. 2001; Righetti and Lucarelli 2007). However, the removal of sediment cores from sediment deposits may cause certain types of disturbance (see Dück et al. 2019). Through technical measures, coring disturbances can be mitigated (see section 2) but never fully avoided. For instance, (McIntyre 1971) reported on the necessity to use coring tubes with a diameter of ≥0.1 m to overcome sampling problems at the sediment-water interface. In particular, the escape of gas bubbles from the sediment during coring or core transportation may disturb the sediment structure. Although, technical methods such as freeze coring preserve the gas bubbles in the sediment (Dück et al. 2019), freezing and thawing may also alter the sediment structure, making this method unsuitable for erosion studies. Yet, we are aware that a non-quantifiable error from core removal and transportation exists in all erosion studies where sediment cores are employed.

Regarding the method of core allocation for data analysis, four limitations must be mentioned:

First, we assume that the BD is as a representative bulk parameter for sediment characteristics to assign sediment layers to each other for subsequent analyses. We allowed a maximum deviation of 7.5% between two layers when assigning them to each other. In doing so, we quantified the error from this frequently used method in sediment research (e.g., Righetti and Lucarelli 2007;

Gerbersdorf et al. 2007). Consequently, a maximum uncertainty interval of ±7.5% can exist. This may also explain the scatter in the data, particularly in the case of the SBT sediments (see Beckers et al. 2021). As described in section 2, some sediment samples could be collected for characterizing analyses prior to the start of an erosion experiment directly from the SETEG flume. This procedure should be preferred in principle, but it depends strongly on the sediment characteristics and the possibilities to obtain representative samples from the erosion flume. However, in this case, the sediment characteristics directly correspond to the measured erosion thresholds and no error from assigning different layers to each other exist (see Beckers et al. 2021).

Second, the procedure to analyze the erosion data for detecting critical erosion thresholds offers advantages over a visual determination since it works analytically and is thus not biased by different user opinions. Potential problems arise from the fact that a small flaw in the surface, maybe due to the vertical slicing (see Beckers et al. 2019), might lead to local sediment movement at the beginning of an erosion experiment. Since PHOTOSED is very sensitive and detects even small erosion events (Beckers et al. 2020), this could result in an initial rise of the erosion volume. We overcome this challenge by applying a pseudo-automatic routine, which requires confirmation by the operator before a threshold is finally stored, allowing to cross-check the individual frames in case of ambiguity. Furthermore, we consider two erosion thresholds (as explained in section 2) to consider the multiple different threshold concepts employed by various authors (see Debnath and Chaudhuri 2010; Sanford and Maa 2001).

Third, we focused on a collection of promising parameters to describe the sediment characteristics. Although they encompass physical, chemical, and biological parameters, we do not claim to have included all relevant parameters (e.g., Berlamont et al. 1993; Grabowski et al. 2011). As mentioned, parameters such as gas content in the sediment were not considered although it may affect the erodibility (Lick and McNeil 2001; Jepsen et al. 2000) and must be considered in future studies on the erodibility of natural reservoir sediments.

Fourth, although our data set was comparably large (see Beckers et al. 2021), it was not large enough to ensure statistical significance for all considered parametric functional relationships

(Table 3 and 4, Figure 4 and 5). Therefore, it is advisable to increase the data pool and we welcome if other researchers utilize our data in their work.

SUMMARY AND CONCLUSIONS

In this study, we presented critical erosion thresholds as well as a collection of physico-chemical and biological sediment characteristics for the deposits of two reservoirs located in southern Germany, namely Großer Brombachsee (GBS) and Schwarzenbach reservoir (SBT). Critical erosion thresholds were evaluated from experimental data obtained with an erosion flume and an advanced photogrammetric system that can detect and quantify erosion events at high spatial and temporal resolution. We considered two erosion thresholds (expressed as critical shear stresses) by using a slope criterion applied to the cumulative erosion volume: i) the threshold for incipient particle (surface) erosion and ii) the threshold indicating a change in the erosion behavior/regime. Based on a large data set measured at various depth-dependent sediment layers (Beckers et al. 2021), we explored the functional relationships between the erosion thresholds and the evaluated sediment parameters. Based on the presented results, the following conclusions can be summarized:

1. The GBS sediments were characterized by an increasing bulk density, clay and silt content, and cation exchange capacity as well as by decreasing contents of sand and total organic carbon over the sediment depth.
2. The SBT sediments were characterized by a comparatively low bulk density (1.02 g cm^{-3} on average), with no clear trend of sedimentological characteristics over sediment depth. Furthermore, the SBT sediments were, in comparison to the GBS sediments, characterized by lower clay and silt contents and a lower cation exchange capacity, but by higher sand and total organic carbon contents. In general, the SBT sediments were characterized by high biological activity.
3. The sediment deposits of the GBS were on average 10 times more resistant against erosion compared to those of the SBT.
4. For the GBS deposits, strong positive correlations were observed between critical erosion

thresholds and clay content, and to a less extent with bulk density. Strong negative correlations were observed between erosion thresholds and total organic carbon content. The correlations of erosion thresholds and sediment characteristics consistently decreased over depth.

5. In contrast, for the SBT sediments, strong negative correlations were found between the erosion thresholds and the clay content, which can be attributed to the comparatively higher sand content (by approx. a factor of 6). The increased sand content was strongly associated with increasing erosion thresholds in the first 10 cm of the sediment core, but this relation diminished in deeper layers. We attributed this effect to high biological activity in deeper layers, which complicated the elucidation of clear functional relationships for the SBT deposits.

Future experimental erosion studies are required to consider more physico-chemical and biological sediment parameters from different reservoir deposits consisting of various fine sediment mixtures. This will help to increase the data pool for statistical analysis in pursuit of better understanding of the functional relationships between sediment stability and sediment characteristics. To foster a standardized approach and facilitate the comparison between different studies, multiple critical erosion thresholds using advanced quantitative methods should be considered, an example of which was presented in this paper.

Acknowledgements

This study was carried out within the project CHARM - Challenges of Reservoir Management - Meeting Environmental and Social Requirements. The project is funded by the Ministry of Science, Research, and Arts of the federal state of Baden-Württemberg, Germany. It is part of the Water Research Network Baden-Württemberg.

We gratefully acknowledge the help of Mr. Ruslan Biserov in conducting various erosion experiments. We also thank colleagues and student assistants involved in the CHARM project.

Data Availability Statement and Supporting Information

All data generated or used during the study are available in a repository online in accordance with funder data retention policies (Beckers et al. 2021). Direct link to data doi.org/10.5281/zenodo.4474529.

Conflict of Interest

The authors have no conflict of interest to declare.

Supplemental Materials

Figs. S1 and S2 are available online in the ASCE Library (ascelibrary.org)

REFERENCES

Aberle, J. (2008). *Measurement techniques for the estimation of cohesive sediment erosion*. Hydraulic Methods for Catastrophes: Floods, Droughts, Environmental Disasters. Publications of the Institute of Geophysics, Polish Academy of Sciences.

Aberle, J., Nikora, V., and Walters, R. (2006). "Data Interpretation for In Situ Measurements of Cohesive Sediment Erosion." *Journal of Hydraulic Engineering*, 132(6), 581–588.

Annandale, G. (1987). *Reservoir Sedimentation*. Elsevier Science, Burlington OCLC: 1162022726.

Beckers, F., Biserov, R., and Wieprecht, S. (2019). "Experimental Investigation of Sediment Stability at Reservoirs on the Rhône River." *Technical Report 09/2019*, Institute for Modelling Hydraulic and Environmental Systems (IWS), Stuttgart, Germany.

Beckers, F., Haun, S., and Noack, M. (2018). "Experimental investigation of reservoir sediments." *E3S Web of Conferences*, 40, 03030.

Beckers, F., Inskeep, C., Haun, S., Schmid, G., Wieprecht, S., and Noack, M. (2020). "High spatio-temporal resolution measurements of cohesive sediment erosion." *Earth Surface Processes and Landforms*, esp.4889.

Beckers, F., Koca, K., Haun, S., Noack, M., Gerbersdorf, S. U., and Wieprecht, S. (2021). "Data related to the manuscript "Functional relationships between critical erosion thresholds of fine reservoir sediments and their sedimentological characteristics"." *Zenodo*, Data set (Version 1).

549 Berlamont, J., Ockenden, M., Toorman, E., and Winterwerp, J. (1993). "The characterisation of
550 cohesive sediment properties." *Coastal Engineering*, 21, 105 – 128.
551 Black, K. S., Tolhurst, T. J., Paterson, D. M., and Hagerthey, S. E. (2002). "Working with natural
552 cohesive sediments." *Journal of Hydraulic Engineering*, 128(1), 2–8.
553 Briaud, J.-L. (2008). "Case Histories in Soil and Rock Erosion: Woodrow Wilson Bridge, Brazos
554 River Meander, Normandy Cliffs, and New Orleans Levees." *Journal of Geotechnical and*
555 *Geoenvironmental Engineering*, 134(10), 1425–1447.
556 Briaud, J.-L., Govindasamy, A. V., and Shafii, I. (2017). "Erosion Charts for Selected Geomateri-
557 als." *Journal of Geotechnical and Geoenvironmental Engineering*, 143(10), 04017072.
558 Briaud, J. L., Ting, F. C. K., Chen, H. C., Cao, Y., Han, S. W., and Kwak, K. W. (2001). "Erosion
559 Function Apparatus for Scour Rate Predictions." *Journal of Geotechnical and Geoenvironmental*
560 *Engineering*, 127(2), 105–113.
561 Buffington, J. M. and Montgomery, D. R. (1997). "A systematic analysis of eight decades of incipient
562 motion studies, with special reference to gravel-bedded rivers." *Water Resources Research*, 33(8),
563 1993–2029.
564 Burt, N., Parker, R., and Watts, J. H. (1997). *Cohesive Sediments*. John Wiley, Chichester, UK.
565 Daus, M., Koberger, K., Gnutzmann, N., Hertrich, T., and Glaser, R. (2019). "Transferring Water
566 While Transforming Landscape: New Societal Implications, Perceptions and Challenges of
567 Management in the Reservoir System Franconian Lake District." *Water*, 11(12), 2469.
568 de Brouwer, J., de Deckere, E., and Stal, L. (2003). "Distribution of extracellular carbohydrates
569 in three intertidal mudflats in Western Europe." *Estuarine, Coastal and Shelf Science*, 56(2),
570 313–324.
571 Debnath, K. and Chaudhuri, S. (2010). "Cohesive sediment erosion threshold: a review." *ISH*
572 *Journal of Hydraulic Engineering*, 16(1), 36–56.
573 Debnath, K., Nikora, V., Aberle, J., Westrich, B., and Muste, M. (2007). "Erosion of Cohesive
574 Sediments: Resuspension, Bed Load, and Erosion Patterns from Field Experiments." *Journal of*
575 *Hydraulic Engineering*, 133(5), 508–520.

576 Deutsches TalsperrenKomitee e. V., ed. (2013). *Talsperren in Deutschland [Dams and reservoirs*
577 *in Germany]*. Springer Fachmedien Wiesbaden, Wiesbaden.
578 DIN 38412-16:1985-12 (1985). *German standard methods for the examination of water, waste*
579 *water and sludge; test methods using water organisms (group L); determination of chlorophyll-a*
580 *in surface water (L 16)*.
581 DIN EN 13137 (2001). *Characterization of waste - Determination of total organic carbon (TOC)*
582 *in waste, sludges and sediments* (December).
583 DuBois, M., Gilles, K. A., Hamilton, J. K., Rebers, P. t., and Smith, F. (1956). "Colorimetric method
584 for determination of sugars and related substances." *Analytical chemistry*, 28(3), 350–356.
585 Dück, Y., Lorke, A., Jokiel, C., and Gierse, J. (2019). "Laboratory and field investigations on freeze
586 and gravity core sampling and assessment of coring disturbances with implications on gas bubble
587 characterization." *Limnology and Oceanography: Methods*, lom3.10335.
588 Encinas Fernández, J., Hofmann, H., and Peeters, F. (2020). "Diurnal Pumped-Storage Opera-
589 tion Minimizes Methane Ebullition Fluxes From Hydropower Reservoirs." *Water Resources*
590 *Research*, 56(12).
591 Farnebäck, G. (2003). "Two-Frame Motion Estimation Based on Polynomial Expansion." *Image*
592 *Analysis*, G. Goos, J. Hartmanis, J. vanLeeuwen, J. Bigun, and T. Gustavsson, eds., Vol. 2749,
593 Springer Berlin Heidelberg, Berlin, Heidelberg, 363–370.
594 Fukuda, M. K. and Lick, W. (1980). "The entrainment of cohesive sediments in freshwater." *Journal*
595 *of Geophysical Research*, 85(C5), 2813.
596 Gerbersdorf, S. U., Jancke, T., and Westrich, B. (2007). "Sediment Properties for Assessing the
597 Erosion Risk of Contaminated Riverine Sites. An approach to evaluate sediment properties and
598 their covariance patterns over depth in relation to erosion resistance. First investigations in natural
599 sediments (11 pp)." *Journal of Soils and Sediments*, 7(1), 25–35.
600 Gerbersdorf, S. U., Koca, K., de Beer, D., Chennu, A., Noss, C., Risse-Buhl, U., Weitere, M., Eiff,
601 O., Wagner, M., Aberle, J., Schweikert, M., and Terheiden, K. (2020). "Exploring flow-biofilm-
602 sediment interactions: Assessment of current status and future challenges." *Water Research*,

185, 116182.

Grabowski, R. C., Droppo, I. G., and Wharton, G. (2011). "Erodibility of cohesive sediment: The importance of sediment properties." *Earth-Science Reviews*, 105(3-4), 101–120.

Gu, Y., Zhang, Y., Qian, D., Tang, Y., Zhou, Y., and Zhu, D. Z. (2020). "Effects of microbial activity on incipient motion and erosion of sediment." *Environmental Fluid Mechanics*, 20(1), 175–188.

Gularte, R., Kelly, W., and Nacci, V. (1980). "Erosion of cohesive sediments as a rate process." *Ocean Engineering*, 7(4), 539–551.

Harrell Jr, F. E., Dupont, w. c. f. C., and others, m. (2020). *Hmisc: Harrell Miscellaneous*, <https://CRAN.R-project.org/package=Hmisc>.

ISO 14688-1:2017 (2017). *Geotechnical investigation and testing – Identification and classification of soil – Part 1: Identification and description (ISO 14688-1:2017)*.

ISO 23470:2018 (2018). *DIN EN ISO 23470, Soil quality – Determination of effective cation exchange capacity (CEC) and exchangeable cations using a hexamminecobalttrichloride solution (ISO 23470:2018)* (December).

Jepsen, R., McNeil, J., and Lick, W. (2000). "Effects of Gas Generation on the Density and Erosion of Sediments from the Grand River." *Journal of Great Lakes Research*, 26(2), 209–219.

Kern, U., Haag, I., Schürlein, V., Holzwarth, M., and Westrich, B. (1999). "Ein Strömungskanal zur Ermittlung der tiefenabhängigen Erosionsstabilität von Gewässersedimenten: das SETEG-System." *Wasserwirtschaft*, 89, 72–77.

Kimiaghalam, N., Clark, S. P., and Ahmari, H. (2016). "An experimental study on the effects of physical, mechanical, and electrochemical properties of natural cohesive soils on critical shear stress and erosion rate." *International Journal of Sediment Research*, 31(1), 1–15.

Koca, K. and Gerbersdorf, S. U. (2019). "Biofilms stabilize fine sediment in reservoirs: Dynamic interactions between flow, substrate and community." *Proc. of the 10th EcomeetIng*, Stuttgart, Germany, 21-22.02.2019.

Koca, K., Wieprecht, S., and Gerbersdorf, S. U. (2019). "Biostabilization of fine sediment in

river and reservoirs: Exploring the interplay between flow, substrate and community." *Proc. of the International Conference onCohesive Sediment Transport Processes 2019 (INTERCOH)*, Istanbul, Turkey, 13 -17.10.2019.

Kothyari, U. C. and Jain, R. K. (2008). "Influence of cohesion on the incipient motion condition of sediment mixtures." *Water Resources Research*, 44(4).

Krishnappan, B. G., Stone, M., Granger, S. J., Upadhayay, H. R., Tang, Q., Zhang, Y., and Collins, A. L. (2020). "Experimental Investigation of Erosion Characteristics of Fine-Grained Cohesive Sediments." *Water*, 12(5), 1511.

Kuivila, K., Murray, J., Devol, A., and Novelli, P. (1989). "Methane production, sulfate reduction and competition for substrates in the sediments of Lake Washington." *Geochimica et Cosmochimica Acta*, 53(2), 409–416.

Lau, Y. L., Droppo, I. G., and Krishnappan, B. G. (2001). "Sequential erosion/deposition experiments - demonstrating the effects of depositional history on sediment erosion." *Water research*, 35(11), 2767–2773.

Le Hir, P., Monbet, Y., and Orvain, F. (2007). "Sediment erodability in sediment transport modelling: Can we account for biota effects?." *Continental Shelf Research*, 27(8), 1116–1142.

Lick, W. and McNeil, J. (2001). "Effects of sediment bulk properties on erosion rates." *The Science of The Total Environment*, 266(1-3), 41–48.

Malvern Instruments (2007). *Mastersizer 2000 - User Manual*, Vol. MAN0384-1.0. Malvern Instruments Ltd., Worcestershire, United Kingdom, man0384-1.0 edition.

Mayar, M. A., Schmid, G., Wieprecht, S., and Noack, M. (2019). "Optimizing vertical profile measurements setup of gamma ray attenuation." *Radiation Physics and Chemistry*, 164, 108376.

Mayar, M. A., Schmid, G., Wieprecht, S., and Noack, M. (2020). "Proof-of-Concept for Non-intrusive and Undisturbed Measurement of Sediment Infiltration Masses Using Gamma-Ray Attenuation." *Journal of Hydraulic Engineering*, 146(5), 11.

McIntyre, A. D. (1971). "Deficiency of Gravity Corers for sampling Meiobenthos and Sediments." *Nature*, 231(5300), 260–260.

McNeil, J., Taylor, C., and Lick, W. (1996). "Measurements of Erosion of Undisturbed Bottom Sediments with Depth." *Journal of Hydraulic Engineering*, 122(6), 316–324.

Mehta, A. (1991). *Characterization of cohesive soil bed surface erosion, with special reference to the relationship between erosion shear strength and bed density*. Coastal and Oceanographic Engineering Department, University of Florida, Gainesville, Florida.

Mehta, A. J. and Partheniades, E. (1982). "Resuspension of deposited cohesive sediment beds." Cape Town, South Africa, Coastal Engineering Research Council, 1569–1588.

Mitchener, H. and Torfs, H. (1995). "Erosion of mud-sand mixtures." *Coastal Engineering 29 (1996) 1-25*.

Morelle, J., Claquin, P., and Orvain, F. (2020). "Evidence for better microphytobenthos dynamics in mixed sand/mud zones than in pure sand or mud intertidal flats (Seine estuary, Normandy, France)." *PLOS ONE*, 15(8), e0237211 Publisher: Public Library of Science.

Mouris, K., Beckers, F., and Haun, S. (2018). "Three-dimensional numerical modeling of hydraulics and morphodynamics of the Schwarzenbach reservoir." *E3S Web of Conferences*, 40, 03005.

Noack, M., Gerbersdorf, S., Hillebrand, G., and Wieprecht, S. (2015). "Combining Field and Laboratory Measurements to Determine the Erosion Risk of Cohesive Sediments Best." *Water*, 7(9), 5061–5077.

Noack, M., Schmid, G., Beckers, F., Haun, S., and Wieprecht, S. (2018). "PHOTO-SED—PHOTOgrammetric Sediment Erosion Detection." *Geosciences*, 8(7), 243.

Panagiotopoulos, I., Voulgaris, G., and Collins, M. (1997). "The influence of clay on the threshold of movement of fine sandy beds." *Coastal Engineering 32 (1997) 19-43*.

Partheniades, E. (2007). *Engineering properties and hydraulic behavior of cohesive sediments*. CRC, Boca Raton, Fla. ; London OCLC: ocm71239271.

Paterson, D. M., Hope, J. A., Kenworthy, J., Biles, C. L., and Gerbersdorf, S. U. (2018). "Form, function and physics: the ecology of biogenic stabilisation." *Journal of Soils and Sediments*, 18(10), 3044–3054.

Peeters, F., Encinas Fernandez, J., and Hofmann, H. (2019). "Sediment fluxes rather than oxic

684 methanogenesis explain diffusive CH4 emissions from lakes and reservoirs." *Scientific Reports*,
685 9(1), 243.

686 Perera, C., Smith, J., Wu, W., Perkey, D., and Priestas, A. (2020). "Erosion rate of sand and mud
687 mixtures." *International Journal of Sediment Research*, 35(6), 563–575.

688 Perkey, D. W., Smith, S. J., and Priestas, A. M. (2020). "Erosion Thresholds and Rates for Sand-
689 Mud Mixtures." *TR-20-13*, The U.S. Army Engineer Research and Development Center (ERDC),
690 Vicksburg, Mississippi (July).

691 Peterson, B. G. and Carl, P. (2020). *PerformanceAnalytics: Econometric Tools for Performance*
692 *and Risk Analysis*, <https://CRAN.R-project.org/package=PerformanceAnalytics>.

693 R Core Team (2017). *R: A Language and Environment for Statistical Computing*. R Foundation for
694 Statistical Computing, Vienna, Austria, <https://www.R-project.org/>.

695 Raunkjær, K., Hvitved-Jacobsen, T., and Nielsen, P. H. (1994). "Measurement of pools of protein,
696 carbohydrate and lipid in domestic wastewater." *Water Research*, 28(2), 251–262.

697 Righetti, M. and Lucarelli, C. (2007). "May the Shields theory be extended to cohesive and adhesive
698 benthic sediments?." *Journal of Geophysical Research*, 112(C05039).

699 Roberts, J. D., Jepsen, R. A., and James, S. C. (2003). "Measurements of Sediment Erosion and
700 Transport with the Adjustable Shear Stress Erosion and Transport Flume." *Journal of Hydraulic*
701 *Engineering*, 129(11), 862–871.

702 Sanford, L. P. and Maa, J. P.-Y. (2001). "A unified erosion formulation for fine sediments." *Marine*
703 *Geology*, 179(1-2), 9–23.

704 Schäfer Rodrigues Silva, A., Noack, M., Schlabing, D., and Wieprecht, S. (2018). "A data-driven
705 fuzzy approach to simulate the critical shear stress of mixed cohesive/non-cohesive sediments."
706 *Journal of Soils and Sediments*, 18(10), 3070–3081.

707 Segers, R. (1998). "Methane production and methane consumption: a review of processes under-
708 lying wetland methane fluxes." *Biogeochemistry*, 41(1), 23–51.

709 Shapiro, S. S. and Wilk, M. B. (1965). "An Analysis of Variance Test for Normality (Complete
710 Samples)." *Biometrika*, 52(3/4), 591–611.

711 Shields, A. (1936). “Anwendung der Ähnlichkeitsmechanik und der Turbulenzforschung auf die
712 Geschiebebewegung [Application of mechanical similarity and turbulence research to bedload
713 motion].” Ph.D. thesis, Preussischen Versuchsanstalt für Wasserbau, Berlin (June).
714 Thebrath, B., Rothfuss, F., Whiticar, M., and Conrad, R. (1993). “Methane production in littoral
715 sediment of Lake Constance.” *FEMS Microbiology Letters*, 102(3-4), 279–289.
716 Thom, M., Schmidt, H., Gerbersdorf, S. U., and Wieprecht, S. (2015). “Seasonal biostabilization
717 and erosion behavior of fluvial biofilms under different hydrodynamic and light conditions.”
718 *International Journal of Sediment Research*, 30(4), 273–284.
719 Tolhurst, T., Defew, E., de Brouwer, J., Wolfstein, K., Stal, L., and Paterson, D. (2006). “Small-
720 scale temporal and spatial variability in the erosion threshold and properties of cohesive intertidal
721 sediments.” *Continental Shelf Research*, 26(3), 351–362.
722 Tsuneda, S., Aikawa, H., Hayashi, H., Yuasa, A., and Hirata, A. (2003). “Extracellular polymeric
723 substances responsible for bacterial adhesion onto solid surface.” *FEMS Microbiology Letters*,
724 223(2), 287–292.
725 Van Ledden, M. (2003). “Sand-mud segregation in estuaries and tidal basins.” Ph.D. thesis, Delft.
726 van Rijn, L. C. (2020). “Erodibility of Mud–Sand Bed Mixtures.” *Journal of Hydraulic Engineering*,
727 146(1), 04019050.
728 Wei, T. and Simko, V. (2017). *R package "corrplot": Visualization of a Correlation Matrix*,
729 <https://github.com/taiyun/corrplot>.
730 Wickham, H. (2016). *ggplot2: Elegant Graphics for Data Analysis*. Springer-Verlag New York,
731 <https://ggplot2.tidyverse.org>.
732 Wickham, H., François, R., Henry, L., and Müller, K. (2020). *dplyr: A Grammar of Data Manipu-
733 lation*, <https://CRAN.R-project.org/package=dplyr>.
734 Winterwerp, J. C., van Kesteren, W. G. M., van Prooijen, B., and Jacobs, W. (2012). “A con-
735 ceptual framework for shear flow-induced erosion of soft cohesive sediment beds.” *Journal of
736 Geophysical Research: Oceans*, 117(C10), n/a–n/a.
737 Wu, W., Perera, C., Smith, J., and Sanchez, A. (2018). “Critical shear stress for erosion of sand and

738 mud mixtures." *Journal of Hydraulic Research*, 56(1), 96–110.

739 Yang, Y., Gao, S., Wang, Y. P., Jia, J., Xiong, J., and Zhou, L. (2019). "Revisiting the problem of
740 sediment motion threshold." *Continental Shelf Research*, 187, 103960.

741 Young, R. N. and Southard, J. B. (1978). "Erosion of fine-grained marine sediments: Sea-floor and
742 laboratory experiments." *Geological Society of American Bulletin*, 89, 10.

743 Zhang, M. and Yu, G. (2017). "Critical conditions of incipient motion of cohesive sediments."
744 *Water Resources Research*, 53(9), 7798–7815.

745 Zhu, Q., van Prooijen, B., Maan, D., Wang, Z., Yao, P., Daggers, T., and Yang, S. (2019). "The
746 heterogeneity of mudflat erodibility." *Geomorphology*, 345, 106834.

List of Tables

TABLE 1. Overview of removed and analyzed sediment cores

Reservoir	No. of Cores	Sediment Length (Min-Max) [m]	No. of Regions	Removal Date
GBS	9	0.49-0.64	3	25-26.09.2017
SBT	13	0.25-0.56	3	06-07.08.2018

SBT = *Schwarzenbachtalsperre*; GBS = *Groß er Brombachsee*

TABLE 2. Overview of main results including critical erosion thresholds and sediment characteristics of the GBS and SBT deposits. Note: NA denotes “not applicable".

Reservoir	GBS			SBT		
Parameter	MIN	MEAN	MAX	MIN	MEAN	MAX
$\tau_{c,0}$ [Pa]	0.10	2.43	11.34	0.07	0.28	0.81
$\tau_{c,S}$ [Pa]	0.32	3.84	12.48	0.17	0.38	0.99
BD [g cm^{-3}]	1.06	1.20	1.46	0.91	1.02	1.11
Clay [%]	4.58	8.12	12.52	2.10	2.94	3.93
Silt [%]	82.30	88.52	93.09	69.35	76.51	82.18
Mud [%]	93.27	96.65	98.65	71.71	79.45	85.58
Sand [%]	1.35	3.35	6.72	14.42	20.55	28.30
d_{10} [μm]	1.38	1.99	2.92	3.36	4.20	5.34
d_{50} [μm]	6.28	8.37	11.38	17.41	20.83	25.79
d_{90} [μm]	21.96	30.92	40.30	64.95	95.09	147.93
TOC [%]	0.71	2.11	3.70	8.38	11.66	14.73
CEC [cmol kg^{-1}]	71.80	102.96	190.96	46.78	79.39	105.29
CHL-a [μg g^{-1}]	NA	NA	NA	40.68	154.05	412.71
EPS-p [μg g^{-1}]	NA	NA	NA	406.06	758.10	1124.39
EPS-c [μg g^{-1}]	NA	NA	NA	266.33	455.65	739.89

TABLE 3. Correlation coefficients between critical erosion thresholds and sediment characteristics for the GBS deposits separated into depth regions A (0-10 cm) and B (>10 cm). The significance levels are indicated by *p ≤ 0.05, **p ≤ 0.01, and ***p ≤ 0.001.

GBS	A (0-10cm)		B (>10cm)	
	$\tau_{c,0}$	$\tau_{c,S}$	$\tau_{c,0}$	$\tau_{c,S}$
BD [g cm^{-3}]	0.37	**0.66*** **	0.28	**0.54** **
Clay [%]	**0.50***	**0.72*** **	**0.48***	0.38
Silt [%]	-0.32	**-0.40**	-0.40	-0.39
Sand [%]	0	-0.07	0.11	0.20
d_{10} [μm]	**-0.46***	**-0.70*** **	**-0.45***	-0.36
d_{50} [μm]	**-0.44***	**-0.66*** **	0.29	**0.49***
d_{90} [μm]	-0.16	-0.26	0.29	**0.45***
TOC [%]	-0.49	**-0.73** **	-0.38	**-0.51***

TABLE 4. Correlation coefficients between critical erosion thresholds and sediment characteristics for the SBT deposits separated into depth regions A (0-10 cm) and B (>10 cm). The significance levels are indicated by *p ≤ 0.05, **p ≤ 0.01, and ***p ≤ 0.001.

SBT	A (0-10cm)		B (>10cm)	
	$\tau_{c,0}$	$\tau_{c,S}$	$\tau_{c,0}$	$\tau_{c,S}$
BD [g cm^{-3}]	0.03	-0.19	0.31	**0.41***
Clay [%]	**-0.82*****	**-0.71****	-0.13	-0.14
Silt [%]	**-0.71****	-0.46	-0.23	-0.19
Sand [%]	**0.72****	0.47	0.23	0.19
d_{10} [μm]	**0.74****	**0.66***	0.16	0.15
d_{50} [μm]	**0.79*****	**0.61***	0.31	0.22
d_{90} [μm]	**0.62***	0.35	0.16	0.12
TOC [%]	**-0.70****	-0.47	0.26	0
CEC [cmol kg^{-}1]	-0.26	0.06	0.20	-0.07

List of Figures

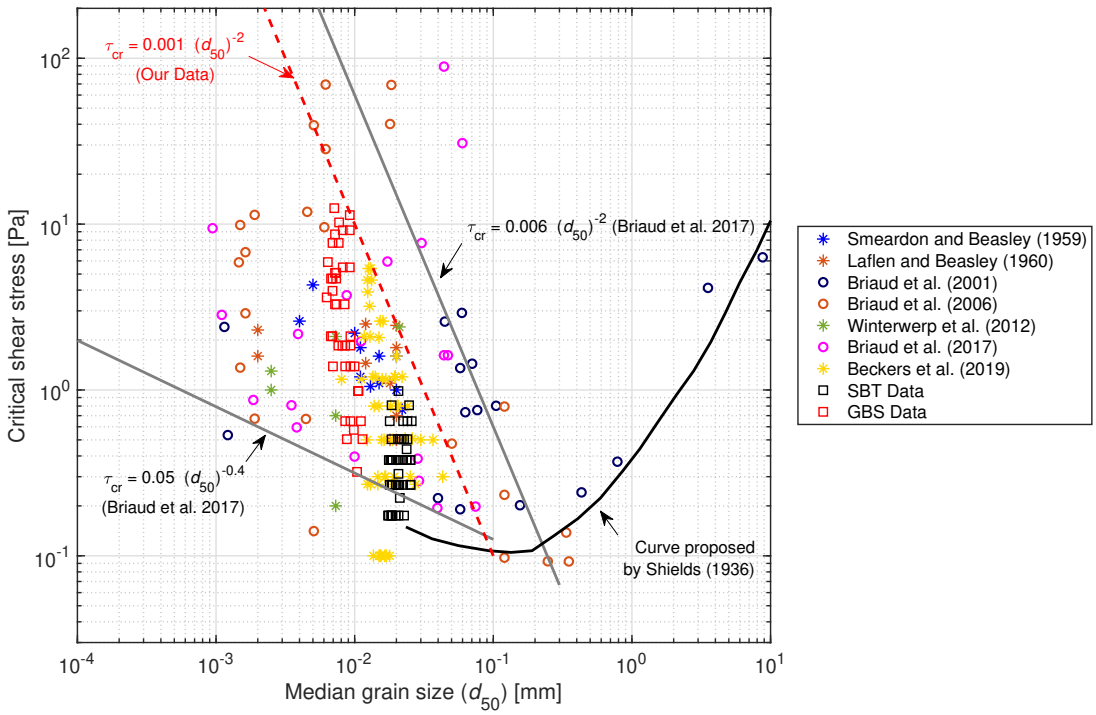

Fig. 1. Erosion data from literature plotted over d_{50} including the limits (upper and lower) suggested by Briaud (2008) and Briaud et al. (2017) and a refined upper limit based on our presented erosion data.

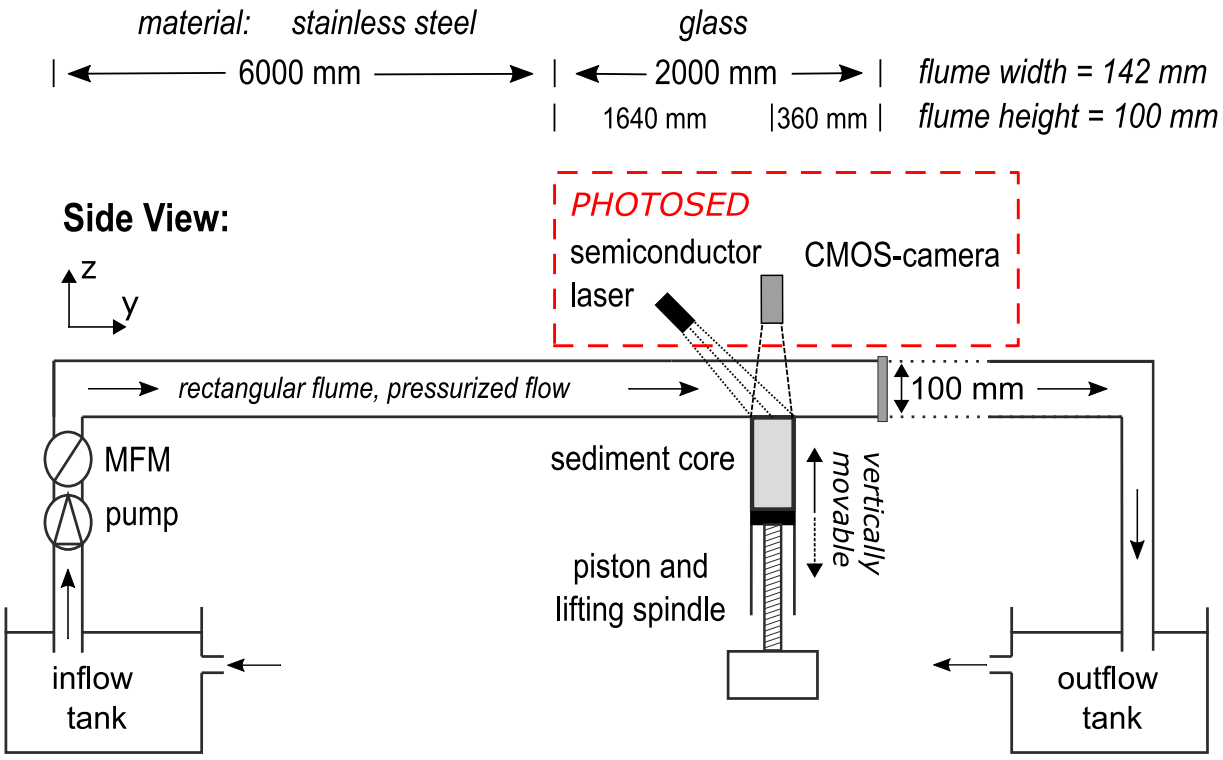

Fig. 2. SETEG/PHOTOSED-system to measure the depth-dependent erosion potential of cohesive sediments and non-cohesive/cohesive sediment mixtures (Beckers et al. 2019).

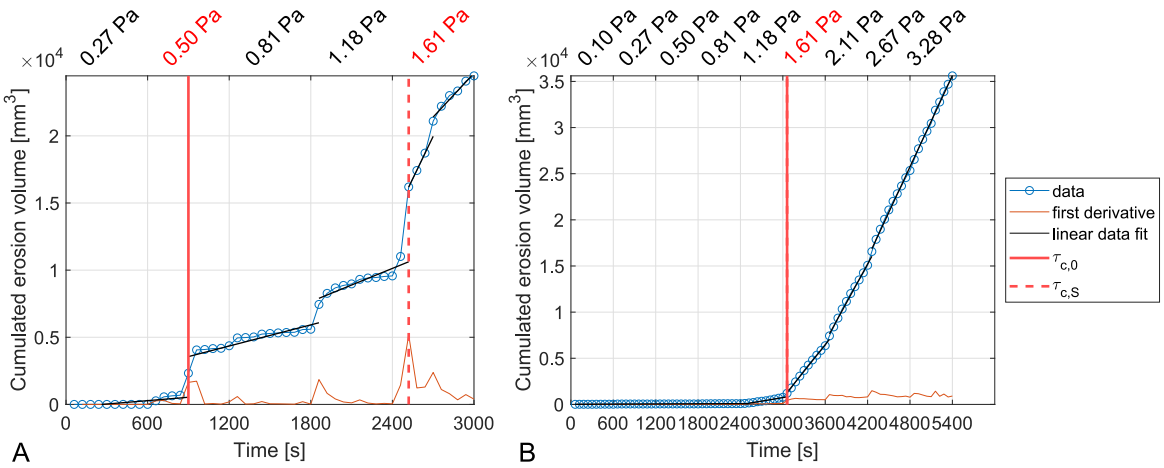

Fig. 3. Procedure to identify the erosion thresholds of a sediment surface by means of a slope criterion applied to the cumulative erosion volume. The initial rise of the volume identifies the erosion threshold $\tau_{c,0}$ and the maximum change in slope identifies the erosion threshold $\tau_{c,S}$. Whereas (A) yields different values for $\tau_{c,0}$ and $\tau_{c,S}$ due to a change in the erosion behavior, (B) yields equal values for $\tau_{c,0}$ and $\tau_{c,S}$ due to constant (steady-state) erosion.

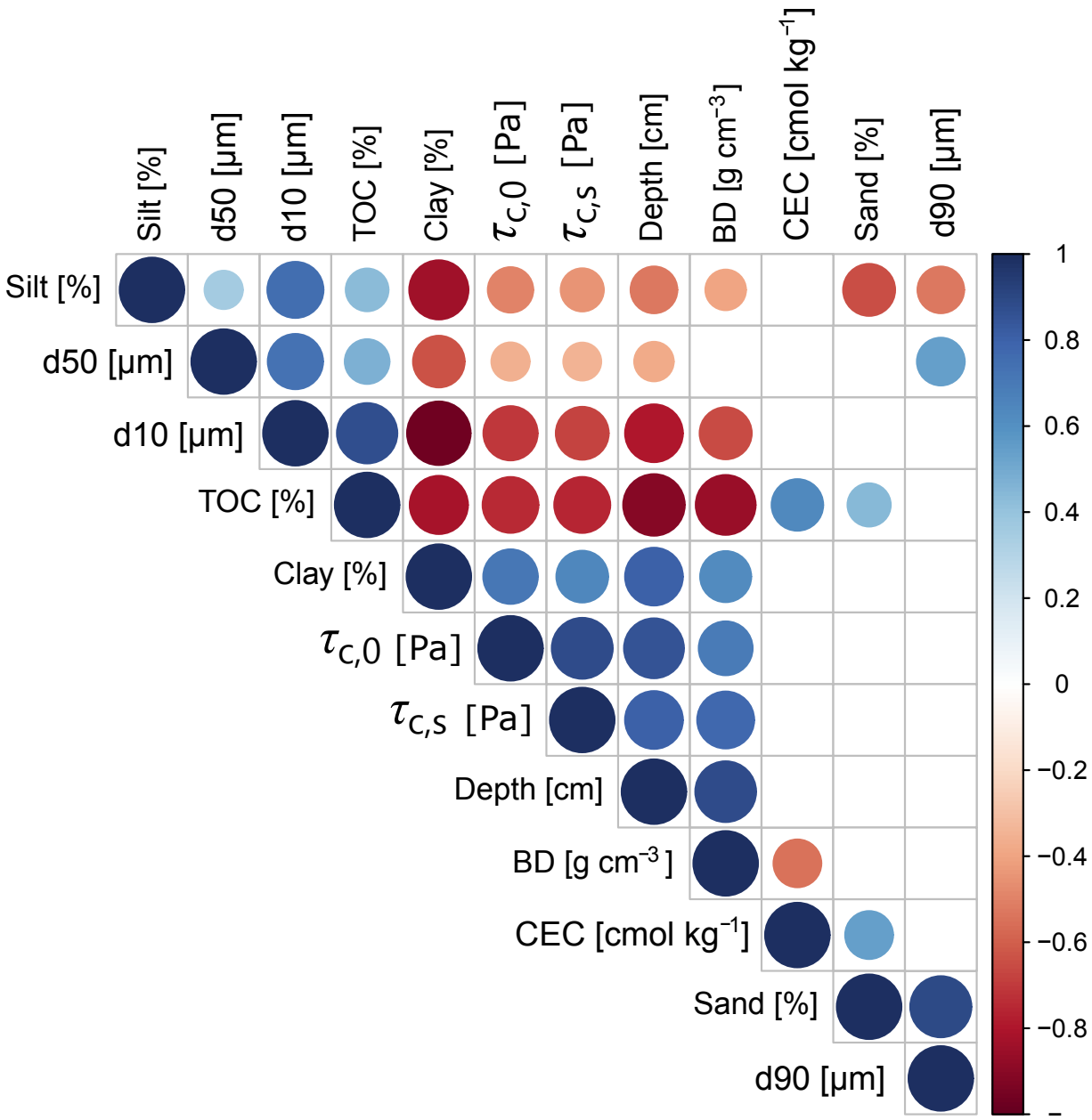

Fig. 4. Correlogram indicating the correlations ($p \leq 0.05$) between the measured sediment characteristics and critical erosion thresholds for the sediment deposits of the GBS. The parameters are arranged with respect to the number of correlating variables. The color scheme denotes positive/negative correlations, whereas the shading as well as the marker size denote the magnitude of correlation.

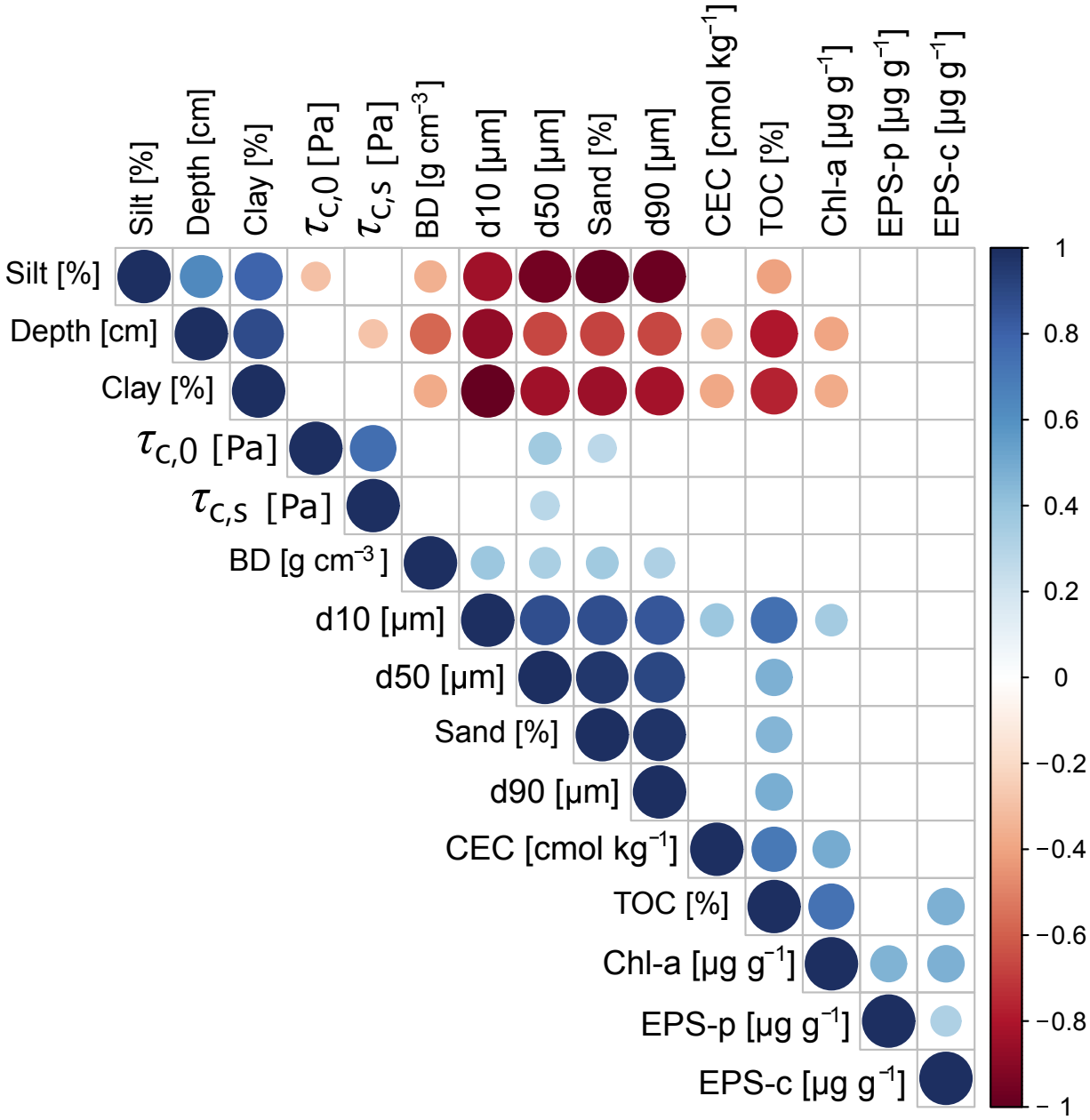

Fig. 5. Correlogram indicating the correlations ($p \leq 0.05$) between the measured sediment characteristics and critical erosion thresholds for the sediment deposits of the SBT. The parameters are arranged with respect to the number of correlating variables. The color scheme denotes positive/negative correlations, whereas the shading as well as the marker size denote the magnitude of correlation.

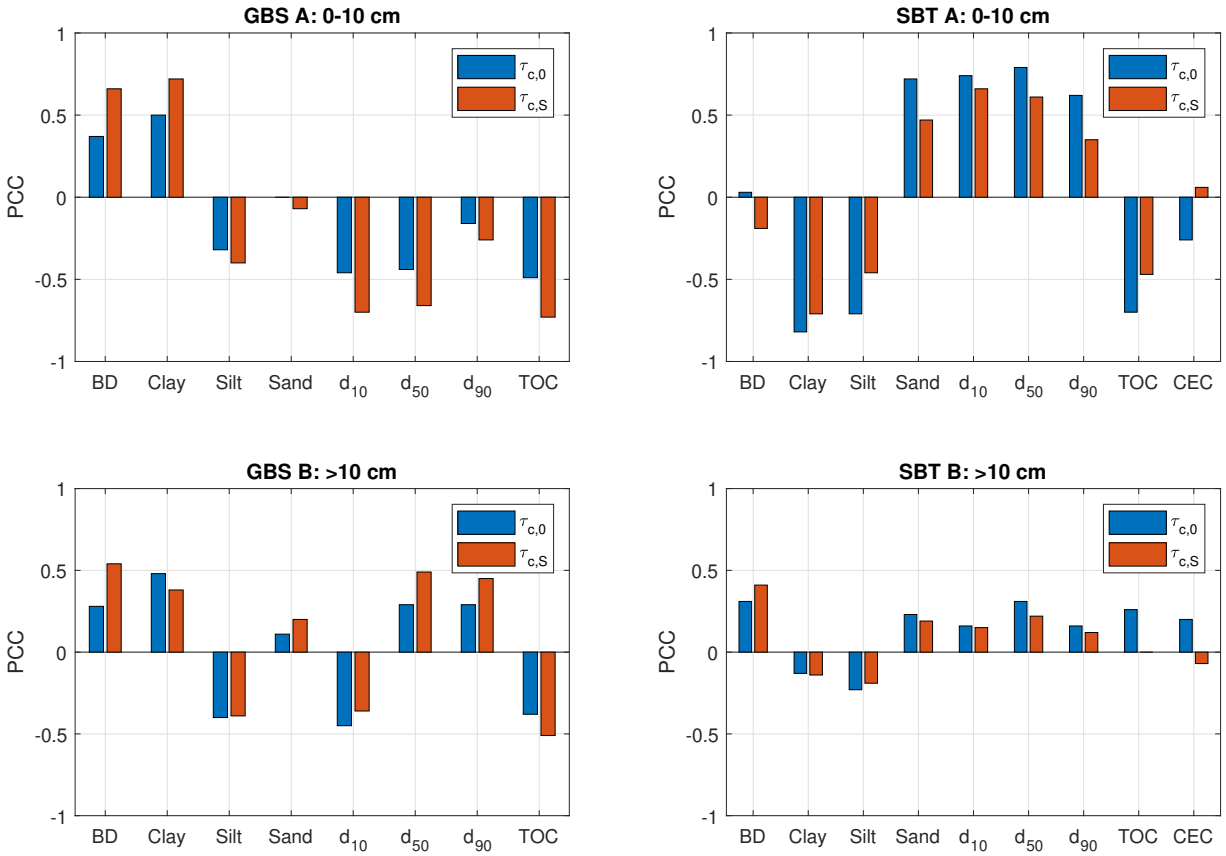

Fig. 6. Variation of correlation coefficients between erosion thresholds ($\tau_{c,0}$ and $\tau_{c,S}$) and sediment characteristics across two regions of sediment depth: A (0-10 cm) and B (>10 cm). The left panels indicate the correlations found for the GBS deposits, whereas the right panels indicate the correlations for the SBT deposits.

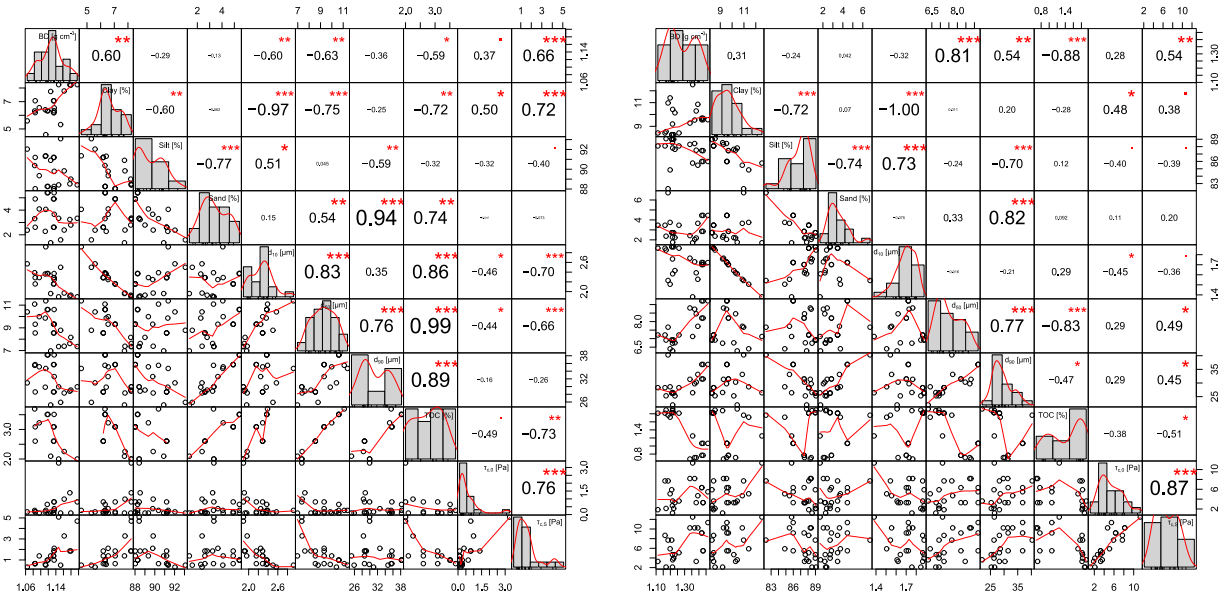

Fig. S1. Multivariate correlations between analyzed sediment parameters and critical erosion thresholds of the GBS deposits for the depth region A (0-10 cm) and B (>10 cm). The distribution of each variable is displayed as a histogram on the diagonal axis with an overlaid kernel density estimation. Below the diagonal axis, the scatter plots with fitted lines are displayed. Above the diagonal axis, the correlation coefficients and significance levels (p-values) of the relationship are indicated by the symbols *** (p = 0 - 0.001), ** (p = 0.001 - 0.01), * (p = 0.01 - 0.05), and ■ (p = 0.05 - 0.10).

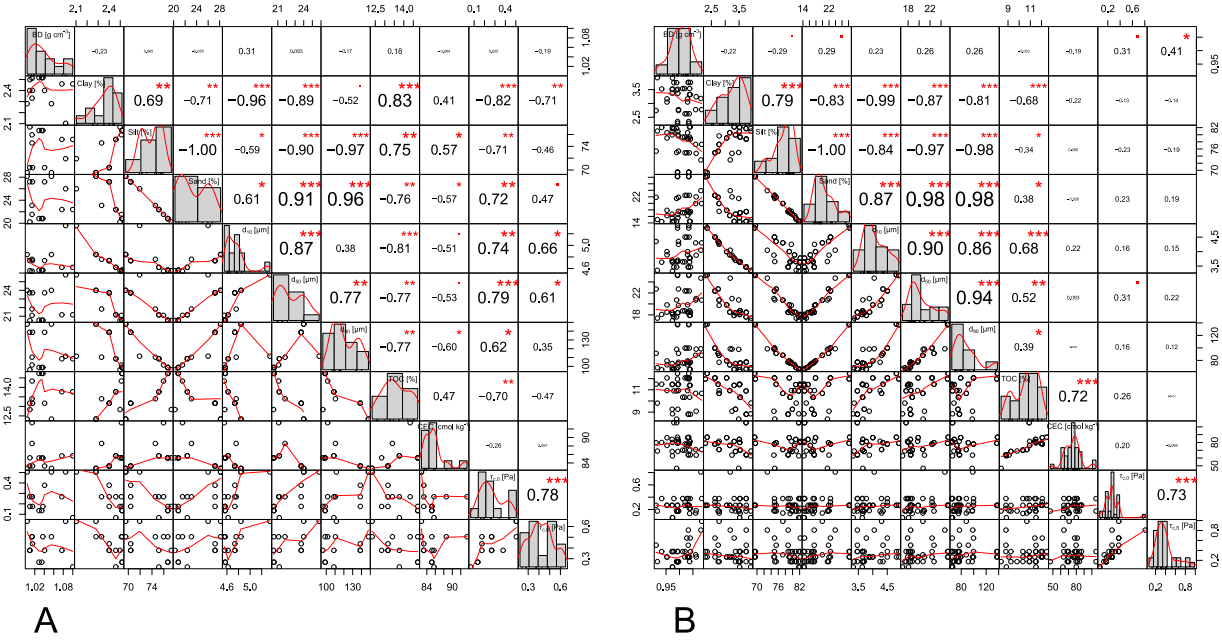

Fig. S2. Multivariate correlations between analyzed sediment parameters and critical erosion thresholds of the SBT deposits for the depth region A (0-10 cm) and B (>10 cm). The distribution of each variable is displayed as a histogram on the diagonal axis with an overlaid kernel density estimation. Below the diagonal axis, the scatter plots with fitted lines are displayed. Above the diagonal axis, the correlation coefficients and significance levels (p-values) of the relationship are indicated by the symbols *** (p = 0 - 0.001), ** (p = 0.001 - 0.01), * (p = 0.01 - 0.05), and ■ (p = 0.05 - 0.10).

Institut für Wasser- und Umweltsystemmodellierung
Universität Stuttgart

Pfaffenwaldring 61
70569 Stuttgart (Vaihingen)
Telefon (0711) 685 - 60156
Telefax (0711) 685 - 51073
E-Mail: iws@iws.uni-stuttgart.de
http://www.iws.uni-stuttgart.de

Verzeichnis der Mitteilungshefte

5 Plate, Erich: *Beitrag zur Bestimmung der Windgeschwindigkeitsverteilung in der durch eine Wand gestörten bodennahen Luftschicht*, und
Röhnisch, Arthur; Marotz, Günter: *Neue Baustoffe und Bauausführungen für den Schutz der Böschungen und der Sohle von Kanälen, Flüssen und Häfen; Gestehungskosten und jeweilige Vorteile*, sowie
Unny, T.E.: *Schwingungsuntersuchungen am Kegelstrahlschieber*, 1967

6 Seiler, Erich: *Die Ermittlung des Anlagenwertes der bundeseigenen Binnenschiffahrtsstraßen und Talsperren und des Anteils der Binnenschiffahrt an diesem Wert*, 1967

7 *Sonderheft anläßlich des 65. Geburtstages von Prof. Arthur Röhnisch mit Beiträgen von* Benk, Dieter; Breitling, J.; Gurr, Siegfried; Haberhauer, Robert; Honekamp, Hermann; Kuz, Klaus Dieter; Marotz, Günter; Mayer-Vorfelder, Hans-Jörg; Miller, Rudolf; Plate, Erich J.; Radomski, Helge; Schwarz, Helmut; Vollmer, Ernst; Wildenhahn, Eberhard; 1967

8 Jumikis, Alfred: *Beitrag zur experimentellen Untersuchung des Wassernachschubs in einem gefrierenden Boden und die Beurteilung der Ergebnisse*, 1968

9 Marotz, Günter: *Technische Grundlagen einer Wasserspeicherung im natürlichen Untergrund*, 1968

10 Radomski, Helge: *Untersuchungen über den Einfluß der Querschnittsform wellenförmiger Spundwände auf die statischen und rammtechnischen Eigenschaften*, 1968

11 Schwarz, Helmut: *Die Grenztragfähigkeit des Baugrundes bei Einwirkung vertikal gezogener Ankerplatten als zweidimensionales Bruchproblem*, 1969

12 Erbel, Klaus: *Ein Beitrag zur Untersuchung der Metamorphose von Mittelgebirgsschneedecken unter besonderer Berücksichtigung eines Verfahrens zur Bestimmung der thermischen Schneequalität*, 1969

13 Westhaus, Karl-Heinz: *Der Strukturwandel in der Binnenschiffahrt und sein Einfluß auf den Ausbau der Binnenschiffskanäle*, 1969

14 Mayer-Vorfelder, Hans-Jörg: *Ein Beitrag zur Berechnung des Erdwiderstandes unter Ansatz der logarithmischen Spirale als Gleitflächenfunktion*, 1970

15 Schulz, Manfred: *Berechnung des räumlichen Erddruckes auf die Wandung kreiszylindrischer Körper*, 1970

16 Mobasseri, Manoutschehr: *Die Rippenstützmauer. Konstruktion und Grenzen ihrer Standsicherheit*, 1970

17 Benk, Dieter: *Ein Beitrag zum Betrieb und zur Bemessung von Hochwasserrückhaltebecken*, 1970

18 Gàl, Attila: *Bestimmung der mitschwingenden Wassermasse bei überströmten Fischbauchklappen mit kreiszylindrischem Staublech*, 1971, vergriffen

19 Kuz, Klaus Dieter: *Ein Beitrag zur Frage des Einsetzens von Kavitationserscheinungen in einer Düsenströmung bei Berücksichtigung der im Wasser gelösten Gase*, 1971, vergriffen

20 Schaak, Hartmut: *Verteilleitungen von Wasserkraftanlagen*, 1971

21 *Sonderheft zur Eröffnung der neuen Versuchsanstalt des Instituts für Wasserbau der Universität Stuttgart mit Beiträgen von* Brombach, Hansjörg; Dirksen, Wolfram; Gàl, Attila; Gerlach, Reinhard; Giesecke, Jürgen; Holthoff, Franz-Josef; Kuz, Klaus Dieter; Marotz, Günter; Minor, Hans-Erwin; Petrikat, Kurt; Röhnisch, Arthur; Rueff, Helge; Schwarz, Helmut; Vollmer, Ernst; Wildenhahn, Eberhard; 1972

22 Wang, Chung-su: *Ein Beitrag zur Berechnung der Schwingungen an Kegelstrahlschiebern*, 1972

23 Mayer-Vorfelder, Hans-Jörg: *Erdwiderstandsbeiwerte nach dem Ohde-Variationsverfahren*, 1972

24 Minor, Hans-Erwin: *Beitrag zur Bestimmung der Schwingungsanfachungsfunktionen überströmter Stauklappen*, 1972, vergriffen

25 Brombach, Hansjörg: *Untersuchung strömungsmechanischer Elemente (Fluidik) und die Möglichkeit der Anwendung von Wirbelkammerelementen im Wasserbau*, 1972, vergriffen

26 Wildenhahn, Eberhard: *Beitrag zur Berechnung von Horizontalfilterbrunnen*, 1972

27 Steinlein, Helmut: *Die Eliminierung der Schwebstoffe aus Flußwasser zum Zweck der unterirdischen Wasserspeicherung, gezeigt am Beispiel der Iller*, 1972

28 Holthoff, Franz Josef: *Die Überwindung großer Hubhöhen in der Binnenschiffahrt durch Schwimmerhebewerke*, 1973

29 Röder, Karl: *Einwirkungen aus Baugrundbewegungen auf trog- und kastenförmige Konstruktionen des Wasser- und Tunnelbaues*, 1973

30 Kretschmer, Heinz: *Die Bemessung von Bogenstaumauern in Abhängigkeit von der Talform*, 1973

31 Honekamp, Hermann: *Beitrag zur Berechnung der Montage von Unterwasserpipelines*, 1973

32 Giesecke, Jürgen: *Die Wirbelkammertriode als neuartiges Steuerorgan im Wasserbau*, und Brombach, Hansjörg: *Entwicklung, Bauformen, Wirkungsweise und Steuereigenschaften von Wirbelkammerverstärkern*, 1974

33 Rueff, Helge: *Untersuchung der schwingungserregenden Kräfte an zwei hintereinander angeordneten Tiefschützen unter besonderer Berücksichtigung von Kavitation*, 1974

34 Röhnisch, Arthur: *Einpreßversuche mit Zementmörtel für Spannbeton - Vergleich der Ergebnisse von Modellversuchen mit Ausführungen in Hüllwellrohren*, 1975

35 *Sonderheft anläßlich des 65. Geburtstages von Prof. Dr.-Ing. Kurt Petrikat mit Beiträgen von*: Brombach, Hansjörg; Erbel, Klaus; Flinspach, Dieter; Fischer jr., Richard; Gàl, Attila; Gerlach, Reinhard; Giesecke, Jürgen; Haberhauer, Robert; Hafner Edzard; Hausenblas, Bernhard; Horlacher, Hans-Burkhard; Hutarew, Andreas; Knoll, Manfred; Krummet, Ralph; Marotz, Günter; Merkle, Theodor; Miller, Christoph; Minor, Hans-Erwin; Neumayer, Hans; Rao, Syamala; Rath, Paul; Rueff, Helge; Ruppert, Jürgen; Schwarz, Wolfgang; Topal-Gökceli, Mehmet; Vollmer, Ernst; Wang, Chung-su; Weber, Hans-Georg; 1975

36 Berger, Jochum: *Beitrag zur Berechnung des Spannungszustandes in rotationssymmetrisch belasteten Kugelschalen veränderlicher Wandstärke unter Gas- und Flüssigkeitsdruck durch Integration schwach singulärer Differentialgleichungen*, 1975

37 Dirksen, Wolfram: *Berechnung instationärer Abflußvorgänge in gestauten Gerinnen mittels Differenzenverfahren und die Anwendung auf Hochwasserrückhaltebecken*, 1976

38 Horlacher, Hans-Burkhard: *Berechnung instationärer Temperatur- und Wärmespannungsfelder in langen mehrschichtigen Hohlzylindern*, 1976

39 Hafner, Edzard: *Untersuchung der hydrodynamischen Kräfte auf Baukörper im Tiefwasserbereich des Meeres*, 1977, ISBN 3-921694-39-6

40 Ruppert, Jürgen: *Über den Axialwirbelkammerverstärker für den Einsatz im Wasserbau*, 1977, ISBN 3-921694-40-X

41 Hutarew, Andreas: *Beitrag zur Beeinflußbarkeit des Sauerstoffgehalts in Fließgewässern an Abstürzen und Wehren*, 1977, ISBN 3-921694-41-8, *vergriffen*

42 Miller, Christoph: *Ein Beitrag zur Bestimmung der schwingungserregenden Kräfte an unterströmten Wehren*, 1977, ISBN 3-921694-42-6

43 Schwarz, Wolfgang: *Druckstoßberechnung unter Berücksichtigung der Radial- und Längsverschiebungen der Rohrwandung*, 1978, ISBN 3-921694-43-4

44 Kinzelbach, Wolfgang: *Numerische Untersuchungen über den optimalen Einsatz variabler Kühlsysteme einer Kraftwerkskette am Beispiel Oberrhein*, 1978, ISBN 3-921694-44-2

45 Barczewski, Baldur: *Neue Meßmethoden für Wasser-Luftgemische und deren Anwendung auf zweiphasige Auftriebsstrahlen*, 1979, ISBN 3-921694-45-0

46 Neumayer, Hans: *Untersuchung der Strömungsvorgänge in radialen Wirbelkammerverstärkern*, 1979, ISBN 3-921694-46-9

47 Elalfy, Youssef-Elhassan: *Untersuchung der Strömungsvorgänge in Wirbelkammerdioden und -drosseln*, 1979, ISBN 3-921694-47-7

48 Brombach, Hansjörg: *Automatisierung der Bewirtschaftung von Wasserspeichern*, 1981, ISBN 3-921694-48-5

49 Geldner, Peter: *Deterministische und stochastische Methoden zur Bestimmung der Selbstdichtung von Gewässern*, 1981, ISBN 3-921694-49-3, *vergriffen*

50 Mehlhorn, Hans: *Temperaturveränderungen im Grundwasser durch Brauchwassereinleitungen*, 1982, ISBN 3-921694-50-7, *vergriffen*

51 Hafner, Edzard: *Rohrleitungen und Behälter im Meer*, 1983, ISBN 3-921694-51-5

52 Rinnert, Bernd: *Hydrodynamische Dispersion in porösen Medien: Einfluß von Dichteunterschieden auf die Vertikalvermischung in horizontaler Strömung*, 1983, ISBN 3-921694-52-3, *vergriffen*

53 Lindner, Wulf: *Steuerung von Grundwasserentnahmen unter Einhaltung ökologischer Kriterien*, 1983, ISBN 3-921694-53-1, *vergriffen*

54 Herr, Michael; Herzer, Jörg; Kinzelbach, Wolfgang; Kobus, Helmut; Rinnert, Bernd: *Methoden zur rechnerischen Erfassung und hydraulischen Sanierung von Grundwasserkontaminationen*, 1983, ISBN 3-921694-54-X

55 Schmitt, Paul: *Wege zur Automatisierung der Niederschlagsermittlung*, 1984, ISBN 3-921694-55-8, *vergriffen*

56 Müller, Peter: *Transport und selektive Sedimentation von Schwebstoffen bei gestautem Abfluß*, 1985, ISBN 3-921694-56-6

57 El-Qawasmeh, Fuad: *Möglichkeiten und Grenzen der Tropfbewässerung unter besonderer Berücksichtigung der Verstopfungsanfälligkeit der Tropfelemente*, 1985, ISBN 3-921694-57-4, *vergriffen*

58 Kirchenbaur, Klaus: *Mikroprozessorgesteuerte Erfassung instationärer Druckfelder am Beispiel seegangsbelasteter Baukörper*, 1985, ISBN 3-921694-58-2

59 Kobus, Helmut (Hrsg.): *Modellierung des großräumigen Wärme- und Schadstofftransports im Grundwasser*, Tätigkeitsbericht 1984/85 (DFG-Forschergruppe an den Universitäten Hohenheim, Karlsruhe und Stuttgart), 1985, ISBN 3-921694-59-0, *vergriffen*

60 Spitz, Karlheinz: *Dispersion in porösen Medien: Einfluß von Inhomogenitäten und Dichteunterschieden*, 1985, ISBN 3-921694-60-4, *vergriffen*

61 Kobus, Helmut: *An Introduction to Air-Water Flows in Hydraulics*, 1985, ISBN 3-921694-61-2

62 Kaleris, Vassilios: *Erfassung des Austausches von Oberflächen- und Grundwasser in horizontalebenen Grundwassermodellen*, 1986, ISBN 3-921694-62-0

63 Herr, Michael: *Grundlagen der hydraulischen Sanierung verunreinigter Porengrundwasserleiter*, 1987, ISBN 3-921694-63-9

64 Marx, Walter: *Berechnung von Temperatur und Spannung in Massenbeton infolge Hydratation*, 1987, ISBN 3-921694-64-7

65 Koschitzky, Hans-Peter: *Dimensionierungskonzept für Sohlbelüfter in Schußrinnen zur Vermeidung von Kavitationsschäden*, 1987, ISBN 3-921694-65-5

66 Kobus, Helmut (Hrsg.): *Modellierung des großräumigen Wärme- und Schadstofftransports im Grundwasser*, Tätigkeitsbericht 1986/87 (DFG-Forschergruppe an den Universitäten Hohenheim, Karlsruhe und Stuttgart) 1987, ISBN 3-921694-66-3

67 Söll, Thomas: *Berechnungsverfahren zur Abschätzung anthropogener Temperaturanomalien im Grundwasser*, 1988, ISBN 3-921694-67-1

68 Dittrich, Andreas; Westrich, Bernd: *Bodenseeufererosion, Bestandsaufnahme und Bewertung*, 1988, ISBN 3-921694-68-X, *vergriffen*

69 Huwe, Bernd; van der Ploeg, Rienk R.: *Modelle zur Simulation des Stickstoffhaushaltes von Standorten mit unterschiedlicher landwirtschaftlicher Nutzung*, 1988, ISBN 3-921694-69-8, *vergriffen*

70 Stephan, Karl: *Integration elliptischer Funktionen*, 1988, ISBN 3-921694-70-1

71 Kobus, Helmut; Zilliox, Lothaire (Hrsg.): *Nitratbelastung des Grundwassers, Auswirkungen der Landwirtschaft auf die Grundwasser- und Rohwasserbeschaffenheit und Maßnahmen zum Schutz des Grundwassers*. Vorträge des deutsch-französischen Kolloquiums am 6. Oktober 1988, Universitäten Stuttgart und Louis Pasteur Strasbourg (Vorträge in deutsch oder französisch, Kurzfassungen zweisprachig), 1988, ISBN 3-921694-71-X

72 Soyeaux, Renald: *Unterströmung von Stauanlagen auf klüftigem Untergrund unter Berücksichtigung laminarer und turbulenter Fließzustände*,1991, ISBN 3-921694-72-8

73 Kohane, Roberto: *Berechnungsmethoden für Hochwasserabfluß in Fließgewässern mit überströmten Vorländern*, 1991, ISBN 3-921694-73-6

74 Hassinger, Reinhard: *Beitrag zur Hydraulik und Bemessung von Blocksteinrampen in flexibler Bauweise*, 1991, ISBN 3-921694-74-4, vergriffen

75 Schäfer, Gerhard: *Einfluß von Schichtenstrukturen und lokalen Einlagerungen auf die Längsdispersion in Porengrundwasserleitern*, 1991, ISBN 3-921694-75-2

76 Giesecke, Jürgen: *Vorträge, Wasserwirtschaft in stark besiedelten Regionen; Umweltforschung mit Schwerpunkt Wasserwirtschaft*, 1991, ISBN 3-921694-76-0

77 Huwe, Bernd: *Deterministische und stochastische Ansätze zur Modellierung des Stickstoffhaushalts landwirtschaftlich genutzter Flächen auf unterschiedlichem Skalenniveau*, 1992, ISBN 3-921694-77-9, vergriffen

78 Rommel, Michael: *Verwendung von Kluftdaten zur realitätsnahen Generierung von Kluftnetzen mit anschließender laminar-turbulenter Strömungsberechnung*, 1993, ISBN 3-92 1694-78-7

79 Marschall, Paul: *Die Ermittlung lokaler Stofffrachten im Grundwasser mit Hilfe von Einbohrloch-Meßverfahren*, 1993, ISBN 3-921694-79-5, vergriffen

80 Ptak, Thomas: *Stofftransport in heterogenen Porenaquiferen: Felduntersuchungen und stochastische Modellierung*, 1993, ISBN 3-921694-80-9, vergriffen

81 Haakh, Frieder: *Transientes Strömungsverhalten in Wirbelkammern,* 1993, ISBN 3-921694-81-7

82 Kobus, Helmut; Cirpka, Olaf; Barczewski, Baldur; Koschitzky, Hans-Peter: *Versuchseinrichtung zur Grundwasser- und Altlastensanierung VEGAS, Konzeption und Programmrahmen*, 1993, ISBN 3-921694-82-5

83 Zang, Weidong: *Optimaler Echtzeit-Betrieb eines Speichers mit aktueller Abflußregenerierung*, 1994, ISBN 3-921694-83-3, vergriffen

84 Franke, Hans-Jörg: *Stochastische Modellierung eines flächenhaften Stoffeintrages und Transports in Grundwasser am Beispiel der Pflanzenschutzmittelproblematik*, 1995, ISBN 3-921694-84-1

85 Lang, Ulrich: *Simulation regionaler Strömungs- und Transportvorgänge in Karstaquiferen mit Hilfe des Doppelkontinuum-Ansatzes: Methodenentwicklung und Parameteridentifikation*, 1995, ISBN 3-921694-85-X, vergriffen

86 Helmig, Rainer: *Einführung in die Numerischen Methoden der Hydromechanik*, 1996, ISBN 3-921694-86-8, vergriffen

87 Cirpka, Olaf: *CONTRACT: A Numerical Tool for Contaminant Transport and Chemical Transformations - Theory and Program Documentation -*, 1996, ISBN 3-921694-87-6

88 Haberlandt, Uwe: *Stochastische Synthese und Regionalisierung des Niederschlages für Schmutzfrachtberechnungen*, 1996, ISBN 3-921694-88-4

89 Croisé, Jean: *Extraktion von flüchtigen Chemikalien aus natürlichen Lockergesteinen mittels erzwungener Luftströmung*, 1996, ISBN 3-921694-89-2, vergriffen

90 Jorde, Klaus: *Ökologisch begründete, dynamische Mindestwasserregelungen bei Ausleitungskraftwerken*, 1997, ISBN 3-921694-90-6, vergriffen

91 Helmig, Rainer: *Gekoppelte Strömungs- und Transportprozesse im Untergrund - Ein Beitrag zur Hydrosystemmodellierung-*, 1998, ISBN 3-921694-91-4, vergriffen

92 Emmert, Martin: *Numerische Modellierung nichtisothermer Gas-Wasser Systeme in porösen Medien,* 1997, ISBN 3-921694-92-2

93 Kern, Ulrich: *Transport von Schweb- und Schadstoffen in staugeregelten Fließgewässern am Beispiel des Neckars*, 1997, ISBN 3-921694-93-0, vergriffen

94 Förster, Georg: *Druckstoßdämpfung durch große Luftblasen in Hochpunkten von Rohrleitungen 1997*, ISBN 3-921694-94-9

95 Cirpka, Olaf: *Numerische Methoden zur Simulation des reaktiven Mehrkomponententransports im Grundwasser*, 1997, ISBN 3-921694-95-7, *vergriffen*

96 Färber, Arne: *Wärmetransport in der ungesättigten Bodenzone: Entwicklung einer thermischen In-situ-Sanierungstechnologie*, 1997, ISBN 3-921694-96-5

97 Betz, Christoph: *Wasserdampfdestillation von Schadstoffen im porösen Medium: Entwicklung einer thermischen In-situ-Sanierungstechnologie*, 1998, SBN 3-921694-97-3

98 Xu, Yichun: *Numerical Modeling of Suspended Sediment Transport in Rivers*, 1998, ISBN 3-921694-98-1, *vergriffen*

99 Wüst, Wolfgang: *Geochemische Untersuchungen zur Sanierung CKW-kontaminierter Aquifere mit Fe(0)-Reaktionswänden,* 2000, ISBN 3-933761-02-2

100 Sheta, Hussam: *Simulation von Mehrphasenvorgängen in porösen Medien unter Einbeziehung von Hysterese-Effekten*, 2000, ISBN 3-933761-03-4

101 Ayros, Edwin: *Regionalisierung extremer Abflüsse auf der Grundlage statistischer Verfahren*, 2000, ISBN 3-933761-04-2, *vergriffen*

102 Huber, Ralf: *Compositional Multiphase Flow and Transport in Heterogeneous Porous Media*, 2000, ISBN 3-933761-05-0

103 Braun, Christopherus: *Ein Upscaling-Verfahren für Mehrphasenströmungen in porösen Medien*, 2000, ISBN 3-933761-06-9

104 Hofmann, Bernd: *Entwicklung eines rechnergestützten Managementsystems zur Beurteilung von Grundwasserschadensfällen*, 2000, ISBN 3-933761-07-7

105 Class, Holger: *Theorie und numerische Modellierung nichtisothermer Mehrphasenprozesse in NAPL-kontaminierten porösen Medien,* 2001, ISBN 3-933761-08-5

106 Schmidt, Reinhard: *Wasserdampf- und Heißluftinjektion zur thermischen Sanierung kontaminierter Standorte*, 2001, ISBN 3-933761-09-3

107 Josef, Reinhold: *Schadstoffextraktion mit hydraulischen Sanierungsverfahren unter Anwendung von grenzflächenaktiven Stoffen*, 2001, ISBN 3-933761-10-7

108 Schneider, Matthias: *Habitat- und Abflussmodellierung für Fließgewässer mit unscharfen Berechnungsansätzen*, 2001, ISBN 3-933761-11-5

109 Rathgeb, Andreas: *Hydrodynamische Bemessungsgrundlagen für Lockerdeckwerke an überströmbaren Erddämmen*, 2001, ISBN 3-933761-12-3

110 Lang, Stefan: *Parallele numerische Simulation instätionärer Probleme mit adaptiven Methoden auf unstrukturierten Gittern*, 2001, ISBN 3-933761-13-1

111 Appt, Jochen; Stumpp Simone: *Die Bodensee-Messkampagne 2001, IWS/CWR Lake Constance Measurement Program 2001*, 2002, ISBN 3-933761-14-X

112 Heimerl, Stephan: *Systematische Beurteilung von Wasserkraftprojekten,* 2002, ISBN 3-933761-15-8, *vergriffen*

113 Iqbal, Amin: *On the Management and Salinity Control of Drip Irrigation,* 2002, ISBN 3-933761-16-6

114 Silberhorn-Hemminger, Annette: *Modellierung von Kluftaquifersystemen: Geostatistische Analyse und deterministisch-stochastische Kluftgenerierung,* 2002, ISBN 3-933761-17-4

115 Winkler, Angela: *Prozesse des Wärme- und Stofftransports bei der In-situ-Sanierung mit festen Wärmequellen,* 2003, ISBN 3-933761-18-2

116 Marx, Walter: *Wasserkraft, Bewässerung, Umwelt - Planungs- und Bewertungsschwerpunkte der Wasserbewirtschaftung,* 2003, ISBN 3-933761-19-0

117 Hinkelmann, Reinhard: *Efficient Numerical Methods and Information-Processing Techniques in Environment Water,* 2003, ISBN 3-933761-20-4

118 Samaniego-Eguiguren, Luis Eduardo: *Hydrological Consequences of Land Use / Land Cover and Climatic Changes in Mesoscale Catchments*, 2003, ISBN 3-933761-21-2

119 Neunhäuserer, Lina: *Diskretisierungsansätze zur Modellierung von Strömungs- und Transportprozessen in geklüftet-porösen Medien*, 2003, ISBN 3-933761-22-0

120 Paul, Maren: *Simulation of Two-Phase Flow in Heterogeneous Poros Media with Adaptive Methods*, 2003, ISBN 3-933761-23-9

121 Ehret, Uwe: *Rainfall and Flood Nowcasting in Small Catchments using Weather Radar*, 2003, ISBN 3-933761-24-7

122 Haag, Ingo: *Der Sauerstoffhaushalt staugeregelter Flüsse am Beispiel des Neckars - Analysen, Experimente, Simulationen -,* 2003, ISBN 3-933761-25-5

123 Appt, Jochen: *Analysis of Basin-Scale Internal Waves in Upper Lake Constance,* 2003, ISBN 3-933761-26-3

124 Hrsg.: Schrenk, Volker; Batereau, Katrin; Barczewski, Baldur; Weber, Karolin und Koschitzky, Hans-Peter: *Symposium Ressource Fläche und VEGAS - Statuskolloquium 2003, 30. September und 1. Oktober 2003,* 2003, ISBN 3-933761-27-1

125 Omar Khalil Ouda: *Optimisation of Agricultural Water Use: A Decision Support System for the Gaza Strip,* 2003, ISBN 3-933761-28-0

126 Batereau, Katrin: *Sensorbasierte Bodenluftmessung zur Vor-Ort-Erkundung von Schadensherden im Untergrund*, 2004, ISBN 3-933761-29-8

127 Witt, Oliver: *Erosionsstabilität von Gewässersedimenten mit Auswirkung auf den Stofftransport bei Hochwasser am Beispiel ausgewählter Stauhaltungen des Oberrheins*, 2004, ISBN 3-933761-30-1

128 Jakobs, Hartmut: *Simulation nicht-isothermer Gas-Wasser-Prozesse in komplexen Kluft-Matrix-Systemen*, 2004, ISBN 3-933761-31-X

129 Li, Chen-Chien: *Deterministisch-stochastisches Berechnungskonzept zur Beurteilung der Auswirkungen erosiver Hochwasserereignisse in Flussstauhaltungen,* 2004, ISBN 3-933761-32-8

130 Reichenberger, Volker; Helmig, Rainer; Jakobs, Hartmut; Bastian, Peter; Niessner, Jennifer: *Complex Gas-Water Processes in Discrete Fracture-Matrix Systems: Up-scaling, Mass-Conservative Discretization and Efficient Multilevel Solution,* 2004, ISBN 3-933761-33-6

131 Hrsg.: Barczewski, Baldur; Koschitzky, Hans-Peter; Weber, Karolin; Wege, Ralf: *VEGAS - Statuskolloquium 2004,* Tagungsband zur Veranstaltung am 05. Oktober 2004 an der Universität Stuttgart, Campus Stuttgart-Vaihingen, 2004, ISBN 3-933761-34-4

132 Asie, Kemal Jabir: *Finite Volume Models for Multiphase Multicomponent Flow through Porous Media*. 2005, ISBN 3-933761-35-2

133 Jacoub, George: *Development of a 2-D Numerical Module for Particulate Contaminant Transport in Flood Retention Reservoirs and Impounded Rivers,* 2004, ISBN 3-933761-36-0

134 Nowak, Wolfgang: *Geostatistical Methods for the Identification of Flow and Transport Parameters in the Subsurface,* 2005, ISBN 3-933761-37-9

135 Süß, Mia: *Analysis of the influence of structures and boundaries on flow and transport processes in fractured porous media*, 2005, ISBN 3-933761-38-7

136 Jose, Surabhin Chackiath: *Experimental Investigations on Longitudinal Dispersive Mixing in Heterogeneous Aquifers,* 2005, ISBN: 3-933761-39-5

137 Filiz, Fulya: *Linking Large-Scale Meteorological Conditions to Floods in Mesoscale Catchments,* 2005, ISBN 3-933761-40-9

138 Qin, Minghao: *Wirklichkeitsnahe und recheneffiziente Ermittlung von Temperatur und Spannungen bei großen RCC-Staumauern*, 2005, ISBN 3-933761-41-7

139 Kobayashi, Kenichiro: *Optimization Methods for Multiphase Systems in the Subsurface - Application to Methane Migration in Coal Mining Areas*, 2005, ISBN 3-933761-42-5

140 Rahman, Md. Arifur: *Experimental Investigations on Transverse Dispersive Mixing in Heterogeneous Porous Media,* 2005, ISBN 3-933761-43-3

141 Schrenk, Volker: *Ökobilanzen zur Bewertung von Altlastensanierungsmaßnahmen,* 2005, ISBN 3-933761-44-1

142 Hundecha, Hirpa Yeshewatesfa: *Regionalization of Parameters of a Conceptual Rainfall-Runoff Model*, 2005, ISBN: 3-933761-45-X

143 Wege, Ralf: *Untersuchungs- und Überwachungsmethoden für die Beurteilung natürlicher Selbstreinigungsprozesse im Grundwasser,* 2005, ISBN 3-933761-46-8

144 Breiting, Thomas: *Techniken und Methoden der Hydroinformatik - Modellierung von komplexen Hydrosystemen im Untergrund*, 2006, ISBN 3-933761-47-6

145 Hrsg.: Braun, Jürgen; Koschitzky, Hans-Peter; Müller, Martin: *Ressource Untergrund: 10 Jahre VEGAS: Forschung und Technologieentwicklung zum Schutz von Grundwasser und Boden,* Tagungsband zur Veranstaltung am 28. und 29. September 2005 an der Universität Stuttgart, Campus Stuttgart-Vaihingen, 2005, ISBN 3-933761-48-4

146 Rojanschi, Vlad: *Abflusskonzentration in mesoskaligen Einzugsgebieten unter Berücksichtigung des Sickerraumes,* 2006, ISBN 3-933761-49-2

147 Winkler, Nina Simone: *Optimierung der Steuerung von Hochwasserrückhaltebeckensystemen,* 2006, ISBN 3-933761-50-6

148 Wolf, Jens: *Räumlich differenzierte Modellierung der Grundwasserströmung alluvialer Aquifere für mesoskalige Einzugsgebiete*, 2006, ISBN: 3-933761-51-4

149 Kohler, Beate: *Externe Effekte der Laufwasserkraftnutzung*, 2006, ISBN 3-933761-52-2

150 Hrsg.: Braun, Jürgen; Koschitzky, Hans-Peter; Stuhrmann, Matthias: *VEGAS-Statuskolloquium 2006,* Tagungsband zur Veranstaltung am 28. September 2006 an der Universität Stuttgart, Campus Stuttgart-Vaihingen, 2006, ISBN 3-933761-53-0

151 Niessner, Jennifer: *Multi-Scale Modeling of Multi-Phase - Multi-Component Processes in Heterogeneous Porous Media*, 2006, ISBN 3-933761-54-9

152 Fischer, Markus: *Beanspruchung eingeerdeter Rohrleitungen infolge Austrocknung bindiger Böden,* 2006, ISBN 3-933761-55-7

153 Schneck, Alexander: *Optimierung der Grundwasserbewirtschaftung unter Berücksichtigung der Belange der Wasserversorgung, der Landwirtschaft und des Naturschutzes*, 2006, ISBN 3-933761-56-5

154 Das, Tapash: *The Impact of Spatial Variability of Precipitation on the Predictive Uncertainty of Hydrological Models,* 2006, ISBN 3-33761-57-3

155 Bielinski, Andreas: *Numerical Simulation of CO_2 sequestration in geological formations*, 2007, ISBN 3-933761-58-1

156 Mödinger, Jens: *Entwicklung eines Bewertungs- und Entscheidungsunterstützungssystems für eine nachhaltige regionale Grundwasserbewirtschaftung*, 2006, ISBN 3-933761-60-3

157 Manthey, Sabine: *Two-phase flow processes with dynamic effects in porous media - parameter estimation and simulation,* 2007, ISBN 3-933761-61-1

158 Pozos Estrada, Oscar: *Investigation on the Effects of Entrained Air in Pipelines,* 2007, ISBN 3-933761-62-X

159 Ochs, Steffen Oliver: *Steam injection into saturated porous media – process analysis including experimental and numerical investigations*, 2007, ISBN 3-933761-63-8

160 Marx, Andreas: *Einsatz gekoppelter Modelle und Wetterradar zur Abschätzung von Niederschlagsintensitäten und zur Abflussvorhersage, 2007,* ISBN 3-933761-64-6

161 Hartmann, Gabriele Maria: *Investigation of Evapotranspiration Concepts in Hydrological Modelling for Climate Change Impact Assessment*, 2007, ISBN 3-933761-65-4

162 Kebede Gurmessa, Tesfaye: *Numerical Investigation on Flow and Transport Characteristics to Improve Long-Term Simulation of Reservoir Sedimentation*, 2007, ISBN 3-933761-66-2

163 Trifković, Aleksandar: *Multi-objective and Risk-based Modelling Methodology for Planning, Design and Operation of Water Supply Systems*, 2007, ISBN 3-933761-67-0

164 Götzinger, Jens: *Distributed Conceptual Hydrological Modelling - Simulation of Climate, Land Use Change Impact and Uncertainty Analysis*, 2007, ISBN 3-933761-68-9

165 Hrsg.: Braun, Jürgen; Koschitzky, Hans-Peter; Stuhrmann, Matthias: *VEGAS – Kolloquium 2007,* Tagungsband zur Veranstaltung am 26. September 2007 an der Universität Stuttgart, Campus Stuttgart-Vaihingen, 2007, ISBN 3-933761-69-7

166 Freeman, Beau: *Modernization Criteria Assessment for Water Resources Planning; Klamath Irrigation Project, U.S.*, 2008, ISBN 3-933761-70-0

167 Dreher, Thomas: *Selektive Sedimentation von Feinstschwebstoffen in Wechselwirkung mit wandnahen turbulenten Strömungsbedingungen*, 2008, ISBN 3-933761-71-9

168 Yang, Wei: *Discrete-Continuous Downscaling Model for Generating Daily Precipitation Time Series*, 2008, ISBN 3-933761-72-7

169 Kopecki, Ianina: *Calculational Approach to FST-Hemispheres for Multiparametrical Benthos Habitat Modelling,* 2008*,* ISBN 3-933761-73-5

170 Brommundt, Jürgen: *Stochastische Generierung räumlich zusammenhängender Niederschlagszeitreihen*, 2008, ISBN 3-933761-74-3

171 Papafotiou, *Alexandros: Numerical Investigations of the Role of Hysteresis in Heterogeneous Two-Phase Flow Systems*, 2008, ISBN 3-933761-75-1

172 He, Yi: *Application of a Non-Parametric Classification Scheme to Catchment Hydrology*, 2008, ISBN 978-3-933761-76-7

173 Wagner, Sven: *Water Balance in a Poorly Gauged Basin in West Africa Using Atmospheric Modelling and Remote Sensing Information*, 2008, ISBN 978-3-933761-77-4

174 Hrsg.: Braun, Jürgen; Koschitzky, Hans-Peter; Stuhrmann, Matthias; Schrenk, Volker: *VEGAS-Kolloquium 2008 Ressource Fläche III*, Tagungsband zur Veranstaltung am 01. Oktober 2008 an der Universität Stuttgart, Campus Stuttgart-Vaihingen, 2008, ISBN 978-3-933761-78-1

175 Patil, Sachin: *Regionalization of an Event Based Nash Cascade Model for Flood Predictions in Ungauged Basins*, 2008, ISBN 978-3-933761-79-8

176 Assteerawatt, Anongnart: *Flow and Transport Modelling of Fractured Aquifers based on a Geostatistical Approach,* 2008, ISBN 978-3-933761-80-4

177 Karnahl, Joachim Alexander: *2D numerische Modellierung von multifraktionalem Schwebstoff- und Schadstofftransport in Flüssen*, 2008, ISBN 978-3-933761-81-1

178 Hiester, Uwe: *Technologieentwicklung zur In-situ-Sanierung der ungesättigten Bodenzone mit festen Wärmequellen,* 2009, ISBN 978-3-933761-82-8

179 Laux, Patrick: *Statistical Modeling of Precipitation for Agricultural Planning in the Volta Basin of West Africa,* 2009, ISBN 978-3-933761-83-5

180 Ehsan, Saqib: *Evaluation of Life Safety Risks Related to Severe Flooding,* 2009, ISBN 978-3-933761-84-2

181 Prohaska, Sandra: *Development and Application of a 1D Multi-Strip Fine Sediment Transport Model for Regulated Rivers,* 2009, ISBN 978-3-933761-85-9

182 Kopp, Andreas: *Evaluation of CO_2 Injection Processes in Geological Formations for Site Screening,* 2009, ISBN 978-3-933761-86-6

183 Ebigbo, Anozie: *Modelling of biofilm growth and its influence on CO_2 and water (two-phase) flow in porous media,* 2009, ISBN 978-3-933761-87-3

184 Freiboth, Sandra: *A phenomenological model for the numerical simulation of multiphase multicomponent processes considering structural alterations of porous media*, 2009, ISBN 978-3-933761-88-0

185 Zöllner, Frank: *Implementierung und Anwendung netzfreier Methoden im Konstruktiven Wasserbau und in der Hydromechanik*, 2009, ISBN 978-3-933761-89-7

186 Vasin, Milos: *Influence of the soil structure and property contrast on flow and transport in the unsaturated zone*, 2010, ISBN 978-3-933761-90-3

187 Li, Jing: *Application of Copulas as a New Geostatistical Tool*, 2010, ISBN 978-3-933761-91-0

188 AghaKouchak, Amir: *Simulation of Remotely Sensed Rainfall Fields Using Copulas*, 2010, ISBN 978-3-933761-92-7

189 Thapa, Pawan Kumar: *Physically-based spatially distributed rainfall runoff modelling for soil erosion estimation*, 2010, ISBN 978-3-933761-93-4

190 Wurms, Sven: *Numerische Modellierung der Sedimentationsprozesse in Retentionsanlagen zur Steuerung von Stoffströmen bei extremen Hochwasserabflussereignissen*, 2011, ISBN 978-3-933761-94-1

191 Merkel, Uwe: *Unsicherheitsanalyse hydraulischer Einwirkungen auf Hochwasserschutzdeiche und Steigerung der Leistungsfähigkeit durch adaptive Strömungsmodellierung*, 2011, ISBN 978-3-933761-95-8

192 Fritz, Jochen: *A Decoupled Model for Compositional Non-Isothermal Multiphase Flow in Porous Media and Multiphysics Approaches for Two-Phase Flow*, 2010, ISBN 978-3-933761-96-5

193 Weber, Karolin (Hrsg.): *12. Treffen junger WissenschaftlerInnen an Wasserbauinstituten*, 2010, ISBN 978-3-933761-97-2

194 Bliefernicht, Jan-Geert: *Probability Forecasts of Daily Areal Precipitation for Small River Basins,* 2011, ISBN 978-3-933761-98-9

195 Hrsg.: Koschitzky, Hans-Peter; Braun, Jürgen: *VEGAS-Kolloquium 2010 In-situ-Sanierung - Stand und Entwicklung Nano und ISCO -,* Tagungsband zur Veranstaltung am 07. Oktober 2010 an der Universität Stuttgart, Campus Stuttgart-Vaihingen*,* 2010*,* ISBN 978-3-933761-99-6

196 Gafurov, Abror: *Water Balance Modeling Using Remote Sensing Information - Focus on Central Asia,* 2010, ISBN 978-3-942036-00-9

197 Mackenberg, Sylvia: *Die Quellstärke in der Sickerwasserprognose: Möglichkeiten und Grenzen von Labor- und Freilanduntersuchungen,* 2010, ISBN 978-3-942036-01-6

198 Singh, Shailesh Kumar: *Robust Parameter Estimation in Gauged and Ungauged Basins,* 2010, ISBN 978-3-942036-02-3

199 Doğan, Mehmet Onur: *Coupling of porous media flow with pipe flow,* 2011, ISBN 978-3-942036-03-0

200 Liu, Min: *Study of Topographic Effects on Hydrological Patterns and the Implication on Hydrological Modeling and Data Interpolation,* 2011, ISBN 978-3-942036-04-7

201 Geleta, Habtamu Itefa: *Watershed Sediment Yield Modeling for Data Scarce Areas,* 2011, ISBN 978-3-942036-05-4

202 Franke, Jörg: *Einfluss der Überwachung auf die Versagenswahrscheinlichkeit von Staustufen,* 2011, ISBN 978-3-942036-06-1

203 Bakimchandra, Oinam: *Integrated Fuzzy-GIS approach for assessing regional soil erosion risks,* 2011, ISBN 978-3-942036-07-8

204 Alam, Muhammad Mahboob: *Statistical Downscaling of Extremes of Precipitation in Mesoscale Catchments from Different RCMs and Their Effects on Local Hydrology,* 2011, ISBN 978-3-942036-08-5

205 Hrsg.: Koschitzky, Hans-Peter; Braun, Jürgen: *VEGAS-Kolloquium 2011 Flache Geothermie - Perspektiven und Risiken,* Tagungsband zur Veranstaltung am 06. Oktober 2011 an der Universität Stuttgart, Campus Stuttgart-Vaihingen*,* 2011*,* ISBN 978-3-933761-09-2

206 Haslauer, Claus: *Analysis of Real-World Spatial Dependence of Subsurface Hydraulic Properties Using Copulas with a Focus on Solute Transport Behaviour,* 2011, ISBN 978-3-942036-10-8

207 Dung, Nguyen Viet: *Multi-objective automatic calibration of hydrodynamic models – development of the concept and an application in the Mekong Delta,* 2011, ISBN 978-3-942036-11-5

208 Hung, Nguyen Nghia: *Sediment dynamics in the floodplain of the Mekong Delta, Vietnam,* 2011, ISBN 978-3-942036-12-2

209 Kuhlmann, Anna: *Influence of soil structure and root water uptake on flow in the unsaturated zone,* 2012, ISBN 978-3-942036-13-9

210 Tuhtan, Jeffrey Andrew: *Including the Second Law Inequality in Aquatic Ecodynamics: A Modeling Approach for Alpine Rivers Impacted by Hydropeaking,* 2012, ISBN 978-3-942036-14-6

211 Tolossa, Habtamu: *Sediment Transport Computation Using a Data-Driven Adaptive Neuro-Fuzzy Modelling Approach,* 2012, ISBN 978-3-942036-15-3

212 Tatomir, Alexandru-Bodgan: *From Discrete to Continuum Concepts of Flow in Fractured*

Porous Media, 2012, ISBN 978-3-942036-16-0

213 Erbertseder, Karin: *A Multi-Scale Model for Describing Cancer-Therapeutic Transport in the Human Lung,* 2012, ISBN 978-3-942036-17-7

214 Noack, Markus: *Modelling Approach for Interstitial Sediment Dynamics and Reproduction of Gravel Spawning Fish,* 2012, ISBN 978-3-942036-18-4

215 De Boer, Cjestmir Volkert: *Transport of Nano Sized Zero Valent Iron Colloids during Injection into the Subsurface*, 2012, ISBN 978-3-942036-19-1

216 Pfaff, Thomas: *Processing and Analysis of Weather Radar Data for Use in Hydrology*, 2013, ISBN 978-3-942036-20-7

217 Lebrenz, Hans-Henning: *Addressing the Input Uncertainty for Hydrological Modeling by a New Geostatistical Method*, 2013, ISBN 978-3-942036-21-4

218 Darcis, Melanie Yvonne: *Coupling Models of Different Complexity for the Simulation of CO_2 Storage in Deep Saline Aquifers*, 2013, ISBN 978-3-942036-22-1

219 Beck, Ferdinand: *Generation of Spatially Correlated Synthetic Rainfall Time Series in High Temporal Resolution - A Data Driven Approach*, 2013, ISBN 978-3-942036-23-8

220 Guthke, Philipp: *Non-multi-Gaussian spatial structures: Process-driven natural genesis, manifestation, modeling approaches, and influences on dependent processes*, 2013, ISBN 978-3-942036-24-5

221 Walter, Lena: *Uncertainty studies and risk assessment for CO_2 storage in geological formations*, 2013, ISBN 978-3-942036-25-2

222 Wolff, Markus: *Multi-scale modeling of two-phase flow in porous media including capillary pressure effects,* 2013, ISBN 978-3-942036-26-9

223 Mosthaf, Klaus Roland: *Modeling and analysis of coupled porous-medium and free flow with application to evaporation processes,* 2014, ISBN 978-3-942036-27-6

224 Leube, Philipp Christoph: *Methods for Physically-Based Model Reduction in Time: Analysis, Comparison of Methods and Application*, 2013, ISBN 978-3-942036-28-3

225 Rodríguez Fernández, Jhan Ignacio: *High Order Interactions among environmental variables: Diagnostics and initial steps towards modeling*, 2013, ISBN 978-3-942036-29-0

226 Eder, Maria Magdalena: *Climate Sensitivity of a Large Lake*, 2013, ISBN 978-3-942036-30-6

227 Greiner, Philipp: *Alkoholinjektion zur In-situ-Sanierung von CKW Schadensherden in Grundwasserleitern: Charakterisierung der relevanten Prozesse auf unterschiedlichen Skalen*, 2014, ISBN 978-3-942036-31-3

228 Lauser, Andreas: *Theory and Numerical Applications of Compositional Multi-Phase Flow in Porous Media*, 2014, ISBN 978-3-942036-32-0

229 Enzenhöfer, Rainer: *Risk Quantification and Management in Water Production and Supply Systems*, 2014, ISBN 978-3-942036-33-7

230 Faigle, Benjamin: *Adaptive modelling of compositional multi-phase flow with capillary pressure*, 2014, ISBN 978-3-942036-34-4

231 Oladyshkin, Sergey: *Efficient modeling of environmental systems in the face of complexity and uncertainty*, 2014, ISBN 978-3-942036-35-1

232 Sugimoto, Takayuki: *Copula based Stochastic Analysis of Discharge Time Series*, 2014, ISBN 978-3-942036-36-8

233 Koch, Jonas: *Simulation, Identification and Characterization of Contaminant Source Architectures in the Subsurface*, 2014, ISBN 978-3-942036-37-5

234 Zhang, Jin: *Investigations on Urban River Regulation and Ecological Rehabilitation Measures, Case of Shenzhen in China*, 2014, ISBN 978-3-942036-38-2

235 Siebel, Rüdiger: *Experimentelle Untersuchungen zur hydrodynamischen Belastung und Standsicherheit von Deckwerken an überströmbaren Erddämmen,* 2014, ISBN 978-3-942036-39-9

236 Baber, Katherina: *Coupling free flow and flow in porous media in biological and technical applications: From a simple to a complex interface description,* 2014,

ISBN 978-3-942036-40-5

237 Nuske, Klaus Philipp: *Beyond Local Equilibrium — Relaxing local equilibrium assumptions in multiphase flow in porous media,* 2014, ISBN 978-3-942036-41-2

238 Geiges, Andreas: *Efficient concepts for optimal experimental design in nonlinear environmental systems*, 2014, ISBN 978-3-942036-42-9

239 Schwenck, Nicolas: *An XFEM-Based Model for Fluid Flow in Fractured Porous Media*, 2014, ISBN 978-3-942036-43-6

240 Chamorro Chávez, Alejandro: *Stochastic and hydrological modelling for climate change prediction in the Lima region, Peru*, 2015, ISBN 978-3-942036-44-3

241 Yulizar: *Investigation of Changes in Hydro-Meteorological Time Series Using a Depth-Based Approach*, 2015, ISBN 978-3-942036-45-0

242 Kretschmer, Nicole: *Impacts of the existing water allocation scheme on the Limarí watershed – Chile, an integrative approach*, 2015, ISBN 978-3-942036-46-7

243 Kramer, Matthias: *Luftbedarf von Freistrahlturbinen im Gegendruckbetrieb*, 2015, ISBN 978-3-942036-47-4

244 Hommel, Johannes: *Modeling biogeochemical and mass transport processes in the subsurface: Investigation of microbially induced calcite precipitation*, 2016, ISBN 978-3-942036-48-1

245 Germer, Kai: *Wasserinfiltration in die ungesättigte Zone eines makroporösen Hanges und deren Einfluss auf die Hangstabilität*, 2016, ISBN 978-3-942036-49-8

246 Hörning, Sebastian: *Process-oriented modeling of spatial random fields using copulas*, 2016, ISBN 978-3-942036-50-4

247 Jambhekar, Vishal: *Numerical modeling and analysis of evaporative salinization in a coupled free-flow porous-media system,* 2016, ISBN 978-3-942036-51-1

248 Huang, Yingchun: *Study on the spatial and temporal transferability of conceptual hydrological models*, 2016, ISBN 978-3-942036-52-8

249 Kleinknecht, Simon Matthias: *Migration and retention of a heavy NAPL vapor and remediation of the unsaturated zone*, 2016, ISBN 978-3-942036-53-5

250 Kwakye, Stephen Oppong: *Study on the effects of climate change on the hydrology of the West African sub-region*, 2016, ISBN 978-3-942036-54-2

251 Kissinger, Alexander: *Basin-Scale Site Screening and Investigation of Possible Impacts of CO_2 Storage on Subsurface Hydrosystems*, 2016, ISBN 978-3-942036-55-9

252 Müller, Thomas: *Generation of a Realistic Temporal Structure of Synthetic Precipitation Time Series for Sewer Applications*, 2017, ISBN 978-3-942036-56-6

253 Grüninger, Christoph: *Numerical Coupling of Navier-Stokes and Darcy Flow for Soil-Water Evaporation*, 2017, ISBN 978-3-942036-57-3

254 Suroso: *Asymmetric Dependence Based Spatial Copula Models: Empirical Investigations and Consequences on Precipitation Fields*, 2017, ISBN 978-3-942036-58-0

255 Müller, Thomas; Mosthaf, Tobias; Gunzenhauser, Sarah; Seidel, Jochen; Bárdossy, András: *Grundlagenbericht Niederschlags-Simulator (NiedSim3)*, 2017, ISBN 978-3-942036-59-7

256 Mosthaf, Tobias: *New Concepts for Regionalizing Temporal Distributions of Precipitation and for its Application in Spatial Rainfall Simulation,* 2017, ISBN 978-3-942036-60-3

257 Fenrich, Eva Katrin: *Entwicklung eines ökologisch-ökonomischen Vernetzungsmodells für Wasserkraftanlagen und Mehrzweckspeicher,* 2018, ISBN 978-3-942036-61-0

258 Schmidt, Holger: *Microbial stabilization of lotic fine sediments*, 2018, ISBN 978-3-942036-62-7

259 Fetzer, Thomas: *Coupled Free and Porous-Medium Flow Processes Affected by Turbulence and Roughness – Models, Concepts and Analysis*, 2018, ISBN 978-3-942036-63-4

260 Schröder, Hans Christoph: *Large-scale High Head Pico Hydropower Potential Assessment*, 2018, ISBN 978-3-942036-64-1

261 Bode, Felix: *Early-Warning Monitoring Systems for Improved Drinking Water Resource*

Protection, 2018, ISBN 978-3-942036-65-8

262 Gebler, Tobias: *Statistische Auswertung von simulierten Talsperrenüberwachungsdaten zur Identifikation von Schadensprozessen an Gewichtsstaumauern*, 2018, ISBN 978-3-942036-66-5

263 Harten, Matthias von: *Analyse des Zuppinger-Wasserrades – Hydraulische Optimierungen unter Berücksichtigung ökologischer Aspekte*, 2018, ISBN 978-3-942036-67-2

264 Yan, Jieru: *Nonlinear estimation of short time precipitation using weather radar and surface observations*, 2018, ISBN 978-3-942036-68-9

265 Beck, Martin: *Conceptual approaches for the analysis of coupled hydraulic and geomechanical processes*, 2019, ISBN 978-3-942036-69-6

266 Haas, Jannik: *Optimal planning of hydropower and energy storage technologies for fully renewable power systems*, 2019, ISBN 978-3-942036-70-2

267 Schneider, Martin: *Nonlinear Finite Volume Schemes for Complex Flow Processes and Challenging Grids*, 2019, ISBN 978-3-942036-71-9

268 Most, Sebastian Christopher: *Analysis and Simulation of Anomalous Transport in Porous Media*, 2019, ISBN 978-3-942036-72-6

269 Buchta, Rocco: *Entwicklung eines Ziel- und Bewertungssystems zur Schaffung nachhaltiger naturnaher Strukturen in großen sandgeprägten Flüssen des norddeutschen Tieflandes*, 2019, ISBN 978-3-942036-73-3

270 Thom, Moritz: *Towards a Better Understanding of the Biostabilization Mechanisms of Sediment Beds*, 2019, ISBN 978-3-942036-74-0

271 Stolz, Daniel: *Die Nullspannungstemperatur in Gewichtsstaumauern unter Berücksichtigung der Festigkeitsentwicklung des Betons*, 2019, ISBN 978-3-942036-75-7

272 Rodriguez Pretelin, Abelardo: *Integrating transient flow conditions into groundwater well protection*, 2020, ISBN: 978-3-942036-76-4

273 Weishaupt, Kilian: *Model Concepts for Coupling Free Flow with Porous Medium Flow at the Pore-Network Scale: From Single-Phase Flow to Compositional Non-Isothermal Two-Phase Flow*, 2020, ISBN: 978-3-942036-77-1

274 Koch, Timo: *Mixed-dimension models for flow and transport processes in porous media with embedded tubular network systems*, 2020, ISBN: 978-3-942036-78-8

275 Gläser, Dennis: *Discrete fracture modeling of multi-phase flow and deformation in fractured poroelastic media*, 2020, ISBN: 978-3-942036-79-5

276 Seitz, Lydia: *Development of new methods to apply a multi-parameter approach – A first step towards the determination of colmation*, 2020, ISBN: 978-3-942036-80-1

277 Ebrahim Bakhshipour, Amin: *Optimizing hybrid decentralized systems for sustainable urban drainage infrastructures planning*, 2021, ISBN: 978-3-942036-81-8

278 Seitz, Gabriele: *Modeling Fixed-Bed Reactors for Thermochemical Heat Storage with the Reaction System CaO/Ca(OH)$_2$*, 2021, ISBN: 978-3-942036-82-5

279 Emmert, Simon: *Developing and Calibrating a Numerical Model for Microbially Enhanced Coal-Bed Methane Production*, 2021, ISBN: 978-3-942036-83-2

280 Heck, Katharina Klara: *Modelling and analysis of multicomponent transport at the interface between free- and porous-medium flow - influenced by radiation and roughness*, 2021, ISBN: 978-3-942036-84-9

281 Ackermann, Sina: *A multi-scale approach for drop/porous-medium interaction*, 2021, ISBN: 978-3-942036-85-6

282 Beckers, Felix: *Investigations on Functional Relationships between Cohesive Sediment Erosion and Sediment Characteristics*, 2021, ISBN: 978-3-942036-86-3

Die Mitteilungshefte ab der Nr. 134 (Jg. 2005) stehen als pdf-Datei über die Homepage des Instituts: www.iws.uni-stuttgart.de zur Verfügung.